The University of Nottingham

UNITED KINGDOM · CHINA · MALAYSIA

Deposition of Satellited Al-TiC Powders for Coating Applications

Thesis submitted to the University of Nottingham-UK for the degree of Doctor of Philosophy

Kamaal Sahib Makki Al-hamdani

November 2019

Department of Mechanical, Materials, and Manufacturing Engineering

Faculty of Engineering

This page is left intentionally blank

ABSTRACT

Metal matrix composite (MMC) coatings have good wear resistance, given the combined ductility of the metal matrix and high hardness and strength of the ceramic reinforcements. Surface modification by coating deposition is an important approach for improving the functional surface region of materials without replacing the entire component, which is also a cost-effective approach for extension the component working life.

Cold spray (CS) is an important technique used to deposit different types of materials without the need for heating or melting. Because of the dependence of cold spray on deformation of the sprayed and substrate materials, hard particles tend to rebound, while less-ductile materials experience limited deformation during impact. Laser cladding (LC) has some advantages in terms of surface processing over other techniques, including narrow wavelength, low divergence, and a highly coherent beam. However, the use of blended feedstocks within powder-injection LC can lead to the separation of the blended phases that may cause stream.

Satelliting is a simple powder-mixing process recently used to produce composite feedstocks consisting of fine ceramic particles attached to the surfaces of relatively large (parent) metal particles. This is based on adding a small amount of liquid binder to the powder mixture during the mixing process without the need for high energy or heat. The main point of investigation of this research is the use of satellited Al-TiC feedstocks for cold spray and laser cladding processes, along with blended feedstocks with the same compositions for comparison. This is a trails for improving the behaviour of the composite coating by increasing the reinforcement fraction through elimination particles rebounding.

In the first stage of this work, preliminary satelliting processes were performed using TiC as a reinforcing phase, adjusting the fraction of Al powder and the binder to produce a satellited powder. The prepared satellited powder then was used in the CS process to evaluate its cold-sprayability, this was along with pure Al and blended Al/TiC feedstocks for comparison purposes. A seven-fold increase in TiC area fraction was measured in the satellited coating compared to that in the blended coating.

In the second stage, the effects of using the satelliting technique on the deposition and characteristics of composite coatings of a less-ductile Al alloy (A6061) and TiC, fabricated by cold-spray were investigated. The use of satellited feedstock has resulted in increasing the TiC catchment and deposition efficiency by 66% and 78%, respectively, compared to the blended feedstock. The satellited coating presented a reduction of 67% in the interlamellar porosity compared with the blended 6061/TiC coating, while the heat-treated coating exhibited a 70% reduction in interlamellar porosity.

Finally, the behaviour of Al/TiC satellited feedstock under laser cladding was investigated along with a blended feedstock. The blended and satellited and have presented several differences regarding: clad geometry, clad area, TiC fraction and other characteristics. These differences indicated a different interaction of the satellited feedstock with the lase radiations; thus, two interaction mechanisms between the laser radiation and the feedstocks were suggested and demonstrated depending on their morphologies.

Publications

Included in the thesis:

- Al-Hamdani, K.S., Murray, J.W., Hussain, T., Kennedy, A. and Clare, A.T., 2017. Cold sprayed metal-ceramic coatings using satellited powders. Materials Letters, 198, pp.184-187. *(Chapter **4**)*

- Al-Hamdani, K.S., Murray, J.W., Hussain, T. and Clare, A.T., 2019. Heat-treatment and mechanical properties of cold-sprayed high strength Al alloys from satellited feedstocks. Surface and Coatings Technology, 374, pp.21-31. *(Chapter **5**)*

- Al-Hamdani, K.S., Murray, J.W., Hussain, T. and Clare, A.T., 2019. Controlling ceramic-reinforcement distribution in laser cladding of MMCs. Journal of Surface and Coatings Technology. *(Chapter **6**)*

Not included in the thesis:

- Tan, H., Hao, D., Al-Hamdani, K., Zhang, F., Xu, Z. and Clare, A.T., 2018. Direct metal deposition of TiB2/AlSi10Mg composites using satellited powders. *Materials Letters*, *214*, pp.123-126.

- Zhang, F., Mei, M., Al-Hamdani, K., Tan, H. and Clare, A.T., 2018. Novel nucleation mechanisms through satelliting in direct metal deposition of Ti-15Mo. *Materials Letters*, *213*, pp.197-200.

- Wits, W.W., de Smit, M., Al-Hamdani, K. and Clare, A.T., 2019. Laser powder bed fusion of a Magnesium-SiC metal matrix composite. *Procedia CIRP*, *81*, pp.506-511.

Acknowledgement

I feel the words are insufficient to express my great gratitude and thanks to my supervisor, **prof. Adam T. Clare**. I have been so lucky working under his supervision. His leadership and scientific experiences were of great importance in guiding me to the right directions through the research journey toward completing my PhD. This also was supported by the scientific and technical support of my supervisors **Dr Tanvir Hussain** that I have gained much knowledge and experience from. I would like also to greatly thank **Dr James Murray** who was the closest supervisor and he supported me throughout my PhD even in matters out of the research area. They all form a great supervision team, it was not possible to complete my study without them.

I also deeply thank Dr Elisabeth Steer and Dr Nigel Neate for their valuable assistance regarding the SEM and XRD characterisation processes. My deep gratitude also goes to the lab manager Mr Rory Screaton for his assistance in cold spray processes, and to Mr Stuart Branston, the technician of the laser processing lab for his support during laser cladding experiments. Also, I would like to thank my best friends, Mohaimen Al-Thamir and Mustapha Al-Assadi for their support during my PhD study and thesis writing up.

I would like to thank my sponsor, the Ministry of Higher education and scientific research in Iraq and the Iraqi Cultural Attaché - London for their kindness in providing the necessary financial support for the completion of my study. My thanks also go to the University of Thi-Qar, Iraq, especially the College of Engineering, for their support in every way.

Great thanks to my parents, they were with me at every step supporting and encouraging me by their warm words and prays that made me feel myself among them every time. Also, thanks to my loyal brothers *Jamal* and *Talal* and all my sisters for their unlimited and sincere support, and encouragement over the years. Thanks to the spirit of my aunt who was my second mom, you will always be with me. My gratitude to my uncle *Najeeb* and my lovely cousin *Raed* for their support and encouragement along this trip.

Finally, special heartfelt thanks should go to my sweetheart wife *Hawraa* who does not spare any effort to support me while she was under the pressure of the kids and other responsibilities. My great thanks to my lovely daughters *Malak* and *Meqat*, and to my hero son *Ali* and the little one *Mostafa* for being close to me all the time. Their sincere feelings, love, patient, encouragement have eliminated all the difficulties I faced and motivated me to go ahead.

Table of Contents

1 Contents

ABSTRACT i

Publications iii

Acknowledgement v

Table of Contents vii

Table of figures x

1 Introduction 1

1.1 Introduction **1**

1.2 Aims and objectives **2**

1.3 Thesis overview **5**

2 Literature Review 7

2.1 Introduction **7**

2.2 Metal Matrix Composites **8**

2.2.1 Advantages of MMCs **11**

2.2.2 Particulate reinforced MMCs **12**

2.2.3 Aluminium-based matrix composites (AMCs): **13**

2.2.4 TiC-reinforced MMCs **15**

2.2.5 Strengthening mechanism in MMC **16**

2.2.6 How MMCs are made **17**

2.3 Cold Spray **20**

2.3.1 Cold Spray Process **21**

2.3.2 Gas dynamics **24**

2.3.3 Bonding theories **28**

2.3.4 Effect of ceramic particles on the CS coating properties. **30**

2.3.5 Cold spray of Al and Al composites **31**

2.3.6 Cold spray of 6061 alloy **34**

2.3.7 TiC in cold spray **35**

2.3.8 Heat-Treatment of Cold Sprayed Coatings **37**

2.4 Laser Cladding (LC) **40**

2.4.1 Quality and deposition efficiency of laser clads **42**

2.4.2 Laser Cladding of AMCs **45**

2.5 Preparation Methods of Composite Feedstocks **48**

2.5.1 Simple Mixing **50**

2.5.2 Mechanical Alloying **50**

2.5.3 Metal-Coated Particles **51**

2.5.4 Spray Drying of Slurries **52**

2.6 Summary of the Literature Review **54**

2.6.1 Metal Matrix Composites 54
2.6.2 Preparing Methods of Composite Feedstocks 55
2.6.3 Cold Spray 56
2.6.4 Laser Cladding (LC) 58
2.6.5 Knowledge Gaps Definition 59
3 MATERIALS AND METHODOLOGY 61
3.1 Introduction 61
3.2 Materials 62
3.2.1 Aluminium 6082 plate 62
3.2.2 Pure aluminium powder 63
3.2.3 Aluminium alloy 6061 powder 64
3.2.4 Titanium carbide powder (TiC) 65
3.2.5 Binder Polyvinyl alcohol 65
3.3 EQUIPMENT AND EXPERIMENTAL PROCEDURES 66
3.3.1 Feedstock preparation 66
3.3.2 Powder characterisation 67
3.3.3 Cold Spray Experiments 69
3.3.4 Annealing heat-treatment 73
3.3.5 Laser Cladding Experiments 74
4 Cold Spray Deposition of Pure Al-TiC Coatings using Satellited Powders 81
4.1 Introduction 81
4.2 Preparation of composite feedstock for cold spray: 82
4.3 Effect of satelliting on the powder flowability 91
4.4 Effect of satelliting on the in-flight particle momentum 95
4.5 Cold sprayed metal-ceramic coatings using satellited powder 101
4.5.1 Composite feedstocks for cold spray processes. 101
4.5.2 Results and discussion 102
4.6 Cold spray of Satellited powders with different TiC fractions: 110
4.7 Summary 118
5 Heat-treatment and mechanical properties of cold-sprayed high strength Al Alloys from satellited feedstocks 119
5.1 Introduction 119
5.2 Experimental details 120
5.2.1 Materials 120
5.2.2 Cold spray 122
5.2.3 Heat treatment 124
5.2.4 Deposition efficiency 125
5.3 Results and discussion 125
5.3.1 Coating characterisation: Al 6061 vs Al6061- TiC 125

5.3.2 Effect of heat treatment on the satellited coatings 137
5.3.3 Wear behaviour of the deposited coatings 144
5.4 Summary 152
6 Laser cladding of ceramic-reinforcement composites using blended and satellited feedstocks 155
6.1 Introduction 155
6.2 Experimental details 157
6.2.1 Materials 157
6.2.2 Feedstock preparation 157
6.2.3 Blown-powder laser cladding 160
6.2.4 Pre-placed powder laser cladding 162
6.2.5 Microhardness and dry-sliding wear 162
6.2.6 Powder and clad characterisation 163
6.2.7 Deposition efficiency 164
6.3 Results and discussion 164
6.3.1 Clad characterisations results 164
6.3.2 Powder behaviour and deposition mechanisms 171
6.3.3 Effect of the process parameters on the clad form 179
6.3.4 Deposition efficiency 181
6.3.5 Invariance upon pre-placed powder laser cladding 183
6.4 Microstructural characterisation of the deposited clads 184
6.5 Microhardness and dry-sliding wear behaviour of the deposited clads 192
6.5.1 Microhardness measurements 192
6.5.2 Dry-sliding wear results 194
6.6 Summary 200
7 Conclusions and Future Work 203
7.1 Conclusions 203
7.2 Recommendations for future work 207
References 209
Appendixes 231
Appendix 226

Table of figures

Figure 2-1: Examples of composite structures with (a) particulate, (b) discontinuous fibres, (c) discontinuous fibres, and (d) continuous fibres [16]. 10
Figure 2-2: Physical and mechanical properties of composites compared with the two most commonly used alloys, i.e., steel and aluminium[19]. 11
Figure 2-3: Illustration of cold spray system [80]. 21
Figure 3-1: (a) SEM image showing the morphology of the pure Al powder; (b) particle size distribution of the pure Al powder. 63
Figure 3-2: (a) SEM image showing the morphology of the Al 6061 powder; (b) particle size distribution of the Al 6061 powder. 64
Figure 3-3: (a) SEM image showing the morphology of the TiC powder; (b) particle size distribution of TiC powder. 65
Figure 3-4: A schematic diagram of the cold spray system used in this research. 70
Figure 3-5: The cold spray system showing (a) the combined whole system, (b) the spraying gun and table, and (c) the powder feeder. 71
Figure 3-6: A schematic of the cold spray deposition path of (a) single track and (b) full surface coating. 72
Figure 3-7: Digital images of cold-sprayed samples; (a) single tracks and (b) full surface coating. 72
Figure 3-8: A schematic diagram of the powder injection laser cladding process. 75
Figure 3-9: Digital images of the powder injection laser cladding system used in this work. 76
Figure 3-10: Powder bed set up prior to the pre-placed powder bed laser cladding. 79
Figure 4-1: SEM images of the satellited powder (mix_1) at (a) X500, and (b) X1000. 83
Figure 4-2: SEM of the satellited powder (mix_1) after (a) sieving the prepared powder; (b) increasing the binder by (20%). 84
Figure 4-3: (a) SE and (b) BSE images of the substrate surface after cold spraying; (c) a BSE image of a crater produced by satellited particle, and (d) Al and TiC deposits. 86
Figure 4-4: SEM images of the (a) virgin TiC, and (b) virgin Al powders used in satelliting of mix_3. 88
Figure 4-5: SEM images of the processed powder show the agglomeration of particles due to the high amount of binder. 89
Figure 4-6: (a) SE and (b) BSE, SEM images of the satellited powder (Al/12TiC) after reducing the binder by 20%. 90
Figure 4-7: A BSE image of a cross-sectional view of satellited particles (Al/12TiC). 91
Figure 4-8: Rheology analysis of the virgin and composite powders, results are the average of three tests. 92
Figure 4-9: The reduction in the velocity of a satellited particle with increasing TiC fraction. 97
Figure 4-10: The change in the momentum of a satellited particle with different TiC fractions. 100
Figure 4-11: SEM image of the (a) blended (Al/12TiC) and (b) satellited (Al/12TiC) feedstocks. 101
Figure 4-12: Cross-sectional BSE images at two magnifications and high magnification SEM images of the cold sprayed coatings showing particle/surface deformation of different feedstocks; (a and b) pure Al, (c and d) blended, and (e and f) satellited. 103

Figure 4-13: The percentage TiC area fraction in the different composite coatings, (b) the average thickness and the percentage areal porosity for the coatings, error bars represent the maximum and minimum values. 104
Figure 4-14: The average thickness of the deposited coatings, error bars represent the maximum and minimum values..... 105
Figure 4-15: Mean percentage of areal porosity of the deposited coatings, error bars represent the maximum and minimum values. 106
Figure 4-16: Cross-sectional SEM images at two magnifications of individual deposited particles; (a and b) pure Al, (c and d) blended, and (e and f) satellited. 107
Figure 4-17: Schematic diagrams for two coating mechanisms using: (a) blended feedstock, (b) satellited feedstock..... 109
Figure 4-18: BSE images showing the morphologies of the satellited powders with two magnifications; (a and b) Sat_20 (c and d) Sat_28 (e and f) Sat_36. 112
Figure 4-19: Low and high magnifications BSE images of the cold-sprayed coatings using (a) Sat_20 and (b) Sat_28 satellited powders..... 113
Figure 4-20: TiC fractions in the deposited coating sections measured using Image-J software, error bars represent the max and min values..... 114
Figure 4-21: The average thickness of the deposited coating sections, error bars represent the max and min values. 115
Figure 4-22: Interlamellar porosity levels in the deposited coating sections (average), measured by Image-J, error bars represent the max and min values. 117
Figure 5-1: SEM SE images showing the morphology of (a) virgin 6061 powder (b), virgin TiC powder, (c) blended feedstock (6061-TiC) and (d) satellited feedstock (6061-TiC). 121
Figure 5-2: The particle size distribution of (a) 6061 powder (b), TiC powder, (c) blended feedstock (6061-TiC) and (d) satellited feedstock (6061-TiC). 122
Figure 5-3: Top-view SEM images of the sprayed substrate surface, showing deposited splats and craters produced by a 6061 particle at low (a) and high (b) magnification..... 126
Figure 5-4: Cross-sectional BSE images showing the different structures of the cold sprayed coatings; (a) 6061 coating, (b) blended 6061-TiC, (c) as-sprayed 6061-TiC satellited coating and (d) heat-treated 6061-TiC satellited coating..... 127
Figure 5-5: SEM images of individual deposited particles showing the effect of fine ceramic particles on the particle/surface bonding. 130
Figure 5-6: The average thickness measurements of the deposited coatings. 131
Figure 5-7: The deposition efficiency of the deposited coatings..... 132
Figure 5-8: The percentage porosity by area of the deposited coatings, showing the effect of the addition of TiC and heat-treatment on coating porosity. 135
Figure 5-9: TiC area fraction in the coating section showing the contribution of satelliting in increasing the embedded ceramic..... 136
Figure 5-10: X-ray diffraction patterns of the deposited coatings..... 139
Figure 5-11: Microhardness measurements at the centreline of the deposited coatings. Error bars represent the maximum and minimum hardness values. 139
Figure 5-12: SE images of microhardness indents of the deposited coatings at 50 gf (lift column) and 10 gf (right column); (a and b) AS-6061, (c and d) AS-blended 6061-TiC, (e and f) AS-satellited 6061-TiC, (g and h) HT-satellited 6061-TiC. 142
Figure 5-13: The average SWR of the deposited coatings, showing the effect of the reinforcement and heat treatment on reducing the SWR. 144
Figure 5-14: (a and d) 3D-views of the entire wear tracks, and SEM images of the coatings (labelled above) at low (b and e) and high (c and f) magnifications..... 146

Figure 5-15: (a and d) 3D-views of the entire wear tracks, and SEM images of the coatings (labelled above) at low (b and e) and high (c and f) magnifications. 148
Figure 5-16: BSE and EDX analysis images of the counter-body surface showing; (a) BSE, (b) Fe and (c) Al. 151
Figure 6-1: SEM images showing the morphology of (a) Al powder (b), TiC powder, (c-d) blended (Al/20TiC); and (e-f) satellited (Al/20TiC). 159
Figure 6-2: The particle size distribution of (a) virgin Al powder, (b) TiC powder, (c) simply blended powder (Al/TiC) and (d) satellited powder (Al/TiC). 160
Figure 6-3: BSE images of the cross-sectional of the blended feedstock clads (sample numbers are shown at the corners) 166
Figure 6-4: BSE images of the cross-sectional of the satellited feedstock clads (sample numbers are shown at the corners) 167
Figure 6-5: The clad area of the blended and satellited clads at different Eeff and PDD values measured by Image-J software, error bars represent the standard error of three clad sections. 168
Figure 6-6: The dilution of the blended and satellited clads at different Eeff and PDD values measured by Image-J software, error bars represent the standard error of three clad sections. 170
Figure 6-7: XRD patterns of the blended and satellited clads deposited at low E_{eff} (104 J/mm^2). 171
Figure 6-8: TiC area fraction in the clad sections of blended and satellited clads deposited at E_{eff}=104 J/mm^2 and different PDD values, error bars represent the standard error values. 172
Figure 6-9: BSE images present the TiC distribution in identical blended (a-b) and satellited clads (c-d), both were deposited at E_{eff} =122 J/mm^2 and PDD = 0.0056 g/mm^2. 173
Figure 6-10: Schematic of the mechanism of the interaction between the laser beam and the blended feedstock. 175
Figure 6-11: Schematic of the mechanism of the interaction between the laser beam and the satellited feedstock. 177
Figure 6-12: BSE images show the difference in the level of TiC dissolution at the blended (a-c) and satellited (d-f) clads deposited at PDD of 0.0037 (g/mm^2) and E_{eff} of 122 (J/mm^2). 178
Figure 6-13: Clad formability according to different E_{eff} and PDD values; (A) Blended feedstock, and (B) Satellited feedstock. 180
Figure 6-14: Deposition efficiency of the blended and satellited feedstocks at Eeff=122 (J/mm2) and PDD=0.0037 (g/mm2); error bars represent the standard errors of the measurements. 182
Figure 6-15: BSE cross-sectional images of the pre-placed powder clads deposited at Eeff=122 using (a) blended, and (b) satellited powders. 183
Figure 6-16: BSE images showing the microstructure of the blended clads deposited at three different laser energy densities; (a - c) 104 J/mm^2, (d - f) 122 J/mm^2, and (g -i) 140 J/mm^2; (scale bar in K is 10 µm). 184
Figure 6-17: XRD patterns of the blended and satellited samples that were deposited at PDD of 0.0056 g/mm^2 at different values of E_{eff}, showing the formation of new phases when high E_{eff}s were used. 186
Figure 6-18: WDS maps showing (a) BSE image, and concentration of (b) Al, (c) C, and (d) Ti in the section of the blended clad deposited at PDD of 0.0056 g/mm2 and 140 J/mm2. .. 187

Figure 6-19: BSE images showing the microstructure of the satellited clads deposited with different magnifications; (a-c) 104 J/mm^2, (d-f) 122 J/mm^2, and (g-i) 140 J/mm^2. 188
Figure 6-20: WDS maps showing (a) BSE image, and the concentration levels of (b) Al, (c) C, and (d) Ti in the satellited clad section deposited at 140 J/mm^2 and 0.0056 g/mm^2..... 190
Figure 6-21: Microhardness measurements of blended and satellited clad matrices deposited at different Eeff values; error bars represent the standard errors of 10 measurements. 193
Figure 6-22: The average SWR of the blended and satellited clads; error bars represent the standard errors of three measurements. 195
Figure 6-23: Images of the worn surfaces of the blended clads; the first column: 3D-views of the entire wear tracks; second column: low magnification SEM images; and third column: high magnification SEM images. Laser energy is labelled on the right. 197
Figure 6-24: Images of the worn surfaces of the satellited clads; first column: 3D-views of the entire wear tracks; second column: low magnification SEM images; and third column: high magnification SEM images. Laser energy was labelled at the right-hand side. 198

List of abbreviations

MMC	Metal matrix composite
CGDS	Cold gas dynamic spray
SEM	Secondary electron microscopy
SE	Secondary electrons
BSE	Back scattered electrons
EDX	Energy dispersive x-ray spectrometers
XRD	x-rays diffraction
EPMA	Electron Probe Micro-Analysis
WDS	Wavelength dispersive spectrometers
v_{cri}	Critical velocity
σ_{TS}	Particle tensile strength
T_i	Impact temperature
T_m	Melting temperature
T_R	Reference temperature
C_p	Heat capacity
ρ_p	Particle material density
M	Mach number
v_g	Gas velocity
γ	The ratio of specific heats (C_p/C_v)
R	Gas constant
M_w	Gas molecular weight
V_p	Particle velocity
V_g	Gas velocity
d_p	Particle diameter
p_o	Nitrogen pressure
ρ_s	Particle density
C_d	Drag coefficient
L_d	Length of the diverging part of the nozzle (m).
P_o	Gas stagnation pressure (bar).
P	Laser power
V	Laser scanning speed
E_{eff}	Laser effective energy
PDD	Powder deposition density
PVA	Polyvinyl alcohol
SI	Stability index
FRI	Flow rate index
DED	Direct energy deposition
F	Powder mass feeding rate
$\boldsymbol{\lambda}$	Wavelength
d_{hkl}	Spacing between lattice planes
θ	Scattering angle
N	Applied load (Vickers hardness)
d	Mean diagonal length (Vickers hardness)
SWR	Specific wear rate

1 Introduction

1.1 Introduction

Many engineering components need improved properties, such as high wear and corrosion resistance, to perform their desired function. Surface coating is a method of improving the functional surface region of material without replacing the entire component. Ceramic materials can be coated on component surfaces to improve hardness and wear behaviour. Metal matrix composites (MMC) are useful materials to deposit as wear resistant coatings, as they can combine the hardness of the ceramic phase with the ductility of the metal matrix.

Cold gas dynamic spray, or simply cold spray (CS), has proven to have advantages over competing processes such as thermal spray. Cold spray uses a supersonic gas stream to accelerate powder particles to velocities of 500–1000 m/s [1]. Due to the kinetic energy of the incident particles, materials can attach and form an integrated film via plastic deformation, and do not require to be molten or semi-molten [2].

Laser-cladding is a competing surface modification technique for depositing materials onto the surfaces of components. A range of materials can be deposited, including hard-wearing ceramics. Laser cladding typically provides good metallurgical bonds, with minimal dilution and low distortion of the deposited coatings, which are hard to achieve by other techniques. In recent years, the literature on laser-cladding shows an increased interest in depositing composite coatings containing various volume fractions of ceramic particles [3]. The reinforcing particulates (including carbides, borides and nitrides) can be prepared separately and added directly to the molten metal with stirring to obtain good distribution for the reinforcement [4].

In this project, the deposition of MMC coatings is conducted using CS and laser cladding technologies. Post heat treatment is also applied on some cold spray coatings,

to investigate the effect of post-heat treatment on the cold sprayed coating properties of the structure, density and cohesion. The microstructure of the deposited coatings is inspected using Optical Microscopy (OM) and Scanning Electron Microscopy (SEM) imaging. Other characterisation techniques conducted include energy-dispersive X-ray spectroscopy (EDS), Wavelength Dispersive Spectrometers (WDS), X-ray diffraction (XRD), micro-hardness, and dry-sliding wear testing.

1.2 Aims and objectives

Satelliting is a process which can be used to produce powders, which consist of major particles (usually metals) covered by a layer of minor particles (often ceramics) with a sufficient bond strength between the major and minor particles, due to the effect of an added binder. This project aims to determine if the satellited powder can be successfully cold sprayed to deposit composite coatings and to determine if the satellited powder can maintain the properties of the two phases, of satellited particles (ductile and hard) in the deposited coating, and ultimately yield superior functional mechanical properties. It also aim to investigate the behaviour of the satellited materials within laser cladding processes.

In this work, a composite powder prepared by satelliting process will be used as a feedstock for cold spray and laser cladding, along with a blended feedstock for comparison purposes. This is to examine the potential effects of the satelliting process on overcoming challenges of cermet cold spray and laser deposited coatings, including the uniformity of reinforcement's distribution in the coating, weakness in the coating/substrate interface area, pore density, and critically the rebounding of hard particles. A Post-processing heat treatment process will be performed on some cold sprayed coatings to study its effect on coating characteristics and response toward wear.

In order to achieve these aims, the project has been divided into the following objectives.

1. **Satelliting and blending of Al-TiC powders:** satellited materials are prepared to be used as composite feedstocks for cold spray and laser cladding. This includes characterisation of the starting and processed powders and optimisation of satelliting parameters to produce composite Al-TiC powder, which suits the related process. In addition, pure aluminium and blended feedstocks are prepared for the same purpose in order to compare the feedstocks and investigate the effect of the preparation processes on powder morphologies and the deposited coatings.
2. **Characterisation of cold sprayed Al and Al-TiC composite coatings:** Cold-sprayed coatings produced using Al, blended Al-TiC, and satellited Al-TiC feedstocks are investigated, to explore the effect of the feedstock type on coating characteristics. A comprehensive study of coating characteristics, including coating density, thickness, and TiC fraction in the coating section is reported. The deposition mechanism of each feedstock is then established and clarified, to explain the impact of the new preparing method on cold spray deposition.
3. **Cold spray of Al6061 and Al6061-TiC composite coatings:** The satellited feedstock is then used as a trial to improve the deposition of high-strength Al alloy (6061). Coating characteristics, including coating density, thickness, and TiC fraction in the coating section are studied. This will include a comparative study of the three feedstock coatings (Al6061, blended Al6061-TiC, and Al6061-TiC).

4. **Post-treatment of the cold-sprayed Al6061-TiC composite coatings:** Al6061-TiC satellited coating is subjected to an annealing heat treatment at 345°C for two hours. This treatment is applied to improve the density and cohesion of the sprayed coatings. The annealed coatings are then analysed to determine the effect of the thermal treatment on coating structure and wear behaviour.
5. **Wear performance of cold-sprayed Al6061-TiC composite coatings:** The microhardness and wear behaviour of the cold-sprayed Al and Al6061-TiC composite coatings are systematically studied. The hardness results and wear data are studied and correlated with relevant coating microstructure. Thus, the improvements arising from the composite structure and annealing effect are clarified.
6. **Laser deposition of blended and satellited Al-TiC powders:** The interaction mechanisms of both feedstocks (blended and satellited) with the laser beam in laser cladding are investigated. The behaviour of Al-TiC satellited feedstock was investigated along with a blended feedstock. The aim of this is to understand the effect of satelliting on the laser-powder interaction process. The effects of the interaction mechanisms of both powder types on clad characteristics (microstructure, clad area, dilution, and formability), are explained under an optimised set of processing parameters. Processing maps for each type of material, are established to yield a parameter window for this material system.
7. **Microhardness and wear performance of Al-TiC clads:** In order to understand the effect of the different feedstock behaviours within laser deposition cladding on strengthening the matrix material, the average hardness

values of the matrix are measured for the different clads. Dry sliding-reciprocated wear testing was performed to study the effect of each feedstock on clad wear behaviour. The worn surfaces are characterised, and the wear behaviour of each sample is correlated with the relevant clad microstructure.

1.3 Thesis overview

This thesis will comprise of seven chapters:

1. ***Chapter 1*** provides a brief introduction to research aims and objectives to meet to achieve these aims. This includes a brief statement about the importance of MMCs and the deposition processes that can be used to create MMC coatings, e.g. cold spray and laser cladding. This chapter includes a summary of the thesis chapters and contents.
2. ***Chapter 2*** is a literature review which identifies the research gaps which are tackled in this thesis. The main sections in this chapter include an overview of metal matrix composites, the preparation methods of composite feedstocks, the fundamentals and key studies of cold spray process and finally, the fundamentals and key studies of laser cladding process.
3. ***Chapter 3*** presents a description of the materials, equipment, and methodology used to carry out the research including the mechanical tests that were used, the metallographic techniques, sample preparation and testing.
4. ***Chapter 4*** investigates the use of the satelliting process for preparing composite feedstocks for cold spray processes. Preliminary satelliting processes were performed with different Al powders and different amounts of binder to produce a range of satellited powders. The prepared satellited powder was then used to evaluate its ability to be cold-sprayed. Optimisation processes were performed on the satelliting processes for obtaining a satellited powder suites cold spray. Thus,

the main aim is to produce satellited particles that have the ability to carry the fine ceramic particles with good flow characteristics during cold spray. For comparison and evaluation purposes, three types of powders were used within cold spray; pure Al, blended Al/TiC and satellited Al/TiC.

5. ***Chapter 5***, in this chapter, cold spraying is used to create Al6061 and Al6061-TiC coatings on an A6082 aluminium substrate. The satelliting technique was used to prepare the composite feedstock to eliminate the rebounding of the fine ceramic fraction in the CS process. Annealing heat treatment was applied to the composite CS coatings to improve porosity and cohesive properties of the coating structure. Additionally, a detailed hardness study is performed to evaluate hardness prior to and after heat treatment, so the effect of heat treatment on the matrix as well as overall composite properties can be understood. Dry-sliding wear testing is performed to evaluate the contribution of the reinforcement material, as well as the effect of heat treatment on practical mechanical properties.
6. ***Chapter 6***, in this chapter, two Al-20TiC feedstocks were prepared by different preparing methods; simple blending and satelliting for LC processes. Several characteristics like clad area, dilution and porosity were calculated. The effects of the process parameters on these characteristics were explained and discussed by adopting two combined process parameters: effective energy and powder deposition density. The best operation parameters that lead to the deposition of quality clad for each feedstock were identified. Further, the microhardness and wear behaviour of two sets of samples (one set from each feedstock) were investigated along with a blended feedstock.
7. ***Chapter 7*** presents a summary of the main contributions of this research, along with an outline of possible strategies for future work.

2 Literature Review

2.1 Introduction

This chapter presents an overview of the literature in composite materials and coatings, with a particular focus on aluminium-ceramic coatings. The fundamentals of cold spray and laser cladding are discussed. A review of composite-powder preparation methods is also presented. Section 2.2 presents a general overview of metal matrix composites, with emphasis on the aluminium matrix composites. Section 2.3 is concerned with the preparation methods of composite powders, including simple mixing, mechanical alloying, metal-coated powders, and spray drying of slurries. Section 2.4 presents a brief description of the cold spray deposition technique, including bonding theories and the effect of ceramic particles on CS coating properties. Section 2.5 presents an overview of the technique of laser cladding and the materials systems, particularly aluminium-ceramic composites. Finally, section 2.6 summarises the gaps in the literature which will be tackled in this thesis.

2.2 Metal Matrix Composites

A composite material is a combination of at least two separate phases, which have been bonded together, thus being considered as a material with autonomous properties [5]. Typically, there are two phases; a reinforcing phase dispersed appropriately in a matrix phase. The common shapes of the reinforcement phase are the fibrous, particulate and whisker, while the matrix phase is usually a metal or plastic matrix [5]. The structure of composite materials can be distinguished from layered or laminated components, or from microscopic structures of multi-material. Thus, the components of the composite materials remain physically independent during the production stages of the composite material. This difference makes composite materials differ from traditional alloys (i.e. eutectics or precipitation alloys) [5]. Wherein the different phases in the alloys are all formed during solidification or heat-treatment after a homogeneous melt.

The metal matrix composite (MMC) is a composite in which the matrix consists of a metal reinforced with a fraction (at least a few percent by volume) of another material [6]. Metal matrix composites can offer desirable physical and mechanical properties that make MMCs a very attractive candidate material for numerous applications [7]. For instance, MMCs have been used in numerous applications that required advanced wear resistance and stiffness like aerospace (compressor rotor, fan blades, sidewalls and structure, etc.) [8], electronics [9] and other important industries. Therefore, considerable progress has been achieved in the development of light MMCs recently [10]. Thus, much research has considered the use of metal–matrix composites (MMCs) to meet most demands of several industries [11]. The main driver for these composites has come from the wide applications in several

industries including aerospace e.g. airframes and spacecraft structures, automotive and electronic industries [12]. Ceramic-reinforced composites have also experienced an important growth over the last few decades, given their good ductility, toughness and thermal conductivity. In addition, the ceramic characteristics provide high mechanical properties like high hardness and young's modulus [13].

With regards to the matrix, nearly all the important metallic systems have been investigated for use in MMCs, including Fe, Al, Be, Ti, Mg, Ni, Co, and Ag. By far aluminium and its alloys have the largest share of usage amongst the matrix materials in MMCs [14]. In the area of reinforcements, ceramics are the most used materials in MMCs because they offer a desired combination of stiffness, strength, and low density [14]. Ceramic-reinforced MMCs are desirable given their combination of metallic properties; such as high ductility, toughness, and thermal conductivity alongside ceramic characteristics of high hardness, high strength and Young's modulus [13]. The common types of ceramic used as reinforcement materials are Al_2O_3, SiC, TiC, B_4C and TiB_2. Also, some metallic materials have been used as reinforcements such as tungsten, molybdenum, tantalum and their alloys [15].

According to the morphology of the reinforcement material, MMCs can be divided into three major classes of reinforcement; continuous fibre, whisker or chopped fibre and particulate reinforcement. Normally, the selection of the reinforcement morphology is directed by the required property-cost combination. Figure 2-1 shows schematics of composite structures with different types of reinforcement.

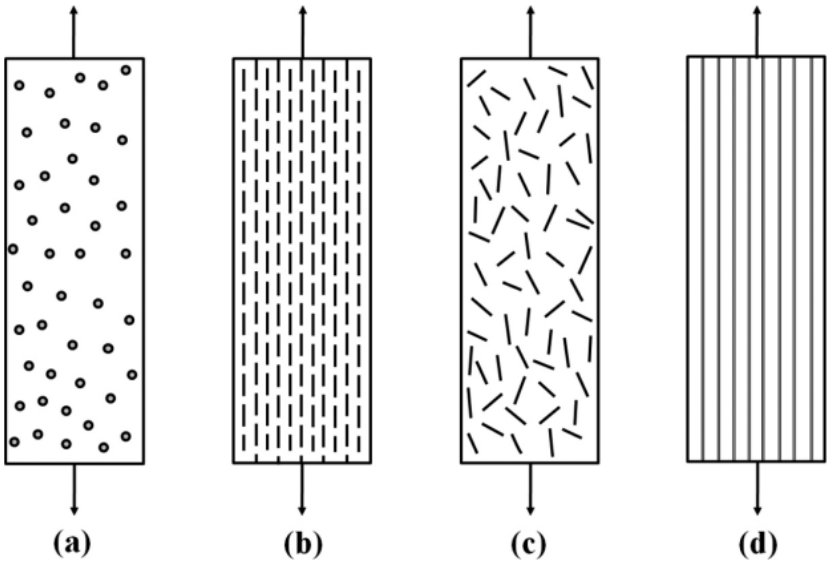


Figure 2-1: Examples of composite structures with (a) particulate, (b) discontinuous fibres, (c) discontinuous fibres, and (d) continuous fibres [16].

The particulate reinforcements, seen in Figure 2-1 (a), are usually cheaper than other types and they produce relatively moderate mechanical properties, however, isotropic enhancement in properties can be achieved [7]. Particulate reinforcements have different geometries like spherical, platelet, cubic, angular with dimensions that are nearly equal in every direction [16]. The strengthening mechanism in the particulate reinforcements composites is indirect strengthening, as dislocation punching will occur in the matrix material [17]. Whisker-reinforced materials (Figure 2-1, b) can be manufactured with a lower cost, in addition to providing significantly improved properties in the plane or direction of their orientation. Commonly, MMCs reinforced by continuous fibres (Figure 2-1 (d)) offer high mechanical properties in the direction of the fibre orientation, but the production cost is relatively high. In fibre reinforced composites, the applied load is carried directly by the reinforcement phase (direct strengthening). The applied load can be transferred from the weaker matrix through the matrix/reinforcement interface [18].

2.2.1 Advantages of MMCs

The biggest advantage of composite materials is that they have light weight as well as high yield strength/stiffness (see Figure 2-2). By choosing an appropriate combination of matrix and reinforcement material, a composite can be made which meets all the requirements of a particular application [19].

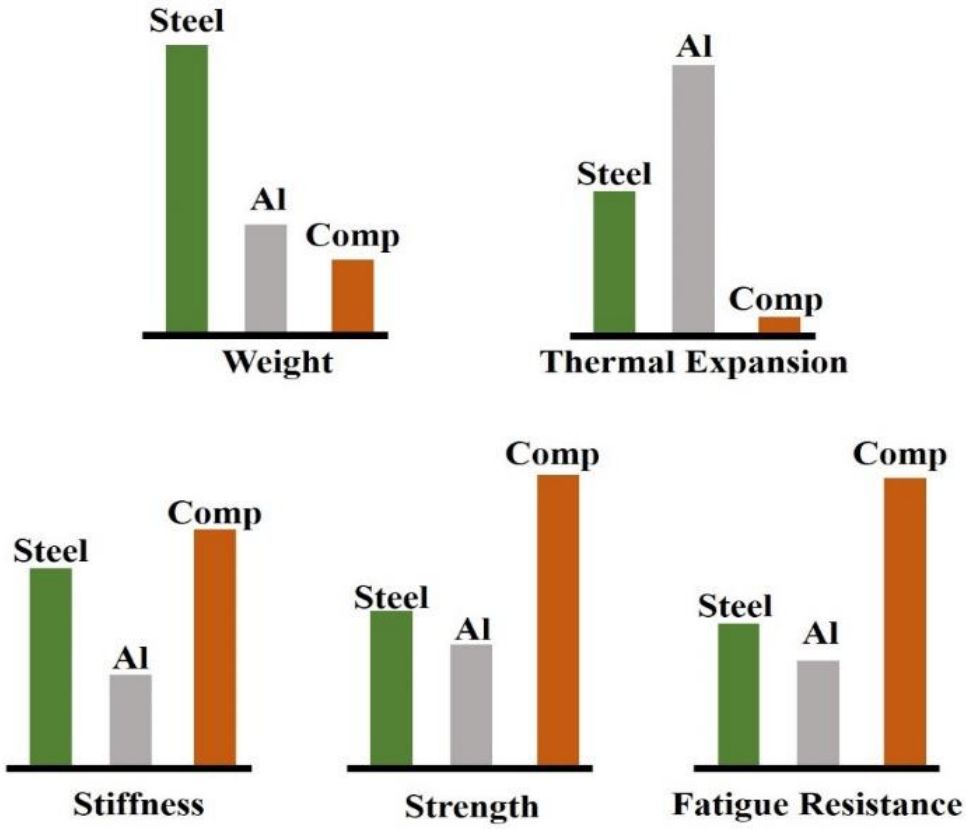


Figure 2-2: Physical and mechanical properties of composites compared with the two most commonly used alloys, i.e., steel and aluminium[19].

Composites also provide design flexibility due to many of them being moulded into complex shapes. The most applicable properties of composite materials include, [20]:

- High stiffness and high strength
- High Young's modulus
- High fatigue strength, especially at elevated temperatures
- High corrosion resistance
- Low density
- High thermal and electrical conductivity
- High wear resistance

Therefore, MMCs are particularly attractive as a replacement for conventional materials in many engineering applications. MMCs are metallic alloys (aluminium, titanium, copper, magnesium, etc.) with reinforcement materials (aluminium oxide, silicon carbide, boron carbide, graphite, etc.) in forms of fibres, whiskers and particles. Therefore MMCs are widely used in various fields of application such as the automotive, aerospace, aircraft and sports, as well as other advanced industries [21].

2.2.2 Particulate reinforced MMCs

Particulate reinforced metal matrix composites are useful for important applications [22] like advanced aerospace (bolts, pistons, valves, high-strength and heat-resistant material) [23] and automotive (engine pistons, engine blocks, and connecting rods) [24]. The attraction of particle reinforced MMCs is due to their cost-effectiveness, isotropic properties and ability to be processed using similar technology used for monolithic materials [6]. Finer reinforcements have superior strengthening effect compared to the coarse reinforcements [25]. These composites have a high similarity to isotropic properties when compared to long fibre-reinforced composites [26].

Both the strength and ductility of particulate MMCs increase when small-size particle reinforcements are used [27]. Another study found that strain hardening in MMCs increases with decreasing particle sizes and increasing volume fraction of the reinforcement phase [28]. Sova et al. stated that fine ceramic particles have a strong effect on surface activation of soft metals in cold spray processes [29] by removing oxide/contamination layers, producing micro-asperities on the impact surfaces, and interlocking deposit. This leads to an increase in the deposition efficiency of the fine-ceramic feedstock compared to pure metal feedstocks. It is known that coarse ceramic powder hinders the cold sprayed coating growth and produces surface erosion, which makes DE decrease accordingly [29]. Moreover, the uniformity of the reinforcement distribution in the matrix materials is one of the main challenges in the processing of particulate MMCs [30]. This is because the distribution of the reinforcing particles has a significant impact on the quality and mechanical properties of the produced MMC [31].

Three approaches can be used to improve the behaviours and properties of the MMCs. The first is the use of fine ceramic particles within the reinforcement phase. The second is the increase in the fraction of the reinforcement phase. Thirdly the homogeneous distribution of the reinforcing particles in the matrix. An appropriate selection of the preparing powder method with optimised process parameters is important to the factors of achieving the best results in the produced MMC components or coatings.

2.2.3 Aluminium-based matrix composites (AMCs):

Aluminium-based matrix composites have been classified as an applicable choice for corrosive and wear environment applications. The improved wear resistance in

AMCs can be owing to three main mechanisms; first, the high mechanical properties of the reinforcement particles [32]. The second is the matrix strengthening owing to the presence of the particles within the matrix. The third mechanism is the improved toughness due to the ageing process in some Al alloys. Specifically, aluminium and its alloys with magnesium, silicon, copper, manganese and zinc are the most common matrix materials after iron for the fabrication of MMCs [33]. This is due to the combination of the mechanical properties of the ceramics and Al alloys, which present good ductility, without losing the corrosion resistance of Al alloys [34, 35].

Aluminium-matrix composites (AMCs) are an example of such a material type, which can possess both corrosion resistance and hard-wearing properties [32, 34, 35]. AMCs that have high specific stiffness and high strength are used in long-term applications in which lightweight components are highly recommended [36]. These applications include high-speed rotating machinery, shafts, robots, brake parts, and engine structure. Additionally, aluminium is able to alloy with a large number of elements, including magnesium, silicon, copper, manganese and zinc, hence providing specific, tailorable properties to the resultant composite [33].

Ceramic-metal composite coatings are widely used to enhance the surface properties and performance of engineering components in the abrasive and corrosive environments [37, 38]. There remains an industrial need to produce metal-ceramic coatings for aluminium components [11], where the high production cost of these composites is a significant barrier to their exploitation. Thus, deposition of ceramic-metal composite coatings has been widely used to enhance engineering component surfaces properties in order to develop their behaviour

against harsh conditions like working in abrasive and corrosive environments [38],[23]. This is due to the possibility of maintaining the combination of the ductility of the metal matrix and the high hardness of the ceramic [39].

In recent years, particulate reinforced metal matrix composites have attracted the attention of many researchers, engineers and designers as promising advanced engineering and structural materials for automobile and advanced aerospace applications. Especially, 6xxx series particulate reinforced aluminium metal matrix composites, (AMCs) [4-6] have been studied extensively because of their relatively low cost, design flexibility, isotropic properties and ease of handling. Also, the processing problems and commercial difficulties associated with continuously reinforced AMCs are contributory to the recent interest in the particulate composites. In AMCs, aluminium /aluminium alloy is used as the matrix phase, and the reinforcing phase is usually non-metallic and ceramic such as Silicon carbide, Titanium carbide, tungsten, boron, aluminium oxide, fly ash, Zirconium, and titanium boride. The most commonly used ceramics are SiC, Al_2O_3, TiB_2, boron and graphite. By varying the composition, size, shape and weight percentages of the reinforcement, the properties of AMCs can be tailored.

2.2.4 TiC-reinforced MMCs

Transition metal carbides (TMCs), e.g. TiC, usually present a combination of the high hardness of covalent-bond solids, the good thermal and electric conductivity of transition metals, and the high melting point of the ionic crystals [40]. TiC has been selected as a useful reinforcement material among many ceramic types owing to its excellent properties like high melting temperature (3067 ^{o}C), high hardness (28 GPa), low density (4.93 g/cm3), and thermodynamic stability [41, 42]. TiC thus

has attracted a growing interest owing to the good mechanical and thermal properties, and its good wettability with aluminium [43]. It became a well-known choice as a reinforcing phase in MMCs that used for many important applications where wear and corrosion are the main sources of failure, including abrasive industries, cutting tools [11], automotive and aerospace applications [44, 45].

In MMCs, TiC is one of the most useful materials for improving the mechanical properties (hardness, stiffness, tensile) [11, 46], enhancing the thermal and electrical conductivity [47] and achieving low-density composites [47]. Karantzalis et al. have observed that the elastic modulus of Al/TiC composites increases with increasing the volume fraction of the added reinforcement [48]. They also stated that the increase in the elastic modulus in the AL/TiC composites is greater than for commercial AI-SiC and Al-Al_2O_3 powder or liquid-route manufactured composite. This is attributed to effective load transfer in the Al/TiC system because of the strong interfacial bonding between Al and TiC particle surfaces due to the nucleation of solid Al on the TiC particle surfaces [48]. Also the use of TiC as a reinforcing phase enhances the stability of composites that operate at elevated working temperature(s) [49, 50].

2.2.5 Strengthening mechanism in MMC

Two categories of strengthening mechanisms have been recognised in MMCs, direct strengthening and indirect strengthening [51]. Direct strengthening takes place when the applied load is carried directly by the reinforcement phase; the load can be transferred from the weaker matrix through the matrix/reinforcement interface [18]. Thus, as the direct strengthening increases with increasing the reinforcement surface area, the fibre reinforcements have better strengthening

action due to the high surface area compared to other reinforcement types. Indirect strengthening occurs when reinforcement particles hinder dislocation motion in the matrix material [52]. Also, the indirect strengthening can be produced as a result of the change in microstructure and properties of the matrix after the addition of reinforcement [51]. When the thermal stress is greater than the yield stress of the matrix, dislocation punching will occur in the matrix producing 'indirect strengthening' of the matrix material [17]. The thermal stresses are usually induced due to the mismatch between the matrix and reinforcement.

Direct strengthening of the composites is controlled by the shape and the volume fraction of the reinforcement particles [53]. Dislocation hardening (indirect strengthening) is also dependent on the particle size as well as volume fraction [54]. Kim et al. [28] have carried out finite element analyses to study the effects of particle size on the mechanical properties in particulate metal matrix composites. They pointed out that strength and ductility of particulate MMCs increases with decreasing particle size of the reinforcing particles. Consequently, the use of fine particles as reinforcement can improve the strengthening effect in the composites as well as increasing the reinforcement fraction.

2.2.6 How MMCs are made

Several techniques are used for manufacturing metal matrix composites; the main aim of these techniques is to introduce a reinforcement phase in the matrix material (metal). Mainly, these techniques involve processing in the liquid state and solid state. Deposition techniques are commonly used to produce MMC protection coatings on base materials [55], while in situ processes are used to form reinforcement phases which form as a result of reactions at high temperature in

melting or sintering processes [56]. Fabrication processes of MMCs can be briefly listed as follows [57]:

1. ***Liquid State Processes***: Casting or molten penetration includes penetration of liquid metal in a bundle of fibres, or passage of fibre bundles through a molten metal bath. For particulate MMCs, the powder of the reinforcement material is added to the molten metal with stirring to achieve a good dispersion of the reinforcement. The main limitation of the liquid processes is the difficulties with fibre reinforcement wetting by the molten matrix material. Moreover, due to the high temperatures of the molten metals, the fibre and the molten metal can react, which can lower fibre properties. This led to only a few MMCs (relatively) have been produced by simple liquid processes.
2. ***Solid-State Processes***: This approach can be used for producing MMC by creating sufficient bonding between the solid phases of the matrix and the reinforcements. The required adhesion can occur by two means. The first is the diffusion bonding when an inter-diffusion at an elevated temperature occurs at metal surfaces which are in contact. This leads to the joining of contact surfaces. Deformation processing is also utilized to produce metal/metal composites; the two metallic phases co-deform producing minor phases that elongate and become a fibrous reinforcement phase in nature in the matrix.
3. ***Powder metallurgy processes***: Cold pressing and sintering, or hot pressing are used to produce metal matrix composites. These processes are suitable for fabricating particulate, fibre, and whisker reinforced MMCs. The solid-state processes allow to control the direction of the fibre layers, orientated properties then can be obtained. However, Solid State Processes have some disadvantages such as

the long processing time, high sintering temperature/pressure, and product size limitation.

4. ***Deposition Techniques***: Several deposition techniques are used for MMC fabrication including spray deposition, chemical vapour deposition (CVD), laser deposition, immersion plating, electroplating, spray deposition, chemical vapour deposition (CVD), and physical vapour deposition (PVD). Deposition processes allow the degree of interfacial bonding to be controlled easily, as well as layer thickness while the main disadvantage of the deposition processes is high time consumption.
5. ***In Situ Processes***: In this approach, the reinforcement phase forms in situ, the common reinforcements are TiB_2, TiC, SiC, etc. within an Al, Ni, Fe or an intermetallic matrix. Thus, the issues regarding the combining of separate components are avoided in in-situ processes.

Several techniques have been adopted for creating MMCs such as stir casting, squeeze casting, spray deposition, liquid infiltration, and powder metallurgy [49]. However, most of the Al-based ex-situ composites have many drawbacks like agglomeration, poor wetting and heterogeneity in microstructure [58, 59]. Synthesis of MMCs coating by the addition of ceramic powders to the molten metal usually results in poor interfacial bonding [60]. A major technical problem occurs with the formation of aluminium carbide (Al_4C_3) phase at the interface during fabrication of aluminium (Al) based silicon carbide (SiC) reinforced composite as SiC is thermodynamically unstable in Al [61].

Also, the important challenge for metal matrix composite process through liquid metallurgy route is avoiding the segregation of reinforcement and obtaining a

uniform distribution of the particles [48, 61, 62]. Thus, most of MMCs have been produced using solid state powder metallurgy techniques such as powder blending and consolidation, diffusion bonding and vapour deposition [63].

2.3 Cold Spray

Cold spray (CS) is a widely used process over the last decades, the amount of research papers, as the patents and applications on this process have grown exponentially [64]. Cold spray has received this attention due to its many advantages among other deposition technologies [65]. The main advantage of cold spray is its ability to deposit thick coatings in the solid-state without the use of heat [66]. This is because cold spray relies on plastic deformation below the melting point in the impacting region [67]. This increases the range of materials eligible for cold spraying as many materials have thermal sensitivity, e.g. phase transformation, oxidation, and dilution at the elevated temperatures [68]. Another advantage of cold spray is the ability to deposit metal coatings like titanium on aluminium substrates, whereas thermal spray (for example) can form a brittle Al-Ti phase at the coating-substrate interface because of the high temperature of thermal spray [69]. This makes cold spray a useful technology for a wide range of applications [70], including biomedical implants like Ti-hydroxyapatite coatings [71]. Also, cold spray is widely used for fabricating different automotive parts such as cylinder walls, tubes and flanges [72]. Further, it has been successfully used for deposition high-performance alloys, i.e. Inconel 718, which has been used in harsh working conditions like the combustors, nuclear reactor, gas turbine blades, and aerospace industry sector [73].

2.3.1 Cold Spray Process

Cold spray operates using low or no heating to deposit materials onto substrates. It is useful for the deposition of a range of materials, even those with sensitivity to temperatures like nano-crystalline and amorphous materials [74]. In this process, each powder particle, to be successfully deposited, should reach a velocity above its critical velocity, which is the minimum velocity in which the deposition in cold spray occurs. Common spraying velocities are between 300 and 1200 m/s [75]. Once these particles impact the substrate surface, they undergo plastic deformation, which causes localized heating and welding at the interfacial surface [76]. High particle velocities are achieved by accelerating particles through a supersonic gas jet [77].

The nozzle is used to accelerate the sprayed particles in CS processes; the nozzle type is chosen depending on the exit velocity of a particular application [78]. A De-Laval nozzle type is typically used in CS processes which is a tube that is pinched in the middle, making an hourglass-shape. A solid-state plastic deformation process makes particles adhere to the substrate surface [79]. Figure 2-3 clarifies the main parts of a typical CS system.

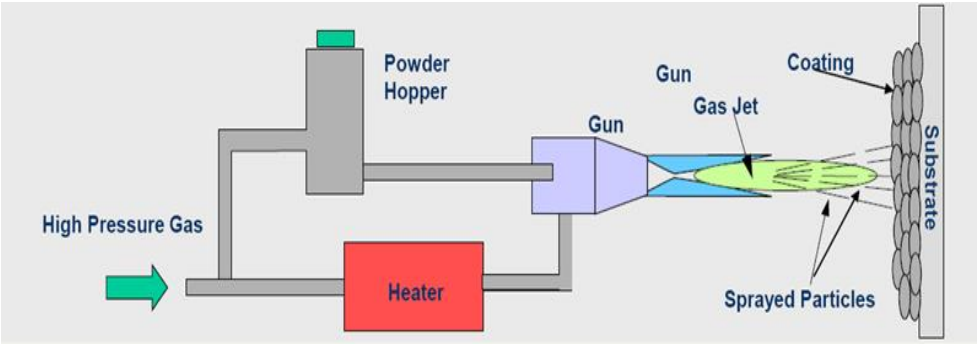


Figure 2-3: Illustration of cold spray system [80].

CS relies upon repeated high plastic deformation of incident particles to form a coating. CS coatings can be produced with low levels of porosity and oxidation [81]. Fine reinforcements have a significant effect on enhancing composite properties [82]. However, low ductility materials (e. g. ceramics) are more difficult to deposit by CS [83], since they can rebound when impacting substrate surfaces, resulting in a reduced deposition rate. Thus, hard materials often need to be combined with more ductile materials for successful cold spraying [84].

However, cold spray has a limitation of dependence on the high plastic deformation that makes cold spray inappropriate for depositing non-plastic materials like carbides, oxides, nitrides and borides due to their low deformability. Hard materials, to be deposited within cold spray, need to combine with ductile materials in order to get sufficient deformation during spraying [85]. Otherwise, most of the hard particles rebound once they impact the substrate surface, and this leads to a decrease in their fraction in the deposited coating.

On the other hand, hard particles, e.g. ceramics, can produce micro-asperities which facilitate the bonding of the incoming particles through increasing the local deformation [29]. Also, the creation of micro-asperities increases the contact area between the coating and the substrate; improving the adhesion. Shkodkin et al. have found that the deposition of the metal-ceramic mixture is higher than the metal feedstock at certain conditions of cold spray due to the roughening action of the ceramic particles [86]. However, the deposition efficiency of the mixture reduced with the further increase of ceramic content, because of the high rebound of ceramic particles.

Different mixing methods have been used in previous studies to prepare composite feedstocks for cold spray; the easiest of which is by blending different powders like ceramics as a reinforcement and ductile metal (or alloy) powder as a matrix [87]. However, this is not effective method due to the inability to deposit coatings containing high volume fraction of ceramic (more than 40%), because a large portion of the hard phase (about 70%) could rebound out the substrate [83]. It has been found that cold sprayed coating compositions are different from that of simply mixed feedstocks because the deposition efficiencies of the constituent powders are not the same at the same processing parameters [88]. In other words, this will lead to the production of coatings with inhomogeneous composition.

The mechanically alloyed (pre-alloyed) composite powders are often used in cold spray, although this process has some drawbacks like high-energy consumption and the heterogeneity of the produced powder [89]. Typically, it needs further processing (e.g. sintering when high volume fracture of ceramic is needed). In addition, the alloyed particles usually have a rough surface that may affect their flowability during spraying [83]. Also, the alloyed powders can undergo high strain hardening and deformed morphology, which impede the deformability and flowability of the particles during cold spray [90]. Furthermore, pre-coated hard particles like diamond particles were recently used as a starting material in cold spray by coating them with a ductile metal layer [91]. This study suggested that the thin ductile clad of the metal experiences high plastic deformation when impacting the substrate surface or the built coating, while the diamond particles may impact with other diamond particles inserted in the coating.

Thus, there is a great challenge regarding the utilisation of ceramic particles in ceramic-metal coating deposition within cold spray processes. This challenge is to deposit composite coating with an acceptable fraction of ceramic embedded to the coating. Increasing the number of ceramic particles in the coating would improve the quality and deposition of the coating due to the peening action, roughening of the substrate surface, and creation of micro-asperities. Moreover, the available feedstock preparing methods of the composite feedstocks have significant drawbacks regarding the cold spray requirements processes. These drawbacks include high processing cost, work hardening of the powder and heterogeneity of the reinforcement phase.

2.3.2 Gas dynamics

A powder particle in the CS process, to be successfully deposited, should reach a velocity above its critical velocity [92]. The following formula (Equ 2- 1) can be used to estimate the critical velocity of a particle within a specific set of process conditions of cold spray [93]:

$$v_{cri} = \sqrt{\frac{4\sigma_{TS}\, F_1 \left(1 - \frac{T_i - T_R}{T_m - T_R}\right)}{\rho_p} + F_2 C_p (T_m - T_i)} \qquad \text{Equ 2- 1}$$

Where: σ_{TS} is particle tensile strength, T_i is the impact temperature that depends on the thermomechanical properties of the sprayed particle). C_p and ρ_p are particle specific heat capacity and density, T_R is the reference temperature (273 K), and F1 and F2 are empirical constants. However, the suggested formula (Equ 2- 1) has ignored the effect of the particle size on the critical velocity. Schmidt et al. have stated that the increase in the critical velocity of the smaller particles compared to

the larger particles from the same material is due to several reasons []. The high temperature gradients within a small particle can hinder the occurrence of shear instabilities as a result of the high cooling rates. Also, the strain-rate is higher in smaller particles and hence severe strain-hardening can occur. In addition the shear strength in the jetting region will be higher for smaller dimensions. Moreover, surface contaminations such as oxide shells have higher fractions in the smaller particles due to the smaller dimensions compared to the larger ones, then they will have a significant influence on bonding. All these effects can lead to an increased critical velocity for finer particles [94].

The nozzle creates thrust through the expansion of the exhaust stream to ambient pressure [95]. According to the continuity and Euler's equation of an adiabatic, isentropic, inviscid flow, a relation between the change in the area of flow and the flow velocity (called Area-Mach relation) can be driven as in Equ 2- 2 [96]. Accordingly, when the flow reaches the shock state at the nozzle throat, M=1, dA/A=0, and higher dA/A will lead to a higher Mach i.e. high velocity.

$$\frac{dA}{A} = (M^2 - 1)\frac{dV}{V} \qquad \text{Equ 2- 2}$$

The gas flow and particle acceleration are divided into three stages: the mixing and flow of gas and powder mixture, the particle movement and acceleration in the divergent part of the nozzle, and the particle movement and acceleration in the free jet space [97]. Several factors affect the particle velocity like the expansion ratio and divergent section length of the nozzle; the morphology, size, and density of the particles. The sonic conditions for flow gas can only be achieved for appropriate stagnation gas pressures. After achieving the sonic condition, the increase of the pressure at the nozzle inlet does not result in a sensible increase in the gas velocity.

Dykhuizen et al. [98] have expressed a formula (Equ 2- 3) for determining the gas velocity (v_g) at the supersonic conditions:

$$v_g = M\sqrt{\frac{\gamma\, R\, T}{M_w}} \qquad \text{Equ 2- 3}$$

Where M is local Mach number, γ is the ratio of specific heats (C_p/C_v), R is the gas constant (kJ/kg°K), T is gas temperature, and Mw is the gas molecular weight. However, there is a clear difference between gas velocity and particle velocity; this is because of the variation of the drag force [97]. Eskin et al. assumed that particles gain radial velocity components owing to collisions with other particles of various sizes, this redial motion causes a particle-wall collision that affects particle velocity in the axial direction [99]. Thus, the influence of these factors has been summarized by Alkhimov et al in an empirical equation (Equ 2- 4) [100]:

$$V_p = \frac{V_g}{1 + 0.85\sqrt{d_p/x}\sqrt{\rho_s V_g^2/p_o}} \qquad \text{Equ 2- 4}$$

Where, V_p is the particle velocity, V_g is the gas velocity (Equ 2- 3), d_p is the particle diameter, x is the axial position, p_o is the nitrogen supply pressure measured at the entrance of the nozzle, and ρ_s is the particle density. In addition, Assadi et al. [101] established a formula (Equ 2- 5) for estimating the achievable particle velocity for a given set of process parameters and particle characteristics. Thus, by using this equation, the particle velocity can be directly estimated, taking in consideration both particle characteristics and process parameters in a combined formula, as follows:

$$v_p \approx \left[\frac{c_2}{\sqrt{R\,T_o}} + \sqrt{\frac{\rho_p d_p}{C_d L_d p_0}}\right]^{-1} \qquad \text{Equ 2- 5}$$

Where;

v_p: In-flight particle velocity (m/s).

R: Gas constant (J/kg.K^o).

ρ_p: Particle material density.

C_d: Drag coefficient = 0.47.

P_o: Gas stagnation pressure (bar).

C_2: Fitting parameter (0.45 for Helium).

T_o: Gas stagnation temperature= 290 ^{o}K.

D_p: Particle diameter (m).

L_d: Length of the diverging part of the nozzle (m).

Helium (He) and nitrogen (N) are usually used as carrier gases which accelerate powder particles to supersonic velocities using converging-diverging nozzles. Also, it is recommended that cold spray is conducted with an inert gas to avoid oxidation during processing [76]. Helium is a comparatively costly gas, yet it has the capability to generate high velocities because of its high sonic speed [102]. According to the ideal gas law and consequently the velocity of the carrier gas (Equ 2- 3), helium is a better carrier gas than the high molecular weight, diatomic gases at the same temperature. Namely, the low molecular weight (and, hence, large R), monoatomic (and, hence, large γ and, in turn, high T*), is associated with a supersonic speed [102], hence for nitrogen: R=0.297 (kJ/kg ^{o}K), ρ=1.2506 (kg/m^3), while for helium; R=2.08 (kJ/kg ^{o}K), ρ=0.1785 (kg/m^3). Thus, helium can be used as a carrier gas to accelerate the sprayed materials in room temperature with relatively low gas pressure, i.e. limited conditions.

2.3.3 Bonding theories

Adiabatic shear instability (ASI) was proposed to be the main bonding mechanism in cold spray processes of metal powders [77, 103-105]. The ASI in CS processes occurs when a high plastic deformation takes place at the interface between the impact surfaces like particle-substrate, this leads to adiabatic heating that produces a softening in the contacted surfaces [106]. ASI occurs when the sprayed particles exceed their critical velocity, which is the minimum velocity in which the deposition in cold spray occurs [92].

The critical velocity depends on the size and properties of the sprayed particle and also on the substrate material [92]. Whereas the high plastic strain results in a softening at the interface due to the adiabatic heating, this causes a jetting of the contact surfaces and thus a bonding between the particle and substrate occurs [77]. These assumptions were established depending on numerical analysis of metal particle impact, while the deposition mechanism was not observed experimentally due to the short time of impact and the small particle size [107].

However, Hassani-Gangaraj et al. argued that the jetting that leads to a bonding creation in cold spray could occur in different ways and not only by the ASI [108]. They proposed that jetting in cold spray could occur due to an interaction of strong pressure waves with the expanding edge of the impact particle. They also showed that the jetting has been observed with and without the adiabatic softening with a slight difference in the lip size [108]. Hussain has suggested that two bonding mechanisms contribute to a strong bond in the cold spray deposits [109]. The proposed mechanisms are the metallurgical bonding at the substrate/coating and the bonding of the substrate material extrusion during particle impacts.

Xie et al. found that the peening effect of sprayed particles leads to the fragmentation of the cracked Al oxide layer, which is commonly covering the Al substrate, into nano-sized pieces [110]. This promotes the local deformation of substrate and particle surfaces. They also mentioned the contribution of the peening effect in enhancing the coating cohesion owing to the compaction of the nano-pores, which leads to metal-to-metal contact at the inter-splat interface [110]. Moreover, when the thickness of the oxide layer increases, the particle deformation and material jetting will be restrained [109]. Mechanical interlocking is the primary mechanism of bonding between the deposited splats promoted by the metallurgical bonds at the interface surfaces [69].

In summary, regardless of the mechanism of jet formation in cold spray, the jetting of the impacting surfaces is the leading factor of bonding, and it requires to sever local deformation to occur. Also, the metallurgical bonding needs clean surfaces and tight contact to achieve contact at the atomic level, which mostly requires to break the oxide layers. The peening action of the sprayed materials also has an important effect on the coating bonding and cohesion due to the compaction, oxide breaking, and pores coalescence. Therefore, the higher the local deformation in the impact surfaces, the higher the bonding strength; and the oxide-free surfaces are preferred to guarantee good contact for metallurgical bonding. Consequently, the use of modified feedstock that allows higher local deformation, increased peening effect, and good interfacial contact can effectively enhance the cold spray coating quality.

2.3.4 Effect of ceramic particles on the CS coating properties.

Particle-reinforced MMCs are important material category because of the combination in properties i.e. high strength and toughness of metals and the high hardness and strength of ceramics. This combination can offer favourable behaviour in harsh working environments such as corrosion resistance, wear resistance, and chemical stability that increase the service life of components [111].

Low ductility materials (e.g. ceramics) are more difficult to deposit since they can rebound when impacting substrate surfaces [112]. As the ceramic particles are not deformed due to the low plasticity, but they can interlock with the metallic materials [113]. Pure ceramic powders like TiO_2 with a particle size range of 3 to 50 µm; however, the deposition was restricted to the first layer resulting from the deformation of the substrate materials [114]. Fan et al. have used nano TiO_2 in cold spray but the coating thickness was only several microns per pass [115]. Thus, brittle materials often need to be combined with more ductile materials for successful cold spraying [112].

Two suggested mechanisms explained the role of ceramic particles in enhancing the deposition of aluminium in cold spraying [116]. Firstly, the creation of micro-asperities improves the mechanical bond between the Al particles. Secondly, breaking up of the oxide layer, which usually forms on some metal surfaces, prepares oxide-clean surfaces that facilitate the bonding process [117]. The use of fine ceramics has a significant impact on the deposited coating as the fine size leads to a reduction in the mean free path (the mean distance between the reinforcing particles) and thus an improvement in the mechanical properties [118]. Additionally, it is found that fine ceramic particles more effectively contribute to

the cohesion of cold sprayed coatings, while the loose coarse ceramic particles are more detrimental to coating cohesion due to rebounding and substrate erosion [117].

Accordingly, ceramic particles have many benefits within cold spray, including the formation of micro-asperities, breaking up of oxide layers, and a good peening effect. These can improve the bonding of the deposits and enhance the cohesion of the cold sprayed coatings due to the compaction and the interaction (interlocking) with the matrix materials. Therefore, the presence of ceramic particles can greatly improve material deposition and the quality of the cold spray coating, in addition to the improvement in mechanical behaviour as composite coatings.

2.3.5 Cold spray of Al and Al composites

Aluminium is a good candidate material for cold spraying owing to its low density, good formability, and high ductility [119]. The critical velocity of deposition of Al within CS is ranged between 680–700 m/s [69] which is achieved by most of CS systems. Thus, several studies have investigated the deposition of Al by cold spray on different types of substrates, from different sides of view. Tao et al. have deposited a pure Al coating on a magnesium alloy substrate (AZ91D) by CS [119]. Their results showed that there are grain interfaces and subgrains formed adjacent to the boundaries of particles indicating severe plastic deformation occurred in these regions. Al coatings showed improved corrosion resistance compared to the bulk Al [119]. In another study, pure Al powder was cold sprayed onto different types of substrate materials [120]. They observed that the initiation of Al deposition was poor for non-metallic substrates, as no metallurgical bond has occurred between the particle and substrate. While the metallic substrates that are harder than

Al particles facilitated deposition; even though the deposition on the Al alloy substrate was restricted because of the presence of the oxide layer [120].

Irissou et al [121] have deposited Al and Al-Al_2O_3 coatings via cold spray using different particle sizes of Al powder, and different concentrations of Al_2O_3 in the starting powder. They found that Al coatings that were conducted using the larger Al particles (81 µm in average) are harder than those were conducted with the smaller size Al powder (36 µm in average); they thought that the large particles caused high peening in the relevant coatings which increased the coating hardness. The same study stated that the addition of the ceramic to the Al feedstock improved material deposition by increasing the substrate roughness through creating more asperities [121].

Diab et al. have deposited pure aluminium powder on AZ31B extrusion flat and round coupons by using cold spray [122]. It is stated that the Al coating provided good corrosion protection for the substrate in an acidic environment. However, the strength of corrosion fatigue (the fatigue in a corrosive environment) of the coated sample was not improved; this is due to the lower fatigue strength of pure Al coating compared to AZ31B material [122]. Atomized Al powder was cold sprayed on AZ91E substrate, then a heat-treatment (400 °C for 20 h) was applied on the deposited coating [123]. This thermal treatment was used to enable diffusion that promotes metallurgical bonding produced by cold spray. In addition, two diffusion layers of Al_3Mg_2 and $Mg_{17}Al_{12}$ formed, offering a corrosion resistance which is similar to that of Al [123]. Further, Al powder was cold sprayed on a copper substrate using sonic and supersonic micro-nozzles [124]. This study demonstrated that the fine Al and Cu particles could be accelerated to their critical velocity of deposition by using the supersonic and sonic micro-nozzles.

Although Al coatings provide acceptable corrosion protection, they have limited wear resistance due to the ductility of al and its alloys. Namely, the addition of ceramic to the coating to form an aluminium matrix composite allows obtaining simultaneously good wear and corrosion resistance, while keeping low the density of the substrate-coating system. For instance, Lopez et al. have observed that the Al-50SiC composite coating has presented hardness and adhesion strength measurements higher than Al coating by 35% and 54%, respectively; while the wear volume loss in the Al-50SiC coating was 97% lower than Al coating [125]. Many advantages have been achieved by embedding hard particles, e.g. ceramic in the cold-sprayed coatings, such as strengthening of the coating by the construction of a composite structure, improving material deposition and enhancing coating cohesion by reducing the porosity [126].

However, non-plastic materials have some difficulties in deposition since they can rebound due to impact from the substrate. It is widely shown that wear resistance increases with an increase in the volume fraction of reinforcements [127]. Cold spray is a promising technique to deposit aluminium-ceramic coatings. However, some limitations are inherent to the technique due to the low temperature and the high velocity of the sprayed particles, which limits the contact time between Al and ceramic particles during the spraying process [128]. These characteristics may cause the breaking of the ceramic reinforcement, tending to form high porosity coatings, which increase with reinforcement percentage. These factors hinder, in most cases, the good mechanical properties of the coating in wear applications [125].

In summary, cold-sprayed pure aluminium coatings have been widely investigated and can be successfully deposited on different substrates. They provide good corrosion protection for the coated substrates. However the mechanical properties were not improved due to the low mechanical properties of pure Al. Thus, the addition of ceramic particles as a reinforcement is a useful method for improving the mechanical properties of the Al coatings and the deposition of matrix material.

2.3.6 Cold spray of 6061 alloy

Al 6061 alloy has exhibited high corrosion resistance and considerable formability among other aluminium alloys, as well as offering a greater strength to weight ratio [129]. It is broadly used in many automobile, aerospace and mineral processing components because of their ideal combination of low density and high electrical/thermal conductivity [130]. In addition, A6061 composites that are reinforced with ceramic particles have been effectively used because of their higher possessing properties such as high strength at high operation temperature, good fatigue and stiffness [11].

However, the high strength of 6061 alloy can restrict its deposition within cold spray processes because of its dependence on local deformation. Thus, limited studies have been reported on depositing 6061 alloy powder or its composites. Rokni et al. reported that 6061 alloys presented a lack of deformation within cold sprayed deposits even when using high-temperature processing (400 ^{o}C) owing to its relatively high strength. This has led to the production of a high-porosity coating [131, 132]. Gavras et al. have established microstructural mechanisms of the fatigue crack growth for cold-sprayed parts produced by using 6061 aluminium alloy powder [133]. They investigated the effects of the characteristic of materials and

post-spraying annealing heat treatment on the crack growth behaviour of the deposits. In another study, cold-sprayed 6061 alloy coating showed higher strength and lower elongation than the wrought and annealed alloys due to strain hardening associated with the cold spray process [134].

Consequently, there are limited studies regarding the deposition of Al 6061 via cold spray as the deposition of dense 6061 coatings using cold spray is a challenge at room temperature. Also, the effects of reinforcement particles on the deposition and quality of the cold sprayed Al 6061 coatings should be studied to present the opportunities of using cold spray for deposition quality composite Al 6061 based coatings.

2.3.7 TiC in cold spray

Al composites can yield wear resistance significantly larger than that of the aluminium alloy [135]. Thus, reinforcing the Al alloys with such reinforcements can effectively improve the wear behaviour of AMCs. Transition metal carbides (TMCs), e.g. TiC, generally present a combination of the high hardness of covalent-bond solids, the outstanding thermal and electric conductivity of transition metals, and the high melting point of the ionic crystals [40]. TiC is a useful reinforcement material among many ceramic types owing to its excellent properties like high melting temperature (3067 °C), high hardness (28 GPa), low density (4.93 g/cm^3), and thermodynamic stability [41, 42]. TiC thus has attracted a growing interest owing to the good mechanical and thermal properties, and its good wettability with aluminium [43]. And it became well-known choice as a reinforcing phase in MMCs that used for many important applications where wear and corrosion are the main sources of failure including abrasive industries, cutting tools [11], automotive and aerospace applications [44, 45].

With regards to MMCs, TiC is one of the distinguished candidates for many purposes such as improving the mechanical properties (hardness, stiffness, tensile) [11, 46] enhancing the thermal and electrical conductivity and achieving low-density composites [47]. Karantzalis et al. have observed that the elastic modulus of Al/TiC composites increases with increasing the volume fraction of the added reinforcement [48]. They also stated that the increase in the elastic modulus in the Al/TiC composites is greater than for commercial Al-SiC and Al-Al_2O_3 powder or liquid-route manufactured composite. This is attributed to effective load transfer in AL/TiC system because of the strong interfacial bonding between Al and TiC particle surfaces [48]. In addition, it is stated that the use of TiC as a reinforcing phase enhances the stability of composites that operate at elevated working temperature(s) [49, 50].

TiC has been widely used as a reinforcement phase for producing composite coatings using different deposition techniques like laser cladding [136-140], HVOF thermal spray [141-145], and plasma spraying [146-150]. Emamian et al. have found that the in-situ formation of TiC in the Fe–TiC composite coating which was deposited by laser cladding has resulted in excellent wear and high hardness for the coating [151]. In another study, increasing the content of TiC ceramic particles has led to a clear increase in the microhardness of the cladding layer, while the inhomogeneity of the TiC particles resulted in larger fluctuation of the microhardness measurements [152].

However. There is very limited research about the usage of TiC as reinforcement in cold spray coating. Munagala et al. have used spherical TiC powder and irregular Ti6Al4V powders to deposit cold sprayed Ti6Al4V and Ti6Al4V-TiC MMC

coatings on mild steel substrates [153]. They have studied the dry sliding wear behaviour, the Ti6Al4V-TiC coatings showed a lower wear rate compared to Ti6Al4V coatings. Although high gas pressure and working temperature 4 MPa and 800 °C were used, the composite coating has presented a porosity three times higher than the Ti6Al4V coating; this was because the fragmentation of TiC particles during cold spray [153]. They also found that TiC particles facilitate the formation of tribo-layers on the coating surface, which resist the localized deformation during the wear test and reduce the wear rate of the composite coating [153]. In another study [154], ball-milled nanostructured TiC-Ti powder was prepared and used within cold spray using 40 bar carrying gas at 800°C. Their results showed that the composite TiC-Ti cold sprayed coating exhibits improved wear characteristics than commonly used biomedical materials.

Accordingly, TiC is an important ceramic material that was used in different deposition processes for producing cermet coatings owing to the high mechanical properties and thermal stability. Increasing the amount of TiC in MMCs and improving the distribution can effectively enhance the quality and mechanical properties of the relevant composites. Also, there are very limited studies on using TiC as a reinforcing phase in cold spray processes for depositing particulate composite coatings. Hence the sprayed composite coatings had higher levels of porosity comparing with the non-composite coatings, even with using higher gas pressure and temperature.

2.3.8 Heat-Treatment of Cold Sprayed Coatings

The term ‘heat treatment’ refers to the thermal processes that are applied to change the metallurgical structure of components [155]. By modifying the metallurgical

structure, the mechanical and physical characteristics of the components are modified to meet specific application requirements [156]. Aluminium and its alloys have metallurgical features (i.e. precipitation hardening and recrystallization) that offer a range of opportunities for applying heat treatment processes in order to achieve required combinations of physical and mechanical characteristics [157].

Some heat treatments have a significant effect on the microhardness of Al6061 matrix alloy and its composites. It is reported that the quenching process followed by artificial ageing resulted in the improved hardness of matrix alloy and its composites[158]. The same study has revealed that the heat treatment of Al6061 also has a significant effect on the ultimate tensile strength (UTS) of matrix alloy and the composites. It is believed that the enhancement in the mechanical properties was due to the formation of precipitates that can hinder the dislocations in the matrix [158]. In addition, high-temperature heat treatment can contribute to improving the cohesion between metal and ceramic particles in the coating; coating porosity may also be eliminated after this treatment. Furthermore, the increase in hardness of the composite due to ageing as well as the formation of the hard precipitates, the aged composite is expected to provide high resistance against dislocations [159].

Pitchuka et al. have applied annealing heat treatment at 300 °C for one hour on cold-sprayed amorphous/nanocrystalline Al coating [160]. They found that the scratch wear resistance of the annealed coating is higher than the as-sprayed coating; this was due to the denser structure of the annealed coating. The structure densification was resulted due to the solid-state diffusion in the inter-splat boundary regions in the annealed sample [161]. Chavan et al. have studied the effects of

process parameters and thermal treatments on the characteristics of cold-sprayed silver coatings [162]. They observed that the heat-treated coating had improved electrical conductivity due to the decrease in cold work effects, the reduction in porosity, the reduction in inter-splat cracks, and an increase in grain size.

Li et al. have cold-sprayed copper coatings on copper substrates, and applied annealing treatment at two temperatures of 350 °C and 650 °C for different durations [163]. It is observed that the pores clearly coalesced in the annealed coating, which led to decreasing the microhardness and electrical resistivity. Li et al. [164] reported that the annealing of Ti and Ti-6Al-4V coatings at 850 °C for 4 hrs has led to an improvement of the inter-splat metallurgical bond between the CS splats owing to the diffusion at grain boundaries. Gavras et al. have evaluated the deposition and heat treatment of cold sprayed Al 6061 coating [133]. They stated that the annealed Al coating had enhanced ductility and inter-particle bonding due to the diffusion processes. This enhancement has led to a considerable improvement in the growth of fatigue cracks in the annealed 6061 coating [133].

Consequently, applying heat treatment, e.g. annealing on the cold-sprayed coatings have several advantages such as enhanced ductility and inter-particle bonding which lead to an enhanced cohesion in the sprayed coating. Also, the annealing can increase the mechanical and electrical properties, and remove the residual stresses that occur due to the cold spray. Thus, these observations can confirm the impact of annealing on enhancing the CS coating porosity by diffusion at the splat boundaries.

2.4 Laser Cladding (LC)

Laser has been widely used for surface processing owing to its valuable advantages among other surface modification technologies. These advantages are related to the characteristics of the laser beam, with a narrow wavelength, low divergence, and highly coherent beam. These features enable the laser to make precision and localized treatment in the targetted surface with controlled depth and high travelling speed. The high heating energy makes the laser beam able to change the solid surface phase when the beam interacts with it [165]. The common types of lasers that used in industrial purposes are the carbon dioxide (CO_2) laser, the fibre laser, the neodymium-doped yttrium aluminium garnet (Nd:YAG) laser, and the diode laser [166].

On the other hand, there are some limitations regarding the use of laser technologies due to the large heat energy of laser. The common problems within laser deposition and laser alloying processes are the cracking and residual stresses [167, 168]. Several reasons are related to these defects including the high cooling rate in the processed surfaces, laser scanning speed, deposition rate, and the difference of the thermal expansion coefficient between coating and substrate or between reinforcements and the matrix in MMC coatings [169-171]. Additionally, dissolution of many chemical compounds like carbides, oxides, and nitrides is a further factor for evaluating the laser coatings quality that can affect the mechanical properties according to the new composition [172].

The principle of LC is the deposition of the clad/coating by melting the feedstock materials and a thin layer of the substrate with a high-energy laser beam that is

normal to the targetted surface [173]. Then, rapid solidification of the molten materials produces the coating on the substrate. Thus, it is allowed to use mixtures of various powders as feedstock materials to deposit coatings with the desirable composition [174-176]. Thus, LC has been broadly used for different purposes/applications such as deposition of protective clads, repairing of worn-out surfaces and manufacturing of near-net-shape products [174].

The clad materials in laser cladding processes are delivered in three common techniques. The pre-placed powder technique is used where the cladding material is applied to the substrate surface in the form of slurry [177]. When the cladding materials are heated by the laser beam, a melt front progresses through the powder bed, from the top surface which faces the laser radiations toward the substrate. When adequate laser energy is available, the melt front will melt a portion of the substrate surface allowing the clad material to merge with the substrate material [173]. This process leads to the formation of a metallurgical bond between the substrate and the clad, and it causes dilution of the substrate depending on the provided laser energy. However, a narrow processing parameter window can be used, it is also time-consuming and not efficient for depositing complex-geometry shapes.

In the second technique, the clad materials are carried by wire feeding mean. There are some limitations with using this technique like the high dilution rates and poor process control [178]. Laser cladding by powder injection is reported as an effective technique compared with other processes and is the only one that has found practical use, due to the effectiveness in energy delivery and high level of process control and repeatability [179]. A carrier gas is used for delivering the starting

material which is in powder form, to the melt pool [180]. The laser beam melts the sprayed powder and a shallow layer of the substrate in order to produce a metallurgical bond between the clad and substrate. A clad track then is formed by a feed motion to the substrate during the continual deposition process. Among the different alternatives to perform this process, powder injection has been proved to be the most flexible, robust, and effective way to supply the precursor material for the laser cladding process as asserted by Steen [181].

2.4.1 Quality and deposition efficiency of laser clads

The quality clads can be defined as a uniform-continuous clad with high density and homogenous microstructure, and with a strong metallurgical bond to the substrate with low dilution [182]. Therefore, numerous studies have been done to understand the effects of the processing parameters on the clad quality. It is known that the laser deposition processes are based on both the heat provided by the laser to the substrate and powder, along with the mass transfer between the feeding powder and melted substrate surface [179]. It is reported that the most influencing processing parameters in laser cladding are: laser power P (kW), laser scanning speed V (mm/s) and powder mass feeding rate F (g/min) [183].

Two combined parameters are thus determined in order to examine the effect of the processing parameters on clad quality and formability. The first, the effective energy (E_{eff}), is an indicator that provides an amount of the delivered energy to the process by the laser [151]. This energy is basically in charge of heating/melting the substrate surface and powder stream [179]. Whereas the second is the powder deposition density (PDD) that provides a measure of the powder feeding rate during

the process [179]. The powder deposition density (PDD) is recognised as a function of effective deposition area.

Dense structure leads to an improvement in the micro-hardness measurements of the deposited clads [184]. Thus, decreasing the clad porosity can be an effective way to improve the mechanical properties of clads. The porosity in the laser cladding coating could be related to several sources including gas entrapped during deposition, instability of powder flow, atmospheric conditions of the process, and oxidation level [185]. Incomplete melting commonly occurs due to the lack of diffusion which usually occurs owing to insufficient energy delivered to the melting pool [186]. By increasing the laser density, the volume of melting pool increases owing to the higher laser energy absorbed by the materials [187]. This can offer longer solidification time, allowing gases to escape, which reduces the porosity level.

Lee stated that, for optimal DE in the laser cladding processes, the powder has to be melted by the laser energy [188]; and the sprayed materials should not rebound away from the surface [189]. Thus, reducing the amount of rebounding particles within laser cladding is reported as an effective factor that enhances the deposition efficiency within laser cladding [188]. Moreover, Lee stated that the higher powder feed rate leads to more randomness in particle movements within the laser beam; this can offer longer interaction time between the material particles and laser radiation [188]. The increased interaction time occurs due to the longer path of the particles because they impact each other. In addition, Devesse et al. have mentioned that fine particles are pulled outward by the gas flow due to the light weight, this results in a lower particle density in the central area of the laser beam [190]. Most

of the laser radiation can be interrupted by the ceramic particles in the composite feedstocks due to the low heat conductivity of ceramic particles [191]. Where the formation of the molten area on the substrate surface can increase the catchment of the incoming particles [192], which means improving the deposition of the sprayed materials. This is achieved by reducing the rebounding from the substrate surface that occurs when particles impact the substrate out of the melt pool.

The ability of the materials to absorb laser radiation is one of the most important factors that affect the interaction between the laser and the processed materials [193]. Thus, the high reflective materials (i.e. Al and Ag) are difficult to laser process within laser cladding; Ag, for example, needs laser power 20 times higher than steel [194]. Moreover, aluminium has high reflectivity (~90%), as the reflectivity increase with the electrical conductivity at a given wavelength [195]. This higher reflectivity is a detrimental issue with the laser processing of Al due to the high energy required for melting Al. The effect of high reflectivity can be eliminated for large scale components by surfaces modification processes such as machining, etching, deforming and texturing to improve their absorption [196]. However, it is a large challenge to modify the surface of powder materials as they have microscale surfaces.

In contrast, ceramic materials have good laser absorbability with low electric conductivity. For example, TiC particles have high electrical resistivity (8×10^{-3} $\Omega*$m compared with 2.7×10^{-8} $\Omega*$m of Al), which means it has high laser absorbability [197]. This may explain why the laser absorption coefficient of TiC is greater than aluminium absorption coefficient at a certain wavelength [180]. These characteristics give TiC a preference for laser absorption compared with Al

and other reflective metals [191]. These different optical characteristics between metals and ceramics can make the interaction between the laser and the sprayed materials complex when composite feedstocks are used.

2.4.2 Laser Cladding of AMCs

Laser deposition of metal matrix composite (MMC) coatings has been widely explored, using often pre-mixed composite powders as feedstock materials. The stability of ceramic (carbides, oxides, etc.) particles in laser clads indicates their wear resistance because these particles tend to dilute when a high-energy laser is applied [198]. The results of these studies explained that the wear resistance was significantly improved in composite coatings, wherein the wear rate has been highly reduced, in some coatings by 99% compared with the substrate without coating [198]. It is known that the increase in the reinforcement fraction increases the mechanical properties of the MMCs [199] by increasing the strengthening action in the composites. This is due to the fact that the increase in reinforcement fraction leads to an increase in the amount of dislocation punching [6].

Farahmand et al. (2015) examined the properties of deposited laser clads with different fractions of WC particles in the mixture. Crack-free coatings with dense and homogeneous structure were achieved when the percentages of WC were less than 50% [170]. Li et al. (2014) investigated the effect of adding Y_2O_3 to the TiB-TiC coating; and they emphasised that the wear resistance was meaningfully improved by adding Y_2O_3 to the TiB-TiC composite coating, because of the refinement of the primary phase structure [200]. The influence of laser density on the resistance of slurry erosion in laser coatings was investigated by Farahmand et al. [201], their results showing that there is a negative relationship between laser

energy and the erosion resistance of Ni-WC coatings. They stated that the finer grains of the Ni matrix and WC contributed to improving the hardness and erosion resistance of the composite. Du et al. [202] used the laser to fabricate a TiB2-TiC-Fe nano-composite coating. The produced coating structure consisted of TiB_2, TiC, Fe_3 and α-Fe. It was also found that higher scanning speed promotes carbides stability in the deposited coating due to the higher cooling rate, which decreases the carbide dilution [202].

One of the most important benefits offered by aluminium-based matrix composites (AMCs), is the possibility of controlling the properties to suit various applications by using an appropriate combination of matrix, reinforcement and processing means [203]. Hence, ceramic-reinforced AMCs are expected to offer a synthesis of desirable properties such as higher strength, stiffness and wear resistance, in parallel with satisfactory ductility and toughness [13]. Therefore, AMCs have been classified as an applicable choice for the corrosive and wearable environment applications [32]. Specifically, aluminium and its alloys with magnesium, silicon, copper, manganese and zinc are the most common matrix materials after iron for the fabrication of MMCs [33]. This is due to the fact that the mechanical properties of the ceramics have been well combined with these of AMCs without forfeiting the ability of aluminium alloys to resist the corrosion [34, 35].

The Al-TiC feedstocks, with different fractions of TiC powder, were pre-placed and laser cladded on Ti–6Al–4V substrate surfaces by Li et al. [204]. They demonstrated that Ti3Al/TiAl + TiC ceramic layer could form by using a proper parameter window of laser cladding. They also observed that the wear resistance of the deposited layer was two times larger than that of the substrate material.

Emamian et al. have used a mixture of Ti, Fe, and graphite powders to deposit composite clads on AISI 1030 substrate [205]. They also found that an in-situ TiC has formed in the deposited coatings and the microstructure of the composite coatings has clearly varied by changing the laser cladding parameters. Moreover, Sampedro et al. studied the use of laser cladding for deposition Ti6Al4V and Ti6Al4V/TiC composite coatings on Ti substrates [206]. They investigated the influence of process parameters on clad geometry and wear behaviour, whereas an improved wear resistance was achieved by the right selection of the process parameters [206].

Further, Yan et al. have successfully used ball-milled mixtures of Co alloy, TiC, and CaF_2 powders within powder injection laser cladding to deposit self-lubricating composite coatings on copper alloy substrates [207]. It is observed that the microstructure of the self-lubricating composite coatings consisted of fine-spherical TiC particles and fine-spherical CaF_2 solid lubrication particles which were uniformly spread in a Co binder. The self-lubricating composite coatings have presented highly improved wear resistance compared with other studies reported by the authors [207].

In summary, the laser energy has been widely used for surface processing owing to its valuable advantages among other surface modification technologies; this made LC has been broadly used for different applications. Particularly, LC with powder injection was classified as an effective technique compared with other processes due to the effectiveness in energy delivering and a high level of process control and repeatability. Aluminium coatings received wide attention for different applications within LC processes, where the mechanical properties of the ceramics have been

well combined with these of AMCs without forfeiting the ability of aluminium alloys to resist the corrosion. TiC-reinforced composite coatings have been widely investigated, and the use of TiC has a significant role in improving the wear behaviour of the TiC-reinforced composites. Otherwise, reducing the amount of rebounding particles is an effective way to enhance the deposition efficiency and mechanical properties of the MMCs that deposited by laser cladding. Also, preventing the fine particles from being pulled outward by the gas flow due to the light weight can improve the deposition and distribution of the fine reinforcement in the deposited clad.

2.5 Preparation Methods of Composite Feedstocks

High-performance coatings can be developed through appropriate design of the initial powders for MMCs. For instance, to achieve high deposition efficiency with the stability of powder feeding rate, the common range of particle size in cold spray, for instance, is 5–50 μm. Also, round-shaped particles are the preferred morphology in the powder [111]. Consequently, the use of a preparation method that keeps these requirements in the prepared powder can lead to enhanced coating structure and material deposition.

Composite powder preparation consists of the selection of the matrix material and the reinforcing phase, in addition to the selection of the production technique. The commonly used processes for composite powder preparation are mechanical alloying or ball-milling, mechanical (simple) blending, spray drying, particle coating or cladding [111]. There are several advantages and disadvantages of each process regarding the powder flow, reinforcement fractions, reinforcement

distribution, and interfacial interaction between consisting phases in the feedstock, discussed in the following section.

2.5.1 Simple Mixing

Simple mixing (SM) or mechanical blending is a simple technique that has been commonly used for preparing composite feedstocks. The wide use of SM is due to the ease of procedure; it is performed by blending two (or more) powders manually or by a mechanical mixer for a certain time. Thus it can be considered an inexpensive process as no further processing is usually needed. However, a sufficient uniformity of the reinforced phases cannot be guaranteed in the mixed powders [111]. This could be because of the particles of both phases can agglomerate as they are not restricted by any forces. In addition, the consisting particles have different ranges of velocities due to the differences in particle size, density, or morphology between the blended constituents [208]. This variance in particle velocities causes a variance in deposition efficiencies of the ingredients [209]. This can yield inconsistencies in the coating structure and composition from that of the prepared feedstock.

2.5.2 Mechanical Alloying

The mechanical alloying (MA) or ball milling process is performed by feeding the materials that need to be milled into a rotating drum containing the milling balls [210]. The milling process takes place through the impact of grinding balls and the abrasion of powder particles between the milling balls when the drum is rotating. The parameters of the ball-milling process include weight ratio of milling balls to powder, milling ball size, type and volume of the milling medium, milling time and rotation speed [211].

Ball-milling can overcome some limitations of the simple mixing process to some extent, due to it depending on crushing and cold-welding, but the ingredient

materials can be affected (refined) by the milling balls [212]. These effects produce finer and homogeneous powders as the reinforcement particles are crushed and inserted in the matrix particles. Thus, by using a designed set of parameters, the size and distribution of the ingredient phases can be controlled. On the other hand, the selection of milling parameters is tricky, especially when near-spherical shape appropriate size ranges are needed [111]. Also, ball-milling can cause serious damage to brittle materials such as carbon nanotubes [213]. The strength of the matrix material often increases due to the created stresses and work hardening during the milling process [213]. Furthermore, high-energy ball milling can induce chemical reactions[214], producing nanoparticles and nano-composites like SmCo5 [215] and FeCo [216], which may affect the morphology and behaviour of the milled powder.

2.5.3 Metal-Coated Particles

Particle coating (or cladding) is reported to be an effective approach for producing the composite powders. The particle coating is usually achieved by depositing a metal film on hard-phase particles by different means. The coating or cladding processes include: chemical vapour deposition [217], plasma chemical vapour deposition (CVD) [218], ion beam assisted deposition (IBAD) [219]. By using this approach, composite powders with different volume fractions of the coating material can be produced through controlling the film thickness on the coated hard particles [111]. Metal-coated powders have been used to enhance the wettability and adhesion in the deposited composite coatings [220]. The coated powders, which are prepared from different material systems, are used in different deposition

techniques such as laser cladding [221], selective laser melting [222], cold spray [223] and thermal spraying [224].

The electroless plating is a methods of depositing metals and alloys by electrochemical reactions. In this process, the chemical reaction proceeds continuously on selected surfaces, producing uniform coatings with unique properties on a wide variety of substrates [225]. However, it is found that clean and oxide-free substrate surfaces are important factors for obtaining high quality composite powders with a uniform thickness layer on the coated particle surfaces [226]. Thus, pre-cleaning process may be necessary in the electroless plating methods.

However, this method is a relatively high-cost process. In addition, the soft layer thickness should be optimised, as a thick layer is required to confirm successful bond to the hard phase, while too thick layer may decrease the overall coating hardness [111]. Particle coating also faces some difficulties regarding the production of fine particles due to the thickness of the cladded layer; this makes the use of coated particles limited or complicated in such processes like cold spray.

2.5.4 Spray Drying of Slurries

In this process, the components are mixed with a liquid in order to form a slurry. The slurry is then atomised and dried by using hot gas. The prepared composite powders used by this approach, are usually homogeneous and have a sphere-like shape. Composite powders produced by spray-drying often need a post-sintering treatment to enhance the cohesion strength [111]. Additionally, the organic solvents

which are used to form the slurry can affect the wear resistance and hardness of the deposited coatings [227].

In summary, three preparation methods are used to produce ceramic-metal feedstocks for cold spray technology: blending of different powders, agglomerating-sintering or mechanical alloying, and cladding or coating of powders [228]. However, blending is not an effective method due to the incapability to deposit coatings containing a high volume fraction of ceramic (more than 40%), because a large portion of the hard phase (about 70%) could rebound from the substrate [83]. Mechanical alloying has some drawbacks with regard to the heterogeneity of the produced powder; it needs extra processes (e.g. sintering when high volume fracture of ceramic is needed). The alloyed particles have a rough surface that may reduce powder flowability [83]. A main technical shortcoming of CS is the dependence on the material deformability for the coating formation, normally only ductile materials can be used [91]. Thus, one of the important challenges regarding the deposition of composite coatings is to find an appropriate process to prepare the feedstock.

As a result, the preparation processes of composite powders play an important role in accomplishing the requirements of the deposition processes. These requirements include the uniformity of the reinforcement phase, particle size and powder flowability. Different processes are adopted to prepare composite powders for different applications. Each preparing process has benefits and shortcomings regarding the characteristics of the prepared powder. Thus, there is a need to use a preparing method which fulfils most of the deposition process requirements. This

can be achieved by enhancing the characteristics of the produced powders and overcoming the limitation in a cost-effective manner.

2.6 Summary of the Literature Review

2.6.1 Metal Matrix Composites

1. MMCs are particularly attractive as a replacement for conventional materials in many engineering applications such as different automotive parts (cylinder walls, tubes, flanges, etc.), aerospace (compressor rotor, fan blades, sidewalls and structure, etc.), electronics and other important industries.
2. Ceramic-metal composite coatings are widely used to enhance the surface properties and performance of engineering components in abrasive and corrosive environments.
3. Fine reinforcements have superior strengthening effect compared to coarse reinforcements. Thus, the use of fine particles as reinforcements can improve the strengthening effect in the composites.
4. Three effective approaches can be adopted to develop the behaviours and properties of the MMCs: the use of fine ceramic particles as a reinforcement phase, increasing of the reinforcement phase fraction and enhancing the distribution of the reinforcing particles in the matrix.
5. An appropriate selection of the preparing powder method with optimised process parameters is important to the factors of achieving the best results in the produced MMC components or coatings
6. Aluminium and its alloys are most matrix materials in MMCs, and AMCs have been classified as an applicable choice for wide corrosive

and wearable environment applications. The improved wear resistance in AMCs can be owing to three main mechanisms; first, the high mechanical properties of the reinforcement particles. The second is the matrix strengthening owing to the presence of the particles within the matrix. The third mechanism is the improved toughness of the AMCs due to the ageing process of some Al alloys.

7. TiC has been selected as a powerful reinforcement material among many ceramic types owing to its excellent properties such as the high hardness, the outstanding thermal and electric conductivity, and the high melting point.

2.6.2 Preparing Methods of Composite Feedstocks

1. The preparation processes of composite powders play an important role in accomplishing the requirements of the deposition processes. These requirements include the uniformity of the reinforcement phase, particle size and powder flowability.
2. Eliminating the segregation of reinforcement and obtaining a uniform distribution of the reinforcement particles are important factors for achieving quality composites. Thus, most of MMCs have been produced using solid-state techniques such as powder metallurgy, powder blending, and consolidation, diffusion bonding and vapour deposition
3. The available feedstock preparing methods of the composite feedstocks have significant drawbacks, particularly regarding the cold spray requirements processes. These drawbacks include high processing cost,

work hardening of the powder and heterogeneity of the reinforcement phase.

2.6.3 Cold Spray

1. Cold spray is an adopted technology for a wide range of applications including fabricating different automotive parts such as cylinder walls, tubes and flanges, field repairs and maintenance, deposition of high-performance alloys which are used in harsh working conditions like the combustors, nuclear reactor, gas turbine blades, and other components in the aerospace industries.
2. The cold spray process has a limitation owing to its dependence on the high plastic deformation that makes cold spray inappropriate for depositing non-plastic materials like carbides, oxides, nitrides and borides due to their low deformability.
3. There is a great challenge regarding the utilization of ceramic particles in ceramic-metal coating deposition within cold spray processes. This challenge is to deposit composite coatings with an acceptable fraction of ceramic embedded to the coating. Increasing the number of ceramic particles in the coating would improve the quality and deposition of the coating due to the peening action, roughening of the substrate surface, and creation of micro-asperities.
4. In cold spray, the higher the local deformation in the impact surfaces, the higher the bonding strength; and the oxide-free surfaces are preferred to guarantee tight contact for a metallurgical bonding.

5. The presence of ceramic particles can greatly improve the material deposition and the quality of the cold spray coating, in addition to the improvement in mechanical behaviour as composite coatings. Ceramic particles have several benefits within cold spray including the formation of micro-asperities, breaking up of oxide layers, and great compaction effect. These offerings can improve the bonding of the deposits and enhance the cohesion of the cold sprayed coatings due to the compaction and the interaction (interlocking) with the matrix materials
6. There are very limited studies on using TiC as a reinforcing phase in cold spray processes for depositing particulate composite coatings. Hence the sprayed composite coatings had higher levels of porosity comparing with the non-composite coatings, even with using higher gas pressure and temperature.
7. There are limited studies regarding the deposition of Al 6061 within cold spray as it is a challenge to deposit dense 6061 coatings using cold spray at room temperature, within cold spray technology. This is because CS significantly depends on the ductility and high deformation of the impact surfaces. Also, the effects of reinforcement particles on the deposition and quality of the cold sprayed Al 6061 coating need to be investigated.
8. Aluminium coatings have limited wear resistance due to the ductility of Al and its alloys. Namely, the addition of ceramic to the coating to form an aluminium matrix composite allows obtaining simultaneously good wear and corrosion resistance, while keeping low the density of the substrate-coating system

9. Embedding hard particles, e.g. ceramic in the cold-sprayed coatings, such as strengthening of the coating by the construction of a composite structure, improving material deposition and enhancing coating cohesion by reducing the porosity.
10. The addition of ceramic particles as a reinforcement is a successful procedure for improving the mechanical properties of the Al coatings, which means a mechanical strengthening for the coated components. Furthermore, the addition of hard particles to the al feedstock improves the deposition Al by different means like increasing the substrate roughness through creating more asperities.
11. Applying a heat treatment, e.g. annealing on the cold-sprayed coatings has several advantages such as enhanced ductility and inter-particle bonding, increasing the mechanical and electrical properties, and removing the residual stresses that occur due to the cold spray. Thus, these observations can confirm the impact of annealing on enhancing the CS coating porosity by diffusion at the splat boundaries.

2.6.4 Laser Cladding (LC)

1. Laser cladding with powder injection is the most flexible, robust, and effective way to supply the precursor material due to the effectiveness in energy delivering and a high level of process control and repeatability.
2. High reflective materials are difficult to laser process within laser cladding; this higher reflectivity is a detrimental issue with the laser processing of Al due to the high energy required for melting Al.

3. Ceramic materials have good laser absorbability, which gives TiC a preference for laser absorption compared with Al and other reflective metals.
4. The interaction between the laser and the composite materials is complex; this is due to the differences in optical characteristics between metals and ceramic.
5. Aluminium coatings received wide attention for different applications within LC processes, where the mechanical properties of the ceramics have been well combined with these of AMCs without forfeiting the ability of aluminium alloys to resist the corrosion.
6. Reducing the amount of rebounding particles is an effective way to enhance the deposition efficiency and mechanical properties of the MMCs that deposited by laser cladding.
7. Preventing the fine particles to be pulled outward by the gas flow due to the light weight can improve the deposition and distribution of the fine reinforcement in the deposited clad.

2.6.5 Knowledge Gaps Definition

According to the literature, there are some limitations regarding the deposition of MMC coatings using cold spray and laser cladding processes. The following problems have been defined and will be tackled in this research:

1. Because of the dependence of cold spray on the high deformation of the sprayed materials, two limitations are presented:

a- Hard particles tend to rebound when hit the substrate or an existing layer. This leads to differences in the composition between the starting materials and deposited coatings

b- Less-ductile materials experience a limited deformation during impact. This produces a porous structure and weak-cohesion coating.

2. The use of blended feedstocks within powder-injection laser cladding can lead to a separation of the blended phases that may cause stream divergence and allow fine particles to be blown-away leaving the high-intensity region. This can lead to inhomogeneous flow, affecting the particle distribution over the clad section, and may promote the formation of unregular clad shapes.

3 MATERIALS AND METHODOLOGY

3.1 Introduction

The experiments performed are described in this chapter. It also provides the details of the processed materials, laser deposition, and cold spray systems. The techniques used for testing the coated samples and characterising used materials will be explained. The principles and practical approaches of the process machinery and instrumentation are described along with their capabilities and limitations for the interpretation of results.

This chapter can be divided into four main sections: materials used, processing equipment and procedures, sample characterisation approaches, and lastly mechanical property testing. 3.2 presents details of the substrate material, powders used for feedstock preparation processes for cold spray and laser cladding. It also includes powder characterisation and flowability analysis techniques. While 3.3 provides details about laser cladding, cold spray and heat treatment systems including the basic principles and the main components with the relevant schematic diagrams.

3.2 Materials

3.2.1 Aluminium 6082 plate

Aluminium 6082-T6 plates with a thickness of 6 mm were used as substrates for both cold spray and laser cladding processes. The plates were supplied by Unicorn Metals Ltd (UK); the nominal chemical composition is shown in Table 3-1 below. It is a medium strength alloy with excellent corrosion resistance with high strength. A6082 has many applications due to the higher strength, it is typically used in highly stressed applications, trusses, bridges, cranes, and transport applications. For cold spray processes, the substrates (made from aluminium 6082-T6) were cut to the desired dimensions (50 × 25 mm) that suit the working table of the cold spray rig and the fixing clamps. The substrate thickness is 6 mm to avoid plate buckling while tightening the substrate on the spraying table. The substrates were ground using 240-mesh SiC grinding paper in order to clean the surface from the oxides and contamination. Surface preparation is also efficient for roughening the surface as it is desirable for enhancing material deposition within cold spray through increasing the contact area between impact surfaces [229]. The ground substrates were rinsed with acetone and dried using a compressed air gun directly prior to processing to remove any contaminations. Optical microscopy was used to check the grinding level of the substrate plates before using.

Other substrates from the same plate (aluminium A6082-T6) were cut to dimensions of 180 mm x 100 mm (6 mm thickness) for laser cladding processes. The substrate surfaces were cleaned and degreased by acetone, sandblasted and then rinsed with acetone before laser processing. The sandblasting is used for roughening substrate surfaces in order to enhance their laser absorption as the

aluminium surface is shiny and can reflect about 90% of the laser radiations [195]. The substrates had four holes of 8 mm diameter to fix the substrate plate onto the processing table by steel screws; this is also used to avoid substrate buckling during the process.

Table 3-1: Nominal chemical composition of the Al 6082-T6 substrate [230].

Element	Si	Mg	Mn	Fe	Cr	Zn	Ti	Cu	Others	Al
Al 6082	0.7-1.3	0.6-1.2	0.4-1.0	0.0-0.5	0.0-0.25	0.0-0.2	0.0-0.1	0.0-0.1	0.0-0.15	Bal.

3.2.2 Pure aluminium powder

Commercially pure, gas atomised Al powder (purity 99.85%) was used as a primary ductile phase of the composite coatings/clads. It is supplied by Angang Group Aluminium Powder Ltd- China. This powder has a spherical shape with 15-45 µm particle size range; d_{50}=25 µm and d_{90}= 39.98 µm. Figure 3-1 shows the morphology of the as-received commercially pure Al powder. This range allows most Al particles to achieve their higher inflight velocity for higher deposition rate.

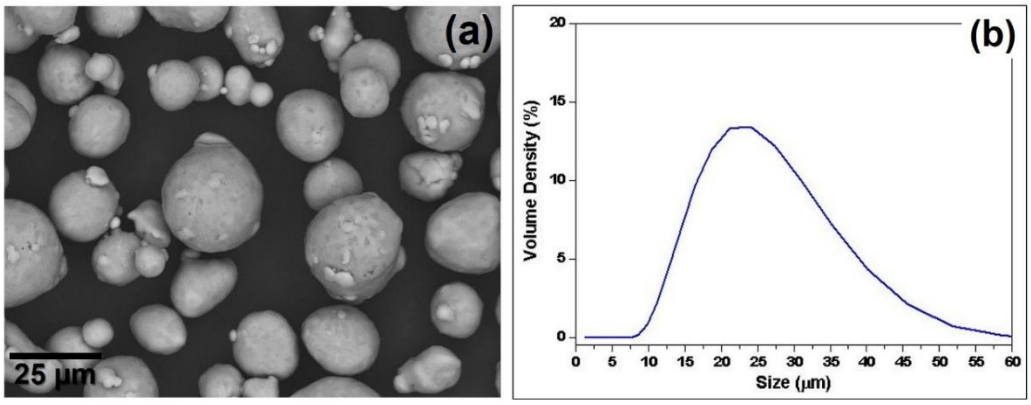


Figure 3-1: (a) SEM image showing the morphology of the pure Al powder; (b) particle size distribution of the pure Al powder.

3.2.3 Aluminium alloy 6061 powder

6061 aluminium alloy powder was used as the parent powder in the satelliting process to prepare a composite satellited feedstock (6061-TiC) for processing by cold spray. 6061 is a high-strength Al alloy and experience limited deformation when impact during cold spray, as porous structures have been observed even with using pre-heating for the working gases, see 2.3.6. The Al powder has an irregular shape with 20-53 µm size range ($D_{(50)}$ = 36.5 µm); provided by LPW Technology, UK. This powder was also used as a 6061 feedstock for comparison (without satelliting). The nominal chemical composition of this powder is shown in Table 3-2. Figure 3-2 shows the morphology and particle size of the virgin Al 6061 powder.

Table 3-2: Nominal chemical composition of the Al 6061 powder.

Element	Si	Mg	Mn	Fe	Cr	Zn	Ti	Cu	Others	Al
Al 6061	0.4-0.8	0.8-1.2	0.0-0.15	0.0-0.7	0.04-0.35	0.0-0.25	0.0-0.15	0.0-0.1	0.0-0.15	Bal

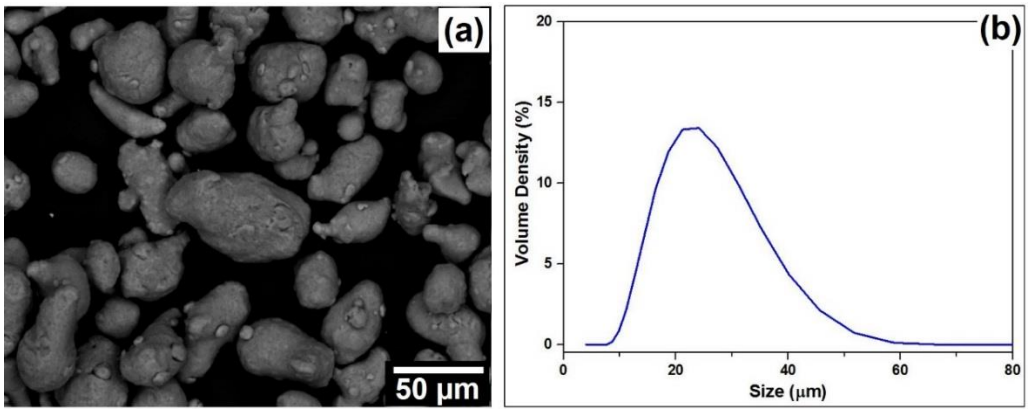


Figure 3-2: (a) SEM image showing the morphology of the Al 6061 powder; (b) particle size distribution of the Al 6061 powder.

3.2.4 Titanium carbide powder (TiC)

The angular TiC powder has a maximum particle size 5 µm, d_{50} = 2.09 µm and d_{90} = 5.22 µm. Figure 3-3 shows the morphology and particle size distribution of the TiC powder. It was supplied by Goodfellow, UK, with a purity of 99.8%. TiC powder was used as a reinforcement material with the aluminium for producing composite feedstocks with both satelliting and simple blending techniques.

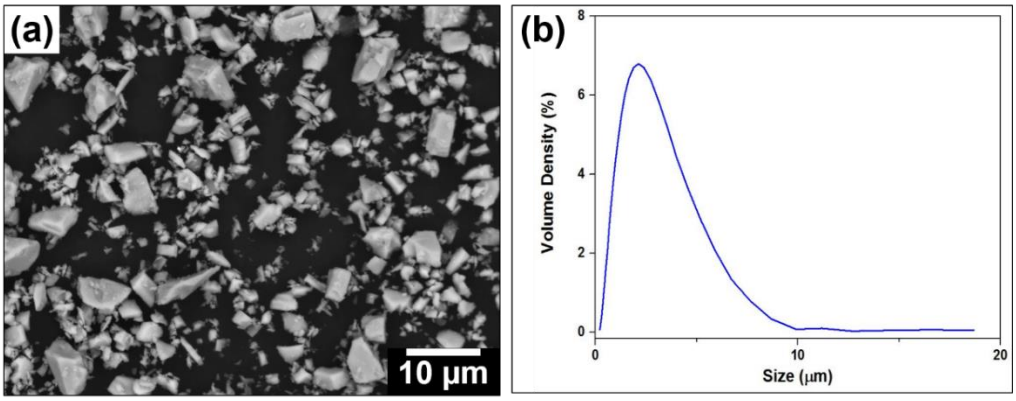


Figure 3-3: (a) SEM image showing the morphology of the TiC powder; (b) particle size distribution of TiC powder.

3.2.5 Binder Polyvinyl alcohol

Polyvinyl alcohol (PVA) is an important water-soluble polymer [231]. It is dissolvable in water and slightly dissolvable in ethanol, but insoluable in other organic solvents. The solution of PVA in water was used as a binder in the satelliting processes. It was lab prepared by dissolving 2.7% of polyvinyl alcohol (PVA) in 97.3% water by volume (4.05 g PVA in 100 g water). Warm water was used to accelerate the preparation process avoiding the use of high-temperature water to reduce the viscosity of the binder in order to enhance its flow and spread.

3.3 EQUIPMENT AND EXPERIMENTAL PROCEDURES

3.3.1 Feedstock preparation

a. Satelliting process

Satelliting is a feedstock preparation method process which can be used to produce powders which consist of parent particles covered by a layer of fine particles [232]. The added binder (PVA) can produce a sufficient bond strength between the major and minor particles due to the effect of the added binder. Satelliting processes were performed as sequential batches of 20-25g. In the dry mixing step, two types of powder (Al and TiC) were mixed with certain weight fractions in a glass beaker for 4-5 minutes. This stage is used to homogenise the mixture by breaking down the agglomerations/clusters in both powders, and also to spread the reinforcement phase over the batch.

The binder is then added using a small spraying bottle to distribute the binder; then the wet mixing step starts to continue for 5 minutes for each patch. This stage is used to homogenise the wet mixture by breaking down the agglomerations/clusters and confirm the binder distribution. The binder liquid was heated up with a water bath at 60 ℃ for 10 minutes before using in order to increase the flowability. Then the whole powder was loaded into a tubular mixer for 30 minutes to complete the mixing process of the whole powder and for further homogenising. The satellited powder is then spread onto a steel tray as a thin layer and placed in the oven at 100 ℃ for 10-12 hours to be dried thoroughly. The steel tray was cleaned and coated with an aluminium foil to avoid powder contamination, where all the utensils (beakers, bottles, stirring rods...etc.) were cleaned and dried before and after the process.

b. Blending process

For comparison purposes, simply blended feedstocks were also prepared by mixing the same fractions of powders (metal and ceramic) but without the addition of the liquid binder. Thus, the preparation process of the blended feedstock involves only two dry mixing steps. In the first dry mixing stage, sequential batches of a mixture (Al and TiC) were stirred together with desired weight fractions in a glass beaker for 4-5 minutes. The purposes of this stage are homogenising the mixture by breaking down the clusters in the virgin powders and spreading the ceramic particles over the batch. While the second stage, the whole powder was loaded into the tubular mixer for 30 minutes to complete the mixing process of the entire composite powder to further homogenise.

3.3.2 Powder characterisation

a. Particle size distribution

The distribution of the particle size of the virgin and prepared powders were examined using Malvern Mastersizer-S (Malvern Instruments Limited, Malvern, UK). The testing process is done by passing powder particles through a laser beam (optical unit), this makes the light scattered. The optical unit in Mastersizer that comprises annular detectors, captures the scattering radiations from a field of particles. Then, based on the Fraunhofer diffraction model, the particle size distribution is evaluated from the scattering pattern of the laser light beam. The waste materials (tested powders) are absorbed and circulated through the machine.

Finally, the raw data of measurements is analysed by a relevant software (V2.18) contained in Malvern instrument to obtain results in the form of volume fractions of each particle size. The result reports typically consist of a table of the volume

fractions of different particle size and a diagram showing the particle size distribution. Three runs of every powder sample (about 25 g) were taken to ensure the repeatability of the results.

b. Powder flowability

Flowability is the capability of the powder to flow desirably in given processing or handling part of equipment [233]. Many factors affect the powder flowability such as particle size, size distribution, shape, surface roughness, chemical composition, moisture content, and other factors. It is expected that different feedstocks have different flow characteristics at same working conditions like temperature and rotation speed of the powder feeder. Thus, to achieve identical powder feed rate, the rotational speed needs to be changed when using different feedstock to obtain comparable results for cold spray and laser cladding. Also, it is important to study the effect of powder processing (e.g. satelliting) on the flow characteristics of the prepared powder. The flowability of each powder (virgin and prepared) were characterised by using FT4 Powder Rheometer, (Freeman Technology Ltd, UK).

The Freeman FT4 Powder Rheometer has adopted as a novel powder flow testing device in the two decades. The test instrument consists of a blade of 48 mm diameter fixed to a vertical rotating steel bar, and a cylindrical glass bore of 50 mm diameter to hold a powder sample of 160 ml volume. This method is empirical and the working principle depends on measuring the flowability of powders by measuring the energy needed to rotate and move the twisted blade into the powder sample. Hence, the recorded flow energy indicates the flow resistance to the rotating blade. This energy is calculated by determining the work required for the

rotation and transmission of the rotating impeller a specific distance into the powder bed [234].

Every run consists of 11 test points; each point represents the energy required for one pass of the blade through the powder sample. The first seven test points are performed at a relatively high tip speed (100 mm/s), where the powder not very sensitive to the blade motion due to the entrapped air prevents a portion of powder particles from contacting the blade surface [235]. While the last four test points that performed at a reduced tip speed (100, 70, 40, and 10 mm/s), the lower speed allows more air to escape producing much contact between the powder and blade surface. Thus, the first seven points are used for measuring the stability of the test as the stability index (SI) = Energy (test7)/ Energy (test 1). While the flowability of the powder is indicated from the last four points by the flow rate index (FRI) = Energy (test11)/ Energy (test 8). FRI represents the reduction in the flow energy when the tip speed (flow rate) is reduced by a factor of 10 [235]. It is also reported that the powders with high compressibility and low transmissibility of forces require low flow energy at lower flow rates compared to low-compressibility powders [235]. A possible explanation is that the moving material around the blade is smaller so that the number of particles which move relative to other particles is smaller, as is the work done by the blade.

3.3.3 Cold Spray Experiments

Cold spray processes of different feedstocks were conducted with a cold gas spraying system constructed at the University of Nottingham. The main components of the cold spray system are shown in the schematic diagram in Figure 3-4. The gun is a steel de-Laval nozzle with a throat diameter of 1.35 mm

and an exit diameter of 4 mm (area expansion ratio of 8.8). The divergent section of the nozzle had a length of 150 mm.

The system worked with room temperature helium at 2.8 MPa for the primary accelerating gas. Nitrogen is used as a powder carrier gas with pressure was fixed approximately 0.1 MPa higher than the primary accelerating gas (2.9 MPa) in order to ensure powder feeding into the primary gas flow. With these working conditions, the inflight speed of an Al particle of 45 µm diameter can reach ~740 m/s according to (Equ 2- 5), which is significantly higher than the critical velocity of a similar Al particle (660 m/s) that was determined by Assadi et al.[77].

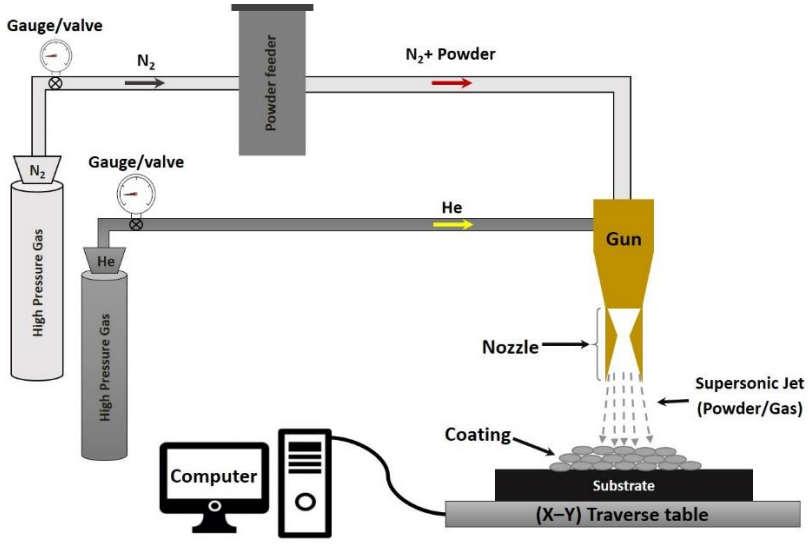


Figure 3-4: A schematic diagram of the cold spray system used in this research.

A commercial powder feeder (Praxair 1264HP, Indianapolis, IN, USA) with a 12-slot feeding wheel was used in the cold-spraying process. The feeder has a changeable rotating speed and is provided with a coating heater to warm up the powder in order to enhance powder flow through the system by reducing the

humidity in the powder. The powder is carried by the carrying gas (N_2) from the feeder exit to the spraying gun (nozzle) inlet through a compressed plastic tube to eliminate electrostatic charging during powder movement. The nozzle-substrate standoff distance was set at 20 mm for all cold spray tracks. Substrates were then fixed from one end on the spraying table by a steel plate and screws. The X–Y traverse table is controlled by computer to governor the relative motion between the nozzle and substrate(s).

The spraying room is provided with a robust extraction system for recycling the powder that has not adhered to the substrate, and to absorb spray gases to keep the space ventilated. It also has sensors to indicate oxygen level in the lab, and also safety glass barrier in addition to the requirements of safety like noise ear defender and masks. Figure 3-5 shows the main components of the cold spray system used in this research.

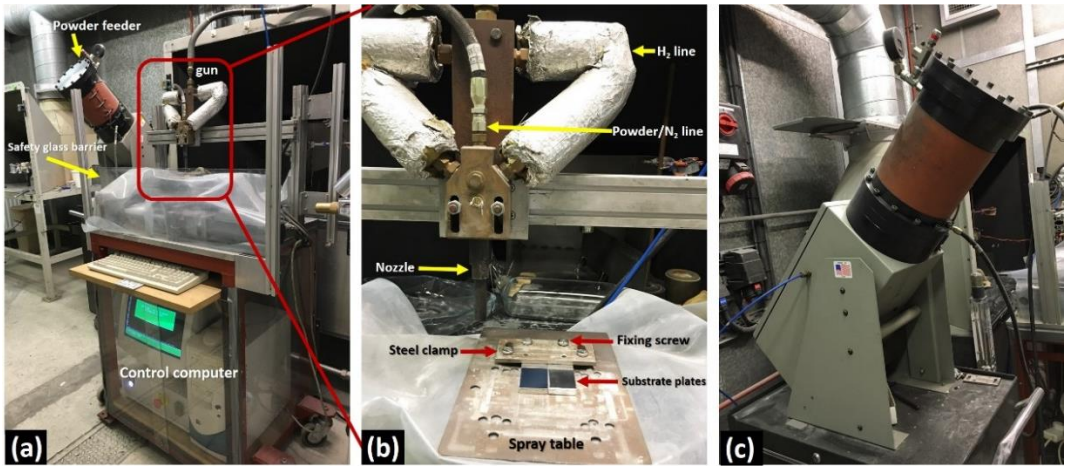


Figure 3-5: The cold spray system showing (a) the combined whole system, (b) the spraying gun and table, and (c) the powder feeder.

Single and overlapped tracks were deposited by cold spray to characterize the deposited materials. Single tracks deposition is usually used for the basic characterisation, and the overlapped tracks are conducted for mechanical testing purposes (e.g. hardness and wear). In single-track cold spray, the table motion was

set to produce a single line with a width of ~4 mm, and the space between each consecutive track centres was kept 10 mm. While for depositing a full-surface coating, an overlap distance of 2 mm was kept between the consecutive tracks. Thus the distance between track centres was 2 mm. Figure 3-6presents a schematic diagram of the spraying path of both single tracks and full coating deposition. Sprayed single tracks and full surface coating samples are presented in Figure 3-7.

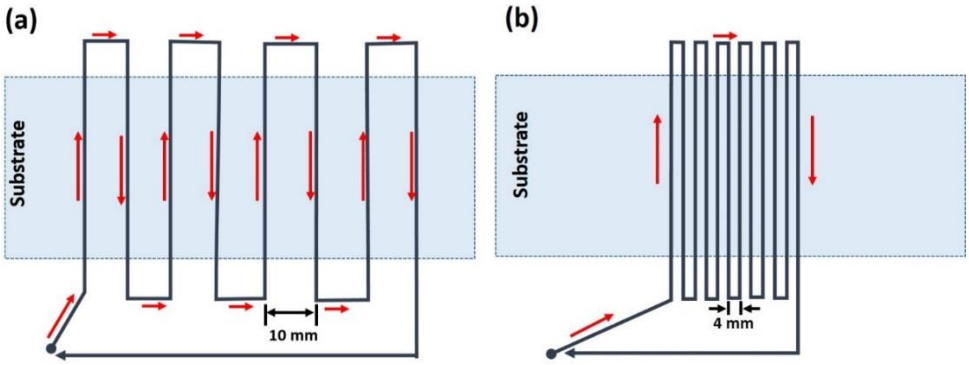


Figure 3-6: A schematic of the cold spray deposition path of (a) single track and (b) full surface coating.

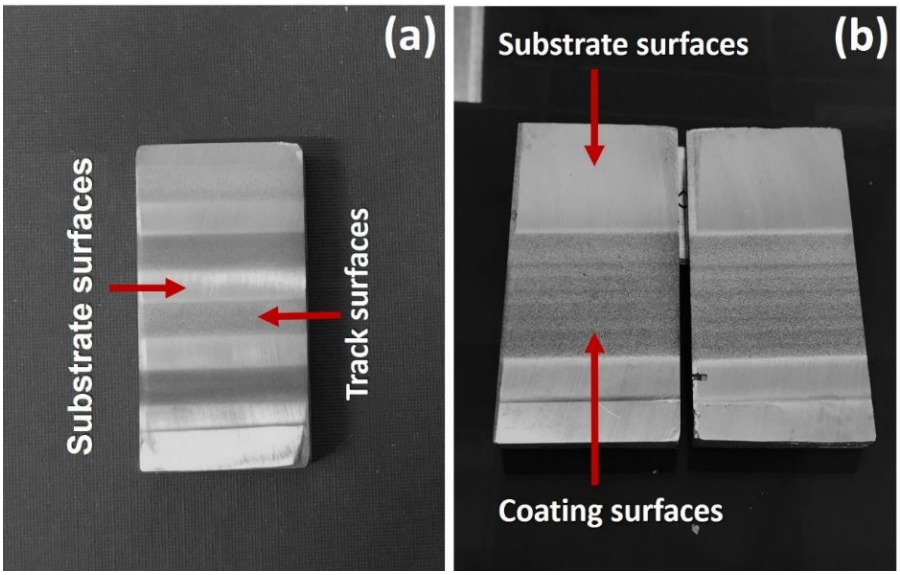


Figure 3-7: Digital images of cold-sprayed samples; (a) single tracks and (b) full surface coating.

Different types of powder were used as feedstocks for cold spray including pure aluminium, 6061 aluminium, satellited Al/TiC, simple-blended Al/TiC, satellited

6061/TiC and blended 6061/TiC. The lowest powder feed rate (with a feeding wheel speed of 0.5 rpm) with high traverse speed of (500 mm/s) were used to obtain individual deposits on a polished substrate for single deposit characterisation.

3.3.4 Annealing heat-treatment

The annealing process has been reported as an effective method for reducing the porosity of cold-sprayed Al coatings [160]. 6061 and 6061-TiC coating samples were subjected to an annealing heat treatment at 345°C for a duration of two hours. These parameters are well understood to relieve the strain hardening effects of cold-worked 6061 components [230, 236]. A Lenton tubular furnace (Lenton Thermal Designs LTD, UK) with an accuracy of ±5°C and heating rate of 10°C/min was used in the thermal treatment experiments. Argon was used as a shielding gas (1 l/min) during the heat treatment process in order to protect the sample surface from oxidation. The samples were furnace cooled to room temperature.

3.3.5 Laser Cladding Experiments

Two types of laser cladding experiments were performed to investigate the effect of the satelliting process on the behaviour of the composed powder within laser cladding. Powder injection laser cladding experiments were carried out using satellited and simple blended feedstocks. Results revealed that there is a clear difference between the two feedstocks when the powder injection method is adopted. This presented a need for another feeding method to examine the hypothesis that is used to explain the mechanism of interaction between the sprayed materials and the laser beam. Therefore, the pre-placed powder bed method was used for laser cladding the same feedstocks on the same substrates. There is a basic difference in the interaction mechanism between the powder injection and pre-placed bed methods; this would help to examine the suggested interaction mechanism of both feedstocks.

The powder-gas jet is focused towards the melt pool on the substrate surface at an appropriate angle [36]. This means that the cladding materials, which are in powder form, are affected by the stream features. Thus, there is a possibility for separation and blowing with different extents according to the characteristics of the particles. In terms of pre-placed powder laser cladding, a layer of the cladding materials is scanned by a laser beam to provide sufficient energy to melt the targeted powder and a layer of the substrate surface. When the cladding materials are heated by the laser beam, a melt front progresses throughout the powder bed, from the surface, which faces the laser radiations toward the substrate. When an adequate laser energy is available, the melt front will melt a portion of the substrate surface allowing the clad material to merge with the substrate material [36].

a. Powder injection laser cladding process

The powder injection laser cladding process is shown in the schematic diagram in Figure 3-8. A 2-kW ytterbium-doped fibre laser (IPG Photonics GmbH, Germany) direct energy deposition (DED) equipment was used in these experiments. The main components of laser cladding equipment were: IPG laser device, maximum power is 2.0 kW operating at wavelength of 1070 nm ± 6; the working table (CNC) controlled by a computer; Praxair (model 1264) powder feeder, USA feeds the powder through a side nozzle was tilted at 28° to the vertical; and operation system.

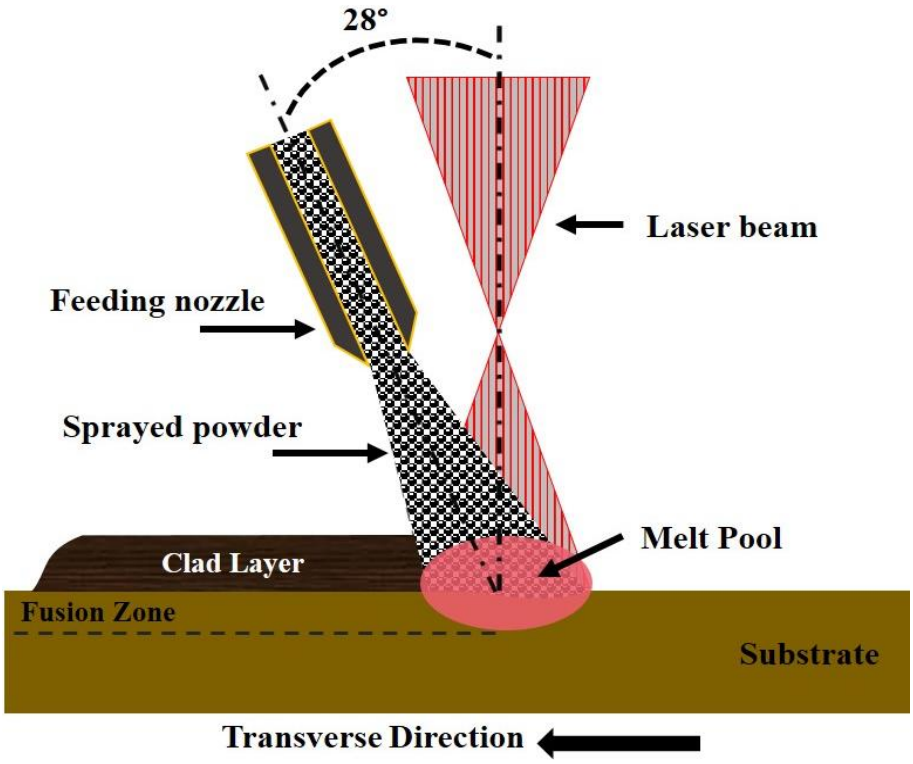


Figure 3-8: A schematic diagram of the powder injection laser cladding process.

The laser beam was transferred, focused, and observed by a beam delivery system (125 mm collimating lens and a 200 mm focussing lens). The feedstock is fed into a laser beam set to produce a beam spot diameter of 3.6 mm. The laser system was mounted on a 4 axis CNC table to traverse the 6082 substrate mounted on the

worktable while the laser beam is kept stationary. The operation space was shielded in an Argon enclosure to avoid oxidation of the deposited clads. The flow rate of a shielding gas was kept constant at 10 l/min; this is also permitted to cool under these conditions.

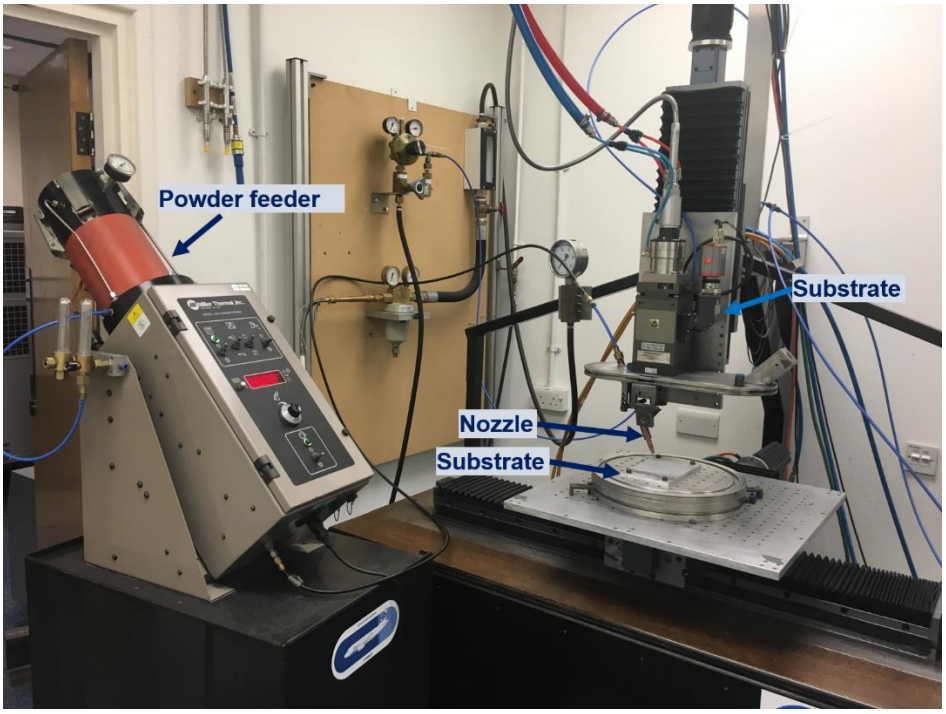


Figure 3-9: Digital images of the powder injection laser cladding system used in this work.

Three effective parameters were chosen as the most influencing processing parameters of laser cladding [183], laser power P(kW), laser scanning speed V (mm/s) and powder mass feeding rate F (g/m). The ranges of these parameters were set according to preliminary experiments. Based on a regular increase in one separate parameter and keeping other constant, the operative parameters that result in the deposition of continuous and well-bonded clads were specified. The use of combined parameters is essential to address the clad quality of the laser cladding process throughout minimizing the number of process variables [179].

Two combined parameters are thus determined in order to examine the effect of the processing parameters on clad quality and formability. The effective energy E_{eff} is adopted as an indicator that provides an amount of the delivered energy to the process by the laser [151]. This energy is basically carrying out heating/melting the substrate surface and powder stream and can be calculated by Equ 3- 1, [179]. Whereas the powder deposition density (PDD) provides a measure of the powder feeding rate during the process [179]. The powder deposition density is recognised as a function of effective deposition area, Equ 3- 2 is used to calculate the PDD.

$$E_{eff} = \frac{P}{V \times D_L} \quad (J/mm^2) \quad \text{Equ 3- 1}$$

$$PDD = \frac{R \times D_L^2}{V D_L \times D_P^2} \quad (g/mm^2) \quad \text{Equ 3- 2}$$

Where P is the laser power (w), V is the scanning speed (mm/s), and DL is the laser spot size (3.6 mm), and R is the powder feed rate in (g/min), and DP is the nozzle diameter (4 mm).

Three individual tracks of every parameter window were deposited on the substrate surface to confirm the repeatability of the process. The behaviour of the satellited feedstock under laser beam then studied to be compared with the blended feedstock. Preliminary starting experiments were done to identify the range of the working parameters of successful clads. The quality clads can be defined as a uniform-continuous clad with high density and homogenous microstructure, owning a strong metallurgical bond to the substrate but with low dilution [27]. Any shortage of one or more of the named characteristics could be defined as a defect in the deposited clad.

Based on preliminary experiments, the ranges of the laser power, scanning speed, and powder feed rate that can produce quality clads were examined. The values of

these parameters were as follows: laser power 1.25, 1.5, 1.75 and 2.0 kW; scanning speed 4, 6, and 8 mm/sec; powder feed rate 2, 4, and 6 g/min. Eventually, three energy densities; 104, 122 and 140 J/mm^2 were used to deposit clads. Similarly, four values of PDD were chosen: 0.0028, 0.0037, 0.0056 and 0.0075 g/mm^2, as these values led to the deposition of sound clads at different laser energy densities. Finally, a 3x4 sample matrix was adopted to examine the difference in behaviour and characteristics of the deposited clads of both feedstocks, see Table 3-3.

Table 3-3: The processing parameters of the laser cladding samples of blended and satellited feedstocks.

Blended samples			Satellited samples		
Sample No.	E_{eff} (J/mm^2)	PDD (g/mm^2)	Sample No.	E_{eff} (J/mm^2)	PDD (g/mm^2)
1	104	0.0028	13	104	0.0028
2	104	0.0037	14	104	0.0037
3	104	0.0056	15	104	0.0056
4	104	0.0075	16	104	0.0075
5	122	0.0028	17	122	0.0028
6	122	0.0037	18	122	0.0037
7	122	0.0056	19	122	0.0056
8	122	0.0075	20	122	0.0075
9	140	0.0028	21	140	0.0028
10	140	0.0037	22	140	0.0037
11	140	0.0056	23	140	0.0056
12	140	0.0075	24	140	0.0075

b. Pre-placed powder bed laser cladding process

Pre-placed powder LC was used to examine the difference in the behavior of blended and satellited feedstocks apart from the spraying materials. Powder beds

of blended and satellited materials with dimensions of 2 × 30 × 100 mm were placed on 6082 aluminium substrate. Two steel plates of 2 mm thickness were used for levelling the powder bed surface by passing another plate over the steel plates to spread the powder between them. Figure 3-10 shows the powder bed set up for the pre-placed powder bed laser cladding. Ar gas was also applied as a sheilding gas, it was located at the upper part of the working space so that the gas jet does not hit the powder bed to avoid the blowing action of the gas stream.

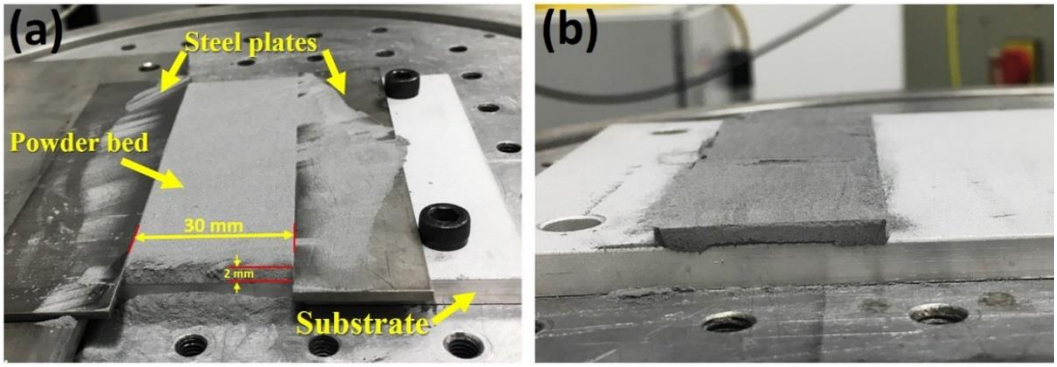


Figure 3-10: Powder bed set up prior to the pre-placed powder bed laser cladding.

4 Cold Spray Deposition of Pure Al-TiC Coatings using Satellited Powders

4.1 Introduction

This fundamental chapter includes all the satelliting trails for preparing a composite feedstock that suits cold spray in order to deposit Al/TiC composite coating by cold spray. The objectives of this investigation include the selection of the best particle size range, the binder amount, and other improvement processes. The aim of this chapter is the production of satellited particles that have the ability to carry fine ceramic particles and maintain the powder flow during cold spray. Preliminary satelliting processes were performed with different Al powders and different amounts of binder to produce a satellited powder. The prepared satellited powder then was used by cold spray to evaluate its cold-sprayability. Optimisation processes have been performed on the satelliting processes for producing satellited powder which suites cold spray. For comparison and evaluation purposes, three types of powders were used by cold spray: pure Al, blended Al/TiC and satellited Al/TiC.

The deposited coating samples were characterised using SEM images and image processing software. The results presented include microstructural evolution, porosity level, coating thickness, and TiC fractions in the composite coatings (blended and satellited). Thereafter, more satellited feedstocks with different TiC fractions were produced and cold-sprayed. The characteristics of the deposited coatings were determined in terms of porosity and coating thickness. Finally, the effects of satelliting on particle velocity and momentum were evaluated and discussed.

4.2 Preparation of composite feedstock for cold spray:

Initial experiments were performed for preparing a satellited Al/TiC composite powder, which achieves the requirements of cold spray processes. Satelliting has a distinct mechanism that depends on bonding two or more types of powder particles together using a binder. The satelliting trials were performed using different particle size ranges for both ductile and reinforcement phases. An irregular Al powder was used as a ductile phase, while an angular TiC powder was used as a reinforcement phase. Powders details are shown in Table 4-1.

Table 4-1: The processing parameters of satellited powder (mix_1).

	Material	Particle size (µm)	Particle shape	Fraction (%)	Added binder amount (%)
Ductile phase	Al	35-53	Irregular	88	2
Hard phase	TiC	<5	Angular	12	

Figure 4-1 shows the satellited AL-TiC powder (mix_1) with the processing parameters presented in Table 4-1. The Al particles are larger and darker, with round shapes, while the TiC particles appear smaller and brighter, with angular shapes. It can be seen that a significant number of TiC particles were attached to the Al particle surfaces. The powder mixture was then dried at 100 °C for 12 h, leaving a neglectable amount (~0.0007 wt.%) of solid PVA remaining in the feedstock after drying.

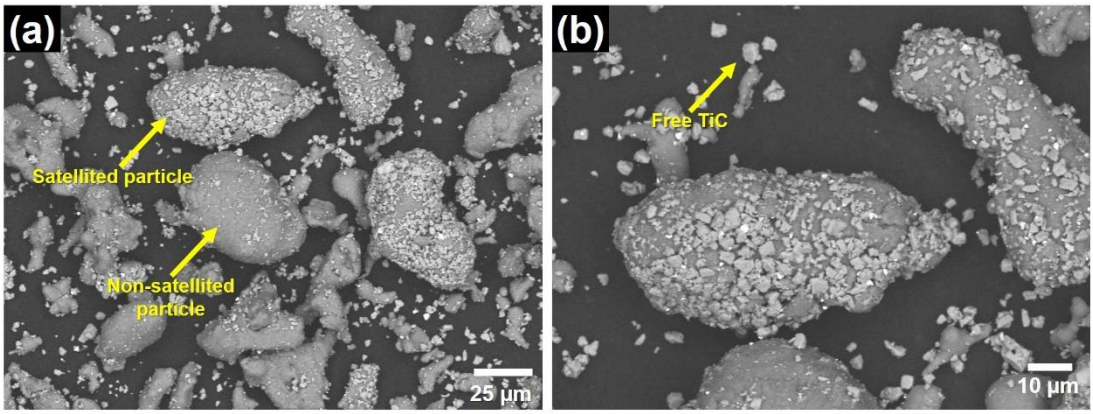


Figure 4-1: SEM images of the satellited powder (mix_1) at (a) X500, and (b) X1000.

It was found that 40% of the Al particles were successfully satellited while the rest were not. This was calculated by counting the number of Al particles which were covered by TiC particles on their surfaces compared with the total number of the Al particles appeared in the SEM image. Image-processing software (Image-J) was used to count the number of the satellited particles. The powder mixture was then dried at 100 °C for 12 h, leaving a neglectable amount (~0.0007 wt.%) of solid PVA remaining in the feedstock after drying.

A lot of free TiC particles can be seen not satellited, indicating an insufficient satelliting level was achieved. The existence of a large amount of loose fine TiC particles in the feedstock is undesirable for cold spray processes, (2.3.4). Therefore, an experimental plan was conducted to further optimise the satelliting process in order to minimise the free TiC, and in turn, increase the proportion of satellited Al particles in the feedstock.

Two approaches were used for enhancing the last satellited powder (mix_1) in order to raise the proportion of satellited particles and reducing the amount of free TiC particles. The first procedure utilised sieving of the satellited powder to decrease

the number of free TiC particles. The second procedure was to increase the amount of the added binder during the satelliting process to enhance the adhesion of free TiC particles to the Al particles. Figure 4-2 (a), shows an SEM image of the satellited powder after sieving.

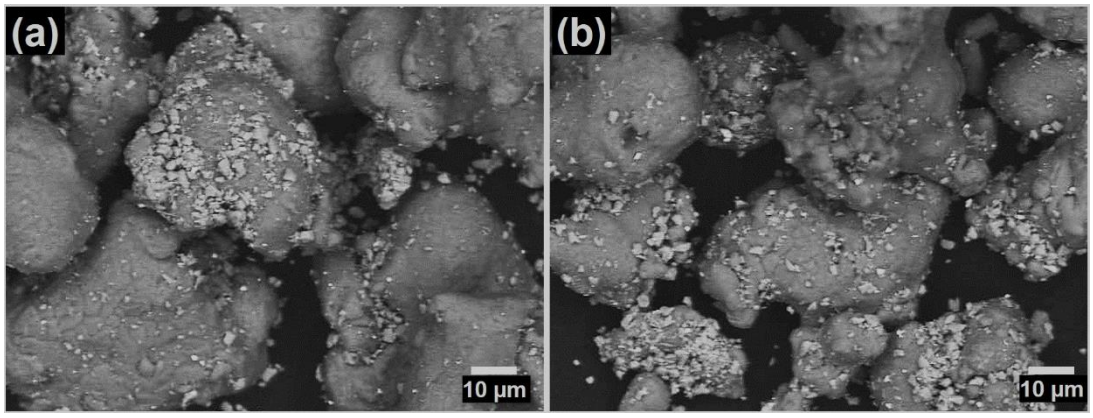


Figure 4-2: SEM of the satellited powder (mix_1) after (a) sieving the prepared powder; (b) increasing the binder by (20%).

It can be seen that the sieving process was effective in reducing the amount of free TiC in the satellited powder, as most of the free TiC particles are not present. However, the fraction of the satellited particles remains the same (40%) because the free TiC were extracted and were not being adhered to the non-satellited Al particles.

Figure 4-2 (b) shows an SEM image of mix_2, the processed powder after increasing the binder amount by 20%. It can be seen that there is a clear reduction in the amount of free TiC particles as they almost disappeared. Moreover, the amount of satellited particles have increased from 40% to ~70% (average of three images results). It seems that the additional binder amount has enabled more TiC particles to adhere to further Al particles compared to mix_1 feedstock. Consequently, this modified satelliting process has provided a promising composite

powder, with an acceptable level of satelliting (70% of the Al particles) with a minimized amount of free TiC particles.

The last satellited powder (mix_2) was used as a feedstock in cold spray preliminary experiments on Al 6082 substrates, to assess the suitability of the feedstock for cold spray using the process parameters shown in Table 4-2.

Table 4-2: Cold spray deposition parameters for single tracks.

Transverse speed (mm/s)	Stand-off distance (mm)	Stagnation pressure of main gas (bar)	Stagnation pressure of carrier gas (bar)
60	20	28	29

Figure 4-3 shows the SEM images of the cold sprayed sample surface. Although there was no continuous coating covering the substrate surface, many deposited particles from both particle types in the satellited powders (Al and TiC) can be seen on the surface. The deposits can be distinguished by the differences in the shape and colour of the particles, especially within the back scattered image (Figure 4-3-d), in which atomic number contras dominates. It is unreasonable to consider these deposited particles as a good coating, but simply scattered particles, given the majority of the substrate surface was not covered.

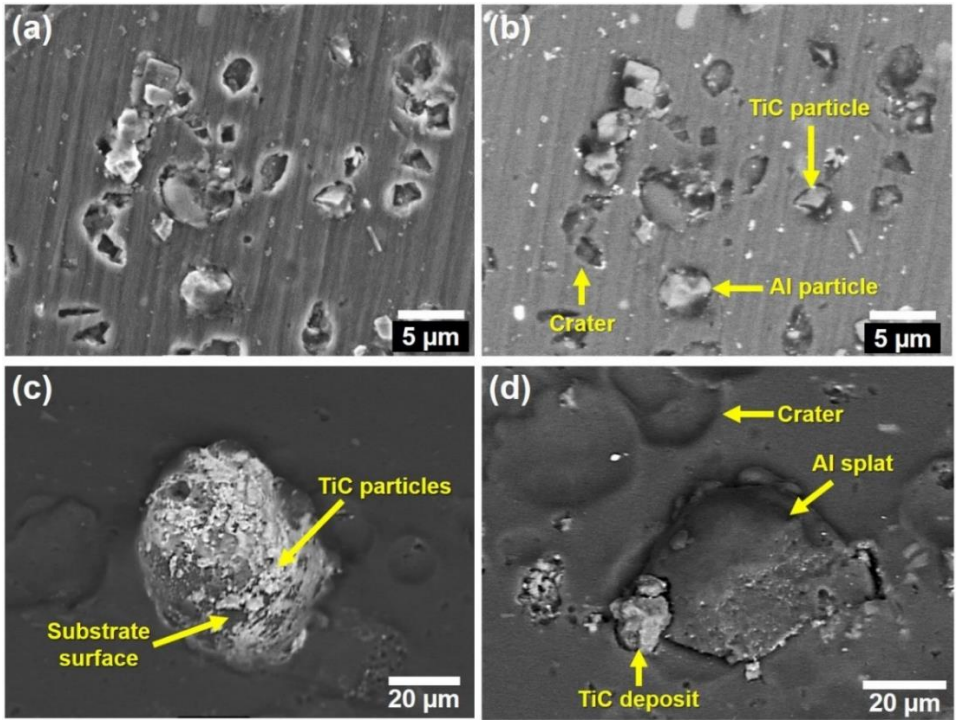


Figure 4-3: (a) SE and (b) BSE images of the substrate surface after cold spraying; (c) a BSE image of a crater produced by satellited particle, and (d) Al and TiC deposits.

In addition, there were several craters on the substrate surface indicating a lack of deposition due to insufficient local deformation at the particle –substrate impact surfaces. The crater sizes are much smaller than the Al particle size as most of the craters have a size below 15 µm, whilst the size range of the Al powder is 35-53 µm. Either the craters were produced by the TiC particles, which should make the craters angular in shape, or the craters may be caused by a weak impact of non-satellited Al particles. Both are possible as both round and angular shaped craters were detected. It is likely that most of the powder particles did not pass the critical velocity that should enable them to undergo sufficient local deformation which is required for deposition.

There are two potential reasons for this low velocity; the first is that most Al particles have a large size that may prevent them from attaining the required

velocity within used operation parameters. The second is related to the hard particles (TiC) on the satellited particle surfaces that may hinder the local deformation of the impacting Al particles. Figure 4-3 (c) shows a crater which is thought to be caused by a satellited Al particle, indicated by the fact the crater surface was covered by a layer of TiC particles. The TiC particles were delivered by a satellited particle and inserted into the crater surface due to the greater level of deformation and hence bonding caused by the satellited particle. However, the Al particle itself did not have sufficient velocity for deformation and bonding, causing the majority of the satellited particles to rebound from the substrate surface. On the other hand, small Al particles were deposited on the substrate (Figure 4-3-d), explained by smaller particles being faster than large particles within the same conditions (Equ 4- 1).

$$v_p \approx \left[\frac{C}{\sqrt{R\,T_o}} + \sqrt{\frac{\rho_p d_p}{C_d L_d p_0}}\right]^{-1} \qquad \text{Equ 4- 1}$$

Where;

v_p: In-flight particle velocity, C: Fitting parameter = 0.45 for Helium.

R: Gas constant = 2077 (J/kg.K^o), T_o: Gas stagnation temperature= 290 K^o.

ρ_p: Particle density (kg/m^3), D_p: Particle diameter (µm).

C_d: Drag coefficient (0.47 for sphere) L_d: Length of the diverging part of the nozzle (0.15 m).

P_o: Gas stagnation pressure (2.8 bar).

Therefore, in order to deposit a sound cold spray coating covering the full substrate surface, a slightly smaller size range of Al powder was used with TiC powder for

preparing a new satellited composite powder. Spherical Al powder (details are shown in 3.2.2) was used as a parent powder, Figure 4-4 (b). The spherical shaped powders are desirable for cold spray processes because they have good flowability compared to other morphologies [237]. Table 4-3 presents the details of the starting materials used to prepare the new satellited powder (mix_3).

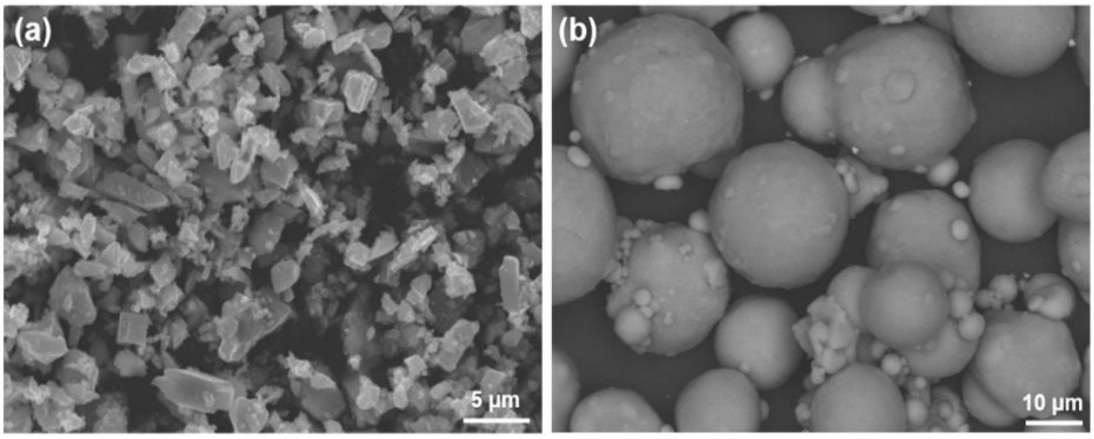


Figure 4-4: SEM images of the (a) virgin TiC, and (b) virgin Al powders used in satelliting of mix_3.

Table 4-3: The processing parameters of the satellited powder (mix_3).

	Material	Particle size	Particle shape	Fraction (%)	Added binder amount (%)
Ductile phase	Al	15-45 µm	Spherical	88	2.4
Hard phase	TiC	<5 µm	Angular	12	

Figure 4-5 shows SEM images of the new satellited powder. It can be seen that the small particles of Al and TiC are agglomerated together, producing many large clusters. It is suggested that the clusters were formed owing to the relatively large amount of the added binder, which makes small particles of both Al and TiC stick to each other. The clusters had a large size compared to the virgin powders, which can affect the flowability and velocity of the powder during cold spraying, subsequently impacting cold spray deposition performance.

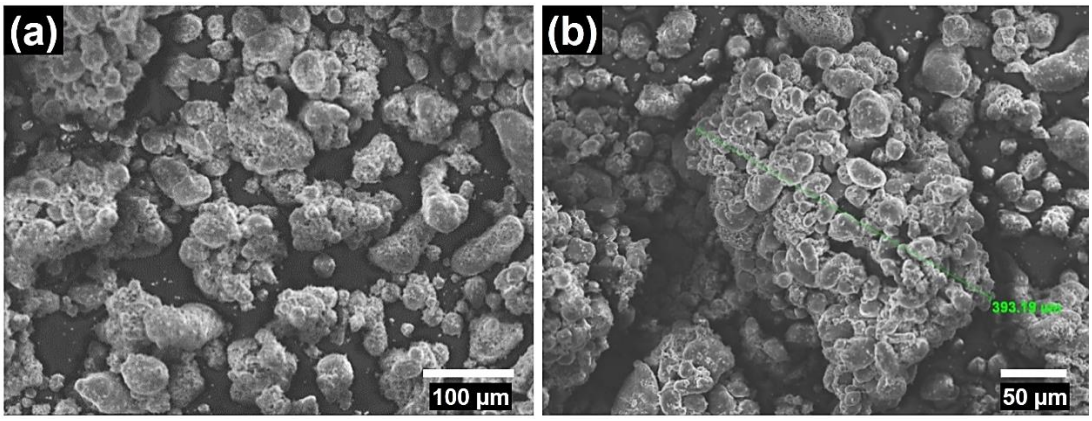


Figure 4-5: SEM images of the processed powder show the agglomeration of particles due to the high amount of binder.

Therefore, further improvement was needed to overcome the clustering in the feedstock. The amount of the added binder hence was reduced from 2.4 to 2%wt. in order to eliminate agglomeration during the satelliting process. SEM images of the final satelliting trial show that most of the fine (TiC) particles were successfully satellited to the Al particles, Figure 4-6. There this newly developed satellited powder can be considered as a more useful feedstock for cold spray in terms of particle shape/size and the low amount of fine loose particles. It can be concluded that the amount of the binder has an important effect on the satelliting processes as there ~60% of Al particles were satellited. Thus, the binder amount should be carefully adjusted according to the particle size distribution and morphology of the powders of starting materials.

Table 4-4: The processing parameters of satelliting (mix_3).

	Material	Particle size	Particle shape	Fraction (%)	Added binder amount (%)
Ductile phase	Al	15-45 µm	Spherical	88	2
Hard phase	TiC	<5 µm	Angular	12	

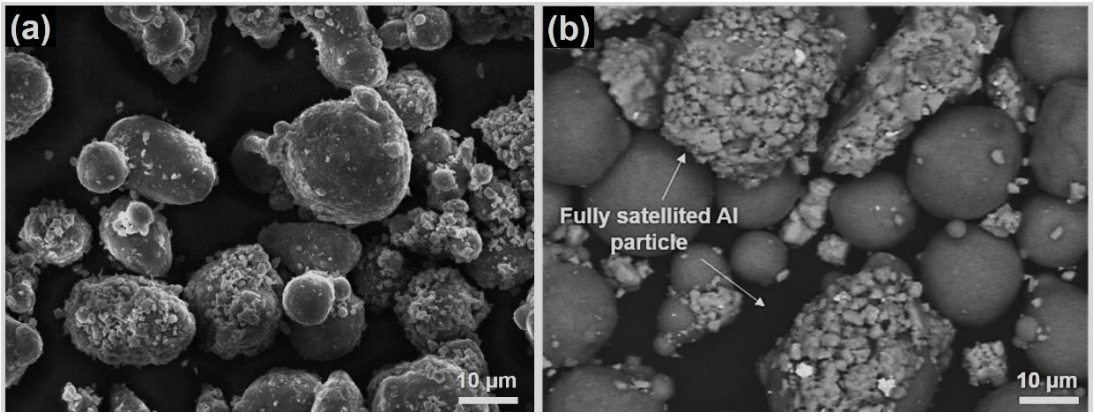


Figure 4-6: (a) SE and (b) BSE, SEM images of the satellited powder (Al/12TiC) after reducing the binder by 20%.

Several features make the large-spherical Al particles appropriate for the satelliting process. Firstly, large particles can easily receive the small-angular particles (TiC in this work) on their surface. This is because of their comparably wide surface area of the Al particles. Otherwise, it is unlikely for the spherical particles to adhere to each other because they have relatively large masses that need a large amount of binder. This can help in eliminating the formation of Al clusters during satelliting. Further, the single-point contact between the spherical particles [238] can deduce the friction force among the moving particles and then the powder flow would be improved.

Accordingly, large-spherical particles can keep their size/shape close to the original after satelliting. This may make satellited particles suitable for CS due to the possibility of getting a sufficient impacting velocity that depends on the particle size with fixing other factors. While very small parent particles could stick together producing large clusters with a complex morphology that can affect their flowability and speed during cold spray. Figure 4-7 shows a cross-sectional view of a satellited particles (mix_3). It can be seen the TiC particles take place on the

surface of the Al particle confirming the sufficient bond between the satelliting components.

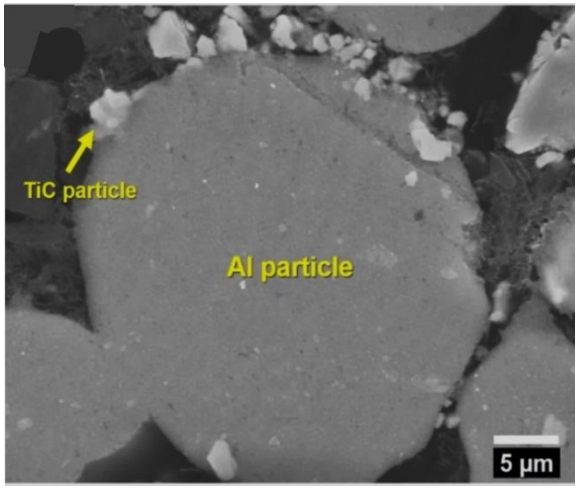


Figure 4-7: A BSE image of a cross-sectional view of satellited particles (Al/12TiC).

Consequently, it is recommended to use a spherical shape powder with a relatively small particle size as a major powder in the satelliting process to generate a cold sprayable powder. This can keep the particle flow and the velocity in an acceptable level to achieve sufficient velocity and in turn, sufficient local deformation which is needed to form bonding in cold spray. In addition, the bonding between the parent and satellite particles can keep them adhered as a block during the later process (spraying). This would be an effective way to change the behaviour of the fine particles during cold spraying which are usually undergo rebounding and blowing, this will be discussed in the next sections.

4.3 Effect of satelliting on the powder flowability

In order to investigate the effect of satelliting on the flow characteristics, the flowability of the virgin and prepared (blended/satellited) powders has been

characterized using FT4 Powder Rheometer (3.3.2). Four types of powder were examined: As-received pure Al, As-received TiC, simply-blended pure Al-20%TiC, and satellited pure Al-20%TiC. Figure 4-8 shows the measurements of the consumed energy during each 11 test points of each type of powder. All data points in this diagram are obtained from the average of three values.

Table 4-5 presents the main characteristics of the tested powders e.g. the stability index (SI) and the flow rate index (FRI). It also shows the basic flow energies (BFE) which were taken from test point number 7 of each sample as a key flowability parameter [235].

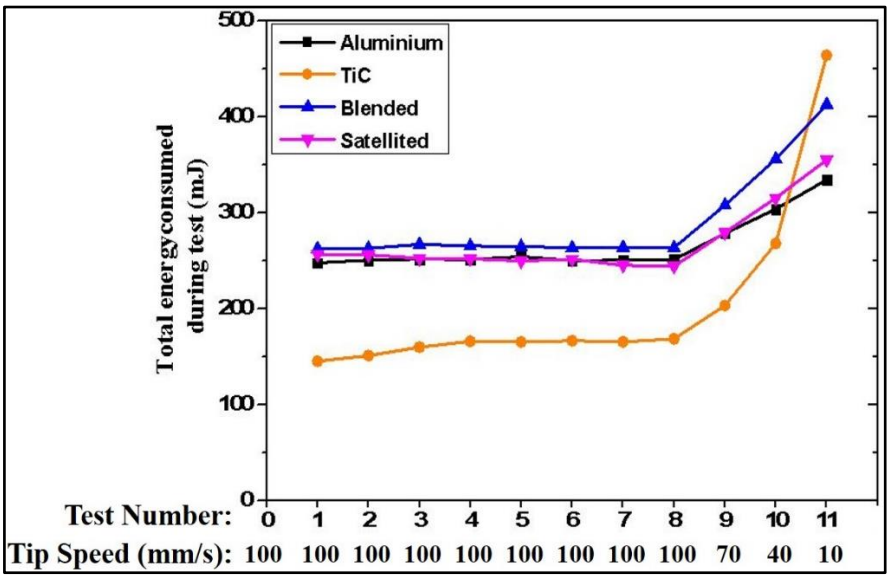


Figure 4-8: Rheology analysis of the virgin and composite powders, results are the average of three tests.

Table 4-5: The main flow characteristics of the tested powders (average of three runs).

	Al	TiC	Blended	Satellited
SI	1.01	1.13	1.01	0.96
FRI	1.33	2.75	1.60	1.41

BFE (mJ)	250.68 ±7	165.63 ±7	264.05 ±8	251.43 ±4

It can be seen that all the powders present a high level of repeatability in the first seven tests indicating stable rheology during the tests. This is confirmed by the values of SI of the powders Table 4-5. The FRI measurements in states that TiC powder has the lower flowability indicating by the larger FRI value (2.75) among other powders, as it consumed the larger energy at the final test point. This can be explained by that the higher surface areas of the fine-angular powders produce higher contact areas, which lead to an increase of the particle-to-particle and particle-to-blade friction [239]. In addition, the low compressibility (the reduction in powder volume in response to applied pressure [240]) of TiC as a ceramic powder can increase the resistance toward blade penetration during the test, consuming higher energy to carry out the test [235].

On the contrary, the pure Al powder presented the lowest FRI of 1.33 Table 4-5, with the lower flow energy among the other powders. The Al powder has a spherical particle's shape with a relatively large particle size (3.2.2). It is known that the spherical particles are most likely to have point contact with other particles that leads to a reduction in the inter-particle friction [241]. This can reduce the powder viscosity and then the flowability is improved [235]. Moreover, it is stated that the gravity and inertia of larger particles are normally greater than the inter-particle adhesion force, which means improved flow [233]. However, the inter-particle adhesion force in the fine particle powders is relatively significant compared to gravity.

Furthermore, the large particles have lower surface areas than small particles; this also contributes to reducing the friction resistance of large-particle powders [242], the required flow energy then decreased. This means that the spherical particles can move with less frictional resistance compared to the angular particles with similar size. Also, the relatively higher compressibility of Al, as a ductile material, compared to TiC made Al powder presents a higher flowability among other powders. This is due to the low force transmissibility and then lower friction and narrower moving zone.

The blended and satellited composite powders presented FRI values of 1.6 and 1.4, respectively; indicating an advanced flowability of the satellited powder compared to the blended. With regard to the blended powder, a combination of angular-fine TiC and spherical-large Al powders was formed. It is expected that the TiC particles take a place in the voids between Al particles, which decreases the compressibility of the blended powder and increase the contact around Al particles and reduce the size of voids, the friction then increases accordingly. This can reduce the flowability of the blended powder as confirmed by the higher dispersed energy by the blended powder (Table 4-5). Therefore, the powders with lower surface areas and higher voids present enhanced flowability results than powders with higher surface area and lower voids which means lower aerate.

It is stated that the satelliting technique significantly reduced the amount of free fine (TiC) particles in the satellited powders, (4.2). This was a result of attaching most fine TiC particles to the parent particle surfaces (Al). Thus, the satellited powder is consisting of relatively large particles and less fine particles with inter-particle voids (similar to the Al powder). Eventually, the satellited particles possess

desirable features that offer the advantages of the spherical particles. Thus, the satellited powder presented the nearest curve to the Al powder in terms of behaviour and consumed energy as most test points in the two curves have very close values, (Table 4-5). This can be confirmed by the measurements of the BFE of the Al and satellited powder as they presented very close values of 250 and 251 mJ, respectively. This similarity between the satellited and Al powders can explain the similar behaviour during the tests that made the results of both powders appear greatly close. Consequently, the satellited powder presents flowability results greatly close to the consisting parent powder (Al), which means a maintaining of good flow characteristics during the later processes.

4.4 Effect of satelliting on the in-flight particle momentum

It is known that the deposition of materials within cold spray is achieved from high-velocity impact and subsequent deformation of impact surfaces [243]. The high-velocity impacts result in adiabatic shear instabilities that provide a sufficient material flow and heat for creating solid bonds at the particle/substrate and particle/splat interfaces. High particle velocities are achieved by accelerating the feedstock materials via injection, using a carrying gas, in a de-Laval nozzle to achieve supersonic velocities (usually more than 500 m/s) [244].

Therefore, the velocity of the impacting particle is an important determining factor for bonding in cold spray studies, and it is worth investigating the effect of the satelliting process on the particle velocity in cold spray. Assadi et al., have established a numerical expression to calculate the approximate inflight particle velocity within cold spray [101]. In this formula, there are two divisions of factors, the first is related to the process variables like nozzle length and gas pressure, while

the second is related to the particle characteristics like the material density and particle size (diameter) as shown in Equ 4- 2.

$$v_p \approx \left[\frac{c_2}{\sqrt{R\,T_o}} + \sqrt{\frac{\rho_p d_p}{C_d L_d p_0}}\right]^{-1} \qquad \text{Equ 4- 2}$$

Where;

v_p: In-flight particle velocity,

R: Gas constant = 2077 (J/kg.K^o),

ρ_p: Particle density,

C_d: Drag coefficient = 0.47,

P_o: Gas stagnation pressure 2.8 bar.

C_2: Fitting parameter = 0.45 for Helium

T_o: Gas stagnation temperature= 290 K^o

D_p: Particle diameter

L_d: Length of the diverging part of the nozzle = 0.15 m.

After satelliting, the attachment of TiC particles on an Al particle surface will increase the Al particle mass, and the whole density will change due to the different density of the attached particles (TiC). For example, the satellited Al particles will receive an additional weight due to the attachment of TiC on their surfaces. Moreover, the added TiC will offer the satellited particle an additional volume that leads to an increase in the particle size by the size of the added TiC, so a new size (diameter) will be produced. A new density then can be calculated from the new weight and size of the satellited particle, and it is larger than the Al density because of the higher density of TiC compared to Al. This increase in particle mass leads to a reduction in the in-flight velocity of the satellited particle due to the increase in both density and particle diameter according to the particle velocity Equ 4- 2.

For example, for a satellited particle consisting of 80%Al and 20% TiC, the Al particles will receive an additional weight of 25% (13.6 %vol.) due to the attachment of TiC, assuming all TiC particles are evenly attached to the Al particles. For an Al particle with an assumed diameter of 45 µm, after receiving

13.6 %vol. TiC, the density of the satellited particle increases from 2.7 g/cm^3 (Al density) to 2.968 g/cm^3 (satellited particle density), this was obtained by determining the gross weight and volume of the satellited particle, depending on the weight and density of both Al and TiC. While the particle diameter increases from 45 (the original diameter) to 46.97 µm, this was calculated by adding the volume of the satellited TiC as a thin layer covering the Al particle surface. Therefore, the particle velocity has decreased from 740 to 711 m/s (4% reduction) due to the increase in both density and diameter of the satellited particle values in the Equ 4- 2. Also, the velocity of the satellited particles may undergo slight reduction due to the deformation of the particle surfaces due to the presence of satellite TiC particles. This may slightly increase the drag coefficient of the satellited particles, unless they maintain their spherical shape after satelliting.

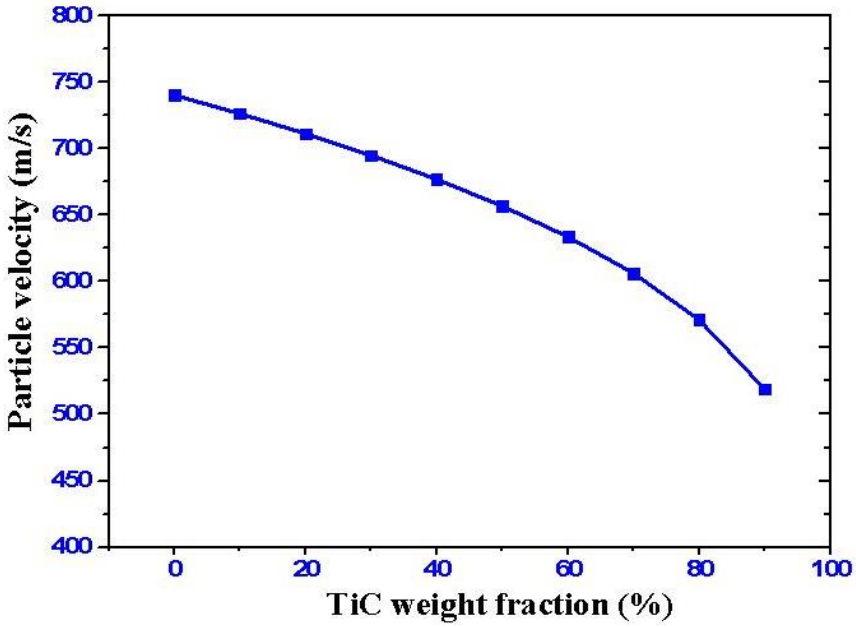


Figure 4-9: The reduction in the velocity of a satellited particle with increasing TiC fraction.

Figure 4-9 shows the decrease in particle velocities due to satelliting with different weight fractions of TiC. The particle velocity decreases with increasing the

satellited TiC, this is due to the increase in both size and density of the satellited particles compared to the non-satellited Al particle with the same size. This should be taken into consideration when satelliting is used for preparing cold spay feedstocks as multiple materials attached together require much higher particle velocity for deposition within the cold spray. Thus, appropriate processing parameters should be set when higher fractions of reinforcement are used.

On the other hand, it is found that the heavy, large cold-sprayed particles undergo a higher deformation compared to others that have less weights and larger maximum velocities [245]. This is because the heavier particles, which have a sufficient momentum, can overcome the effect of the bow shock region which is formed directly above the substrate owing to the impinging of the high pressure gas jet on the substrate. This effect (bow shock) can be avoided in the satellited feedstock as the fine TiC particles have been attached to the Al particles which have relatively large particle size. However, it can affect the fine TiC in the blended feedstock as most of TiC particles have a size range <5 µm. Otherwise, it was reported that the impact of relatively large particles can produce a considerable local plastic deformation due to their larger momentum [246]. Furthermore, Wei et al. have found that the tamping (compaction), which is produced by shot-peening of hard particles, is an effective technique for reducing the interlamellar porosity in the cold spray coatings [245]. They also stated that the large shot-peening particles provide a larger kinetic energy than smaller particles owing to their larger mass. This can result in producing denser coating structures due to the stronger tamping effect of large particles. Thus, it is very important to study the effect of satelliting on the momentum of the satellited particles.

The momentum of the satellited particle can be expressed by the new mass and velocity values of the satellited particle. The change in particle momentum after satelliting can be expressed using the changes in particle mass and velocity in the momentum equation (Equ 4- 3):

$$\boldsymbol{M = v \times m} \qquad \text{Equ 4- 3}$$

For an Al particle (not-satellited), the momentum is:

$M_{Al} = v_{Al} \times m_{Al}$

After satelliting; the particle velocity decreases by 4%, and the mass increases by 25% (assuming each satellited particle consists of 80%wt Al and 20%wt. TiC) thus:

$v_s = 0.96\, v_{Al}$; $m_s = 1.25 \times m_{Al}$

$$M_s = 0.96\, v_{Al} \times 1.25 \times m_{Al} = 1.2\, (v_{Al} \times m_{Al})$$

$$\boldsymbol{M_s = 1.2\, M_{Al}} \qquad \text{Equ 4- 4}$$

According to Equ 4- 4, the satellited particles gained on average 20% higher momentum than the non-satellited Al particles with the same particle size. This may explain the lower level of porosity in the satellited coatings with higher TiC fractions (4.6) due to the greater peening (compaction) action of the satellited particles. Figure 4-10 shows the increase in the momentum of a satellited particle with different weight fractions of TiC. It can be seen that the increase in the TiC fraction in the satellited powder can lead to an increase in the particle momentum despite the reduction in the particle velocity.

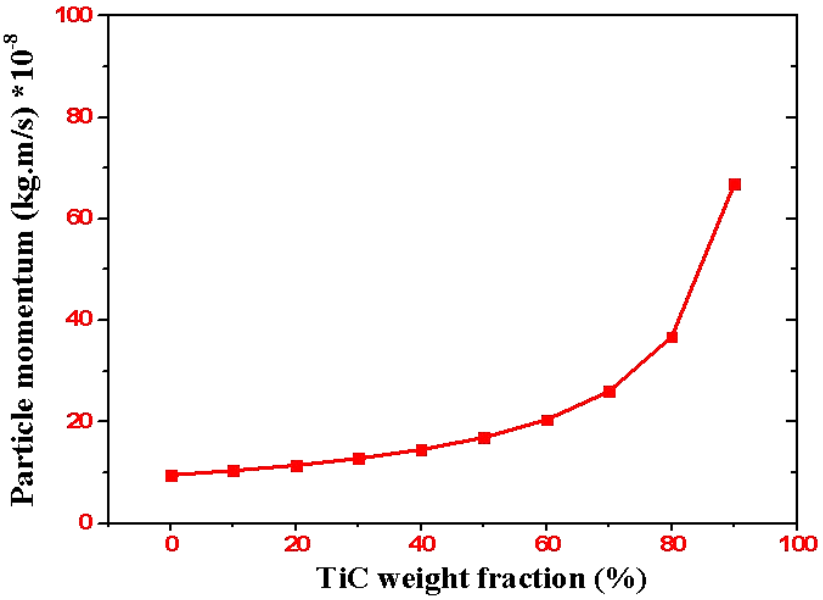


Figure 4-10: The change in the momentum of a satellited particle with different TiC fractions.

It can be concluded that the satellited particle that has a layer of hard particles with higher momentum has the ability to produce micro-asperities and a higher level of plastic deformation in the coating. This can facilitate the material deposition due to the increase jetting of the impact surfaces. In addition, higher particle momentum would produce a denser coating structure by reducing the porosity owing to the hammering (peening) effect of the satellited particles. Furthermore, the penetration of the satellited particles against the bow shock that occurs as a result of the impingement of the supersonic gas jet [247], due to their higher momentum, is an effective approach to avoid scattering of fine particles and then higher fractions of reinforcement can be embedded in cold spray coatings. Accordingly, the satellited particles have a combined effect of peening and material deposition as the peening effect occurs without particle rebounding.

4.5 Cold sprayed metal-ceramic coatings using satellited powder.

4.5.1 Composite feedstocks for cold spray processes.

In order to assess the 'cold-sprayability' of the (*mix_3*) satellited powder the powder was cold sprayed onto Al 6082-T6 plate substrates with dimensions of 6 x 25 x 50 mm. The satellited powder consisted of 88 wt.% Al and 12 wt.% TiC. For comparison purposes, a simply-blended feedstock of Al and TiC was also prepared by mixing the same powders with the same weight fractions but without the use of a liquid binder. A comparison between the mixed and satellited powders can be seen in Figure 4-11, where several Al powder particles are extensively covered in finer TiC particles.

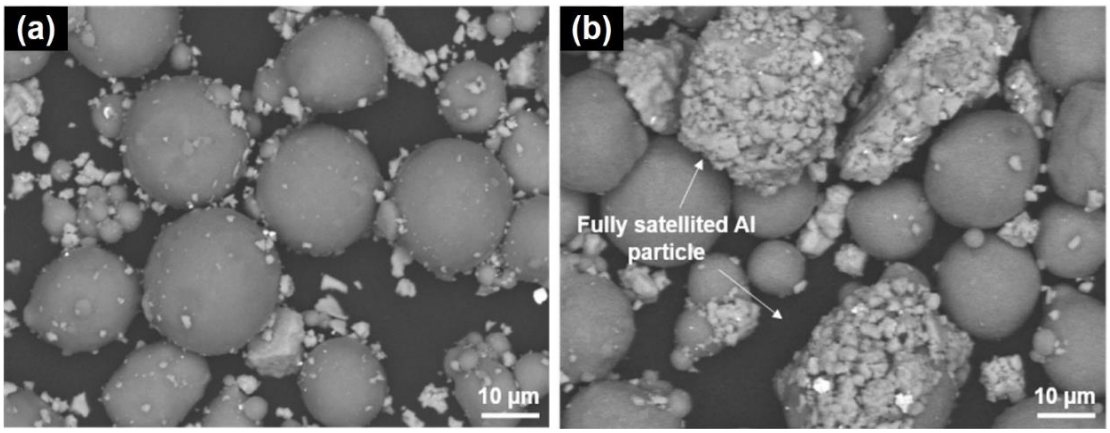


Figure 4-11: SEM image of the (a) blended (Al/12TiC) and (b) satellited (Al/12TiC) feedstocks.

The full details and set up procedure for the CS apparatus used is described in *Materials and Methodology* (3.3.3). The traverse speed of the spraying table in two-dimensions is computer-controlled, with the other three parameters considered as shown in Table 4-6. The main parameters used in the CS experiments (traverse speed, stagnation pressure of the main gas, stagnation pressure of the carrier gas, and the stand-off distance) were kept constant for all material types. Additionally,

fast-scanning using a single pass at 800 mm/s was used to produce individual deposits from pure Al, blended Al -12 wt.% TiC and satellited Al - 12 wt.% TiC.

Table 4-6: Cold spray deposition parameters for single tracks.

Traverse speed (mm/s)	Stand-off distance (mm)	Stagnation pressure of main gas (bar)	Stagnation pressure of carrier gas (bar)
60	20	28	29

4.5.2 Results and discussion

Figure 4-12 shows cross-sectional BSE SEM images of the deposited coatings (Al, blended, and satellited), with higher magnification in the right column. From these images, it is apparent that both interlamellar porosity, as well as the level of TiC deposition, are increased for the satellited coating. Also, the existing of TiC particles on the satellited particle surfaces can improve their distribution over the coating because the TiC may follow the distribution of the parent particles (Al).

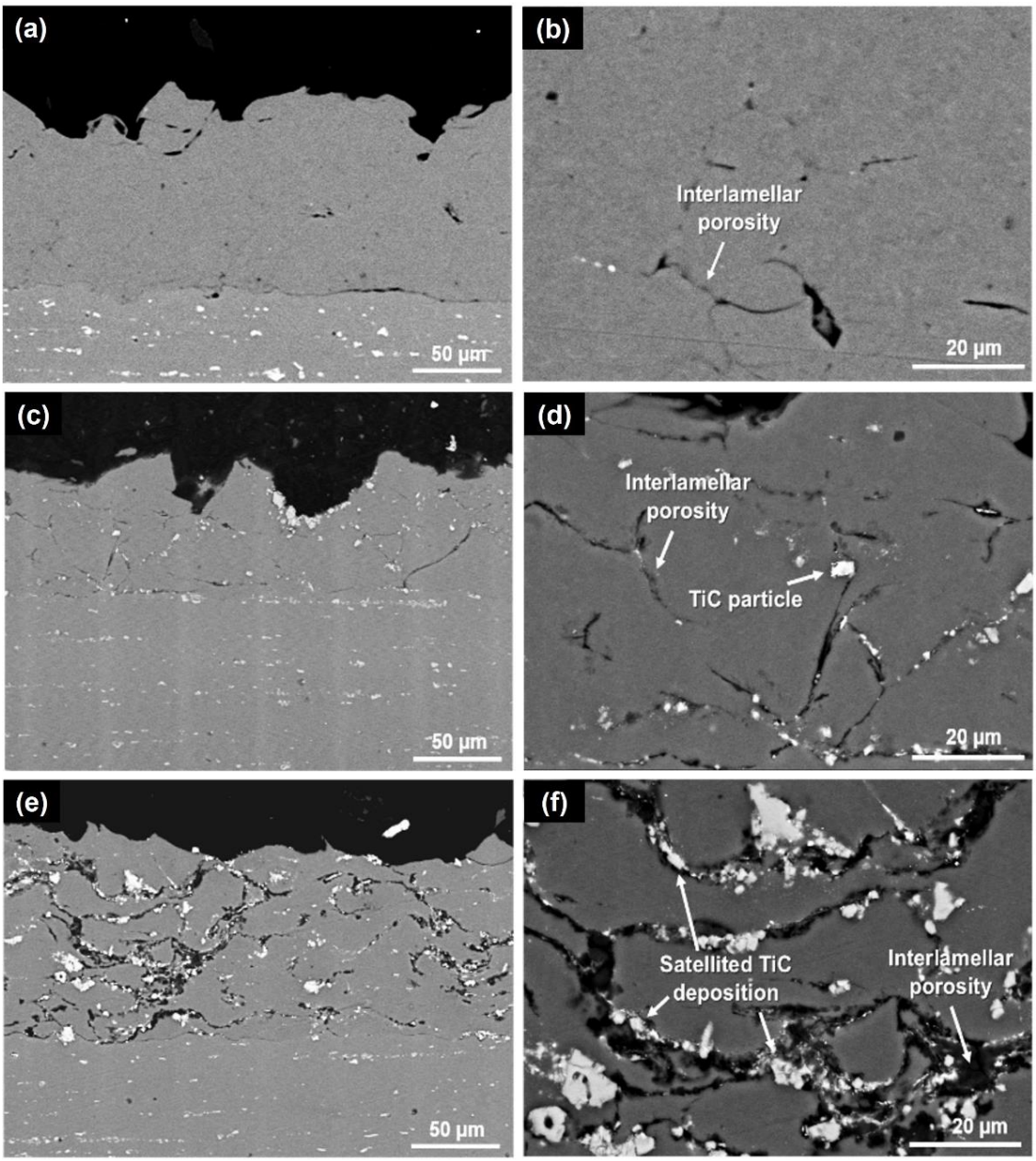


Figure 4-12: Cross-sectional BSE images at two magnifications and high magnification SEM images of the cold sprayed coatings showing particle/surface deformation of different feedstocks; (a and b) pure Al, (c and d) blended, and (e and f) satellited.

Image processing software (Image-J) was used to quantify the difference in porosity, TiC deposition, and coating thickness for the different coating types. Three 260*195 µm representative images of each coating section were analysed, and the average values were considered. Figure 4-13 the TiC area fraction,

measured from the cross-sections, showing a seven-fold increase in mean area fraction for the satellite powder coating compared to the coating made from simply-blended powder.

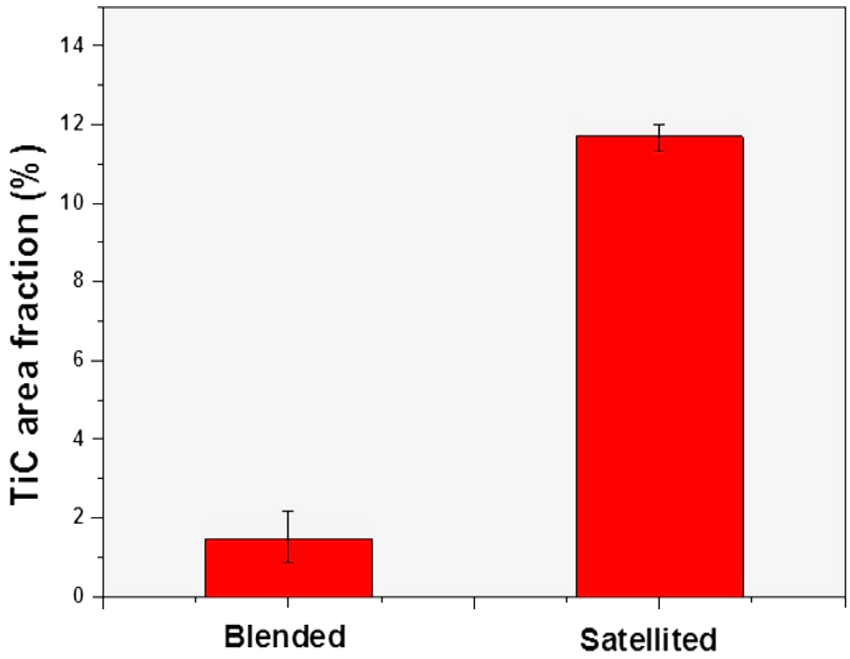


Figure 4-13: The percentage TiC area fraction in the different composite coatings, (b) the average thickness and the percentage areal porosity for the coatings, error bars represent the maximum and minimum values.

Figure 4-14 shows thickness measurements for the three coating types. A slight decrease in blended coating thickness, in comparison with both the Al and satellited coating, was measured. However, this coating was non-uniform in thickness, reaching an approximate minimum of 50 µm and a maximum of 100 µm. The pure Al and satellited coatings had a similar thickness of just over 100 µm and also a similar range of thicknesses and hence process repeatability is shown to be increased.

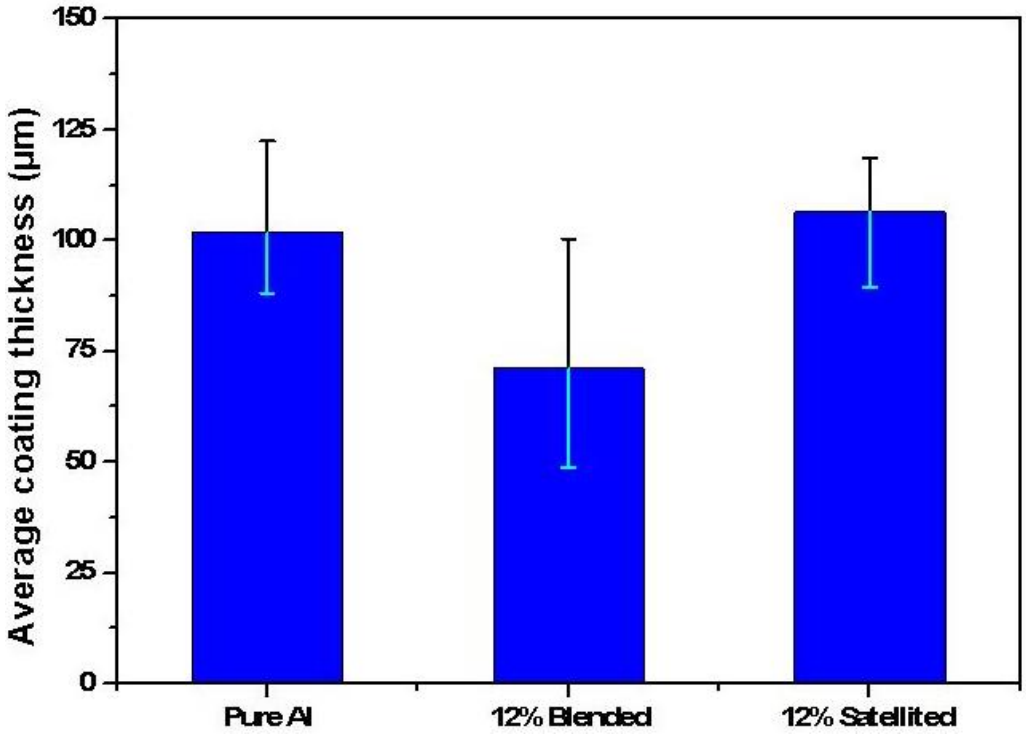


Figure 4-14: The average thickness of the deposited coatings, error bars represent the maximum and minimum values.

Figure 4-15 shows the porosity levels of the deposited coatings. To explain the porosity level within the coatings, we can consider the following. Generally, the cold-sprayed particles undergo two stages of deformation. The first stage is the high strain rate deformation of the particle with another particle or the substrate during bonding and the second stage of deformation is the further reduction in porosity due to peening effect of the other incoming particles on top of the bonded particle [248]. Generally, in cold sprayed coatings, large-plastic deformation considered as the main cause of producing high-density structures [249]. Thus, any lack of deformation at any side of a particle will most likely lead to the generation of interlamellar porosity.

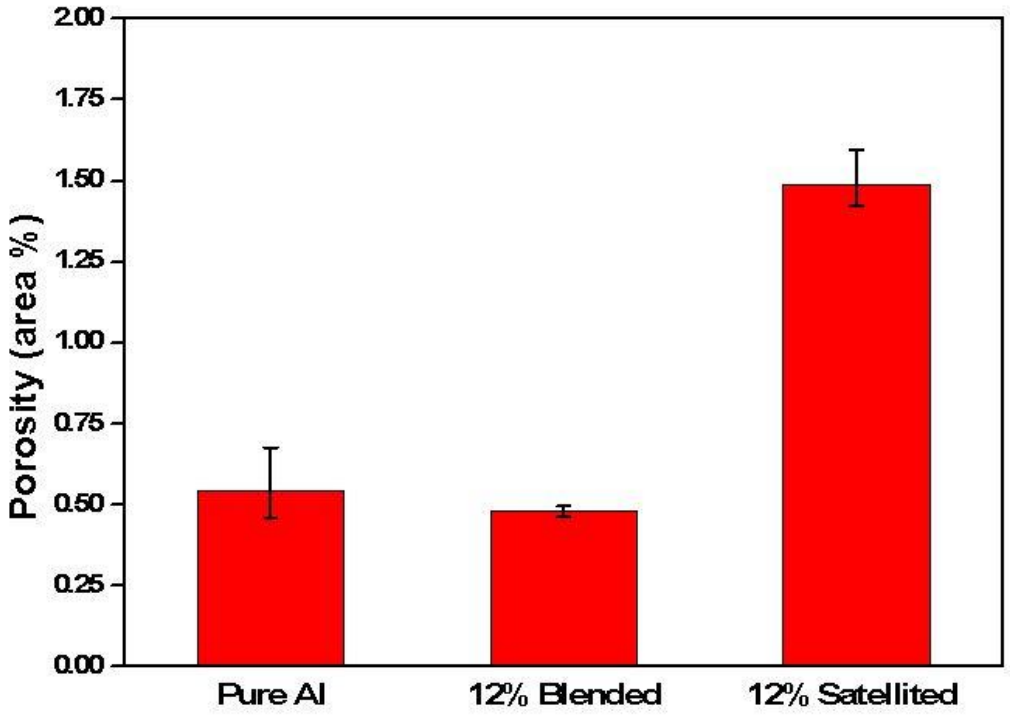


Figure 4-15: Mean percentage of areal porosity of the deposited coatings, error bars represent the maximum and minimum values.

Results confirm that the satellited coating has a relatively higher level of porosity (~1.5%), compared with the other coatings. This is likely due to the high presence of ceramic at the splat boundaries, where the hard phase hinders splat deformation from all sides. With regard to the blended coating, the larger fraction of Al particles and their large size provide deformable areas around TiC particles explains the lower level of porosity of this coating. A similar trend was observed by Guo et al. [66] where free ceramic particles were shown to be surrounded by metal splats in the cold-sprayed coatings.

From the observation of the TiC area fraction in the coatings, it can be concluded that the use of the satellited powder has greatly facilitated ceramic particles to be embedded into the deposited coating. This might be achieved by the elimination of non-ductile particles rebounding during cold spraying. To help elucidate the

difference in deposition mechanisms for the coating types, individual particle analysis was conducted both from the surface and in cross-section.

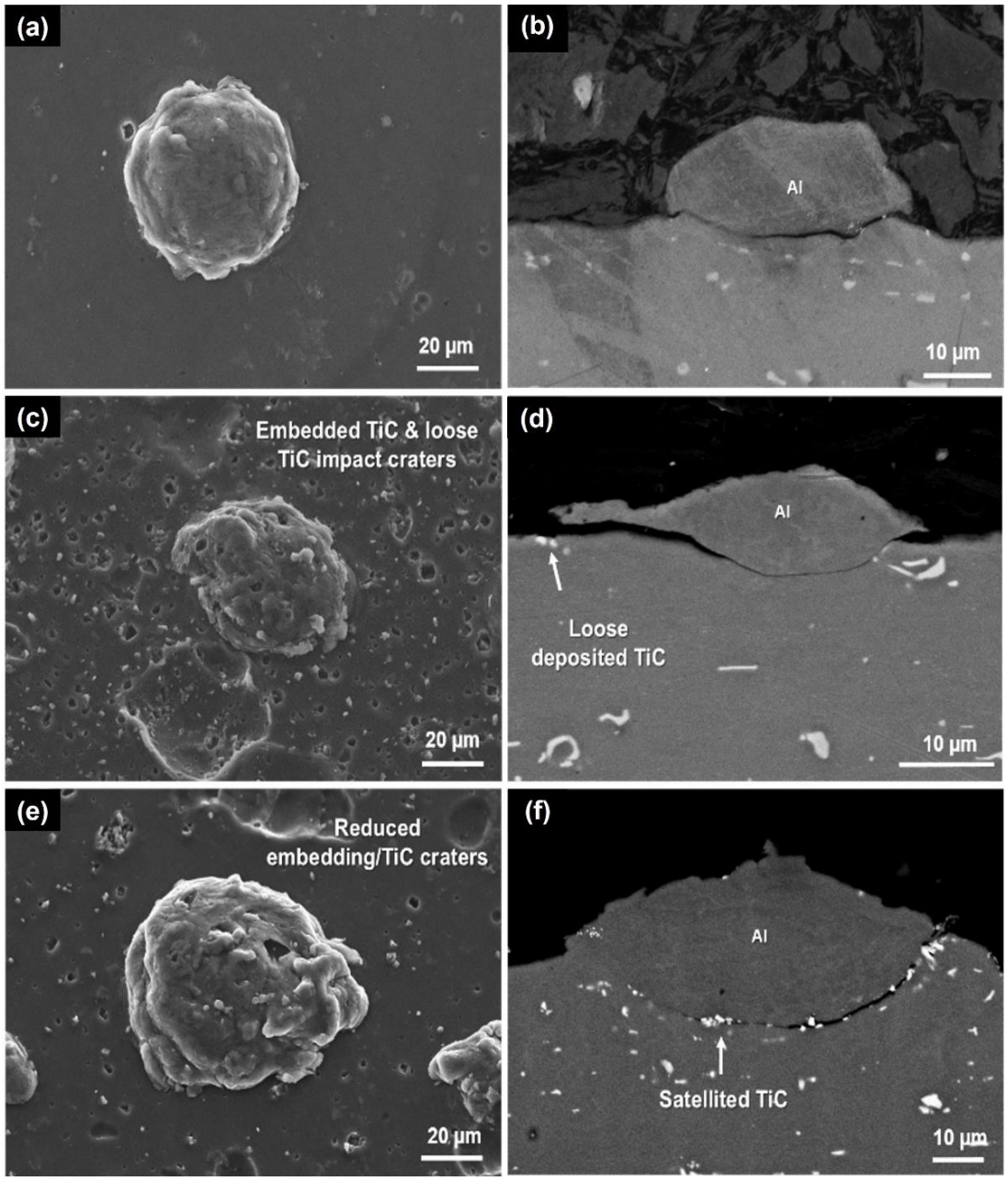


Figure 4-16: Cross-sectional SEM images at two magnifications of individual deposited particles; (a and b) pure Al, (c and d) blended, and (e and f) satellited.

Figure 4-16 shows cross-sections of particles deposited from the three feedstocks. In Figure 4-16 (a) and (b), individual-deposited Al particles can be seen on a

polished Al substrate. Of note is the substantially reduced cratering and embedding of TiC in areas peripheral to the Al particle in the case of the satellited powder. An average of a 74% reduction in cratering (measured using Image-J) in the non-deposit regions of the substrate surface was measured by dividing the number of craters per unit area. This difference can also be seen clearly in Figure 4-16 (c) and (e). This indicates that the satelliting between powder types is maintained to a greater extent throughout the spraying process. It is suggested that a high proportion of ceramic which was attached to the satellited powder will be embedded in the coating which is demonstrated by the high presence of ceramic in the associated coating.

In the blended cross-section, a deformed, deposited particle can be seen, with loose TiC deposited separately in the vicinity of the particle. For the cross-section of the satellited particle, TiC particles can be seen embedded beneath the deformed particle, and a slightly increased interlamellar porosity can be seen as a result. Significantly fewer TiC particles can be seen on top of the deposited particles, most likely due to them becoming detached as a result of impact stresses of the satellite particles.

Figure 4-17 illustrates the proposed mechanisms for the cold-spray process using blended (Figure 4-17 a) and satellited (Figure 4-17 b) powders containing a small, hard particle and a large, more compliant parent particle. In the case of the blended feedstock, the majority of TiC particles arrive separately from the large Al particles and predominantly rebound from the substrate surface after undergoing almost no deformation themselves. The relatively large range of thickness yielded by the blended powder can be explained by the inhomogeneity of the feedstock. A small

number of loose TiC particles remain embedded, but are insufficient to form a good composite coating. The high number of craters and non-satellited ceramic particles embedded in the substrate surface could not form a good coating due to low ductility.

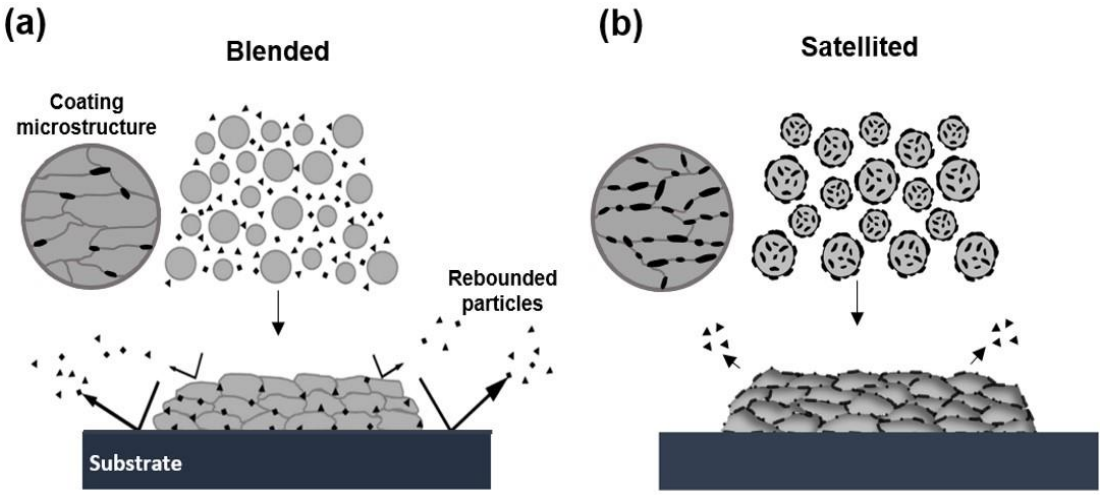


Figure 4-17: Schematic diagrams for two coating mechanisms using: (a) blended feedstock, (b) satellited feedstock

It is suggested that the satellited powder can deliver the majority of the satellited ceramic in the prepared feedstock to the coating. Satelliting can also help in improving the gas-solid flow characteristics by combining the two powders in one satellited phase which may decrease the turbulence in the powder-gas jet. Thus, the incident feedstock is composed of a majority of satellited particles. It is proposed that upon impact with the soft material substrate, particles underneath the incident particles are embedded within the interface between splats. Deposition continues as TiC particles beneath the deposited parent particles are embedded, gradually building up a composite coating. Higher deposition and higher porosity could mean that the satellited particles here need more compaction (peening) for reducing the coating porosity, this can be achieved by increasing the TiC fraction. In addition, there are some TiC particles that can be seen on the top surface of satellited coatings

and it is believed that the bond between TiC and Al particles enabled Al particles to hold ceramic particles after impact.

4.6 Cold spray of Satellited powders with different TiC fractions:

Satellited Al-TiC feedstocks with different TiC fractions were prepared to investigate the capability of satelliting different fractions of the reinforcement phase. This is useful for producing composite coatings with different compositions. Four TiC fractions were used to produce four satellited feedstocks, the basic details of the feedstocks are presented in Table 4-7.

Table 4-7: The basic details of the deposited coatings.

No.	Feedstock	Coating	TiC (%)	Al (%)	Mixing type
1	12%TiC (mix_3)	Sat_12	12	88	Satelliting
2	20%TiC	Sat_20	20	80	Satelliting
3	28%TiC	Sat_28	28	72	Satelliting
4	36%TiC	Sat_36	36	64	Satelliting

Figure 4-18 shows SEM images of the satellited feedstocks with two different magnifications. It can be seen that sat_20 has a good satellite level in terms of the fraction of the satellited particles and the amount of free TiC particles (Figure 4-18 (a) and (b)), which are almost eliminated in the feedstock. In addition, there are no Al or TiC clusters observed, indicating a successful satelliting process. By increasing the amount of TiC to 28%, some TiC clusters have been observed at the feedstock. There are some larger clusters consisting of Al and TiC particles agglomerated. This can be because of the higher exceed amount of TiC particles

has agglomerated assisted by the liquid binder producing TiC clusters. Al-TiC masses can be produced due to the adherence of some TiC particles to Al particles, Figure 4-18 (c) and (d).

After a further increase of the TiC fraction in the satellited feedstock to 36%wt., the amount of TiC clusters has increased, and the cluster size has increased as well. This is as a result of the presence of a higher amount of free TiC particles that attached to each other producing larger clusters compared to Sat_28. Clusters consisting of both Al and TiC were observed in addition to the TiC clusters, Figure 4-18 (e) and (f)). The existing of the high amount of clusters can significantly affect the flow spraying of the powder. Thus, the last powder (Sat_36) has been excluded after testing it by a funnel flow test prior to clod spray due to the poor flowability, wherein Sat_36 did not flow properly even with shaking the test funnel indicating bad flowability. The large clusters can also cause nozzle clogging during spraying which may lead to the system crashing or other issues.

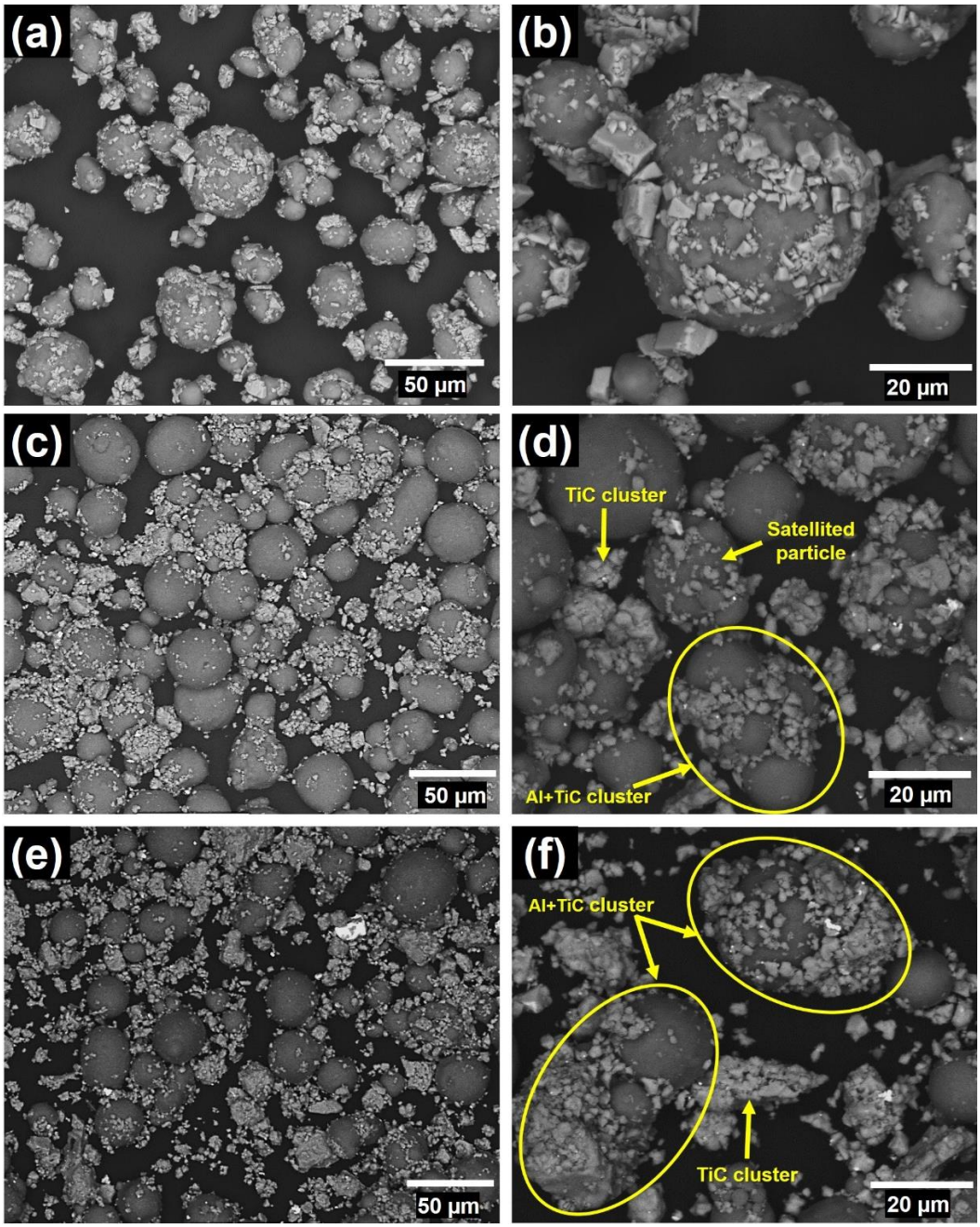


Figure 4-18: BSE images showing the morphologies of the satellited powders with two magnifications; (a and b) Sat_20 (c and d) Sat_28 (e and f) Sat_36.

Figure 4-19 shows typical cross-sectional BSE images of the deposited satellited coatings (Sat_20 and Sat_28) with two different magnifications. The irregular bright particles are TiC particles on the grey metallic Al matrix.

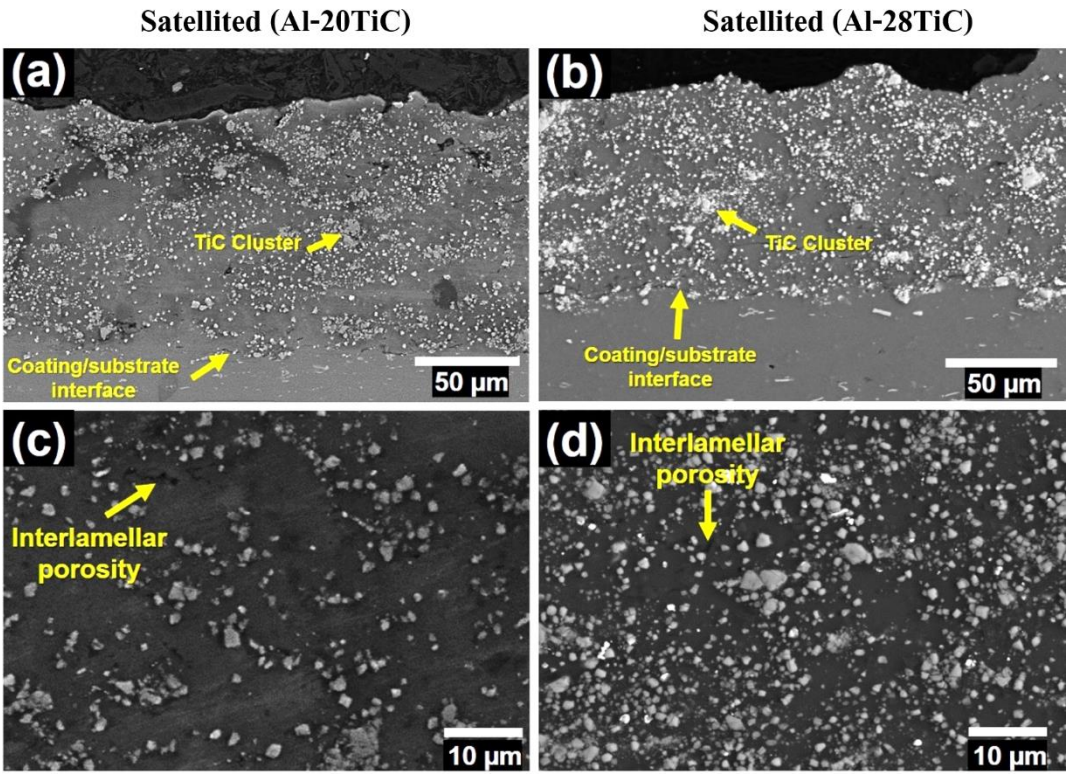


Figure 4-19: Low and high magnifications BSE images of the cold-sprayed coatings using (a) Sat_20 and (b) Sat_28 satellited powders.

The structure of Sat_20 coating is presented in Figure 4-19 (a) and (c). A cold sprayed coating was deposited with good adhesion to the substrate indicated by the disappeared interface line between the coating and substrate. It can be seen that a significant amount of TiC particles are evenly distributed through the coating section with few interlamellar pores. Figure 4-19 (b) and (d) show the cross-section morphology of the Sat_28 coating. The coating structure seems similar to the Sat_20 coating, however with smaller coating thickness and significantly higher TiC fraction including several TiC clusters. Both Sat_20 and Sat_28 coatings contain low interlamellar porosity indicating denser structures compared with Sat_12 coating that presented a greatly higher level of porosity.

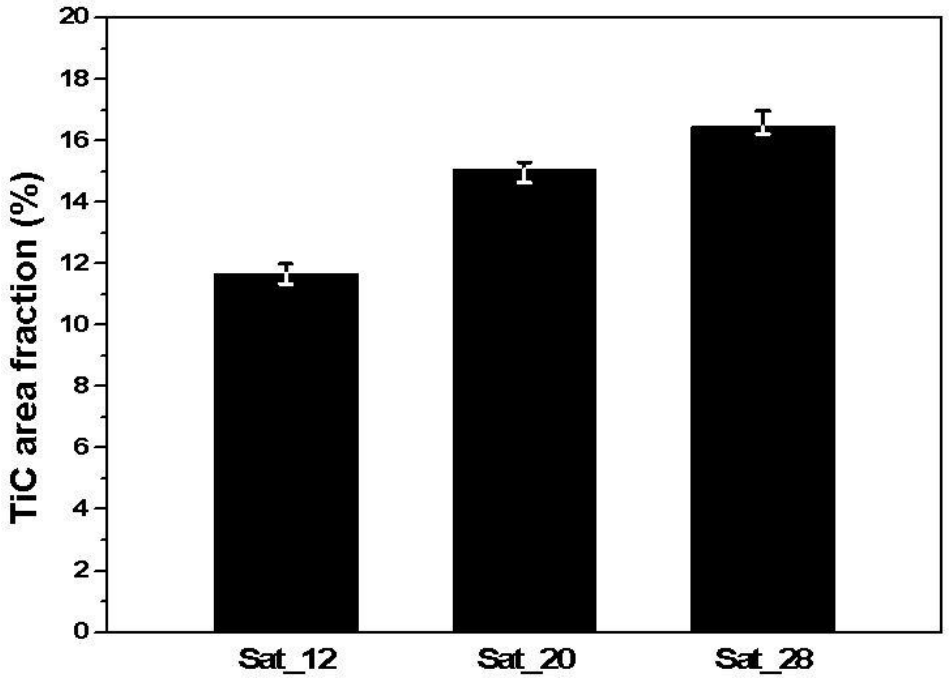


Figure 4-20: TiC fractions in the deposited coating sections measured using Image-J software, error bars represent the max and min values.

It is stated that there is a significant increase in TiC in the Sat_12 coating (Figure 4-12) compared to Blend_12 (4.3). In addition, it can be seen that increasing TiC fraction in the feedstock from 12% to 20% has led to an increase in the amount of ceramic in the coating section, as the Sat_20 coating presented a TiC fraction greater than Sat_12 coating by 30% (Figure 4-20). Furthermore, increasing the amount of TiC in the starting satellited powder from 20% to 28% also led to an increase in the TiC area fraction in the relevant cold sprayed coating by 23% compared with Sat_20 coating. This may confirm the ability of the satellited particles to deliver, for some extent, higher TiC fraction to the cold sprayed coatings.

Figure 4-21 shows the average thickness measurements of Sat_20 and Sat_28 coatings. The increase of TiC fraction in the satellited powder from 12 to 20% has resulted in an increase in the coating thickness by 36% compared with Sat_12

coating. This is indicated by the increased coating thickness of the relevant coatings. The improved material deposition can be explained by the contribution of the TiC in the satellited particles in facilitating the deposition of materials by the creation of asperities and increasing the local deformation of impact surfaces [117]. Also, the effects of satellited particles in promoting the local deformation at the impact surfaces can enhance the material deposition in CS coatings where the plastic deformation is the main factor for bonding. Similar results were also observed showing the clear contribution of ceramic particles in enhancing the bonding between the deposited Al splats as well as between the coating and substrate [126, 250].

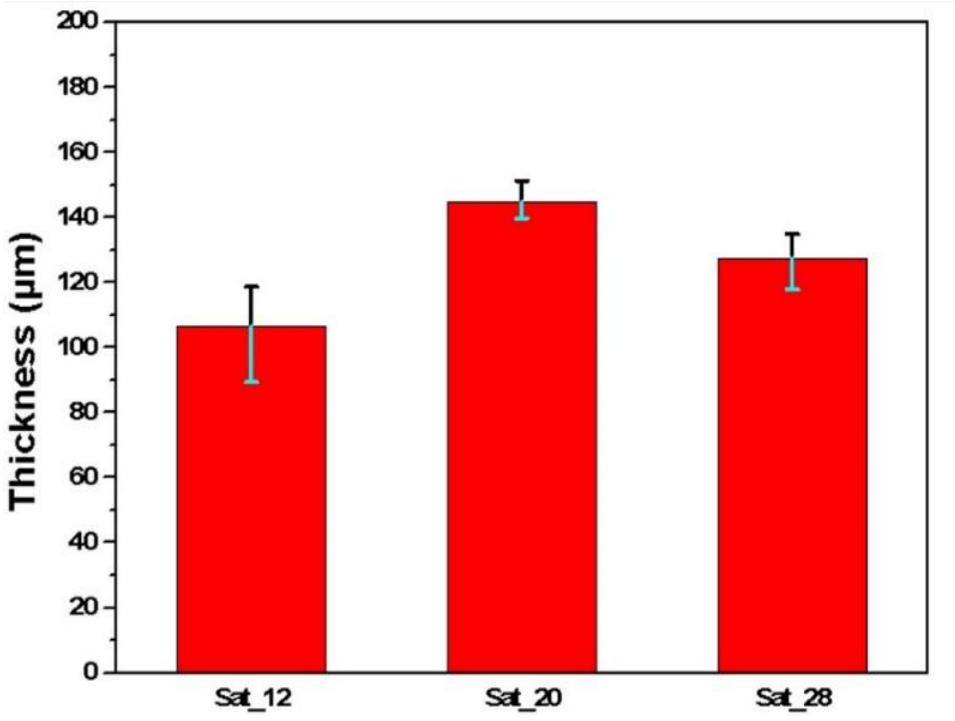


Figure 4-21: The average thickness of the deposited coating sections, error bars represent the max and min values.

The formation of micro-asperities that are caused by the ceramic particles was reported as an effective way for increasing the embedment of TiC and also the

deposition of the matrix material [117]. This is because of the asperities increase the contact area between the splats due to the surface roughening, while the embedded TiC particles produce an interlock between splats [251], and increase the local deformation at impact surfaces [250]. A similar trend was also observed in previous studies, as it was found that the addition of alumina particles to the Al feedstock enhances the deposition efficiency [252]. This was due to the peening and roughening actions of the layers during cold spray deposition.

Figure 4-22 illustrates the porosity levels in the deposited coatings. It is found that porosity has decreased in Sat_20 by a factor of 75% compared to Sat_12. In addition, the Sat_28 coating presented a porosity level close to Sat_20. It is thought that the compaction action of the satellited particles increases with increasing the amount of the satellited TiC particles. This is due to the increase in the momentum of the sprayed particles (Equ 4- 4) that increases the peening action of the sprayed particles [251]. In addition, there are some TiC clusters appeared in the higher TiC fraction satellited feedstocks (Sat_20 and Sat_28), this can increase the peening effect during cold spray which leads to a reduction in porosity level. Eventually, the compaction caused by the peening of the cumulative layers has contributed in the coalescence of some interlamellar pores, and that led to an enhancement of coating porosity measurements.

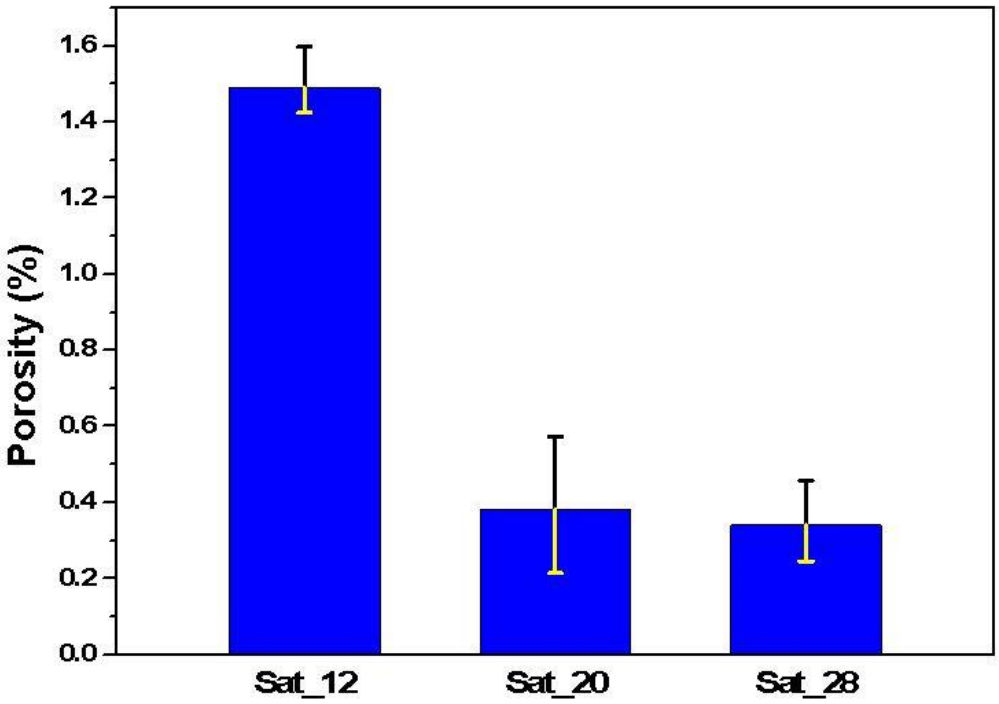


Figure 4-22: Interlamellar porosity levels in the deposited coating sections (average), measured by Image-J, error bars represent the max and min values.

Consequently, the satelliting process has been successfully used to produce cold sprayable composite powders with different TiC fractions; 12 wt.%, 20 wt.% and 28 wt.%. The experimental results have demonstrated that the distinctive deposition mechanism of the satellited feedstock and the high momentum of the satellited particles (4.4) have a great influence on the deposited coating characteristics. It is found that the use of the satellited feedstock significantly increased the embedment of the ceramic particles in cold sprayed coatings due to decreasing ceramic rebounding during spraying.

Additionally, the bond between TiC and Al particles in the satellited feedstock makes TiC restricted with the Al particles. This can improve the TiC distribution over the deposited coating sections. The large momentum of the satellited particles can produce an increased peening action during spraying which increases the

compaction in the deposited coatings. With these features, the satellited feedstock coating showed the higher thickness and a higher percentage TiC area to that of the blended feedstock one. The composite coating of 20% wt. TiC satellited powder (Sat_20), shows a lower level of porosity with a homogeneous structure between the coatings. Finally, Satelliting with this unique deposition technique can surpass the conventional mixing method of composite powders preparation.

4.7 Summary

It is concluded that, by using a unique preparation method 'satelliting' to bond hard TiC particles to larger Al particles, a composite feedstock has been produced. Satelliting has the advantages of a simple production procedure and no mechanical modification of the feedstock. The efficacy of this process is demonstrated by cold-spraying the satellited feedstock and comparing the coating morphology and TiC fraction with an equivalent, blended powder.

The satellited coating results show a significant improvement in yield of TiC embedded in coatings produced by cold spraying. The satellited feedstock shows good flowability which is very close to the starting Al powder. Although there is a slight reduction in the particle velocity, satelliting process maintained the suitability of the satellited powder for cold spray process and improved the peening in the cold-sprayed coatings. This novel approach can enable a range of materials to be used for the production of multi-component coatings via a wide range of processes.

5 Heat-treatment and mechanical properties of cold-sprayed high strength Al Alloys from satellited feedstocks

5.1 Introduction

In the previous chapter, the satelliting technique was used for the elaboration of composite coatings containing TiC particles in a pure Al matrix by cold spray. In the present, the effects of using the 'Satelliting' technique on the deposition and characteristics of A6061-TiC coatings fabricated by cold-spray are investigated. Cold spraying is used to create composite coatings of 6061 aluminium alloy reinforced with TiC particles on an A6082 aluminium substrate using optimised spray conditions previously determined. A6061 coating was also cold sprayed using identical process conditions for comparison. The satelliting technique was used to prepare the composite feedstock to eliminate the rebounding of the fine ceramic fraction in the CS process. Annealing heat treatment was applied to the composite CS coatings to improve porosity and cohesive properties of the coating structure. Additionally, a detailed hardness study is performed to evaluate hardness prior to and after heat treatment so the effect of heat treatment on the matrix as well as overall composite properties can be understood. Dry-sliding wear testing is performed to evaluate the contribution of the reinforcement material to as well as the effect of heat treatment on practical mechanical properties.

5.2 Experimental details

5.2.1 Materials

6061 aluminium alloy (simply 6061) was used as the parent powder and TiC as a reinforcement material in the satelliting process to prepare a composite satellited feedstock (6061-TiC) for processing by cold spray. This powder was also used as a 6061 feedstock for comparison (without satelliting or blending). The nominal chemical composition of this powder is shown in Table 3-2. The TiC powder has an angular shape with a particle size <5 µm with a mean particle size of 3 µm, see 3.2.4, UK. The binder was lab prepared by dissolving a 2.7% of polyvinyl alcohol (PVA) in 97.3% water by volume (4.05 g PVA in 100 g water).

For comparison purposes, simple blended 6061-TiC feedstock was also prepared by mixing the same powders with the same weight fractions but without the use of a liquid binder. Grit blasted 6082 aluminium plates ground using 240-mesh grit were used as substrates for CS with dimensions of 25 x 50 x 6 mm. The nominal chemical composition is shown in Table 3-1. SEM imaging was used to confirm successful satelliting of the powder, as shown in Figure 5-1. Significant coating of the large aluminium particles by TiC can be seen, however it should be noted that some particles are not successfully coated given the stochastic nature of the mixing process and in particular difficulty in achieving a uniform spread of binder.

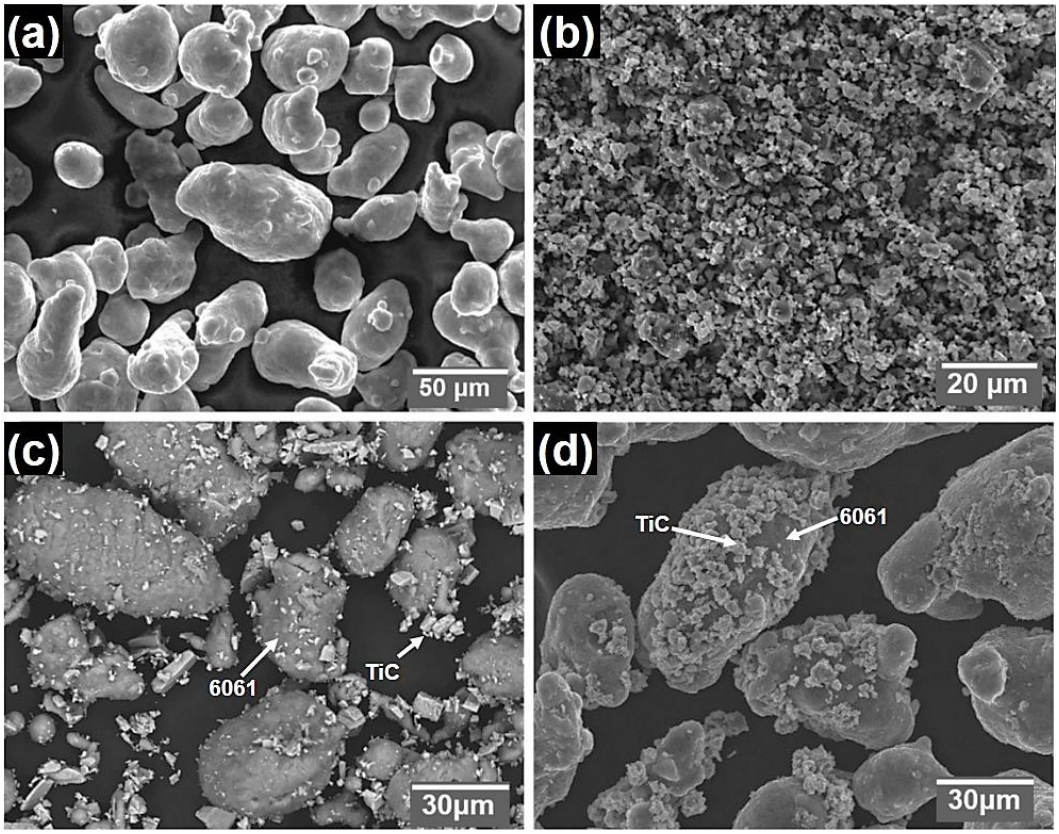


Figure 5-1: SEM SE images showing the morphology of (a) virgin 6061 powder (b), virgin TiC powder, (c) blended feedstock (6061-TiC) and (d) satellited feedstock (6061-TiC).

Figure 5-2 shows the particle size distribution of the 6061 and 6061-TiC feedstocks. This is a useful way of illustrating the extent of satelliting. The results show that the majority of TiC particles were satellited as only 25% of the TiC amount are a presence in the satellited powder as shown in the data in Figure 5-2 (d). This was calculated by converting the volume fraction of the free TiC that presents in the particle size distribution data into weight fraction by considering the density of TiC. This implies that 75% of the added TiC by weight was satellited to the Al particles.

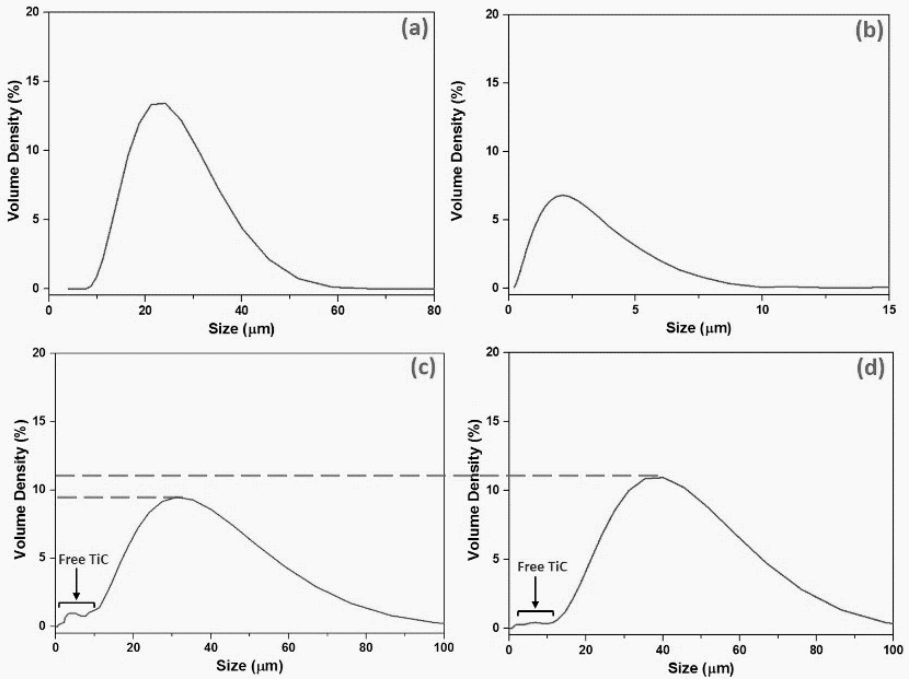


Figure 5-2: The particle size distribution of (a) 6061 powder (b), TiC powder, (c) blended feedstock (6061-TiC) and (d) satellited feedstock (6061-TiC).

5.2.2 Cold spray

Cold-spraying was performed to create individual tracks of 6061, blended 6061-TiC and satellited 6061-TiC on Al substrates. The CS system used for this work is a custom-built system described in detail elsewhere [253]. The system consists of a helium and nitrogen gas pressure system, a commercial powder feeder (Praxair 1264HP, Indianapolis, IN, USA) with a 12-slot feeding wheel, which has a changeable rotating speed. The gun is a steel de-Laval nozzle with a throat diameter of 1.35 mm, an area expansion ratio of ~ 8.8 and a divergent section of 150 mm length. The nozzle exit diameter is 4 mm. The standoff distance between the nozzle and the substrate surface was fixed at 20 mm. The traverse speed of the spraying table in two-dimensions is computer-controlled using an interfaced system. Helium at 2.8 MPa was used in the spraying system for the primary accelerating gas at room temperature, while nitrogen was used as the powder carrier gas at 2.9 MPa. Helium

working gas was used due to its better performance at lower pressures. Substrates were clamped onto the spraying table, which controls the relative motion between the substrate surfaces and the nozzle.

Primarily, fast-scanning cold spray experiments, using a single pass at 800 mm/s, were used to produce individual deposits from Al6061 to evaluate the deposition of the Al. Then, the main parameters used in the CS experiments were kept constant for all material types as shown in Table 5-1. Image-J software (USA) was used to analyse the thickness and porosity of the deposited coatings using three SEM across the length of the coatings using images of 250 x 350 μm to provide averages.

Table 5-1: Cold spray deposition parameters for single tracks.

Transverse speed (mm/s)	Stand-off distance (mm)	Stagnation pressure of main gas (bar)	Stagnation pressure of carrier gas (bar)
60	20	28	29

A Buehler Microhardness machine (USA) was used for microhardness testing on coating cross-sections, using two loads 10 and 50 gf and a dwell time of 15 s. The average of 10 Vickers microhardness measurements was used to provide mean hardness values. The distance between every two consecutive indents was kept 5 times more than the indent size to avoid the influence of nearby indents on the next indent. To examine phase composition of the sprayed coatings, a Siemens D500 X-ray diffraction instrument was used, with a wavelength of 0.15406 nm (Cu k-alpha), a 2θ range of (30^o-90^o) and step size and step time of 0.05° and 2 s, respectively.

Ball-on-flat reciprocating dry-sliding wear tests were performed using AISI steel ball (grade 440c) with a hardness of 800 Hv, and 6 mm diameter as a counter body at 5 N normal load. A CETR Universal Micro-Tribometer 3 (USA), was used for

all wear tests, using a linear displacement amplitude of 5 mm and 1 Hz frequency for a duration of 10 minutes. A sample of 25 x 50 mm of each coating type was prepared for wear tests, using an overlap cold-spray strategy. The coated area was 35 x 25 mm with an average thickness of ~300 μm.

All coating surfaces were polished to a mirror finish using standard grinding and polishing steps, finishing with a 1 μm diamond polish prior to testing. Three tests were performed on each sample to confirm result reliability. An Alicona Infinite Focus variation microscope was used to measure wear track volume. The specific wear rate (SWR) was calculated using the following formula, Equ 5- 1:

$$\text{SWR} = \frac{\boldsymbol{wear\ volume(mm^3)}}{\boldsymbol{load(N)*distance(m)}} \quad (\text{mm}^3/\text{N.m}) \qquad \text{Equ 5- 1}$$

Where the wear volume is the track area (average) multiplied by the track length (5 mm), the load is 5 N and the total worn distance during the test is 6 m. SEM was used to analyse the worn surfaces of wear tracks.

5.2.3 Heat treatment

Satellited 6061-TiC coating samples were subject to an annealing heat treatment at 345°C for a duration of two hours. These parameters are well understood to relieve the strain hardening effects of cold-worked 6061 components [230, 236]. The annealing process has been reported as an effective method for reducing the porosity of cold-sprayed Al coatings [160]. It has also been reported that the metallurgical bond in the cold-sprayed coatings has been enhanced throughout the annealing process due to the solid-state diffusion that occurs [164]. A tubular furnace (Lenton Thermal Designs LTD, UK) with an accuracy of ±5°C and heating rate of 10°C/min was used in these experiments. The samples were furnace cooled

to room temperature. Argon was used as a shielding gas (1 l/min) during the heat treatment process in order to protect the sample surface from oxidation.

5.2.4 Deposition efficiency

The deposition efficiencies were calculated as the ratio of the coating deposition weight to the mass of the sprayed powder during the processing time [254]. The prepared aluminium substrates of 6082-T6 alloy plate were weighed on a digital electronic balance before the spray, then the coated substrates were weighed (after spraying) to calculate the weight of the deposited coatings. The total track length is obtained by multiply the number of the CS passes by the actual sample width, the processing time on each sample then can be determined by dividing the total track length by the traverse speed (60 mm/s).

The actual powder feeding rate was calculated by weighting the dropped powder from the powder feeder during a period of time (30s), with using the same rotational speed of the feeder. The weight of the sprayed powder during the processing time thus obtained by multiply the powder feeding rate by the processing time. The deposition efficiency was then measured by dividing the coating weight by the sprayed powder weight. The above procedure was repeated for each type of feedstock because of the different densities and powder characteristics.

5.3 Results and discussion

5.3.1 Coating characterisation: Al 6061 vs Al6061- TiC

Figure 5-3 shows top views of the sprayed surface containing individual deposits of Al6061 produced by fast-scanning cold spraying, using a single pass at 800

mm/s. It can be seen that there are several deposits on the substrate surface with few craters, Figure 5-3 (a). The high magnification image of the single deposit states that the Al particle was deposited with good bonding to the substrate surface. This can be indicated by the jetting libs that are known as one of the leading mechanisms for successful bonding between deposited splats [255].

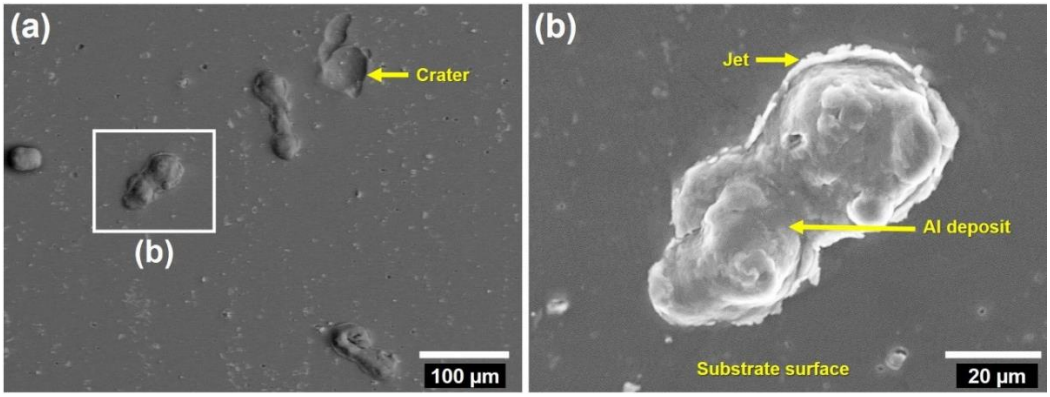


Figure 5-3: Top-view SEM images of the sprayed substrate surface, showing deposited splats and craters produced by a 6061 particle at low (a) and high (b) magnification.

Typical cross-sectional BSE images of the 6061 and 6061-TiC coatings are shown in Figure 5-4. The structure of the 6061 coating is presented in Figure 5-4-a. The 6061 particles were deformed on impact as is typical to cold-spray. Figure 5-4-b shows the cross-section morphology of the blended 6061-TiC coating, wherein the irregular bright particles are TiC particles on the grey metallic matrix. Both 6061 and blended 6061-TiC coatings contain significant interlamellar porosity and open boundaries in their structure, distributed over the coating. In addition, the interface of the coating/substrate can be clearly seen.

Figure 5-4-c shows the cross-section morphology of the satellited 6061-TiC coating. A higher level of local deformation and larger TiC area fraction with an improved distribution can be clearly noticed in the satellited coating. The enhanced

distribution of the ceramic is consistent with the boundaries of aluminium particles. It can be seen that porosity was greatly reduced in the satellited coating, and the coating/substrate interface became much less visible in the 6061-TiC coating indicating an improved adhesion between the coating and the substrate.

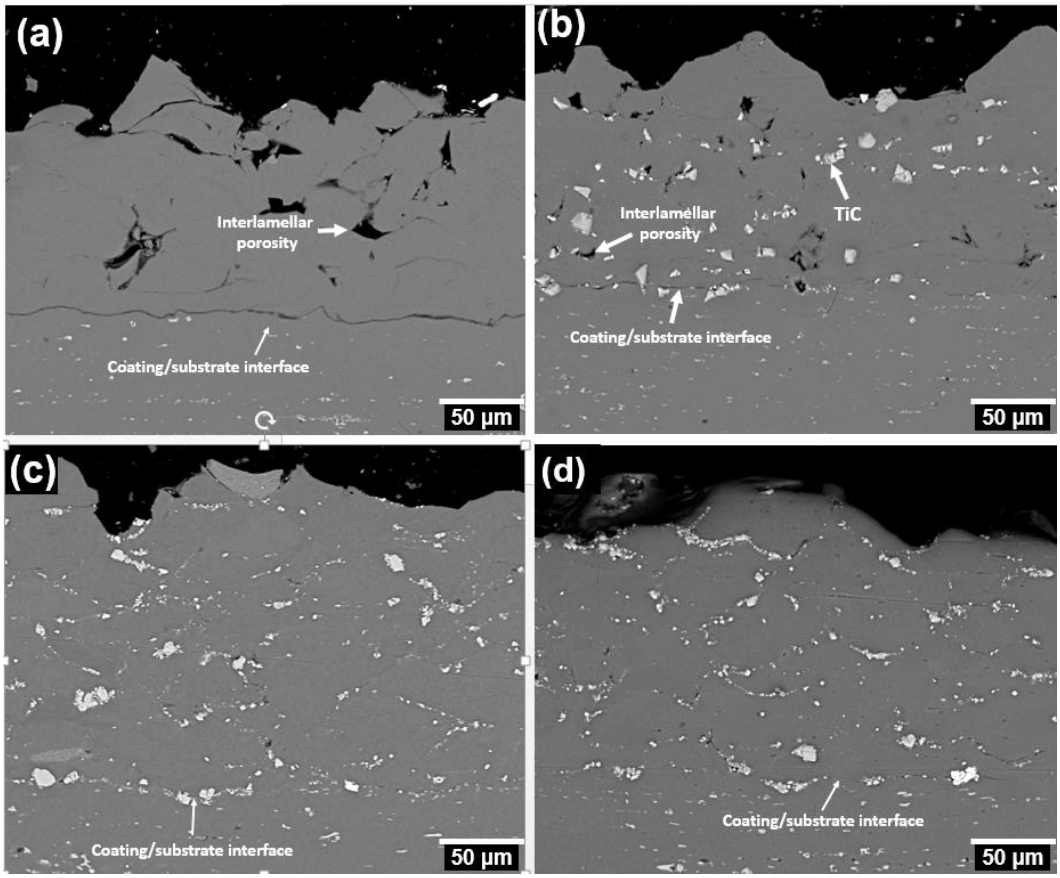


Figure 5-4: Cross-sectional BSE images showing the different structures of the cold sprayed coatings; (a) 6061 coating, (b) blended 6061-TiC, (c) as-sprayed 6061-TiC satellited coating and (d) heat-treated 6061-TiC satellited coating.

As cold spray greatly depends on the deformation of the sprayed materials, an absence of particle deformation can lead to porosity. Significant porosity can be seen in the 6061 coating, which can be explained by a lack of local deformation. Additionally, the appearance of the interface line indicates poor bonding in several substrate-coating interface regions. This is correlated with the low ductility of 6061

that causes limited local deformation of the deposits. Low particle deformation produced poor particle-particle interfacial bonding and created a highly porous structure as shown in Figure 5-4-a. For the blended coating, the presence of the TiC particles has affected the level of porosity. This can be explained by the effect of ceramic particles on increasing the local deformation at the impact surfaces, as the TiC particles appear clearly inserted in the matrix splats. This made the blended coating presents lower porosity than 6061 coating. Figure 5-4-c shows the low porosity, well-bonded coating characteristic of the satellited feedstock. Similar results were also observed showing the clear contribution of ceramic particles in enhancing the bonding between the deposited Al splats as well as between the coating and substrate [126, 250].

Figure 5-5 shows a cross-sectional view of an individual Al6061 deposit taken at a sprayed track using satellited feedstock. It can be seen that there is a clear difference in the interface line appearance with and without the presence of TiC particles. The interface line between the Al splat and substrate surface appears clearly at the free-TiC region (region A), as the splat seems to be separated at this region. On the other hand, the presence of the reinforcement (TiC) particles at the interface between the Al splat and the substrate surface (region B) has made the interface line less invisible, especially at areas surrounding TiC particles. This can indicate that an enhanced bonding between the impact surfaces can be achieved due to the presence of TiC at the interface areas.

The interlocking action of ceramic particles in the cold sprayed coating has been reported in previous studies [256], as the hard particles do not plastically deform within cold spray but they interlock with the metallic matrix. Consequently, as the

TiC particles have a desirable effect in the deposited coatings, increasing the amount of embedded TiC particles would lead to an increase of the advisable effects (adhesion and cohesion) in the relevant coatings. These observations are consistent with the results of Koivuluoto, et al, they found that hard particles play an important role in the activation of metal particles and even substrate surfaces [257]. Therefore, the use of a feedstock that facilitates the embedment of more ceramic particles in the deposited coating can be an efficacious manner to increase these advantages.

In addition, the satellited particles possess relatively large sizes of parent powder, also being covered with a hard-fine ceramic (TiC). This can enable satellited particles to have a higher hammering action than non-satellited particles, allowing higher local deformation and compaction to occur. This may reflect the capability of the satellited feedstock in enhancing the density of cold spray coating owing to the reduction in the interlamellar porosity.

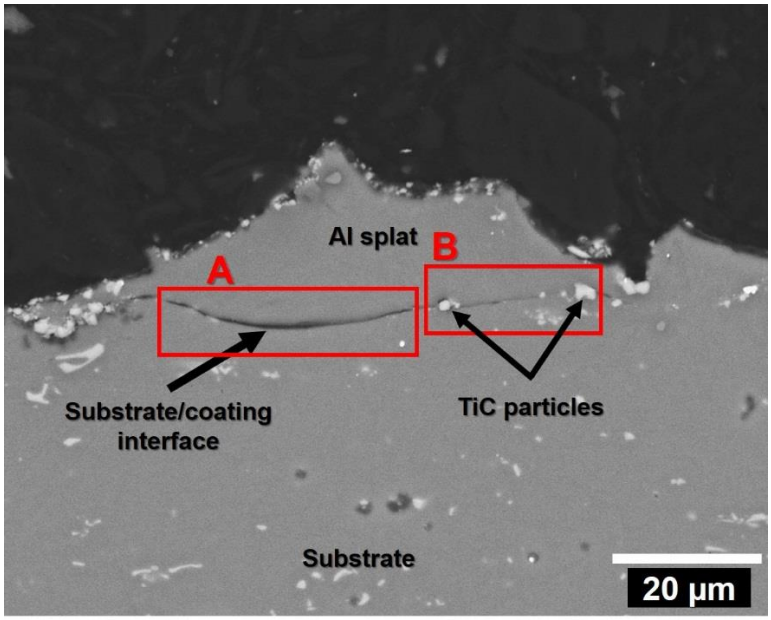


Figure 5-5: SEM images of individual deposited particles showing the effect of fine ceramic particles on the particle/surface bonding.

Figure 5-6 shows the thickness measurements of the as-sprayed 6061 and 6061-TiC blended and satellited coatings. It can be seen that the blended 6061-TiC coating had the lowest thickness (240 µm) among the coatings, while the 6061 presents an average thickness of 268 µm. It is believed that the free TiC particles have the potential to rebound after impact, especially when hitting a low-ductility surface i.e. 6061. This means a significant portion of the reinforcement particles are lost, leading to a reduction in surface activation by producing micro-asperities on the impact surfaces and deposit interlocking. This also caused the 6061 and blended coatings to have similar thickness measures particularly when error bars are taken into consideration.

It is conceivable that impingement of the hard particle results in a peening/densification effect in the deposited coating, reducing interlamellar porosity, and this effect is still present despite a significant rebound of the particles. This would be similar to the shot-peening (SP) particles that are used for tamping CS coating [245], where steel particles mixed and sprayed with Al powder to compact the deposited Al particles before rebounding. However, in case of using the satellited feedstock, the peening effect can be achieved without the rebound of the satellited particles as the TiC embeds and interlock the Al splats. Thus, one the advantages of using the satellited materials within CS is the improvement of both peening and DE at the same time.

The satellited 6061-TiC coating yielded a larger thickness (360 µm) with an increase of 34% and 50% compared to the 6061 and blended 6061-TiC coatings,

respectively. In addition, as represented by the error bars, the satellited 6061-TiC coating was more uniform in thickness than others, reaching a minimum of 340 µm and a maximum of 380 µm.

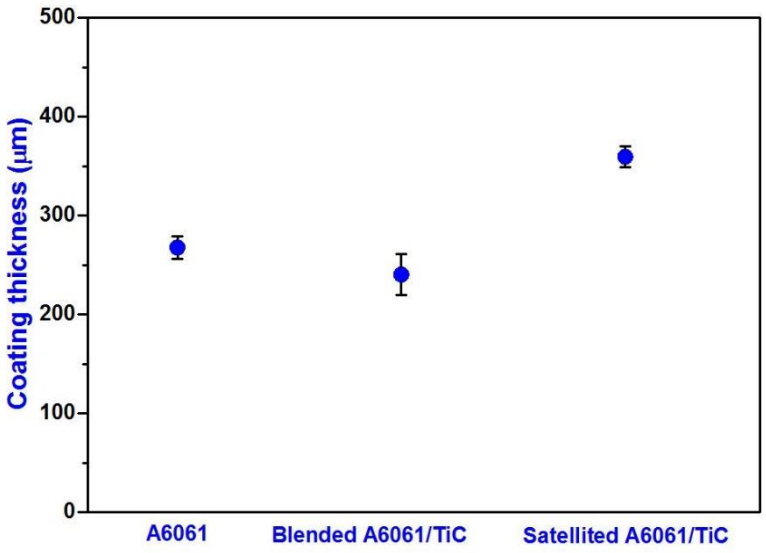


Figure 5-6: The average thickness measurements of the deposited coatings.

Subsequently, the DE of the satellited 6061-TiC coating is clearly higher than the 6061 and blended 6061-TiC coatings, (Figure 5-7). This also confirms the improvement in the material deposition regime of the satellited feedstock when compared with 6061 and blended 6061-TiC coatings because of the presence and behaviour of the satellited hard particles. A similar trend was observed in previous studies; for instance, it was found that the addition of ceramic particles in simple mixing enhances the deposition efficiency (DE) of aluminium composite coatings [252]. This was due to reducing the critical velocity and creation of asperities in the coating during spraying that facilitated the bonding of incoming Al particles. Contrary, the blended coating presented the lower DE among the sprayed coatings with just 18%, this can be explained by the high amount of the rebound TiC that is

considered as weight loss of the blended sample. Moreover, the lack of deformation in the Al6061 particles in the blended feedstock can also affect the deposition in the blended 6061-TiC coating. It is believed that these two deficiencies of the blended feedstock contributed to the lower DE of the blended materials.

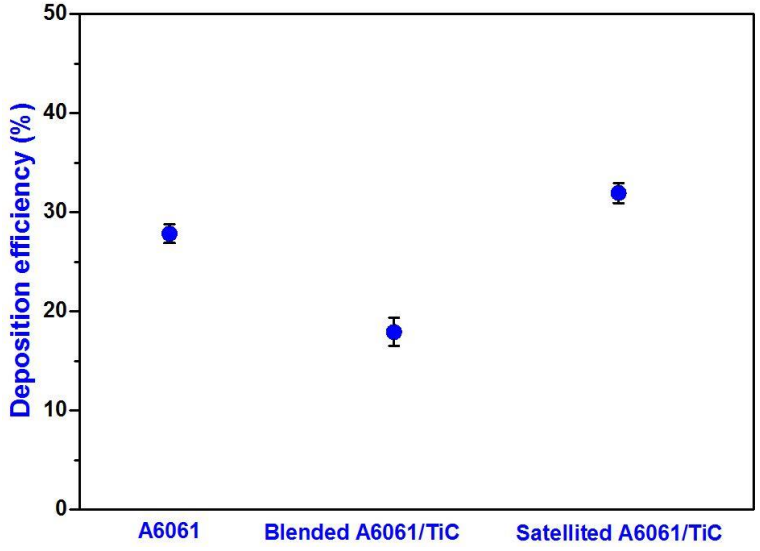


Figure 5-7: The deposition efficiency of the deposited coatings.

In the satellited feedstock, the attachment of TiC particles on an Al particle surface will increase the Al particle mass by 25% compared to a non-satellited Al particle with the same size, assuming all TiC particles are attached to Al particle surfaces, which will reduce the in-flight velocity of the satellited particle due to the increase in both density and particle diameter according to the particle velocity (Equ 5- 2), [101].

$$v_p \approx \left[\frac{C}{\sqrt{R\,T_o}} + \sqrt{\frac{\rho_p d_p}{C_d L_d p_0}}\right]^{-1} \qquad \text{Equ 5- 2}$$

Where;

v_p: In-flight particle velocity,

C: Fitting parameter = 0.45 for Helium.

R: Gas constant = 2077 (J/kg.K^o),

T_o: Gas stagnation temperature= 290 K^o.

ρ_p: Particle density (kg/m^3),

D_p: Particle diameter (µm).

C_d: Drag coefficient (0.47 for sphere)

L_d: Length of the diverging part of the nozzle (0.15 m).

P_o: Gas stagnation pressure (2.8 bar).

For a 45 µm diameter Al particle, after satelliting, the density of the satellited particle increases from 2.7 (Al density) to 2.968 g/cm^3, this was obtained by determining the whole weight and volume of the satellited components. While the particle diameter increases from 45 to 46.97 µm obtained by adding the volume of the satellited TiC as a thin layer evenly distributed on the Al particle surface. Therefore, the particle velocity has decreased by 4% (from 740 to 711 m/s) due to the increase in both density and particle diameter values (4.4).

Further, the satellited particles gained 20% higher momentum than the non-satellited Al particles with the same particle size (Equ 4- 4). This may explain the lower level of porosity due to the greater peening action of the satellited particles. Also, it is known that the deposition of cold-sprayed materials greatly depends upon the mechanical/metallurgical bonding created by local plastic deformation [258]. Thus, the satellited particle that has a layer of hard particles with higher momentum has the ability to produce a higher level of plastic deformation in the coating, increasing material deposition. This can be explained by the effects of TiC on the satellited particles such as producing micro asperities and breaking down the oxide layer and interlocking the Al splats. This can be evident by the higher DE and thickness of the satellited 6061-TiC among the coatings.

Fernandez and Jodoin [116], have proven that the micro-asperities made by the impact of angular ceramic particles have a significant contribution in increasing the DE of Al particles. They showed that these asperities were produced by cutting off the metal and rebounding of the sharp-edged ceramic particles. Namely, it is needed to rebound more ceramic particles to create more asperities for increasing the DE of the matrix metal.

In the case of satellited feedstock, the satellite particles (i.e. TiC) are entrapped between the existing and incoming 6061 particles, causing TiC to be retained in the coating. This will simultaneously increase the deposition of both matrix and ceramic particles because the creation of asperities increases, as the ceramic deforms both incoming and already deposited particles, and the rebounding of TiC decreases. As discussed in the previous chapter, this mechanism of embedment of the TiC is based on TiC remaining attached to the parent particles upon impact (4.5.2). In particular, it has been observed that the trapping of TiC beneath the impacting particle is key to retaining significant TiC content. Consequently, this improvement in material deposition can explain both the larger thickness and higher DE measurements of the 6061-TiC coating compared with the 6061.

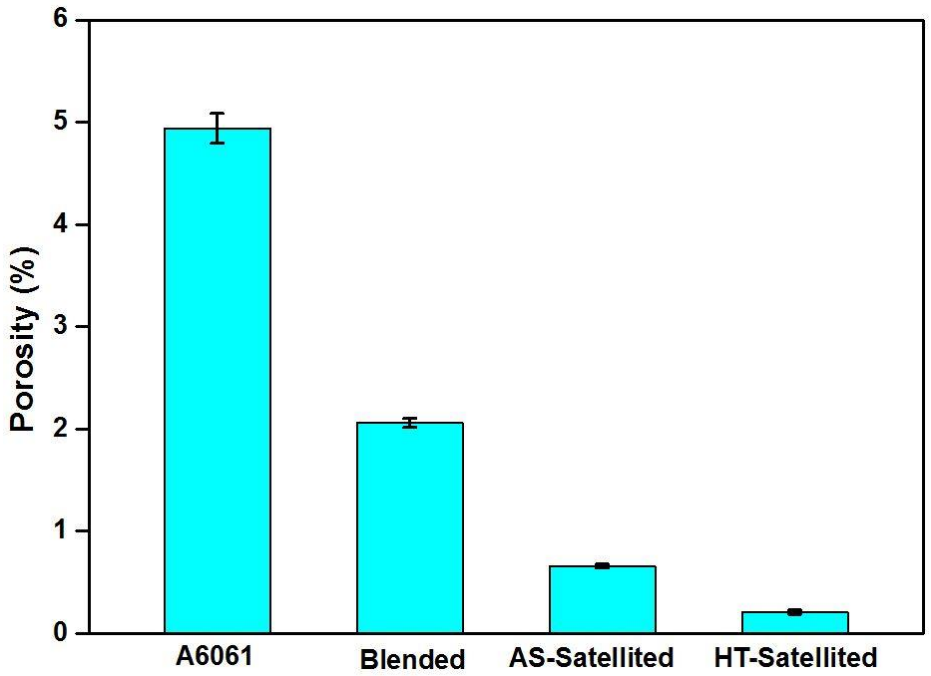


Figure 5-8: The percentage porosity by area of the deposited coatings, showing the effect of the addition of TiC and heat-treatment on coating porosity.

Porosity levels in the deposited coatings are shown in Figure 5-8 The 6061 coating presents a high level of porosity (4.94%) compared to (2.06%) of the blended 6061-TiC coating, and (0.66%) of the satellited 6061-TiC coating. The most likely reason for the interlamellar porosity in CS coatings is the lack of deformation at particle sides [11]. The presence of TiC particles in the blended feedstock decreased the porosity by about 60% compared to the 6061 coating. This can be explained by the effect of hard particles on increasing the local deformation and enhancing bonding of splat surfaces. Similar results were observed by Koivuluoto and Vuoristo [259], in which it was stated that the activation, cleaning (removing impurities and contamination from the impact surfaces) and hammering actions of the ceramic particles (Al_2O_3) have significantly reduced the porosity of the CS Ni-20Cr-Al_2O_3 coating. However, the rebound of an important portion of TiC during the cold spray process decreased the effectiveness of TiC regarding the porosity reduction.

Figure 5-9 presents the TiC area fraction in the blended and satellited coating sections. It is shown that the satellited feedstock presents a clear superiority in depositing hard particles (TiC) in the cold sprayed Al coating. The deposition efficiencies of the ceramic particles of the blended and satellited feedstock were 29% and 48%, respectively. These were calculated by comparing the volume fraction of the TiC between the coating sections and starting materials through converting weight fractions into volume fractions depending on the material densities. Namely, the use of satellited feedstock has contributed in increasing the deposition of the hard particles in the cold-sprayed coating by 65.5%. This can be considered as an important achievement regarding the deposition of hard phases within cermet coating using cold spray.

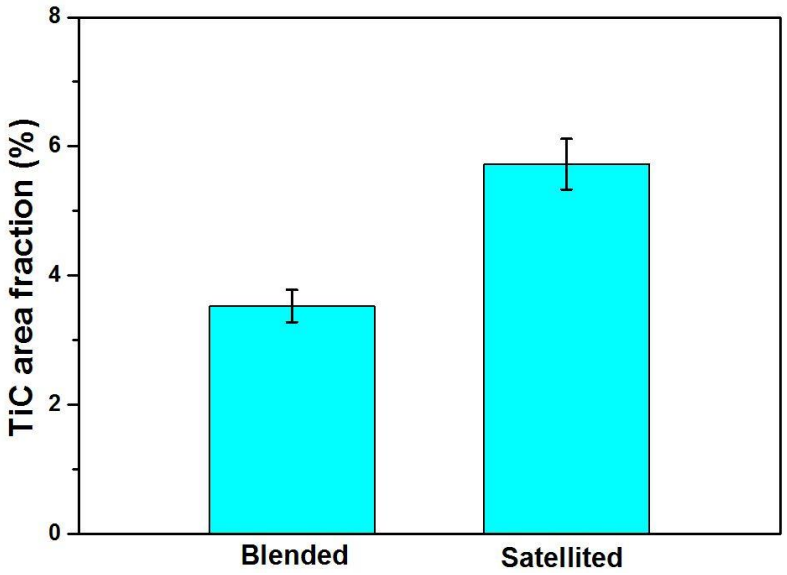


Figure 5-9: TiC area fraction in the coating section showing the contribution of satelliting in increasing the embedded ceramic.

The satellited 6061-TiC coating shows a significant reduction in the interlamellar porosity, it is lower than the 6061 coating and blended 6061-TiC coating by 87 and 68%, respectively. The effect of the TiC particles on coating porosity is similar to

their actions in the case of the blended coating. Moreover, the larger TiC fraction can increase the influence of TiC particles in the satellited coating. In addition, it was found that the hard particles with high momentum allow a higher level of deformation and also increase the peening action in the cold-sprayed layers [260]. Thus, the satellited particles that have a higher momentum (Equation 4) and hard–grainy surface, have the potential to carry out the compaction process in an improved manner. This can explain the eliminated porosity and dense structure of the satellited 6061-TiC coating in comparison to 6061 and blended 6061-TiC coatings.

5.3.2 Effect of heat treatment on the satellited coatings

In order to obtain further improvement in structure density and coating cohesion, the satellited 6061-TiC coating was heat-treated at 345°C for a duration of two hours. This temperature is above the recrystallization temperature of Al, which is 325°C [261]. Figure 5-4-d shows a BSE image of the cross-sectional area of the heat-treated satellited coating. The annealing process caused the reduction in interlamellar porosity and healing of most inter-splat and coating/substrate interface lines.

Although the as-sprayed satelliting coating retained only 0.66% porosity, this was decreased after heat treatment to 0.21%. This level of porosity is 50% of the 6061 based CS coating achieved by Wei, et al. in their ‘fully dense coating’ [262]. Consequently, a superior coating in terms of porosity level and structural cohesion, particularly after heat treatment can be achieved by using the satellited feedstock. Besides, the range of data for porosity for the heat-treated coating is notably reduced.

Similar observations were made in a previous study, in which the interlamellar porosity of cold-sprayed Al coatings significantly decreased after annealing at 300 °C [160] owing to solid-state diffusion in the inter-splat boundary regions. The self-diffusion coefficient of Al at 345°C is 5.23×10^{-16} (cm^2/s) as reported by Messer et al. [263]. Accordingly, the expected diffusion distance of the aluminium atoms after 2 hrs will be 1.94 µm. Thus, it is supposed that an interlamellar pore of 2 µm thickness can be 'sealed' by the diffusion of Al after two hours of annealing at 345 °C. This can explain the consequence of the annealing process regarding the structure densification of CS coatings.

The contribution of the heat treatment processes in improving CS coating structure was reported in previous studies [160, 161, 264], however without demonstrating the potential of diffused materials to reduce the porosity. Li et al. [164] reported that the heat treatment process can be used to improve the inter-splat metallurgical bond between the CS splats due to diffusion at grain boundaries. These observations can confirm the impact of annealing on enhancing the CS coating porosity by diffusion at the splat boundaries.

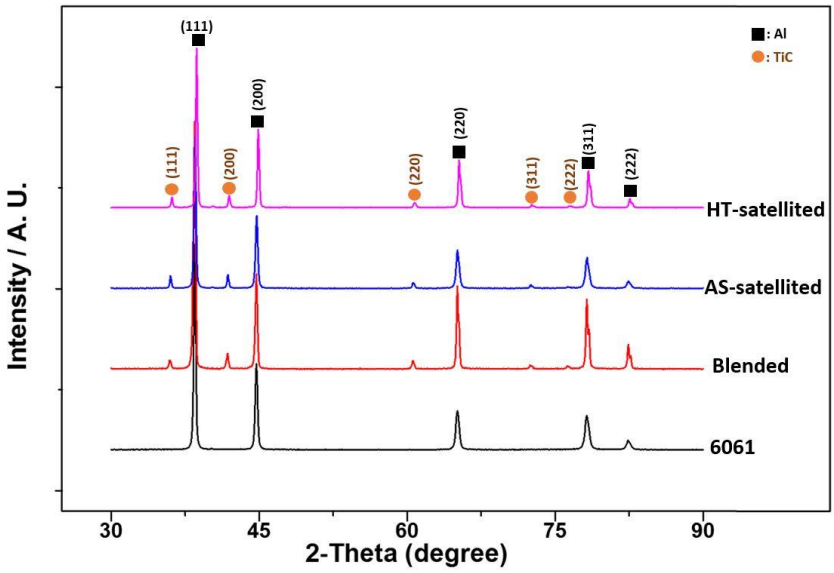


Figure 5-10: X-ray diffraction patterns of the deposited coatings.

XRD analysis was performed on the three coating types. XRD patterns of the as-sprayed 6061, labelled 6061-AS and heat-treated satellited 6061-TiC, labelled as 6061/TiC-HT coating samples are shown in Figure 5-10. Similar patterns were obtained for the blended and both AS and HT satellited 6061-TiC coatings. There is no indication that the heat treatment resulted in the formation of intermetallic components or oxides of the alloy components in the coating.

The annealing temperature was lower than that required for the formation of intermetallic components between Al and TiC [265, 266]. Similarly, it is also clear from Figure 5-10 that there is no noticeable difference in the two patterns of the as-sprayed and heat-treated satellited 6061-TiC coatings, confirming that there were no intermetallic structures formed due to the annealing process in these conditions.

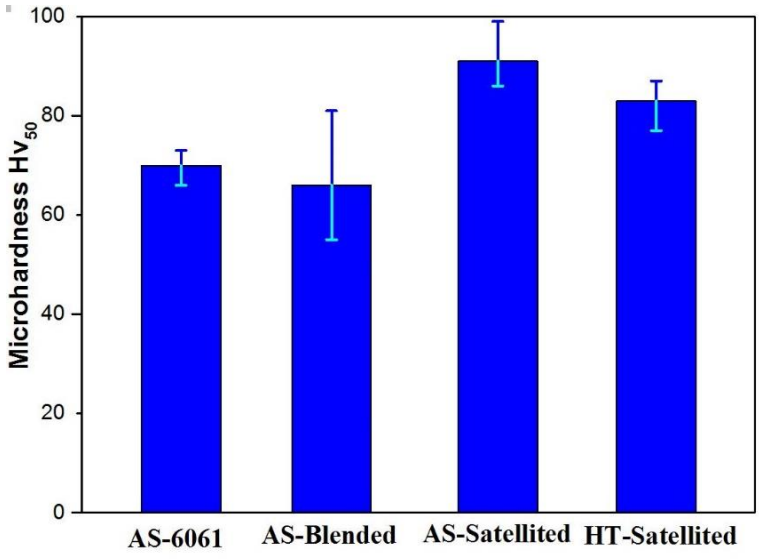


Figure 5-11: Microhardness measurements at the centreline of the deposited coatings. Error bars represent the maximum and minimum hardness values.

A series of 50 gf microhardness measurements were used to evaluate the practical hardness of the coating, by creating indents which incorporate both matrix and ceramic material. Figure 5-11 shows the measured microhardness values of the deposited coatings. The as-sprayed satellited 6061-TiC coating presents the highest mean microhardness value among the coatings at 91 HV0.05 (±1.5). The mean hardness of the heat-treated 6061-TiC was 83 HV0.05 (±0.7), while the as-sprayed 6061 coating yielded 70 HV0.05 (±0.8). The blended 6061-TiC coating presented a hardness similar to the 6061 coating, 67 HV0.05 (±1.8), with a higher range among the coatings confirmed by the larger error bars. This can indicate a non-uniform structure density and TiC distribution of the blended coating. It is known that the high strain hardening of the cold work associated with cold spray leads to the creation of high residual stresses in the CS coatings [267].

The higher hardness of the AS-satellited 6061-TiC coating is related to two combined factors; the higher level of deformation due to the satellited feedstock behaviour (higher momentum), and the presence of a larger amount of the reinforcement in the coating structure. The TiC area fraction also increased by more than 60% in the coating section compared to the blended coating, Figure 5-9. It is known that the reinforcements have a marked effect on the mechanical and microstructural properties of the coatings, and they increase with increasing the amount of the entrapped ceramic particles [268].

After heat treatment, internal residual stresses are expected to be relieved, hence also contributing to a lower measured microhardness in the heat-treated coatings. These results are in agreement with another prior study [269], in which the hardness

of the aluminium alloy (5083) cold-sprayed coating decreased after annealing heat treatment. This was explained by grain recovery, i.e. a reduction in dislocation density, which would also explain the reduced hardness in the case of cold-sprayed coatings which have been subject to work hardening. However, the HT-satellited 6061-TiC coating still has a hardness value higher than the 6061 coating. This is explained by the contribution of the ceramic particles to the resistance to the indentation at this load level. The HT-satellited 6061-TiC coatings showed a minor reduction in mean hardness, however they are similar when considering the error range.

To determine in more detail the contribution of factors to the hardness measurements, Figure 5-12 shows microhardness indents at 10 and 50 gf loads that were made on the deposited coatings, noting the smaller scale of (b, d, f and h). The microhardness of the AS and HT coatings was also measured using a smaller load (10 g) targeting TiC-free areas, as shown in Figure 5-12 (b, d, f and h), in order to determine the contribution of TiC addition and heat treatment on matrix properties. The Vickers microhardness measurements of the Al matrix (HV0.01) in the as-sprayed and heat-treated satellited 6061-TiC coatings were 79 and 65 HV0.01, respectively, compared with 61 HV0.01 of the 6061 coating. The blended 6061-TiC presented a microhardness of 64 HV0.01.

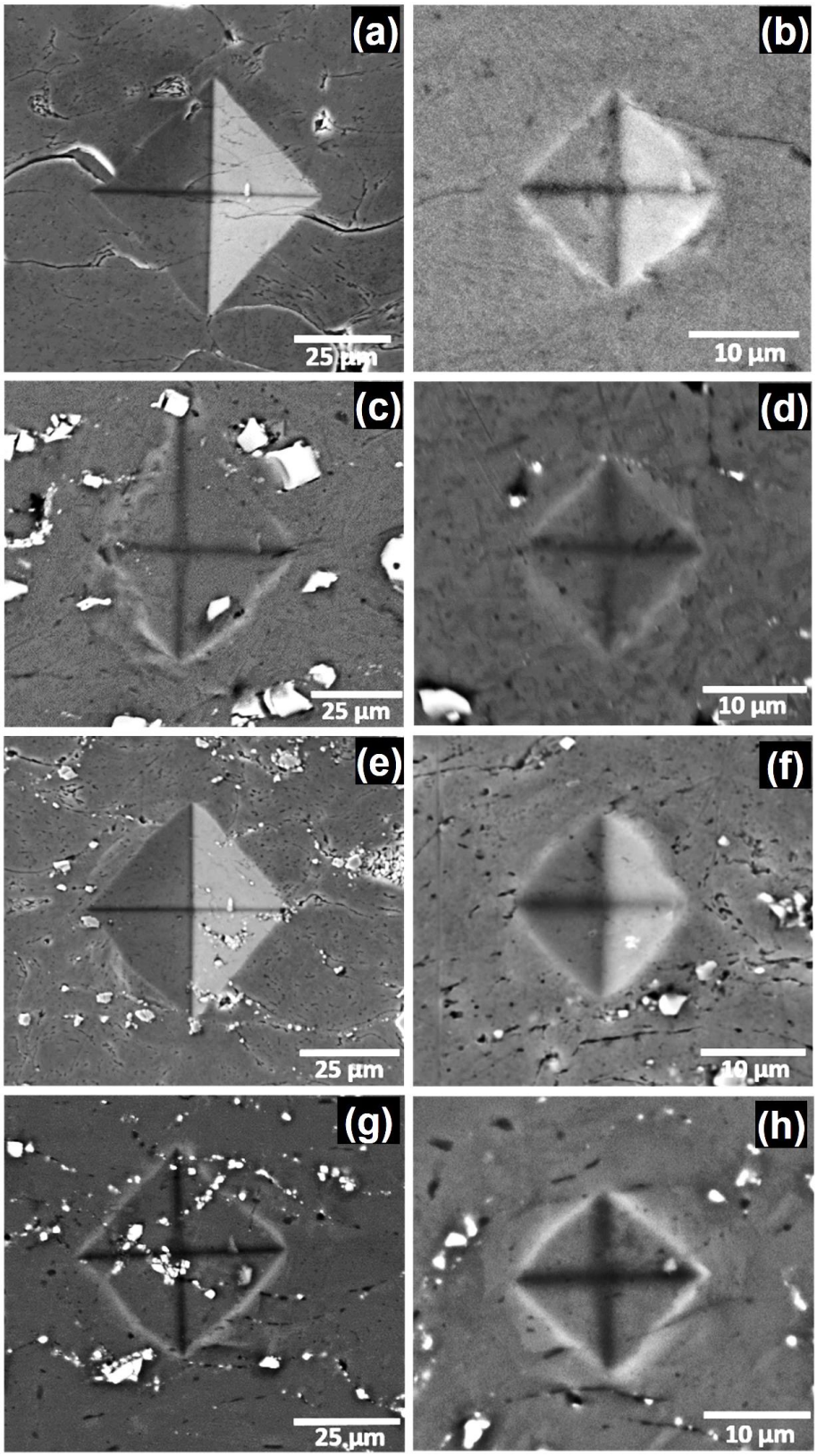


Figure 5-12: SE images of microhardness indents of the deposited coatings at 50 gf (lift column) and 10 gf (right column); (a and b) AS-6061, (c and d)

AS-blended 6061-TiC, (e and f) AS-satellited 6061-TiC, (g and h) HT-satellited 6061-TiC.

The increase of the matrix hardness in the AS satellited 6061-TiC coating can be explained by the increased work hardening in the composite cold-spray coatings, this is likely result of the high level of work hardening caused by the satellited particles during CS process. While the annealed matrix showed lower hardness values than the as-sprayed satellited coating owing to the softening action of the annealing process, however, it still had a hardness higher than the 6061 coating due to the TiC reinforcing effect. It is therefore clear that the addition of TiC provides the majority of the hardness increase as measured by the 50 gf indents for the results in Figure 5-11. These results are consistent with results of a recent study [260], it was found that the higher level of work hardening, caused by the high momentum of hard particles, led to a significant improvement in the matrix hardness and wear resistance of the cold sprayed coatings. In fact, the slightly lower mean hardness value of the heat-treated coating implies that the annealing and softening effect of the heat-treatment plays a more significant role.

When a large load was used (50 gf), some cracks can be seen adjacent to the indents on the AS-6061 and AS-composite coatings, but not at the indent tip. It is observed that cracks do not necessarily start from the indent corners in the sprayed coatings [270], due to the inhomogeneous structure. The inter-splat cracks take the direction parallel to the substrate-coating interface which is consistent with the direction of elongation of splats [271]. On the other hand, there is no cracking or inter-splat cracking observed at the indents made in the heat-treated coatings. This may indicate an improvement in the fracture toughness of the HT coating, owing to

matrix softening and enhancement of the interfacial bonding as a result of the annealing process.

5.3.3 Wear behaviour of the deposited coatings

Figure 5-13 shows the specific wear rate (SWR) of the deposited coatings; 6061, blended 6061-TiC, AS-satellited 6061-TiC and HT-satellited 6061-TiC under dry sliding wear conditions. It can be seen that the SWR of the satellited 6061-TiC coatings (AS and HT) was lower than the other coatings. The SWR of the AS-satellited 6061-TiC was 55% and 20% lower than that of 6061 and blended 6061-TiC, respectively. This can be explained by the contribution of the reinforcing TiC particles in increasing the hardness, as well as reducing porosity, hence resulting in increased wear resistance.

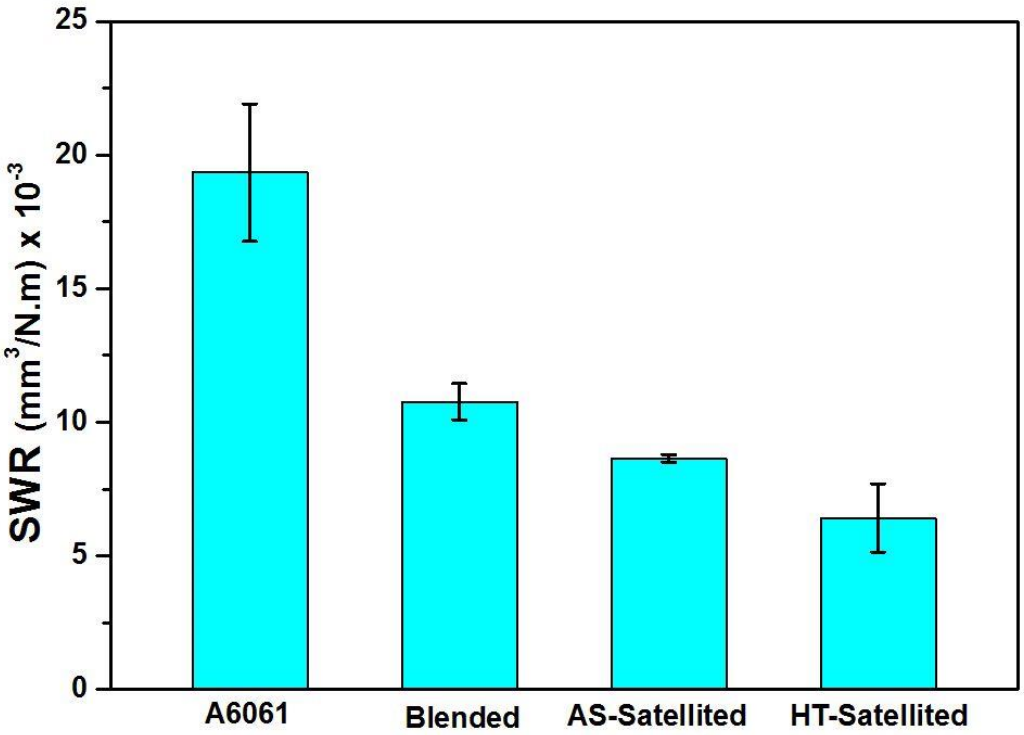


Figure 5-13: The average SWR of the deposited coatings, showing the effect of the reinforcement and heat treatment on reducing the SWR.

Interestingly, the heat-treated 6061-TiC coating presented a mean SWR 25% lower than the AS-satellited 6061-TiC, despite the heat-treated coating yielding lower microhardness values. Therefore, the HT-satellited 6061-TiC coating presents a total reduction of ~70% and 40% in comparison to the 6061 and blended 6061-TiC coating, respectively. A likely explanation for this is the reduced porosity in the heat-treated coating due to annealing improving the resistance of the coating against wear. This is likely explained by a reduction in the incidence of a pull-out based wear mechanism which was observed in the wear tracks in this work. The pulling out of the reinforcing particle has been reported as an important factor in increasing the wear rate in the composite coatings [272]. To further explain the wear behaviour of the deposited coatings, SE images at two magnifications are shown of the wear tracks in Figure 5-14, 3D-view images of the entire wear track are also presented.

The as-sprayed 6061 coating exhibits a wear track morphology with a combination of abrasive scratches and flattened regions of the original splat morphology. Round regions can be seen with similar dimensions to individual deposits. These regions have no indication of grooving implying either a pull-out/delamination mechanism taking place, or these regions are particularly soft. In addition, wear debris has also become trapped between splat-like regions, likely explained by regions of porosity revealed during wear. It is clear therefore that in the case of the 6061 coating the inter-splat porosity and splat-based structure has an adverse influence on the wear mechanism. The blended 6061-TiC coating shows excessive wear on the surface, with a combination of fracture and cracking confirmed by the high magnification image, Figure 5-14-f. It is likely that the low reinforcement amount, weak cohesion

and the high porosity in the blended coating overall produce a more severe wear process.

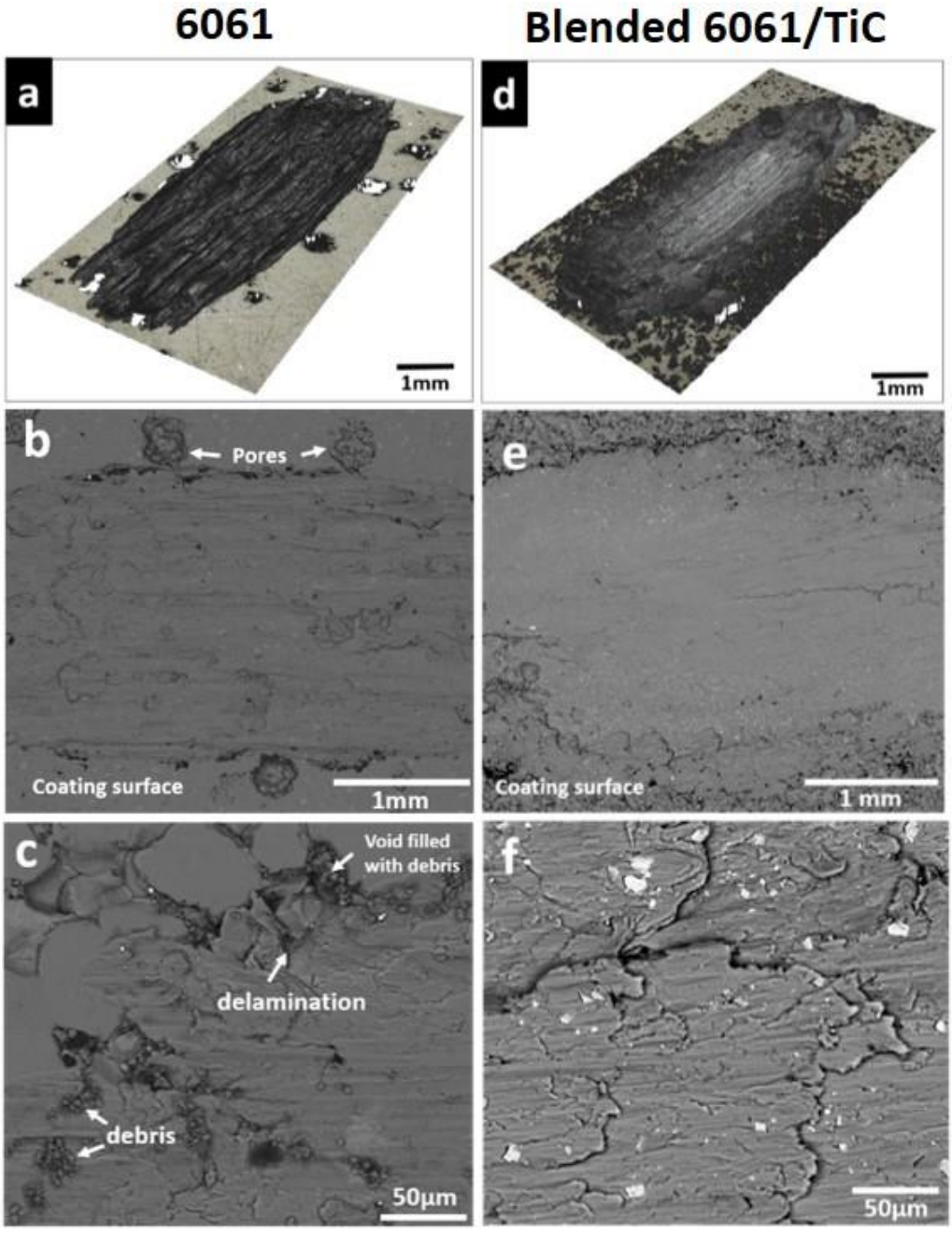


Figure 5-14: (a and d) 3D-views of the entire wear tracks, and SEM images of the coatings (labelled above) at low (b and e) and high (c and f) magnifications

In the case of the satellited 6061-TiC coatings, splats do not appear as part of the wear morphology. Abrasive grooves dominate the surface, with cracking also prevalent. For the HT-satellited 6061-TiC coating, a similar abrasive mechanism can be seen with scratching apparently less prevalent. The SE images of the satellited coating wear tracks at two magnifications are shown in Figure 5-15 with 3D-view images of the entire wear track

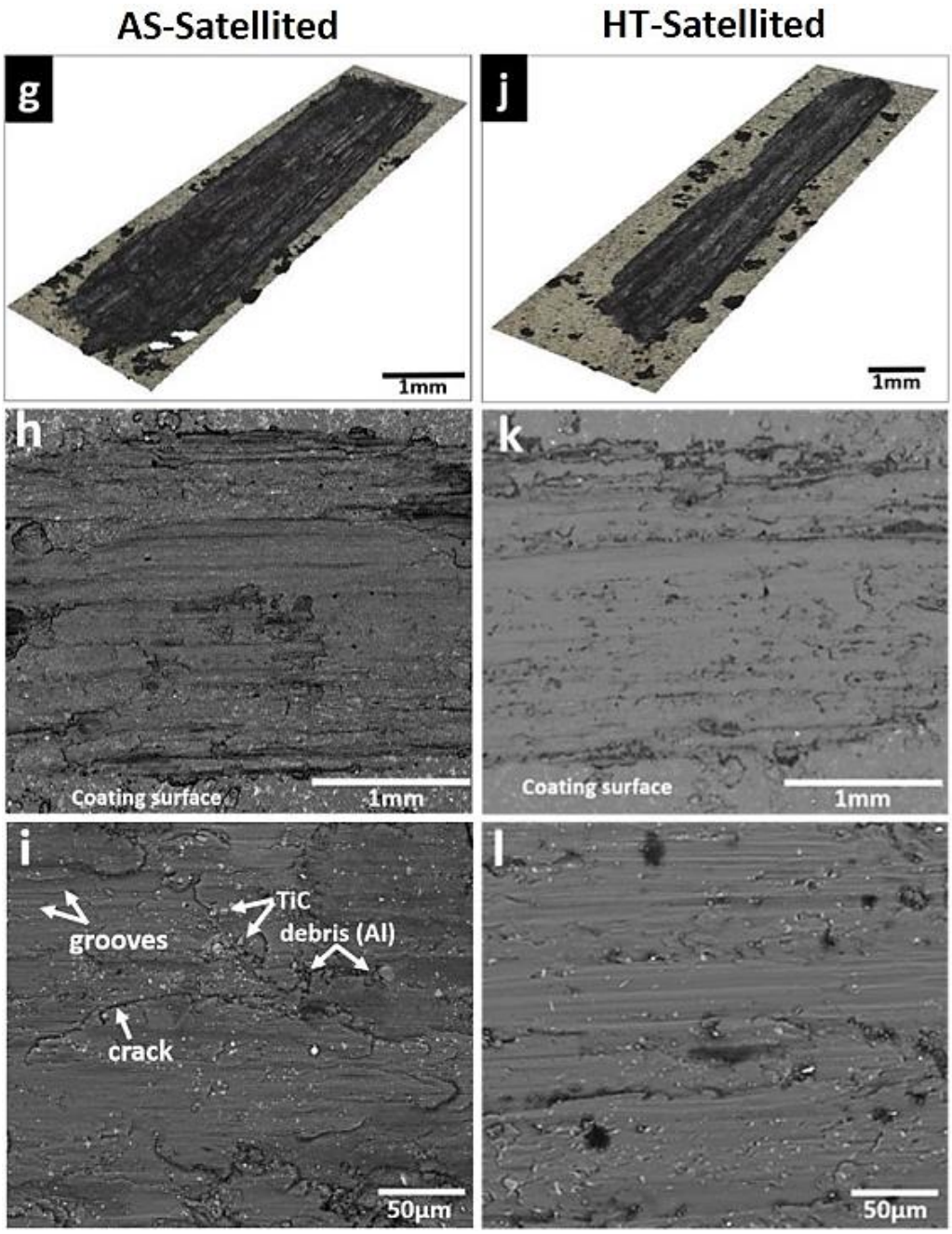


Figure 5-15: (a and d) 3D-views of the entire wear tracks, and SEM images of the coatings (labelled above) at low (b and e) and high (c and f) magnifications.

In the low magnification image, the wear morphology of the heat-treated coating appears somewhat more uniform than the un-treated, providing evidence that more uniform properties pervade the coating, Figure 5-15 (i). Previously, several studies have considered toughness as a significant factor in the improved wear behaviour

of metal matrix-ceramic composites [273, 274]. For instance, Qiao et al. have also noted that there is a correlation with the bonding between the hard particles and the matrix, and the adhesion between splats and the toughness of the composite coating [275].

Moreover, improved bonding between ceramic particles and matrix in composite coatings can also lead to a reduction in the amount of pulled-out ceramic particles, which is a key mechanism in the wear of such materials, and hence this improves the coating wear resistance [276]. Given the reduction of porosity, as a result of the heat treatment process in this work, these mechanisms based on improved cohesion may be contributing factors to the improved wear behaviour.

Accordingly, despite presenting lower microhardness measures, the heat-treated satellited coatings presented lower SWR than the other composite coatings, even the as-satellited coating that has a slightly higher hardness value, Figure 5-11. This means that the hardness value, in this case, is not the dominating factor on the wear. Previously, it is revealed that the hardness, or hardness to Young's modulus ratio, can be adopted as an indicator for the wear resistance of the materials [277].

However, it is found that when the material system has been changed (e.g. addition of reinforcements) or undergoes different processing methods like heat-treatment, the wear mechanism is most probably being different, thus the wear controlling factor differs accordingly [278]. Similar results were observed in other studies [273, 274], where it was revealed that the toughness also has a significant effect on developing coatings behaviour against wear loads. On a related context, it is reported that the annealing of cold-worked aluminium at 345 C^{o} has increased the toughness to the best value [236]. Besides, Qiao et al. mentioned that the toughness

of the coatings has been significantly affected by the bonding between the hard particles and the matrix, in addition to the adhesion between splats [275]. This can explain the superiority of the HT coating over AS ones in terms of wear resistance since the HT coatings present a highly coherent structure in comparison with the AS coatings. It is confirmed that the improved bonding between ceramic particles and binder in the composite coatings, lead to a sensible reduction in the amount of pulled ceramic particles, which in turn improves the coating wear resistance [276].

With regards to the material transfer between the coating and the counter body surface, it seems that there is no transferred material from the counter body to the coating surface. This is due to the high difference in the hardness value of the coating surfaces and counter body (steel 440c). EDX analysis was used to identify the composition of the adhered layer on the counter-body surface, Figure 5-16. However, a great amount of the wear debris has adhered on the steel ball' surface, forming a layer on the steel ball surface. In the last part of the test, the formation of the adhered layer has changed the contact nature between the contacting surfaces from steel-coating contact to a coating-coating wear. This will call off the effect of the counter body morphology; henceforth the wear mechanism becomes more complex.

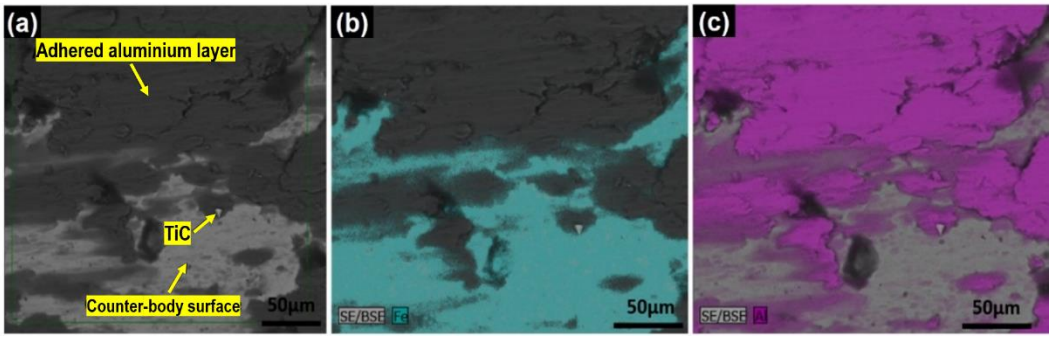


Figure 5-16: BSE and EDX analysis images of the counter-body surface showing; (a) BSE, (b) Fe and (c) Al.

The counter-body surface does not seem to be clearly affected by the deposited coatings, even the higher hardness ones, the worn aluminium thus has transferred and adhered to the steel ball due to its ductility. Moreover, there are no noticeable abrasive scratches on the steel ball surface after using in the test, this may also state that the hardened steel ball surface was not affected during the test.

In conclusion, the wear tracks reflected the microstructure features of the deposited coatings with regards to the porosity, adhesion and ceramic presence. The weak cohesion in the 6061 and blended coatings can be clearly indicated by the amount of the detached particles (Figure 5-14) due to the ploughing action of the counter body. The effect of heat treatment on reducing the porosity of the heat-treated satellited coating can be noticed in the wear track. Wherein a clear reduction in the coating porosity and wear track width can be noticed in the heat-treated satellited coating, pointing to the improved cohesion in the annealed coating, Figure 5-15. Thus, the contribution of TiC particles in strengthening the coating has a clear impact on enhancing the wear resistance of the 6061-TiC coating. Furthermore, the HT-6061-TiC coating yielded the lowest SWR among the deposited coating, explained by enhanced cohesion owing to the heat treatment process.

5.4 Summary

The effects of using satelliting feedstock preparation on the deposition and characteristics of A6061-TiC coatings fabricated by cold-spray were investigated. The use of satelliting is shown to overcome typical defects observed in the deposition of less compliant Al alloys. The key findings of this experimental and characteristic work can be summarised in the following points:

1. The deposition efficiency of the 6061-TiC satellite feedstock was improved by 78% in comparison to that when using a simple 6061 feedstock.
2. The coating porosity reduced by ~70% with using the satellited feedstock.
3. The TiC area fraction increased by 66% in the satellited coating compared to the blended coating.
4. Heat-treatment of the satellited coating at 345^{o}C for 2 hr yielded a reduced porosity of 0.21% from 0.66% for the non heat-treated (satellited) coating. This was explained by reduced inter-particle interfaces and an enhanced coating-substrate interface owing to the solid-state diffusion of Al.
5. The consequence of the annealing process regarding the structure densification of cold spray coatings, which has led to a clear reduction in the interlamellar porosity.
6. The contribution of the satelliting approach is manifested in increased embedment and enhancing the compaction action of TiC in the composite coating.
7. The as-sprayed satellited 6061-TiC coating yielded the highest mean microhardness value among the coatings at 91 HV0.05 (±1.5). The mean hardness of the heat-treated 6061-TiC was 83 HV0.05 (±0.7), while the as-

sprayed 6061 coating yielded 70 HV0.05 (±0.8). The blended 6061-TiC coating presented a hardness similar to the 6061 coating, 67 HV0.05 (±1.8).

8. Under dry-sliding conditions, the specific wear rate of the heat-treated 6061-TiC cold-sprayed coating against a steel ball was reduced by a mean of 25% in comparison to the as-sprayed coating, with good repeatability. This was explained by the contribution of the improved toughness and enhanced structure cohesion after heat treatment, resulting in reduced fracture during wear.

Therefore, satelliting has been proved as a promising powder preparation method that can change the behaviour of the sprayed materials due to the different interaction between the satellited phases. And this can be utilized to overcome the challenges of cold spray regarding the deposition of fine-hard particles and the lack of deformation in high strength alloys within the cold spray.

6 Laser cladding of ceramic-reinforcement composites using blended and satellited feedstocks

6.1 Introduction

MMCs are used in the automotive and aerospace sectors [21]. Particulate reinforced metal matrix composites are of particular interest, as favourable materials for important industries like advanced aerospace applications and automobile [22]. The attraction of particle reinforced MMCs is due to their cost-effectiveness, isotropic properties and ability to be processed using similar technology used for monolithic materials [6]. The laser has some advantages in terms of surface processing over other techniques, including narrow wavelength, low divergence, and a highly coherent beam [279]. Laser cladding with powder injection is a flexible, robust, and effective way to supply the precursor material due to the effectiveness in energy delivery and a high level of process control and repeatability [181].

The interaction between the laser and composite materials is complex, due to the differences in optical and thermal characteristics between the metallic and ceramic materials. Highly reflective materials (e.g. many metals) are difficult to process by laser cladding, and this is particularly the case with Al [194]. In large components the effect of high reflectivity can be eliminated by surface modification processes such as machining, etching, deforming and texturing to improve absorption [196]. However, it is a challenge to modify the surface of powder materials. On the other hand, ceramic materials (i.e. TiC) have good laser absorptivity, giving TiC a preference for laser absorption compared to Al and other reflective metals [191]. Otherwise, reducing the amount of rebounding particles is an effective way to enhance the deposition efficiency and mechanical properties of the MMCs that are

deposited by laser cladding [188]. Thus, preventing the fine particles from being pulled outward by the gas flow, due to the light weight, can improve the deposition and distribution of the fine reinforcement in the deposited clad.

In this chapter, the behaviour of Al/TiC satellited feedstock was investigated along with a blended feedstock. This study aims to evaluate the interaction of satellite feedstocks compared to blended feedstocks in the laser cladding process. The effects of feedstock type and process parameters on the clad characteristics (microstructure, clad quality and formability) were investigated.

6.2 Experimental details

6.2.1 Materials

A6082-T6 aluminium plates were used as substrate materials with dimensions of 180 x 100 x 6 mm, which fit the deposition table and produce an adequate track length for analysis. Table 3-1 shows the nominal chemical composition of the Al 6082-T6 plate material. The substrate surfaces were cleaned, grit blasted and then cleaned with acetone before laser processing. Two types of feedstock were used in this study; simply blended and satellited commercially pure Al with fine TiC powder. The weight fraction of the TiC in both blended and satellited feedstocks was 20%, this fraction yielded a good level of satelliting with low TiC-TiC agglomeration based on previous work of authors (4.6).

The parent powder is a spherical-shaped Al with 15-45 μm particle size range (d_{50}=25 μm) and 99.84% purity, it was provided by Angang Group Aluminium Powder Ltd., China. The TiC powder (99.80% purity) was provided by Goodfellow group, UK; it has an angular shape with a particle size of <5 μm. The liquid binder was lab prepared with a 2.7% (volume fraction) of polyvinyl alcohol (PVA), supplied by GoodFellow/UK, within 97.3% water (3.75 g PVA for 100 ml H_2O).

6.2.2 Feedstock preparation

The blended feedstock was prepared by mixing small batches (20 g) of a mixture (Al and TiC) with the desired weight fractions. The purpose of this stage is to homogenise the mixture by breaking down the clusters in the virgin powders and spreading the ceramic particles over the batch. The full batch of the blended powder was then loaded into a tubular mixer for 30 minutes to complete the mixing process.

Satelliting was performed in sequential batches of 20 g; the dry mixing step is similar to the blending process. However, the binder is added to each patch to be satellited using a small spraying bottle to distribute the binder over the mixed Al-TiC powder, then a wet mixing step performed for 5 minutes for each patch of 20 g. This stage is used to homogenise the wet mixture by breaking down the agglomerations/clusters and confirm the binder distribution. Then the whole satellited powder batch was loaded into a tubular mixer for 30 minutes to complete the mixing process of the whole powder and for further homogenising. Finally, the satellited powder was spread in a metal tray and dried in an oven at 100 ºC for >12 hrs, to dry the powder of binder, leaving ~0.0007 wt.%. This amount was calculated by determining the fraction of PVA in the binder, assuming the full evaporation of the added water after the oven-drying stage. Therefore, both blended and satellited feedstocks consist of 80wt.% commercial pure Al and 20wt.% TiC.

Figure 6-1 shows the morphologies of the starting powders and the prepared feedstocks. The particle size distributions of the Al, TiC and the composite feedstocks are shown in Figure 6-2. Particle size distribution was examined using a Malvern Mastersizer-S (Malvern Instruments Limited, Malvern, UK). The particle size distributions of the satellited feedstock show that about 60% of TiC particles have been satellited to the Al particles. This was calculated by converting the volume fraction of the free TiC that presents in the particle size distribution data into weight fraction by considering the density of TiC. The reduction in the amount of free TiC particles also can be indicated by the reduction in the fine particles region and the increase in the large size peak in Figure 6-2-d. Note the smaller scale of the TiC graph.

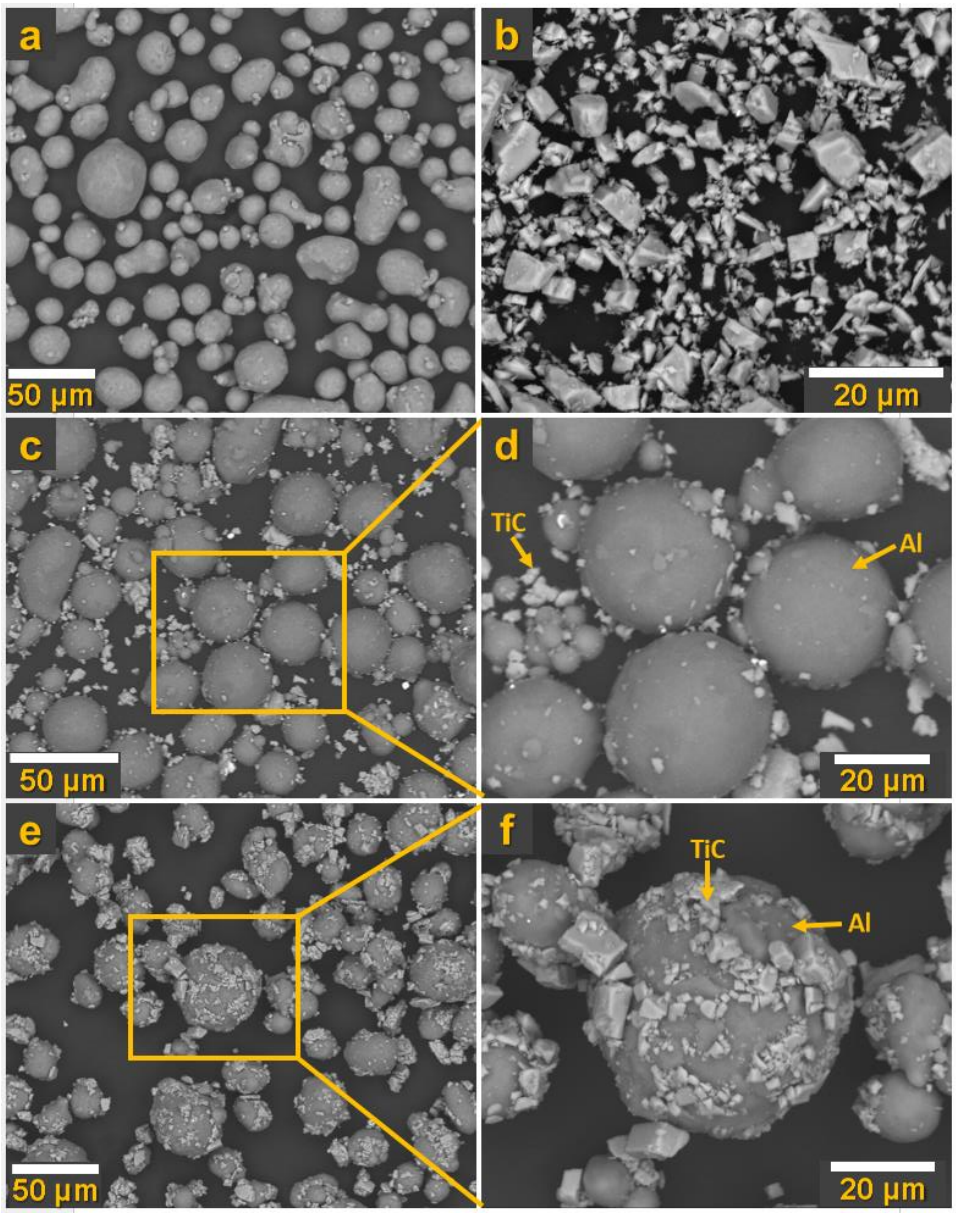


Figure 6-1: SEM images showing the morphology of (a) Al powder (b), TiC powder, (c-d) blended (Al/20TiC); and (e-f) satellited (Al/20TiC).

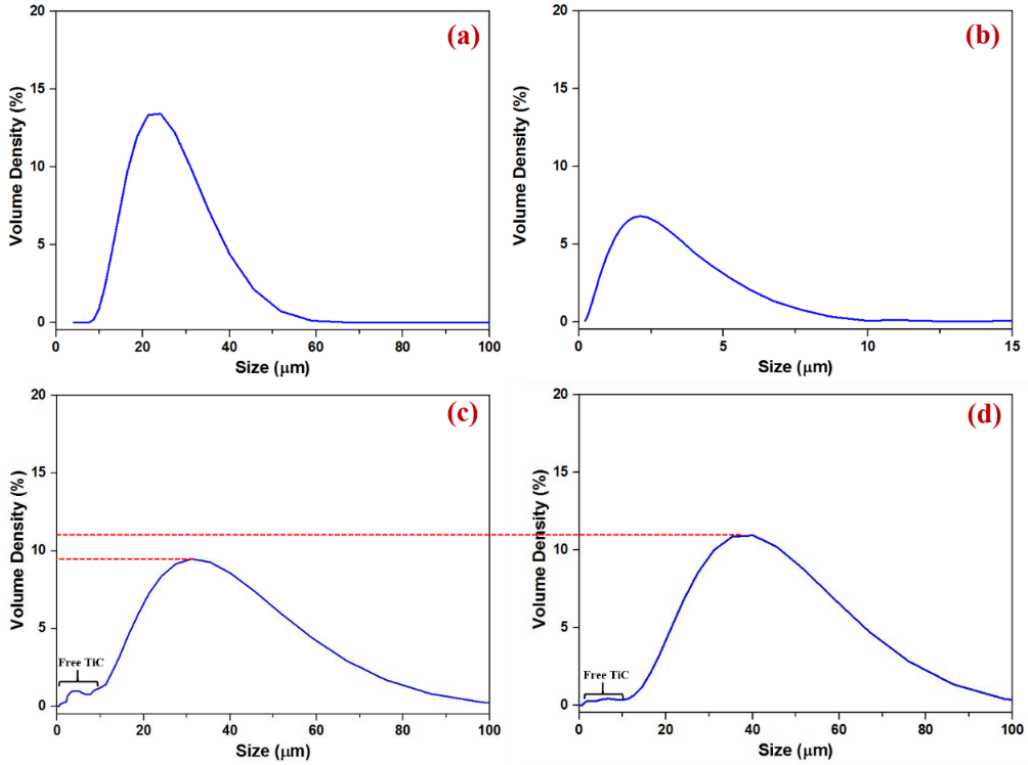


Figure 6-2: The particle size distribution of (a) virgin Al powder, (b) TiC powder, (c) simply blended powder (Al/TiC) and (d) satellited powder (Al/TiC).

6.2.3 Blown-powder laser cladding

A 2-kW ytterbium-doped fibre laser (IPG Photonics) direct energy deposition (DED) equipment was used for laser cladding. The main components of laser cladding equipment were: IPG laser device (GmbH), Germany (maximum power of 2.0 kW operating at 1070 nm wavelength); a CNC controlled working table; model 1264 powder feeder, (Praxair USA) feeding the powder through a nozzle tilted at 28° to the virtical. The feedstock is fed into a laser beam with a beam spot diameter of 3.6 mm. The operation space was shielded in an Argon enclosure to avoid oxidation of the deposited clads. The flow rate of a shielding gas was kept constant at 10 l/min.

Three parameters were varied, being the most critical laser cladding process parameters [183]: laser power P (kW), laser scanning speed V (mm/s) and powder mass feeding rate F (g/min). The range of these parameters in this work was set according to preliminary experiments, and the final parameters that result in the deposition of continuous and bonded clads were identified based on these.

The use of combined parameters is essential to study the effects of laser cladding process parameters on the deposited clads by minimising the number of process variables [179]. Two combined parameters were determined in order to examine the effect of processing parameters on clad quality and formability: The effective energy (E_{eff}) and the powder deposition density (PDD).

E_{eff} is used as an indicator that provides an amount of the delivered energy to the process by the laser [151]. This energy is responsible for heating/melting the substrate surface and powder stream and can be calculated by Equ 6- 1, [179]. PDD provides a measure of the powder feeding rate during the process [179]. PDD is recognised as a function of effective deposition area. While Equ 6- 2 is used to calculate the PDD.

$$\boldsymbol{E_{eff}} = \frac{\boldsymbol{P}}{\boldsymbol{V \times D_L}} \qquad (\mathrm{J/mm^2}) \qquad \text{Equ 6- 1}$$

$$\boldsymbol{PDD} = \frac{\boldsymbol{R \times D_L^2}}{\boldsymbol{V D_L \times D_P^2}} \qquad (\mathrm{g/mm^2}) \qquad \text{Equ 6- 2}$$

Where P is the laser power (W), V is the scanning speed (mm/s), and D_L is the laser spot size (mm), R is the powder feed rate (g/min), and D_P is the nozzle diameter (mm). The behaviour of the satellited feedstock under laser beam was then compared with the blended feedstock. Preliminary experiments were performed to identify the range of working parameters that can be used for successful clads.

Based on preliminary experiments, three energy densities; 104, 122 and 140 J/mm^2 were used to deposit clads. Similarly, four values of PDD were chosen: 0.0028, 0.0037, 0.0056 and 0.0075 g/mm^2, as these values led to the deposition of sound clads at different laser energy densities. Eventually, a 3x4 sample matrix was adopted to examine the difference in behaviour and characteristics of the deposited clads of both feedstocks. Note that the values below are the average of three measurements and the error bars represent the standard error values. Values of E_{eff} and PDD here have units of (J/mm^2) and (g/mm^2), respectively. Three measurements were obtained from different locations along each individual track to confirm the repeatability of the results.

6.2.4 Pre-placed powder laser cladding

The 2-kW ytterbium-doped fibre laser (IPG Photonics) direct energy deposition (DED) equipment was also used to deposit pre-placed powder bed clads. Powder beds of blended and satellited materials with dimensions of 2×30×100 mm were placed on 6082 aluminium substrate. Two steel plates of 2 mm thickness were used for levelling the powder bed surface using another plate to pass over the steel plates to spread the powder between the plates.

6.2.5 Microhardness and dry-sliding wear

In order to understand the effect of the different feedstock behaviours within the laser deposition process on strengthening the material, the average hardness values of the matrix were measured for the different clads. The microhardness of the matrix at different regions was measured using a testing load of 25 g_f; hence the reinforcement particles were avoided. A Buehler Microhardness indenter (USA) was used for microhardness testing on the clad cross-sections using a dwell time of

15s. The distance between every two consecutive indents was >5 x indentor widths to avoid the influence of nearby indents on the next indent.

A CETR Universal Micro-Tribometer 3 (USA), was used for reciprocating dry-sliding wear tests that were performed according to the ASTM G133-05 standard using a linear displacement amplitude of 5 mm and 1 Hz frequency for 10 minutes. A 6 mm-diameter AISI steel ball grade 440C (800 Hv) was used as a counter body at 5 N normal load. The wear tests were performed on the clad top surfaces after grinding to the centre of the clad thickness to eliminate the rough top surface. The ground clad surfaces then were polished to a mirror finish in order to analyse the worn surfaces after the tests. For each sample, three wear tests were performed to confirm result reliability. An Alicona Infinite Focus variation microscope was used to measure wear track volume on the worn surfaces. The specific wear rate (SWR) [280] was calculated using the SWR formula (Equ 5- 1). The wear volume is the averaged track area multiplied by the length of the wear track (5 mm). The total distance wear distance during the test is 6 m.

6.2.6 Powder and clad characterisation

Scanning electron microscopy (SEM) was performed using FEI Quanta 600 using back-scattered electron (BSE) and secondary electron (SE) imaging. Clad characteristics of height, depth, porosity, width and area were manually-calculated by assisting of Image-J software. Dilution is determined by the ratio of the dilution depth to the sum of dilution depth and clad height. The Bruker D500 X-ray diffractometer was used to examine phase composition of the clads with a wavelength of 0.15406 nm (Cu k-alpha), a 2θ range of (30°-90°) and step size and step time of 0.05° and 2 s, respectively.

Three clad samples from each feedstock (blended and satellited) were subjected to microstructural analysis to understand the effect of satelliting on composition and microstructure and hence potential mechanical properties. The selected clads were deposited at a powder deposition density of 0.037 g/mm^2. This PDD value was selected because there are three clads from each feedstock deposited at this PDD value with three different laser energy densities (104, 122, and 140 J/mm^2), wherein a significant microstructure evolution has occurred. This gives an acceptable range of samples that can be used to study the microstructure of different clads from blended and satellited feedstocks.

6.2.7 Deposition efficiency

The deposition efficiency (DE) was calculated by measuring the weight of the deposited clad and the weight of blown powder during the cladding process. The measurements were taken from blended and satellited clads deposited at moderate E_{eff} and PDD. The weight of the substrate was determined by multiplying the measured volume by the density of the substrate material before subtraction from the sample weight. The weight of the blown material was obtained by multiplying the powder feed rate by the cladding time; three trails were practised to confirm the repeatability of results. The cladding (deposition) time of the clad is determined by dividing the clad length by the scanning speed (table speed).

6.3 Results and discussion

6.3.1 Clad characterisations results

Clads of high quality can be defined as a uniform and continuous clad with high density and homogenous microstructure, with a strong metallurgical bond to the substrate with low dilution [182]. Hence, any shortage of one or more of the named

characteristics can be considered as a defect in the deposited clad. In addition to the visual inspection, SE images for the entire clad section and other images at different magnifications can provide further details about every individual clad. Figure 6-3 presents a map of cross-sectional images of the blended feedstock clads deposited at different E_{eff} and PDD values. The cross-sectional images of the satellited feedstock clads are shown in Figure 6-4. The combined parameters can be observed through this map that can demonstrate the sensitivity of the clad section geometry towards the processing parameters as there are clear differences in the clad sections for various values of the E_{eff} and PDD.

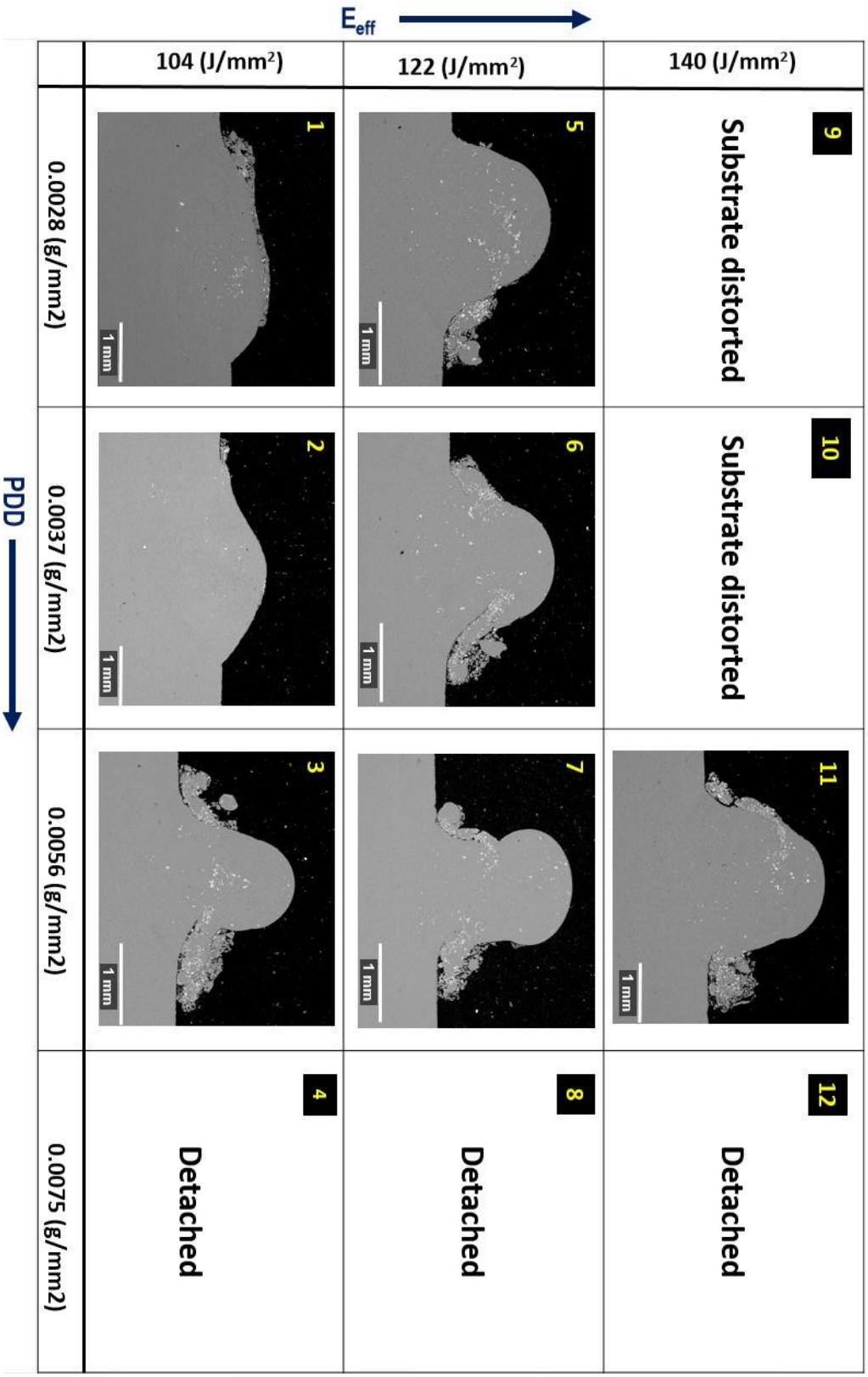


Figure 6-3: BSE images of the cross-sectional of the blended feedstock clads (sample numbers are shown at the corners)

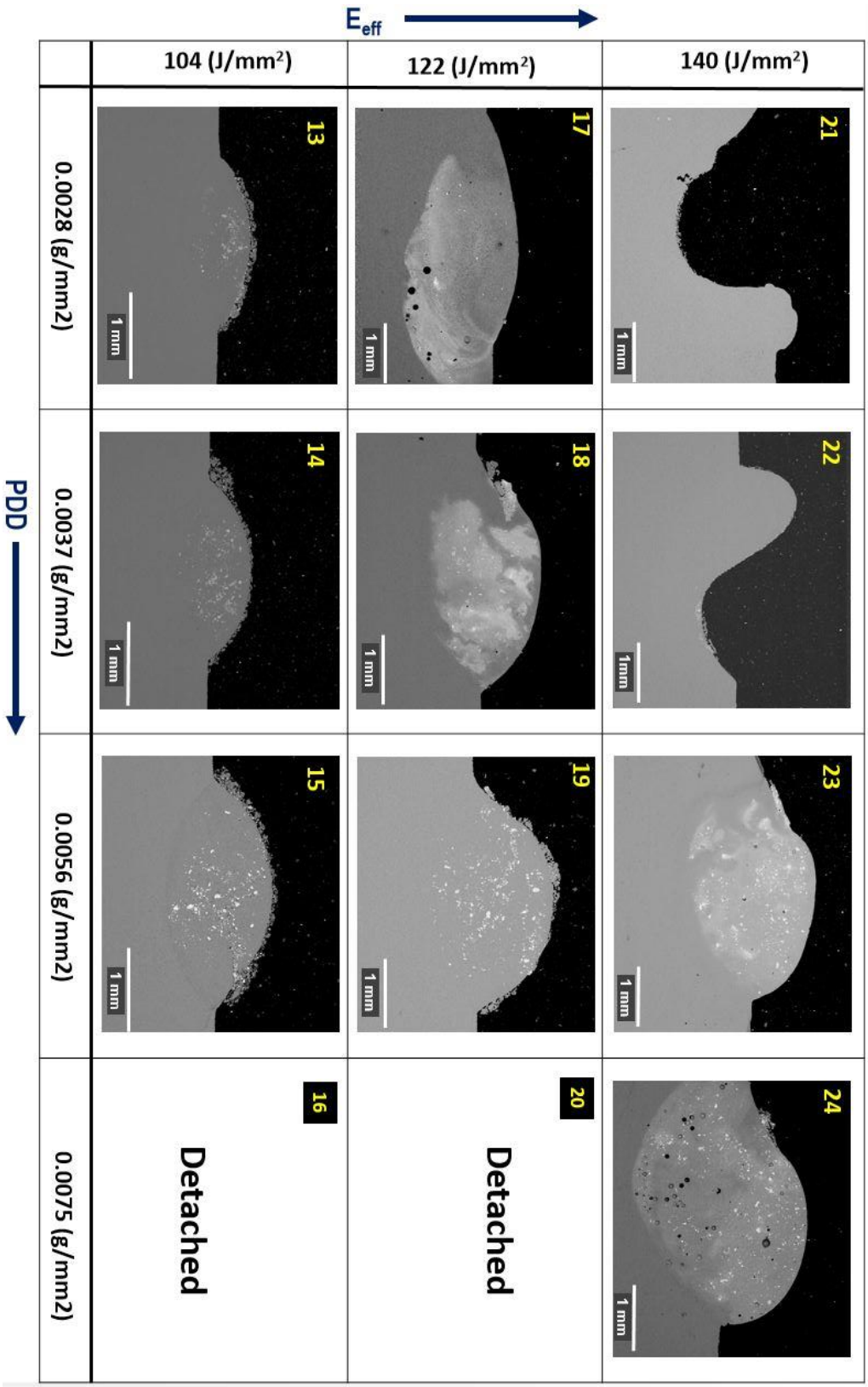


Figure 6-4: BSE images of the cross-sectional of the satellited feedstock clads (sample numbers are shown at the corners)

The most significant features here are the clad area and dilution because the clad area indicates the effectiveness of deposition of material where the larger clad area indicates a higher deposition rate of materials. Dilution measures the amount of the substrate material that is melted by the laser energy and diffused with a clad material [179].

Figure 6-5 shows the clad areas of blended and satellited clads at different E_{eff} and PDD values. For the blended feedstock, the clad area Ac values change from 0.8 to 1.92 mm^2. It is known that for higher deposition efficiency, the majority of the feedstock material has to be melted by the laser [188]. This can be explained by the fact that higher laser energy can melt/deposit more material at a certain time by delivering sufficient heat to the powder and substrate surface. The material deposition increased when the E_{eff} increased, indicated by the clad cross-sectional areas.

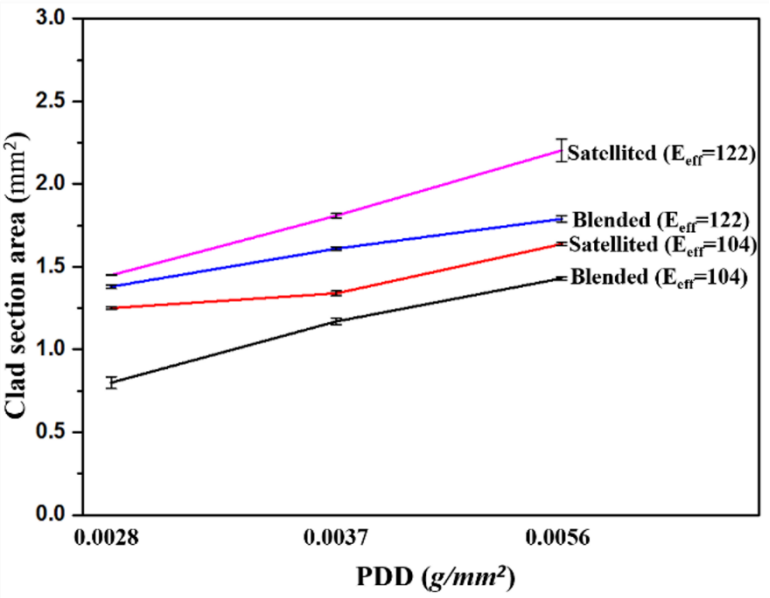


Figure 6-5: The clad area of the blended and satellited clads at different Eeff and PDD values measured by Image-J software, error bars represent the standard error of three clad sections.

When excessive E_{eff} was used, the substrate surface melted overly producing an irregular groove with a discontinuous clad on one side of the groove. When a low PDD is used, a small amount of material is present in the working area. This means a small amount of the laser energy is absorbed by sprayed material and instead a larger proportion of the laser beam energy is delivered to the substrate surface. Thus, a melt pool with larger size is created, which increases melt pool lifetime. At the higher E_{eff} and moderate value of PDD (i.e. 140 J/mm^2 and 0.0056 g/mm^2), there is a deposited clad but with a high dilution area. This is a result of the combined effect of the higher energy and high PDD that absorbs higher laser energy.

The satellited feedstock clads show relatively large clad areas and larger dilution levels compared with the blended feedstock clads. The clad area (A_c) values of satellited clads varied from 1.25 (sample 13) to 4.1 mm^2 (sample 24), presenting wider range and higher sensitivity toward process parameters compared with the blended feedstock. The clad areas at PDD of 0.0037 and 0.0056 g/mm^2 both have increased ~35% by increasing the energy density from 104 to 122, while the increase in the clad area is ~16% at a PDD of 0.0028. This indicates that the use of higher energy density can improve material deposition when more powder is delivered to the working area. Accordingly, the satellited clads present larger clad areas than blended, indicating enhanced exploitation of the laser energy when satellited materials are used.

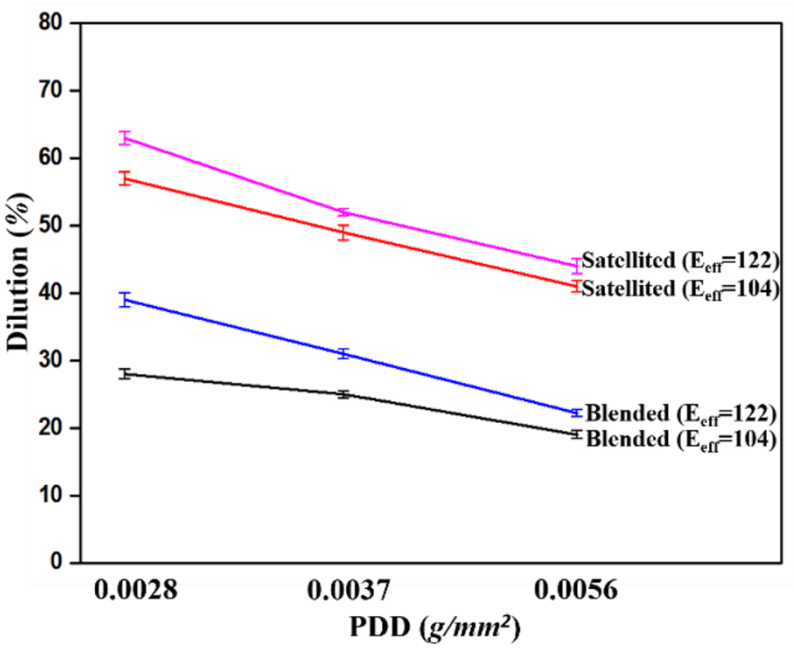


Figure 6-6: The dilution of the blended and satellited clads at different Eeff and PDD values measured by Image-J software, error bars represent the standard error of three clad sections.

Figure 6-6 shows the dilution measurements in the blended and satellited clads at various E_{eff} and PDD values. It can be seen that the dilution increases with increasing laser energy density and decreases with increasing PDD, and the effect of the PDD is greater than that of E_{eff}. It is known that the dilution greatly depends on the laser energy that is provided to the substrate surface [183]. On the other hand, the dilution area clearly decreased by increasing the PDD amount. This can be explained by the shielding effect of the sprayed materials which hinders a significant proportion of laser energy to reach the substrate. With regards to the feedstock type, the satellited feedstock clads have higher dilution than blended clads, as the dilution in the satellited clads has increased by 90% on average compared to the blended clads. This indicates a larger amount of heat has been delivered to the substrate in the case of using the satellited feedstock. Consequently,

both the process parameters and the feedstock type have a clear effect on the clad area and dilution.

6.3.2 Powder behaviour and deposition mechanisms

6.3.2.1 TiC fraction in the deposited clads

The TiC area fractions in different deposited clad sections were quantified using Image-J software. Three clads from each feedstock clad were used to measure TiC fractions in the relevant clads. These clads were deposited at relatively low E_{eff} parameter of 104 J/mm^2, as no dissolution of TiC particles was detected. This was established depending on TiC morphology, XRD patterns, and microstructural observations of clads prepared at 104 J/mm^2. It can be seen that only TiC and Al peaks appeared in the tested samples (as shown in Figure 6-7), similar to that of the starting powder.

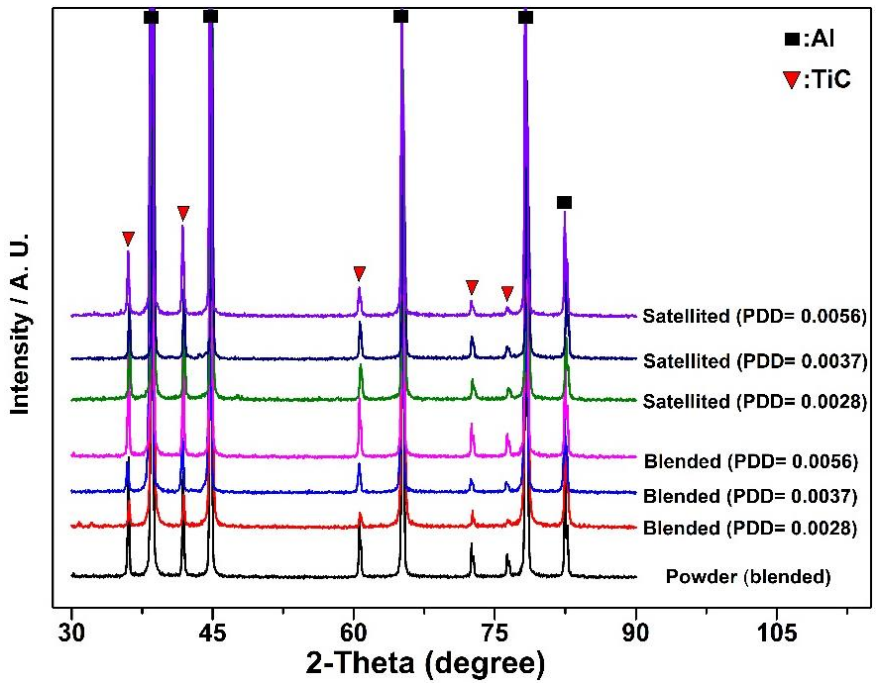


Figure 6-7: XRD patterns of the blended and satellited clads deposited at low E_{eff} (104 J/mm^2).

Figure 6-8 shows the TiC area fractions of the blended and satellited feedstocks at E_{eff} of 104 J/mm^2 and different values of PDD. Automatic particle counting was used to count the areas of individual particles through automatic determining of the image threshold, where black and white binary mode was used for better accuracy. The results showed a significant increase (113% on average) in the TiC fraction in the clad section when the satellited feedstock was used, compared to the blended feedstock.

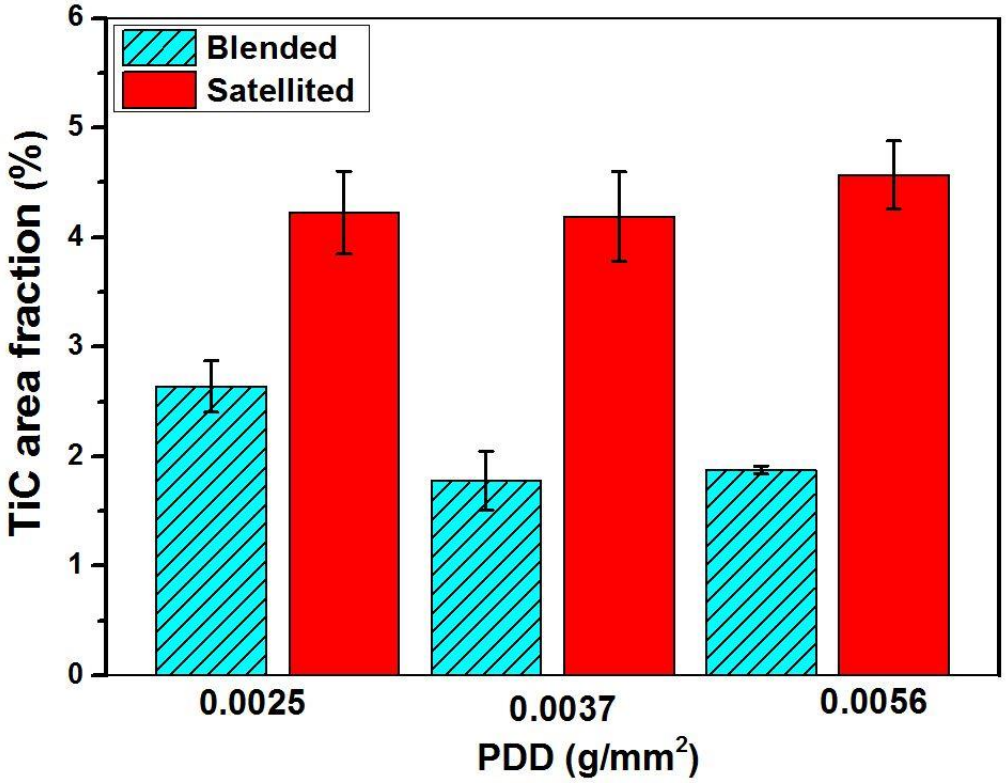


Figure 6-8: TiC area fraction in the clad sections of blended and satellited clads deposited at E_{eff}=104 J/mm^2 and different PDD values, error bars represent the standard error values.

The blended and satellited clads prepared with the same parameter window presented different geometries. Figure 6-9 shows cross-sectional BSE images of blended and satellited clads deposited at the same E_{eff} and PDD of 122 J/mm^2 and 0.0056 g/mm^2, respectively. Separate deposits (side deposits) can be seen attached

to the blended clad (Figure 6-9 a and b), consisting of a high TiC amount bonded by Al. These deposits appear weakly bonded to the clad and substrate surface as the contact area is very small compared to the deposit area. It can be seen that TiC is concentrated inside deposit areas, in comparison to the clad centre.

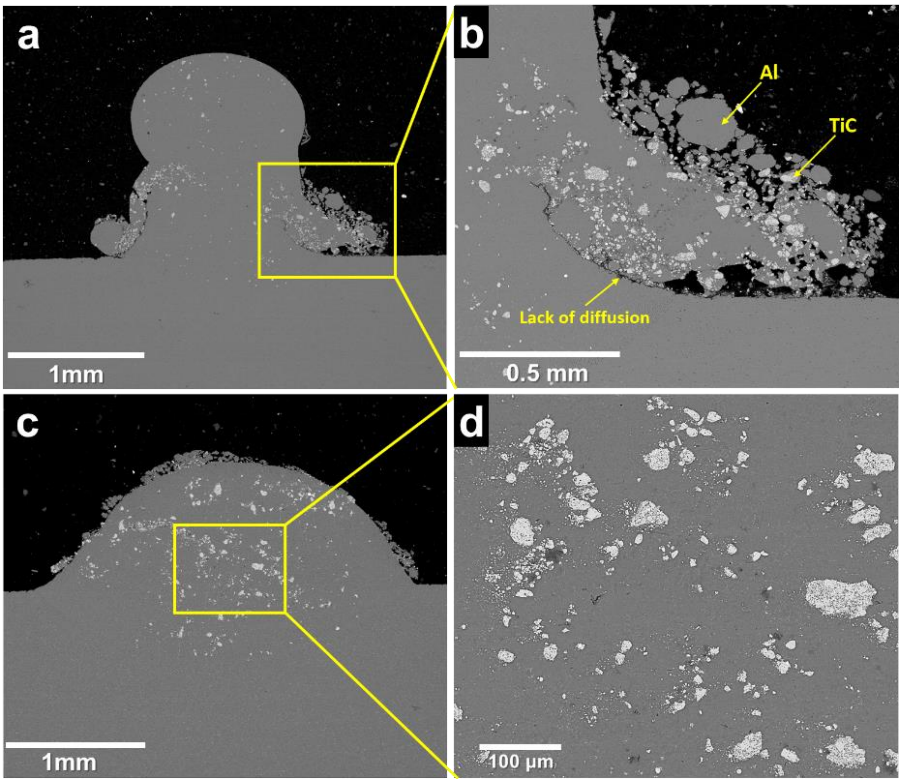


Figure 6-9: BSE images present the TiC distribution in identical blended (a-b) and satellited clads (c-d), both were deposited at E_{eff} =122 J/mm² and PDD = 0.0056 g/mm².

The satellited clads had a more uniform geometry with a larger clad area as the side deposits have disappeared (Figure 6-9 c and d). The satellited clads yielded a higher amount of TiC particles spread over the clad section, particularly in the clad centre, with enhanced distribution.

It is reported that fine particles tend to be pulled outward by the gas flow due to the light weight (lower inertia) [190], this results in a lower particle density in the

central area of the laser beam which has the highest laser intensity according to the Gaussian distribution. Thus, TiC and finer Al particles in the blended feedstock have a high potential for being drawn away from the intended direction. When fine particles are blown to the edge of the laser beam, they are exposed to relatively low laser energy compared to the beam centre owing to the Gaussian distribution of the laser beam intensity. The small-size Al particles at the clad sides could melt due to the relatively low melting point of Al and the higher surface area to volume ratio area of the fine particles size [281]. It is believed that the fine Al particles have melted and surrounded the blown TiC particles (at the clad edge) forming the side deposits. The rest of the blended powder that consists mostly of large Al particles and TiC particles interacted with the laser beam in its high-intensity region and formed the bulk of the clad.

On the other hand, the satellited feedstock has less free TiC and fine particles due to the satelliting effect. Particle size is slightly larger due to the adhesion of TiC particles on the Al particle surfaces (Figure 6-2-d), increasing the momentum of the satellited particles compared with non-satellited particles [282]. Thus, the satellited powder-gas jet has less divergence than the blended, given its improved focusing and directivity stream. These features can reduce the proportion of particles blown away from the cladding region. This can be demonstrated by the higher TiC fraction and enhanced distribution in the satellited feedstock clad compared to the blended clad, Figure 6-9. Accordingly, the satellited feedstock showed superior delivery of TiC to the deposited clads and elimination of side deposits.

6.3.2.2 Interaction between the laser beam and sprayed materials:

To clarify the different behaviours of the blended and satellited feedstocks in laser cladding, schematics were drawn to simplify the interaction mechanism between the laser radiation and the feedstocks depending on their morphologies. Figure 6-10 shows the schematics of laser interaction with the blended feedstock.

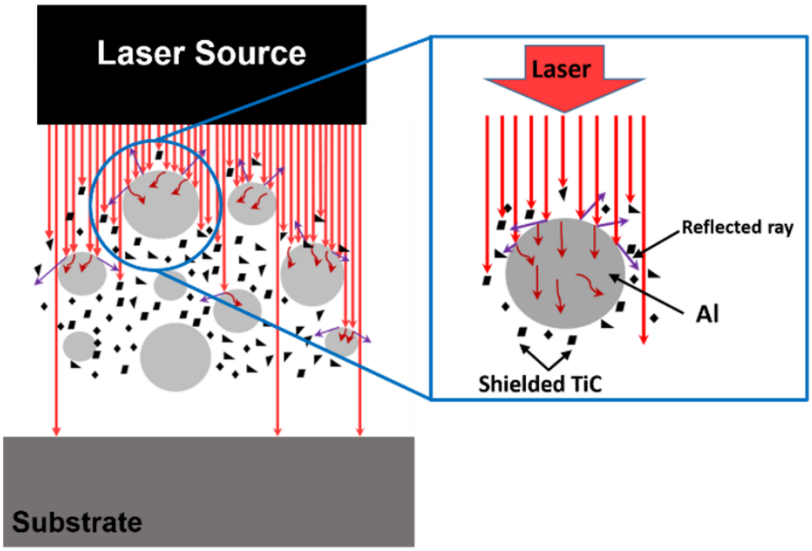


Figure 6-10: Schematic of the mechanism of the interaction between the laser beam and the blended feedstock.

Depending on the nature of the blended feedstock, a mixture of free fine TiC and relatively large Al particles is blown in the space between the feeding nozzle and melt pool. For clearer details, a zoomed view of an individual Al particle is presented in Figure 6-10. The Al particle (grey particle) seems surrounded by a cloud of TiC particles (black-angular). It can be seen that most of the laser radiation is interrupted by the free TiC particles around the Al particle, this is based on the high laser absorption of ceramic particles [283]. The TiC particles have a wide absorption range of wavelength, extending to the visible-light range [284]. Also,

the upper TiC particles may shade several small areas on the Al particle, while the TiC on the sides can prevent laser radiation penetrating downward.

Consequently, a significant proportion of laser radiation can be prevented from passing toward the lower powder layer and substrate surface. This might be evident from the lower dilution in the blended clads compared with the satellited clads deposited with the same parameters, Figure 6-6. The TiC particles that are below the Al particles have been shadowed by the Al particle, so they have reduced heating from laser radiation.

A schematic of the proposed interaction mechanism between the laser and satellited feedstock is shown in Figure 6-11. It can be seen that most TiC particles have attached to the Al particle surfaces, thereby reducing the presence of the free TiC particles. This is consistent with the mechanism of the satelliting process and satellited powder characterisation (Figure 6-1 and Figure 6-2). The magnified view of the satellited particle Figure 6-11 illustrates the interaction of the satellited particles with the laser radiation. The absence or reduction of the free TiC particles would allow more laser radiation to reach the satellited particles and also to penetrate downward between the satellited Al particles. This could mean higher energy will be provided to the sprayed satellited particles and substrate surface. This can increase the possibility of the sprayed materials to melt during spraying between the nozzle and substrate, and this can increase the catchment efficiency of the laser cladding materials [285]. It has been reported that the laser energy is attenuated when the laser passes through the powder layers, which, in turn, reduces the laser intensity [286]. Thus, reducing the interruption of laser radiations by TiC particles would reduce the losses in laser intensity during the processing time.

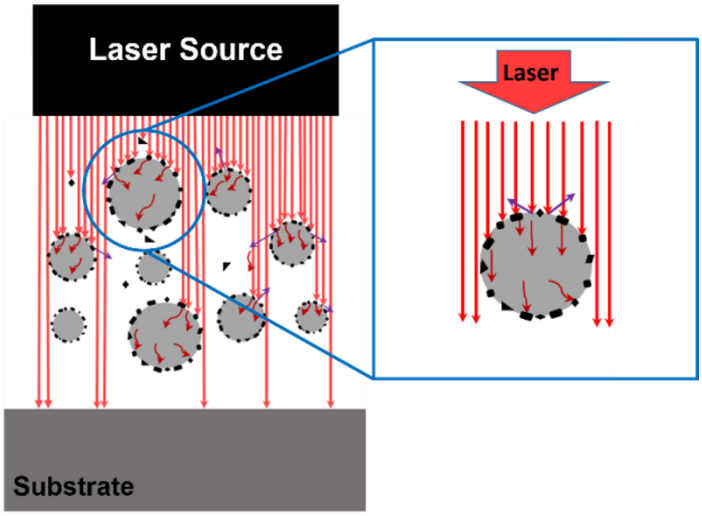


Figure 6-11: Schematic of the mechanism of the interaction between the laser beam and the satellited feedstock.

Moreover, the formation of wider molten area on the substrate surface can increase the catchment of the incoming particles [192]. This is achieved by reducing the rebounding of sprayed particles from the substrate surface that occurs when these particles impact the substrate melt pool [192]. The decrease of the amount of rebounding particles within laser cladding is an effective way to enhance the deposition efficiency in laser cladding [188]. Therefore, the satellited particles allow a higher amount of energy to reach the substrate surface due to the reduction in the amount of free TiC particles that interrupt laser radiation. The satellited feedstock can reduce the rebound of the sprayed particles owing to the improvement in laser beam penetration throughout the blown materials. This may explain the increase in TiC fraction and clad areas of the satellited clads compared to the simply blended clads.

6.3.2.3 Effect of satelliting process on the laser absorptivity of the sprayed materials

TiC is superior for laser absorption compared with Al and other reflective metals [191]. This is because of the laser absorption coefficient of TiC is three times greater than aluminium absorption coefficient at a certain wavelength [180]. In the blended feedstock, Al particles are expected to reflect most of the incident radiation. It is expected that the blended materials absorb lower heat energy compared to the energy provided by the laser beam. This means the efficiency of the heating process is low for the blended Al-TiC feedstock. On the other hand, a significant proportion of TiC particles in the satellited feedstock are attached to the Al particles, Figure 6-1-f. This attachment leads to a reduction of reflective regions on particles, greater transfer of heat through attached particles, and greater efficiency of transfer of laser energy.

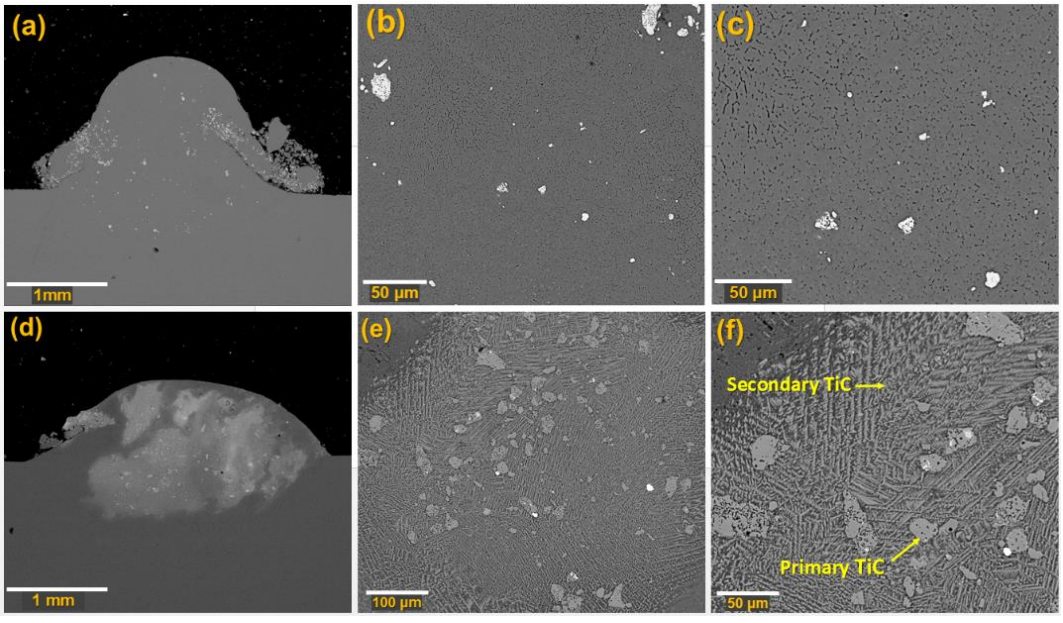


Figure 6-12: BSE images show the difference in the level of TiC dissolution at the blended (a-c) and satellited (d-f) clads deposited at PDD of 0.0037 (g/mm^2) and E_{eff} of 122 (J/mm^2).

The greater dissolution in the satellited clads can be an evidence of the greater heat absorption compared to the blended feedstock, which means higher temperature and larger melt pool are obtained. This is indicated form the different microstructures of identical clads from both feedstocks deposited at the same parameters. Figure 6-12 shows low and high magnification BSE images of blended and satellited clad sections deposited at PDD of 0.0037 (g/mm^2) and E_{eff} of 122 (J/mm^2). The images present a clear difference in the microstructure due to the difference in TiC dissolution level, as well as the amount of TiC present in the centre of the clads. It can be seen that there is no noticeable TiC dissolution in the blended feedstock clad, Figure 6-12 (a-c). In contrast, there is a higher dissolution of the TiC in the cross-section of the satellited clad, Figure 6-12 (d-f), as most of the TiC particles were dissolved, forming a secondary TiC phase with a distinctive structure spread relatively uniformly over the clad section.

6.3.3 Effect of the process parameters on the clad form

Most of the deposited clads have good metallurgical bonds to the substrate with different levels of dilution. The effect of the process parameters on clad geometry is reflected in the variation in the clad shape, clad area, and level of dilution. Figure 6-13 shows the formability map of 'successful' clads with the processing parameters of both blended and satellited feedstocks. Note that some points are missing due to the detachment of clads or the high distortion in the substrate surface due to the high heat input.

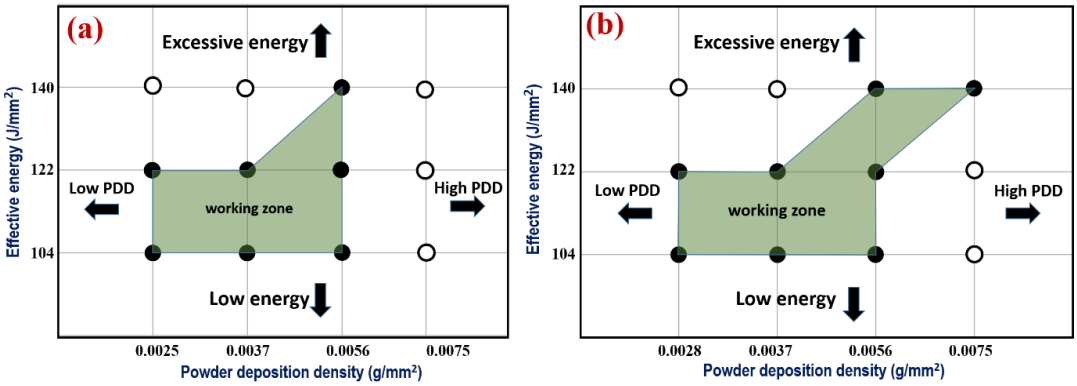


Figure 6-13: Clad formability according to different E_{eff} and PDD values; (A) Blended feedstock, and (B) Satellited feedstock.

The working zones of the satellited and blended feedstocks were defined by connecting the successful clads points of each feedstock on an E_{eff} – PDD diagram, producing a shaded area representing the working zone. Compared to the satellited map (Figure 6-13 b), no clad was formed at highest PDD and lower E_{eff} corner of the blended feedstock, explained by insufficient melting of the deposited layers and the substrate surface. Regarding the numbers of the successful clads, it can be noticed that the satellited clads are more than the blended as there is a deposited satellited clad at high PDD of 0.0075 (g/mm^2) but no blended clad was deposited at the same point. This indicates that satelliting is capable of expanding the process capability for deposition of clads at high PDDs through delivering sufficient laser energy.

Substrate distortion was observed at the higher E_{eff} and lower PDDs for the satellited samples. This can be explained by the Gaussian distribution of the laser beam intensity producing a large thermal gradient at the melted pool. This difference in temperature leads to a significant difference in the surface tension force as the surface tension is dependent on temperature, increasing with decreasing temperature [287]. The difference in the surface tension force may drive the melt

pool material to flow from the high tension region at the melt pool centre to the lower tension region at the edges. This phenomenon is widely known as the Marangoni convection force [288]. Otherwise, another effect may contribute to the formation of grooves in the substrate. The powder-gas jet impact with the pool surface could make the melt pool to rush on the side producing a groove along the cladding line. These observations were reported by Goodarzi et al., [289].

It is thought that when high E_{eff} and low PDD were used, more energy was provided to the melt pool which can make the melt pool boiling. This also can lead to a larger melt pool volume and then longer solidification time was required. This may promote the production of the groove on the substrate surface due to Marangoni and powder-jet actions.

6.3.4 Deposition efficiency

The deposition efficiency (DE) is the ratio between the amount (weight) of deposited materials and the amount of the blown materials. Figure 6-14 shows the deposition efficiency of blended and satellited clads deposited at E_{eff}=122 and PDD=0.0037.

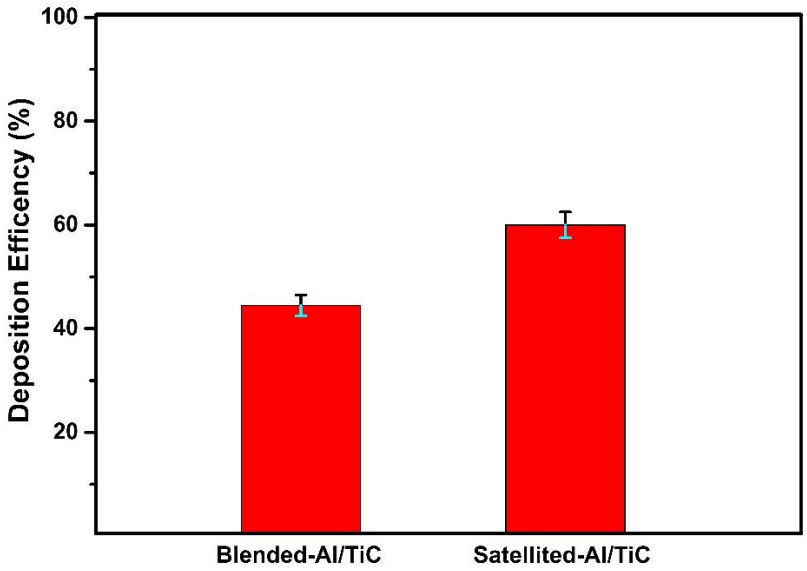


Figure 6-14: Deposition efficiency of the blended and satellited feedstocks at Eeff=122 (J/mm2) and PDD=0.0037 (g/mm2); error bars represent the standard errors of the measurements.

Figure 6-14 states that the DE of the satellited feedstock is ~60%, and it is higher than the DE in the case of using the blended feedstock by 29%. The higher the absorption of laser energy, the higher the probability of particles to melt, explaining the higher DE of the satellited feedstock. Moreover, the TiC particles in the blended feedstock, which were subjected to the blowing action, have a higher potential to rebound as the opportunity to hit the melt pool is less. It is reported that, for optimal DE in the laser cladding processes, the powder has to be melted by the laser energy and should not rebound away from the surface [189]. Therefore, in the satellited feedstock, the higher delivered energy, the eliminated particle rebound, and the homogeneous stream all can contribute in the higher DE compared to the blended feedstock. The larger clad areas of the satellited feedstocks can indicate the enhancement in the materials deposition of the satellited feedstock compared with the blended feedstock.

6.3.5 Invariance upon pre-placed powder laser cladding

The previously discussed laser interaction mechanism (6.3.2) between the laser beam and the feedstock materials helped explain the increased melting apparent in the case of the satellite feedstock. It is also hypothesised that the difference in both the amount and distribution of material delivered to the clad is due to the spraying process. To determine at which point in the process satelliting benefits the laser cladding process, cladding of pre-placed powder was performed.

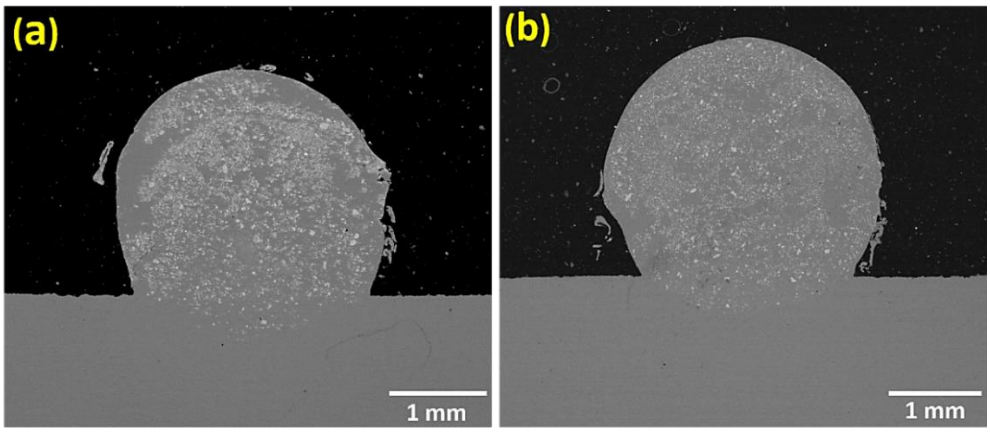


Figure 6-15: BSE cross-sectional images of the pre-placed powder clads deposited at Eeff=122 using (a) blended, and (b) satellited powders.

The cross-sectional BSE images of the deposited clads shown in Figure 6-15 shows that there is no clear difference between the blended and satellited clads in terms of clad uniformity, geometry, and spread of TiC. Both clads have t similar sections and they are well bonded to the substrate without side deposits. This indicates there is no difference in the behaviour of the blended and satellited powders within the laser cladding process when the pre-placed method is used. Accordingly, the satelliting plays a beneficial role earlier in the process, i.e. during powder flow/flight. This would confirm the suggested interaction mechanisms of the satellited and blended feedstocks and side deposits formation. Wherein the

satelliting technique has affected the flow characteristics of the sprayed materials, but it does not affect the powder bed LC process.

6.4 Microstructural characterisation of the deposited clads

Figure 6-16 presents BSE cross-sectional images at three different magnifications of the blended clads made in blown powder mode deposited at a PDD of 0.0056 g/mm^2 with three laser energy densities of 104, 122, and 140 (J/mm^2). The clad produced at a laser energy density of 104 (J/mm^2), presents a microstructure consisting of TiC dispersed in an aluminium matrix, Figure 6-16 (a-c).

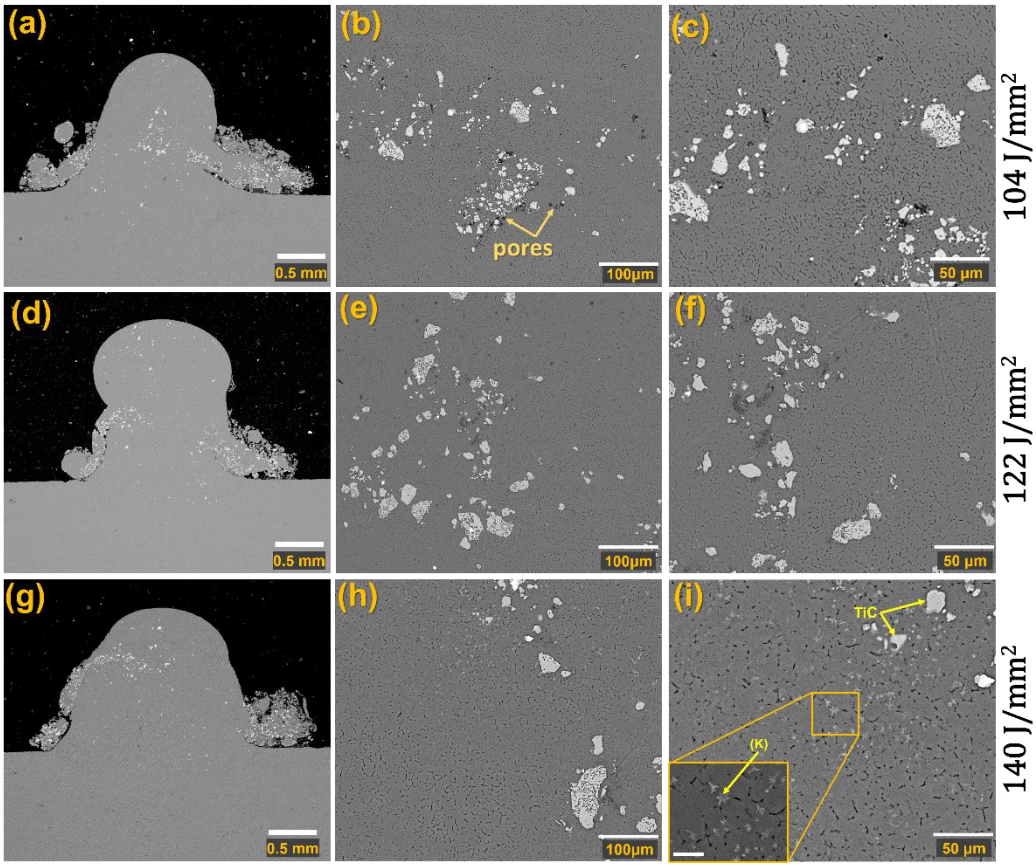


Figure 6-16: BSE images showing the microstructure of the blended clads deposited at three different laser energy densities; (a - c) 104 J/mm^2, (d - f) 122 J/mm^2, and (g -i) 140 J/mm^2; (scale bar in K is 10 µm).

Some pores can be seen in the clad section, this is likely due to incomplete melting in some regions, given their irregular morphologies, hence unlikely to be gas porosity. The incomplete melting commonly occurs due to insufficient energy delivered to the melt pool [186]. Some pores can be seen concentrated close to the TiC clusters, Figure 6-16-b. This may be explained by the lower energy reaching the blended clads as discussed in 6.3.2.2.

The microstructure of the blended clad which deposited at 122 J/mm^2 also appears consisting of TiC particles in an aluminium matrix shown in Figure 6-16 (d-f). It can be seen that the clad section has almost eliminated porosity (reduction of 83%). This is likely explained by the effect of higher laser energy that yields sufficient energy to the melt pool, avoiding incomplete melting.

Higher laser density, i.e. 140 J/mm^2, led to the dissolving of some TiC particles. The blended clad microstructure consists of virgin TiC particles dispersed in an Al matrix. In addition, fine flower-shape structures with bright appearance have appeared spattered around the original TiC particles, Figure 6-16 (i). The XRD pattern of the blended clad deposited at 140 J/mm^2 shows that the consisting phases of the relevant clad are Al, TiC, and a few peaks of Al_5Ti_3, Figure 6-17.

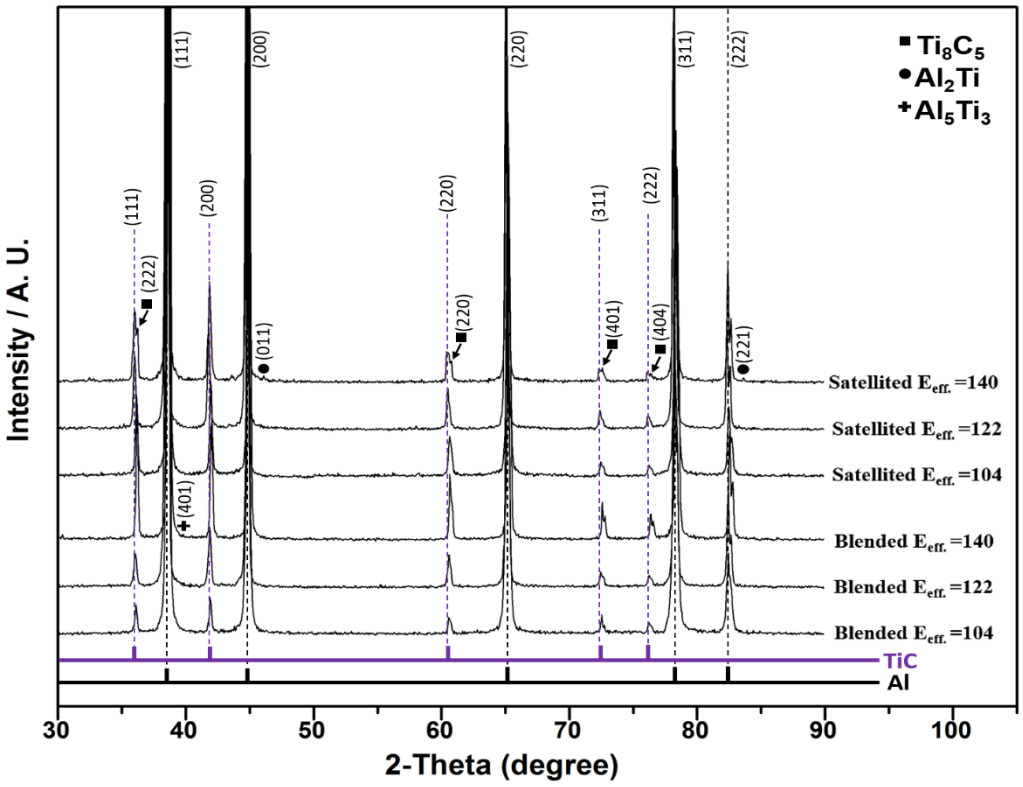


Figure 6-17: XRD patterns of the blended and satellited samples that were deposited at PDD of 0.0056 g/mm^2 at different values of E_{eff}, showing the formation of new phases when high E_{eff}s were used.

Figure 6-18 shows the WDE mapping data of sample 11. Three major elements Al, C, and Ti were presented for a selected region of sample 11 which has been mapped by WDS. It can be seen that structure (labelled K) consists of Al and Ti. This may indicate the formation of Al_5Ti_3 during the cladding process due to the dissolution of TiC high laser energy. This indication is based on the XRD data of the relevant clad as there is a small peak of Al_5Ti_3 appeared in the clad pattern. The microstructure of the blended clads consists of TiC particles dispersed in an Al matrix, while the sample deposited at 140 J/mm^2 includes fine Al_5Ti_3 structure distributed through the matrix in addition to the TiC particles.

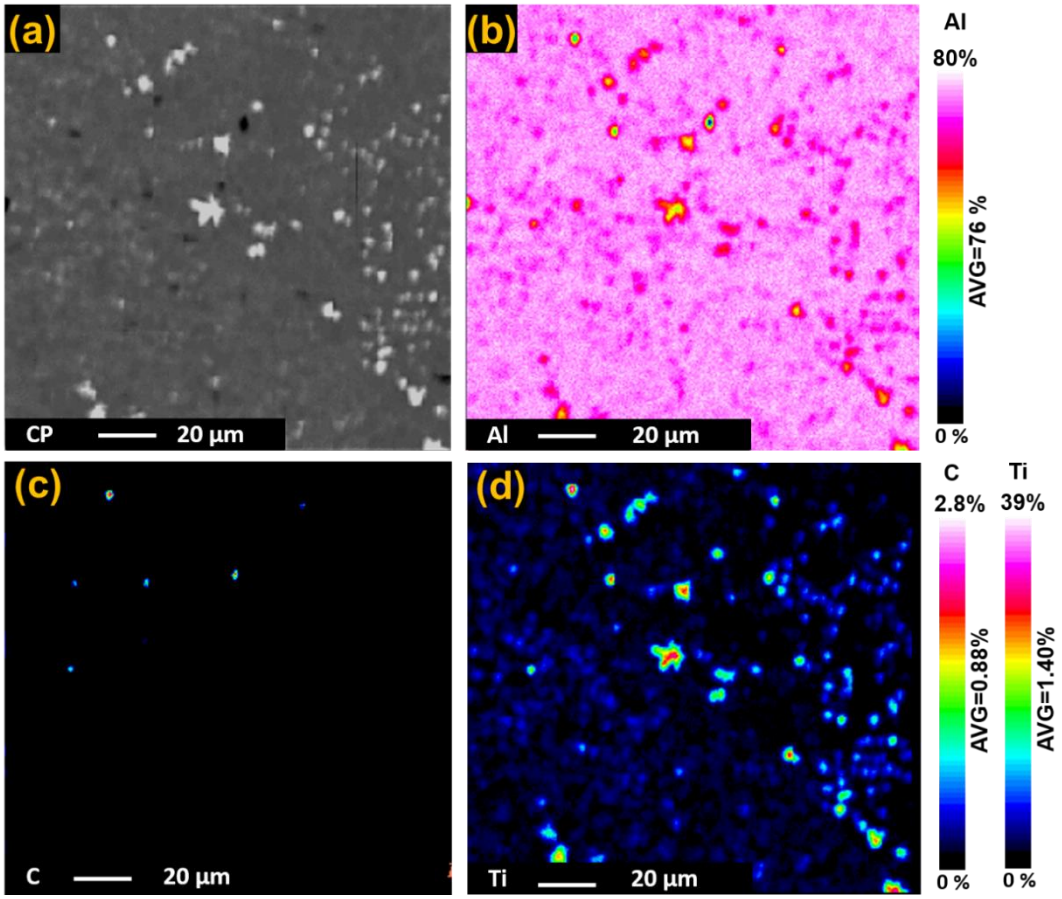


Figure 6-18: WDS maps showing (a) BSE image, and concentration of (b) Al, (c) C, and (d) Ti in the section of the blended clad deposited at PDD of 0.0056 g/mm2 and 140 J/mm2.

Figure 6-19 shows the typical microstructure of the satellited samples that were prepared at 104, 122 and 140 (J/mm^2). The microstructure of the lower laser energy clad (sample 15) shows that there is no noticeable dissolution of TiC particles, this can also be confirmed by the XRD pattern of the sample which deposited at 140 J/mm^2 (Figure 6-17). It seems that the lower energy density (104 J/mm^2) was not sufficient to melt TiC in both blended and satellited feedstocks.

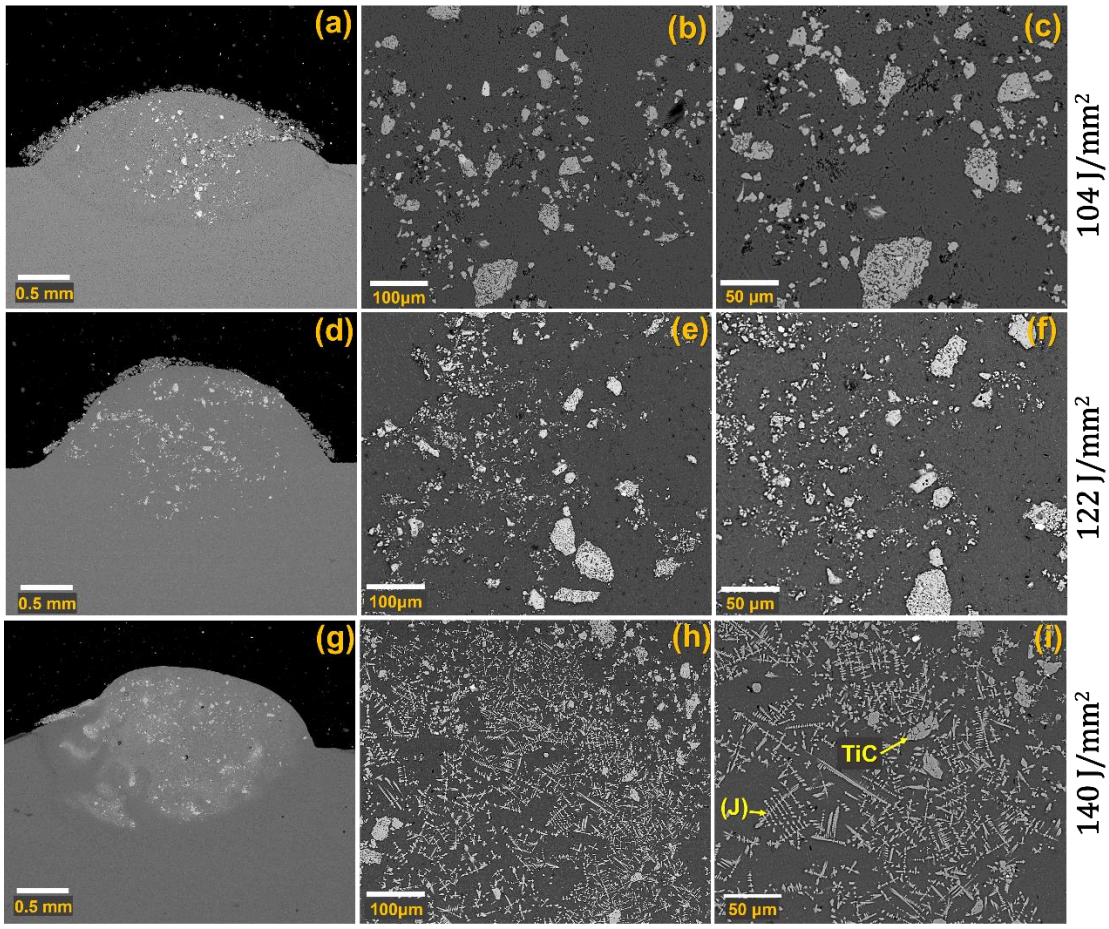


Figure 6-19: BSE images showing the microstructure of the satellited clads deposited with different magnifications; (a-c) 104 J/mm^2, (d-f) 122 J/mm^2, and (g-i) 140 J/mm^2.

At medium laser density (122 J/mm^2), the microstructure of the satellited clad appears to consist of an Al matrix reinforced by virgin TiC. The XRD pattern also confirms this observation as there are Al and TiC peaks. The WDS data of the Al matrix showed no dissolution occurred in the TiC as the at.% of Al was 99.96 ±0.02. This is also indicated by the angular shapes of the TiC particles in the clad section, Figure 6-19 (d-f).

The micro-porosity in the satellited clad at 122 J/mm^2 is 73% lower than the satellited clad at 104 J/mm2. It is known that by increasing the laser energy density, the volume of the melt pool increases owing to the higher laser energy absorbed by

the materials [187]. Consequently, the solidification time increases and a longer time is provided for the melt to fill the pores. This can explain the reduced porosity in the satellited clad at 122 J/mm^2. Interestingly, the difference in TiC amount between the blended and satellited clads can be clearly seen. The satellited clads contain a higher amount of TiC with an even distribution compared with the blended clads, the proposed mechanism of the powder behaviour within laser cladding can explain this observation, see 6.3.2.

The satellited clad deposited at E_{eff} 140 J/mm^2 yielded a different structure consisting of a needle-like structure which is widespread throughout the Al matrix, as shown in Figure 6-19 (g-i). The clad microstructure consists of three main components: intact TiC particles, an Al matrix, and the bright needle-like structure. When the laser energy density increased, a higher amount of TiC is dissolved, e [290]. A smaller amount of the unmelted TiC particles were present compared with other satellited samples deposited at lower Eeff that have no dissolving in TiC.

The XRD pattern of the satellited clad deposited at E_{eff} 140 J/mm^2 indicates that the phases present in the sample are Al, TiC, Ti_8C_5 and Al_2Ti. The WDS mapping of the selected region of the sample (Figure 6-20) shows that the needle structure contains Ti and C, and considering XRD data, this suggests that the columnar structure is Ti_8C_5. WDS mapping results show that the Ti and Al have appeared at the edges of the dendritic TiC. This points to the presence of the Al_2Ti in these regions due to the dilution of the TiC particle edges as a result of the high laser energy delivered to the satellited materials compared to the blended materials.

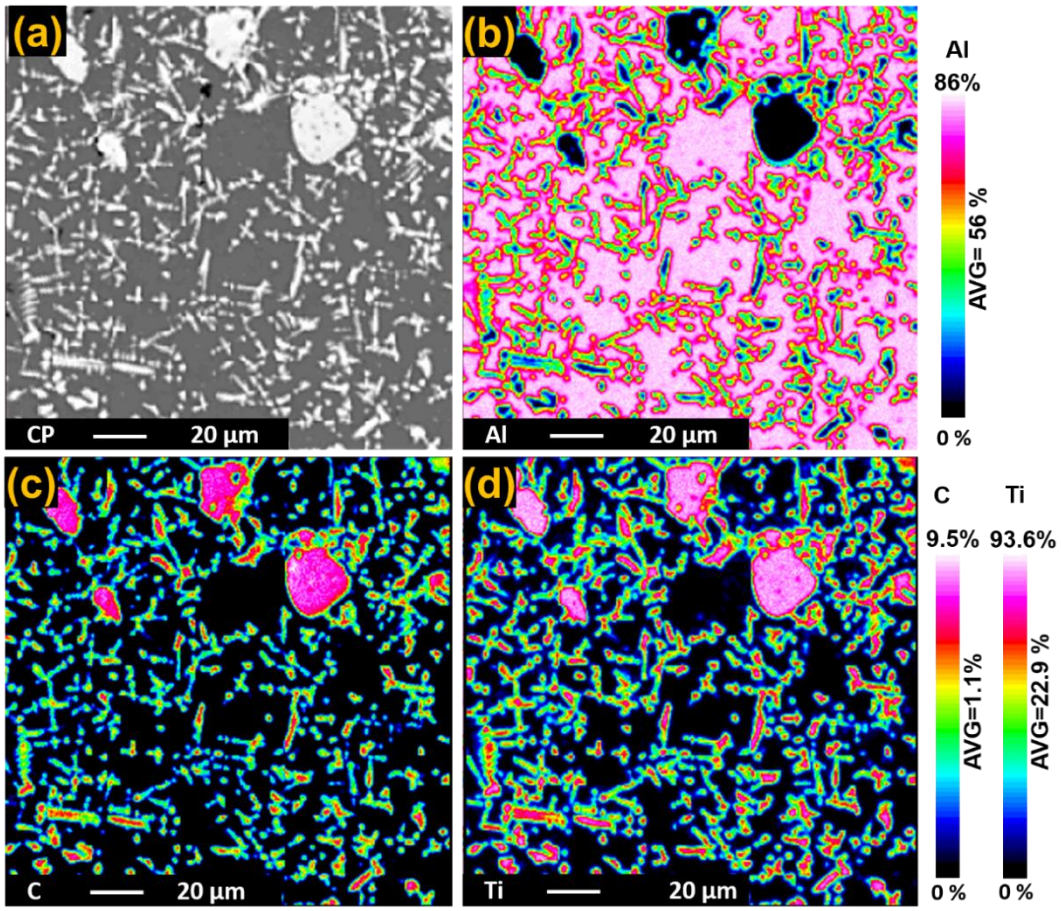


Figure 6-20: WDS maps showing (a) BSE image, and the concentration levels of (b) Al, (c) C, and (d) Ti in the satellited clad section deposited at 140 J/mm^2 and 0.0056 g/mm^2.

The Ti-C phase diagram [291] shows that the titanium carbide with carbon atomic fraction of 38.5 %, which is the same composition of Ti_8C_5, forms at 3065 ºC. Emamian et al. have stated that the clad temperature can be different in different locations [151]. Thus, elevated temperature can be achieved in the clad where the TiC particles (with high laser absorption) concentrate, while lower temperature can also exist at lower TiC areas. Bandyopadhyay et al. state that the precipitation of Al_5Ti_3 starts at 1119 ºC [292]. This indicates that Ti_8C_5 forms at a higher temperature compared with Al_5Ti_3. It is also known that Al_5Ti_3 is not stable and dissolves rapidly when Ti-Al alloys are annealed at temperatures above 800°C

[293]. The formed phases (Ti_8C_5 and Al_5Ti_3) are evidence that the satellited clads absorbed higher laser energy compared to the blended clads deposited at the same process parameters.

Consequently, clear differences in the microstructure between the identical clads that were deposited using blended and satellited feedstocks can be observed this can be attributed to distinct heat transfer regimes in each case. The TiC fractions in the satellited clads are significantly larger compared with blended clads. Also, the dissolution of the TiC at the blended clad that was deposited at E_{eff} of 140 J/mm^2 is less than that in the satellited clads prepared at the same conditions.

The microstructure and phases are different, as new phases including Ti_8C_5 and Al_2Ti formed in the satellited clad that was produced at higher E_{eff} (140 J/mm^2). Previous studies showed that the hardness of Ti_8C_5 is ~953 HV [294] and the hardness of Al_2Ti is ranged between 349-507 HV [295]. The presence of these phases can enhance the strengthening action in the matrix material [296]. Consequently, the modified behaviour of the satellited materials has led to differences in the microstructure between the blended and satellited clads, which can lead to an improvement in the mechanical properties and materials deposition within laser cladding.

6.5 Microhardness and dry-sliding wear behaviour of the deposited clads

6.5.1 Microhardness measurements

To evaluate the mechanical performance of the clads made from blended and satellited feedstocks, microhardness and dry sliding wear testing were performed. Figure 6-21 shows the measured microhardness of the blended and satellited clads deposited at different laser densities. The mean micro-hardness measurements of the matrix of the blended clads were between 37.7 and 51.6 Hv0.025. The clad samples prepared with 104 and 122 J/mm^2 presented close hardness values 37.7 ±0.5 and 40.9 ±0.5 Hv0.025, respectively. The slight increase in the hardness of the sample at 122 J/mm^2 compared to 104 J/mm^2 can be explained by the relatively denser structures of the samples of 122 J/mm^2, as the porosity decreased by 83% when the laser density increased from 104 to 122 J/mm^2.

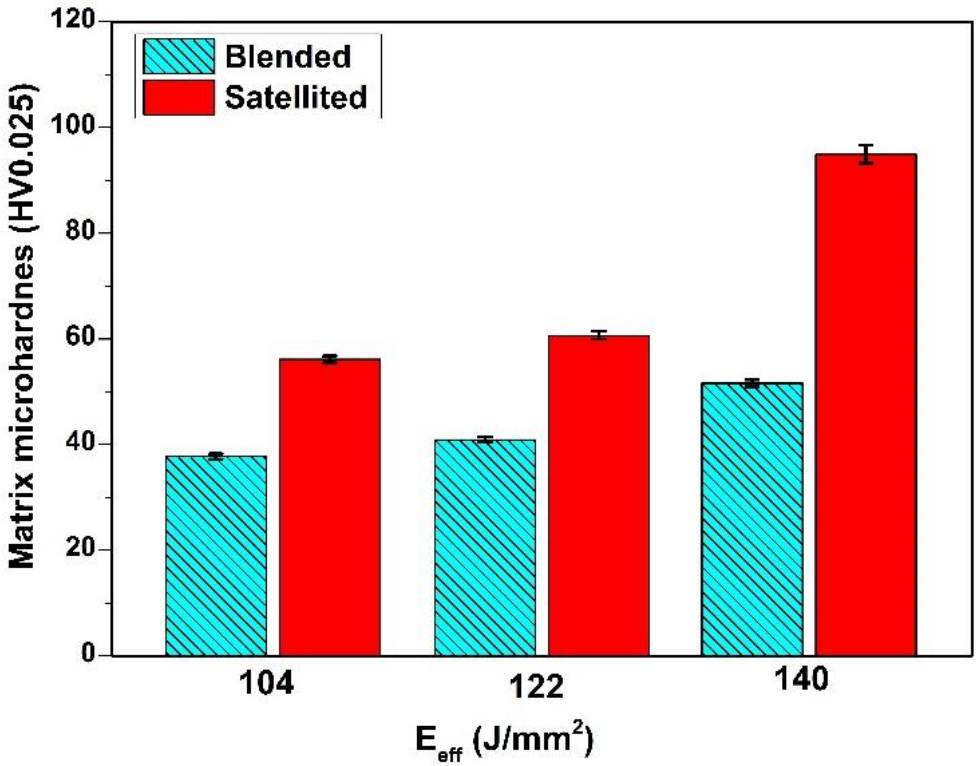


Figure 6-21: Microhardness measurements of blended and satellited clad matrices deposited at different Eeff values; error bars represent the standard errors of 10 measurements.

The blended clad prepared with 140 J/mm^2 yielded the highest hardness among blended clads with 51.6 ±0.6 Hv0.025. It is believed that the presence of Al_5Ti_3 can positively affect the hardness due to the expected strengthening action of Al_5Ti_3 on the matrix. Al_5Ti_3 is known to be a reinforcement of Al-Ti alloys [297]. The formation of stable phases such as Al_5Ti_3 can improve the mechanical properties of the Al-Ti alloy [298, 299]. The formed hard phases behave as reinforcement phases in the matrix and contribute to increased hardness in the composites [300].

With regard to the satellited clads that were prepared at 104 and 122 J/mm^2, the microhardness measurements are 56.1 ±0.6 and 60.6 ±0.7 Hv0.025, respectively. The denser structure of the satellited sample deposited at 122 compared with that at 104 J/mm^2 can explain the slight difference in the clad hardness. As it is reported that the dense structure has led to an improvement in the micro-hardness measurements of the composite clads [184]. In comparison to the blended samples that were deposited at 104 and 122 J/mm^2, the average microhardness values of the satellited samples were higher by 42% and 55%, respectively. This increase can be explained by the significantly higher TiC amount embedded (or dissolved) in the satellited clads compared to the blended clads.

The satellited clad deposited at E_{eff} =140 J/mm^2 yields a matrix hardness of 94.9 ±1.7 Hv0.025, the highest hardness among all clads. Xue et al. [301] have found that the formation of Ti_8C_5 plays an effective role in enhancing the hardness and wear resistance of the composite ceramic. The uniform distribution of the

reinforcement phase is an important factor for the quality of the mechanical properties in the composite coatings [170]. Thus the presence of Ti_8C_5 with the enhanced structure/distribution over the clad section can explain the higher measurement of the hardness of the high E_{eff} satellited sample

In summary, the microhardness results showed a superiority of the satellited clads in comparison with the blended clads due to the higher TiC fractions in the satellited clads. In addition, the higher laser density clads presented higher microhardness measurements. This is due to the formation of the intermetallic Al_5Ti_3 in the blended clad, and the formation of the needle-structure Ti_8C_5 in the satellited clad with good distribution.

6.5.2 Dry-sliding wear results

Three samples from each feedstock, prepared with different energy densities, were tested under dry sliding reciprocating wear testing. The specific wear rate data of the deposited clads (blended and satellited), under dry sliding wear conditions, is shown in Figure 6-22.

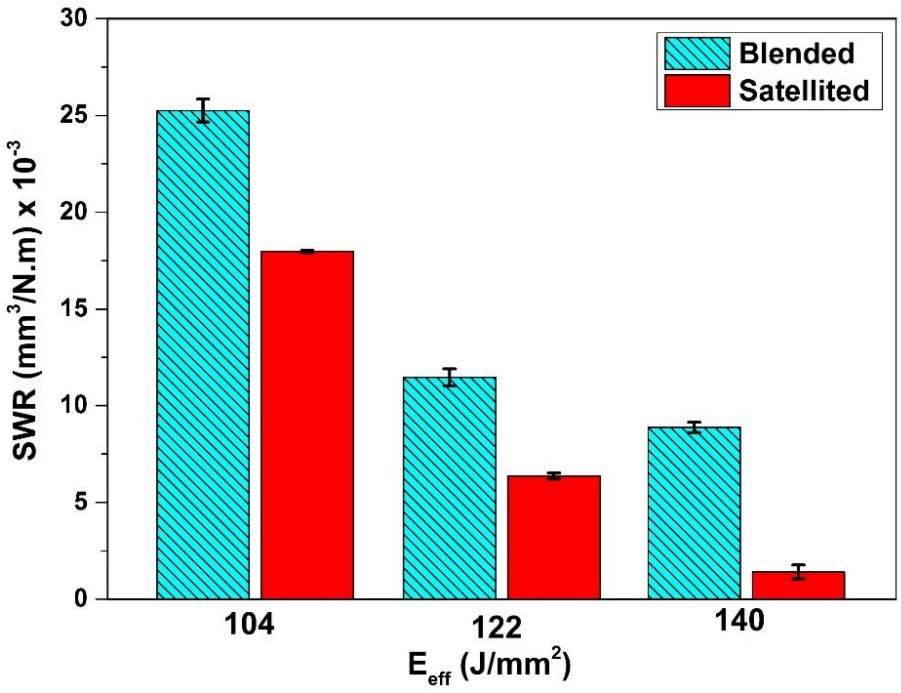


Figure 6-22: The average SWR of the blended and satellited clads; error bars represent the standard errors of three measurements.

In general, the blended and satellited clads that were deposited at higher E_{eff} yielded SWRs lower than clads deposited at lower E_{eff} from the same feedstock. In general, satellited clads yielded an improved wear resistance compared with the blended clads at different values of E_{eff}. There was a reduction of 29% and 44% in the SWR values of the satellited clads compared to the blended clads that were at E_{eff}=104 and 122 J/mm^2, respectively. For clads deposited at higher E_{eff} (140 J/mm^2), the satellited clad presents a SWR significantly lower than the blended clad (84% reduction).

The entire wear scar and worn surface SE images of the blended clads are shown in Figure 6-23. The worn surfaces of the blended clad prepared at E_{eff} of 104 are shown in Figure 6-23 (a-c). It is shown that the worn surface consists of abrasive grooves, delaminated layers, and wear debris. This is likely due to the softness of the Al matrix, and also due to the non-uniform structure owing to the presence of

incomplete melting regions and pores. The worn surface of the blended clad deposited at 122 J/mm^2 appears similar to the sample deposited at 104 J/mm^2 in terms of the surface morphology and the low amount of TiC over the surface, Figure 6-23 (d-f). The track surface presented flat areas with thinner delaminated layers and smaller debris. The blended sample that was deposited at 140 J/mm^2 shows continuous abrasive grooves and thin delaminated layers with little debris. Some debris appears to have been deformed by the counter body and to have been adhered to the surface. The track overall appears narrower than other sample tracks. The higher hardness of the clad at 140 J/mm^2 likely explains its lowest SWR out of the blended clads.

These observations indicate that the plastic deformation dominated the wear behaviour due to the high ductility of the clad surfaces. The worn surface in the high E_{eff} blended clad is similar to that of the lower E_{eff} tracks, although presenting less delamination and wear debris. These features are consistent across the entire track.

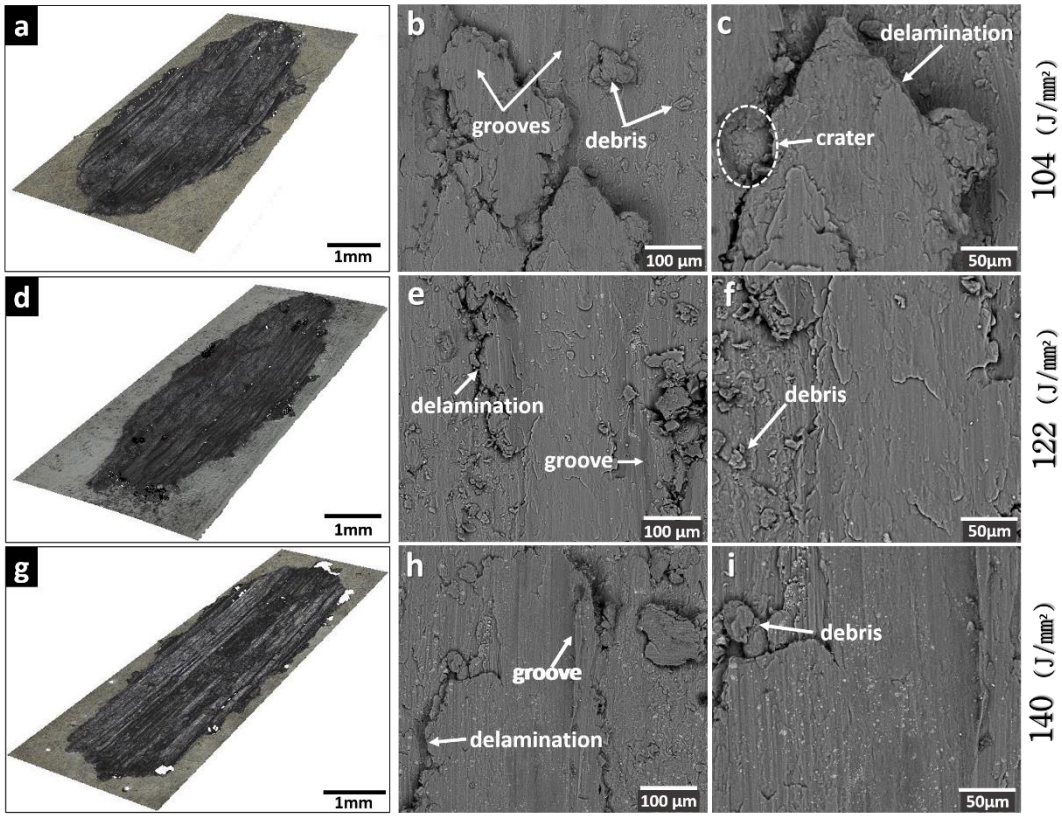


Figure 6-23: Images of the worn surfaces of the blended clads; the first column: 3D-views of the entire wear tracks; second column: low magnification SEM images; and third column: high magnification SEM images. Laser energy is labelled on the right.

Figure 6-24 s shows the entire wear scar and worn surface SE images of the wear track of the satellited clads. Worn surfaces are generally smoother with less delamination and fewer abrasive grooves. It is known that the embedding of ceramic in MMC coatings increases the wear resistance of composite coatings. This is due to the high hardness of the ceramic [302] and also likely enhanced by the improved bonding between the matrix and ceramic particles [303].

Figure 6-24 (a-c) shows abrasive scratches on the worn surface of the satellited clad which was prepared at 104 J/mm^2. Micro-cracks can be seen in the middle of the track owing to the cyclic stresses caused by the counter body movement during the

test. Thin detached layers can be seen at the track centre, leaving some craters. With regards to the satellited sample deposited at E_{eff} of 122 J/mm^2, the worn surface is similar to the lower E_{eff} satellited sample; however, the cracks and grooves are almost disappeared. It can be seen that the track surface is flat without wear debris on the surface and less extensive abrasive grooving.

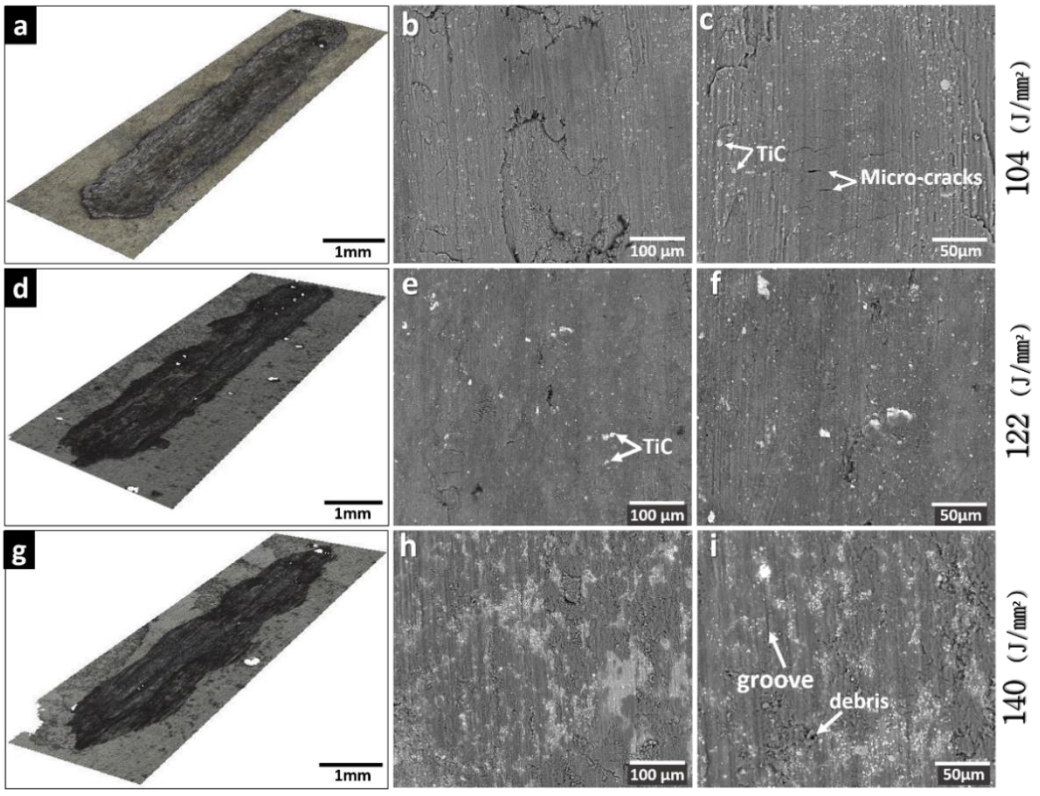


Figure 6-24: Images of the worn surfaces of the satellited clads; first column: 3D-views of the entire wear tracks; second column: low magnification SEM images; and third column: high magnification SEM images. Laser energy was labelled at the right-hand side.

The satellited clad which was deposited at higher energy density (E_{eff} of 140 J/mm^2) presents a wear track morphology reflecting the microstructure of the clad section. The worn surface consists of TiC particles spread over two types of areas: dark area represents the Al matrix, and the bright area represents TiC. The morphology of the

worn track includes fine discontinuous scratches and some micro-cracks in the Al matrix regions, in addition to fine wear debris without noticeable detached layers.

Accordingly, the dry-sliding wear test results showed that there was a clear improvement in the wear resistance when a satellited feedstock was used. This is indicated by the lower SWR measurements of the satellited clads compared with the blended. The main reason for this improvement is related to the presence of higher amounts of titanium carbide (TiC/Ti_8C_5) in the satellited clads compared with the blended clads. Similar observations were reported by Prasad et al., since the presence of TiC particles reduced the penetration depth of the abrasive particles by protecting the Al matrix [304]. The wear results were well-matched with the microhardness results that indicated the superiority of satellited clads over the blended clads. This correlation between wear and hardness results was also reported by Xu et al. [305] who observed that higher hardness composite clads presented lower weight loss and higher wear resistance than lower hardness clads.

6.6 Summary

Simply-blended and satellited Al/20TiC composite feedstocks were prepared and successfully used for laser cladding to investigate the effects of satelliting on the behaviour of the sprayed materials. The conclusions of this investigation can be summarised as follows:

1. The satellited clads yielded larger clad areas than those from blended feedstocks, indicating an enhanced efficiency of the laser cladding process. The blended clads presented dilution levels lower than satellited clads, explained by a lower amount of heat being delivered to the substrate. These differences indicate different behaviour of each feedstock in laser processing that led to differences in the delivered energy and the rate of material deposition.
2. The free TiC particles in the blended feedstock had two main effects. Firstly, they interrupted the laser beam preventing its action directly beneath. Secondly, the TiC particles were blown away from the laser region to a greater extent due to lower mass.
3. The TiC particles that attached to the Al in the satellited feedstock improved the laser absorption of the Al particles by reducing the reflection of the laser from the particle surfaces. In addition, the reduction in the amount of the free TiC particles allows more laser energy to reach more material in line of sight of the beam.
4. The attachment of TiC to the Al particle surfaces increased the momentum of the satellited particles, producing a narrower stream of particles, caused by reduced divergence from the stream, and in turn reducing the number of

particles rebounding from the unmelted substrate. Thus, the TiC fractions in the satellited clads have increased by an average of 113% compared to the blended clads. Reduced divergence of powder in the case of the satellite feedstock was proven through pre-placed powder laser cladding experiments in which similar clad structures were produced.

5. The deposition efficiency of the satellited feedstock clads was greater than the blended clads by ~30%. However, the dilution in the satellited clads was greater than that in the blended, likely due to the higher laser energy delivered to the substrate. Dissolution of the TiC in the satellited clads occurred when high E_{eff} was used.
6. The range of the processing parameters which yielded high quality satellited clads was slightly wider than that of the blended clads. A significant increase in TiC fraction with an enhanced distribution was obtained when the satellited feedstock was used compared with the blended feedstock owing to the reduced divergence of powder.
7. This work introduces satelliting as a promising approach for enhancing the deposition of fine-ceramic reinforced composite coatings with improved ceramic fraction and deposition efficiency by means of laser cladding.

7 Conclusions and Future Work

7.1 Conclusions

This thesis investigated the satelliting technique for preparing composite feedstocks for cold spray and laser cladding deposition processes. For comparison purposes, simply-blended feedstocks with the same composition were also prepared and used within the same deposition processes under the same processing conditions.

Satelliting has the advantages of being a simple production procedure with no mechanical modification of the feedstock. The efficacy of this process is demonstrated by cold-spraying the satellited feedstock and comparing the coating morphology and TiC fraction with an equivalent, blended powder. When pure Al powder was used as a matrix, the satellited coating results showed a significant, sevenfold improvement in yield of TiC embedded in coatings produced by cold spraying. The satellited feedstock also showed good flowability, close to that of the starting Al powder. This was indicated by the measurements of the BFE of the Al and satellited powder as they presented very close values of 250 and 251 mJ, respectively.

In case of using A6061 as a matrix material, satelliting was also shown to reduce the number of defects typically observed in the deposition of less compliant Al alloys and producing a dense A6061-TiC coating fabricated by cold-spray. The use of satellited feedstock has resulted in increasing the TiC catchment and deposition efficiency by 66% and 78%, respectively, compared to the blended feedstock. This indicates an important enhancement in the material deposition and coating reinforcement. The coating porosity also reduced by ~70% using the satellited feedstock, while the TiC area fraction increased >60% in the satellited coating

section compared to the blended coating. Satelliting has caused increased embedment and enhances the compaction (hammering) action of TiC in the composite coating. Post-deposition heat-treatment of the satellited coating at 345^{o}C for 2 hr yielded a reduced porosity of 0.21% from 0.66% for the non heat-treated coating. This was explained by reduced inter-particle interfaces and an enhanced coating-substrate interface owing to the solid-state diffusion of Al.

Under dry-sliding wear conditions, the specific wear rate of the heat-treated 6061-TiC cold-sprayed coating against a steel ball was reduced by a mean of 25% in comparison to the as-sprayed coating, with good repeatability. This was explained by the contribution of the improved toughness and enhanced structure cohesion after heat treatment, resulting in reduced fracture during wear. Therefore, satelliting has been demonstrated as a promising powder preparation method that can change the behaviour of the sprayed materials due to the different interaction between the satellited phases. Wherein the satellite particles have been restricted to the Al particles, i.e. trapping beneath bottom of the satellite deposits; this has increased the deposition of both TiC and A6061 particles within cold spray.

In laser cladding, clads from satellite feedstocks yielded larger clad areas than those from blended feedstocks, indicating an enhanced efficiency of the laser cladding process. The blended clads presented dilution levels lower than satellited clads, explained by a lower amount of heat being delivered to the substrate. These differences indicate different behaviour of each feedstock in laser processing that led to differences in the delivered energy and the rate of material deposition.

The free TiC particles in the blended feedstock had two main effects. Firstly, they interrupted the laser beam preventing its action directly beneath. Secondly, the TiC

particles were blown away from the laser region to a greater extent due to lower mass. It is believed that TiC particles that were attached to the Al in the satellited feedstock improved the laser absorption of the Al particles by reducing the reflection of the laser from the particle surfaces. In addition, the reduction in the amount of free TiC particles allows more laser energy to reach more material in line of sight of the beam. The attachment of TiC to the Al particle surfaces increased the momentum of the satellited particles, producing a narrower stream of particles, caused by reduced divergence from the stream, and in turn, reducing the number of particles rebounding from the unmelted substrate. Reduced divergence of powder in the case of the satellited feedstock was proven through pre-placed powder laser cladding experiments in which similar clad structures were produced.

Two deposition mechanisms explain the differences in the behaviour of both feedstocks within laser cladding. The satellited particles allow a higher amount of energy to reach the substrate surface and Al particles due to the reduction in the amount of free TiC particles that interrupt laser radiation and reducing the laser reflection at the Al particle surfaces. It is likely that the satellited feedstock also reduced the divergence of TiC particles based on the attachment of these particles to the Al particles. These resulted superior laser clads from satellite feedstocks in terms of deposition efficiency and TiC content in deposited coatings with improved uniformity and distribution.

The deposition efficiency of the satellited feedstock clads was greater than the blended clads by ~30%. However, the dilution in the satellited clads was greater than that in the blended, likely due to the higher laser energy delivered to the

substrate. Dissolution of the TiC in the satellited clads occurred when high E_{eff} was used. The range of the processing parameters which yielded high quality satellited clads was slightly wider than that of the blended clads. A significant increase in TiC fraction with an enhanced distribution was obtained when the satellited feedstock was used compared with the blended feedstock owing to the reduced divergence of powder.

In summary, it is believed that the knowledge gaps in the literature that were mentioned in chapter 2 (2.6.5), have been discovered in this thesis. Although there is a slight reduction in the particle velocity, the satelliting process maintained the suitability of the satellited powder for the cold spray process and improved the peening (compaction) in the cold-sprayed coatings. Also, the use of satelliting can be utilized to overcome the challenges of cold spray regarding the deposition of fine-hard particles and the lack of deformation in high strength alloys within cold spray. According to the laser cladding results, satelliting can be considered as a promising approach for enhancing the deposition of fine-ceramic reinforced composite coatings with improved ceramic fraction and deposition efficiency by means of laser cladding.

7.2 Recommendations for future work

Considering the broad investigation of the work undertaken, there are a number of interesting research areas that may require additional investigation to be carried out. These are summarised as follows.

The satelliting approach needs to be widely investigated for exploring the advantages and disadvantages of the satellited material within different deposition processes like selective laser melting, thermal spray. Also, satelliting can be used for preparing powders for powder metallurgy processes of composite materials; this would enhance the distribution of the reinforcements.

Moreover, satelliting can be applied to different materials systems with different powder morphologies to study the effect of powder morphologies on the quality and efficiency of the satelliting. Also, using coarse ceramic as a parent powder and fine metal powder as satellite may affect the behaviour of the satellited powder within cold spray as the deformation will occur at the satellited particle surfaces instead of the cores.

Nano carbon tubes and nano-ceramic can be used as satellite materials in order to produce composite feedstock for different deposition processes. However, there are some challenges should be considered regarding the use of nanomaterials as the agglomeration/clustering may form, and this would affect the flowability and homogeneity of the satellited powder.

It is believed that satelliting can play a vital role in expanding the range of materials that are used as feedstocks for different deposition techniques; this is by overcoming the drawbacks of other traditional powder preparing methods.

References

[1] Sakaki K, Shimizu Y. Effect of the increase in the entrance convergent section length of the gun nozzle on the high-velocity oxygen fuel and cold spray process. Journal of thermal spray technology. 2001;10:487-96.

[2] Lee HY, Jung SH, Lee SY, You YH, Ko KH. Correlation between Al2O3 particles and interface of Al–Al2O3 coatings by cold spray. Applied Surface Science. 2005;252:1891-8.

[3] Wang X, Zhang M, Zou Z, Qu S. Microstructure and properties of laser clad TiC+ NiCrBSi+ rare earth composite coatings. Surface and Coatings Technology. 2002;161:195-9.

[4] Wang XH, Zhang M, Liu XM, Qu SY, Zou ZD. Microstructure and wear properties of TiC/FeCrBSi surface composite coating prepared by laser cladding. Surface and Coatings Technology. 2008;202:3600-6.

[5] Alexander E, Christopher S, Andreas M. Metal matrix composites in industry: an introduction and a survey. Nor well: Kluwer Academic Publishers. 2003.

[6] Chawla N, Shen YL. Mechanical behavior of particle reinforced metal matrix composites. Advanced engineering materials. 2001;3:357-70.

[7] Ibrahim I, Mohamed F, Lavernia E. Particulate reinforced metal matrix composites—a review. Journal of materials science. 1991;26:1137-56.

[8] Singerman S, Jackson J, Lynn M. Titanium metal matrix composites for aerospace applications. Superalloys 1996, proceedings of eighth international symposium on superalloys1996.

[9] Chung DDL. Composite materials for electrical applications. In: Chung DDL, editor. Composite Materials: Functional Materials for Modern Technologies. London: Springer London; 2003. p. 73-89.

[10] Shoukry SN, Prucz JC, Shankaranarayana PG, William GW. Microstructure modeling of particulate reinforced metal matrix composites. Mechanics of Advanced Materials and Structures. 2007;14:499-510.

[11] Shyu R, Ho C. In situ reacted titanium carbide-reinforced aluminum alloys composite. Journal of materials processing technology. 2006;171:411-6.

[12] Everett R. Metal matrix composites: processing and interfaces: Academic press; 2012.

[13] Huang L, Geng L. Discontinuously Reinforced Titanium Matrix Composites: Microstructure Design and Property Optimization: Springer; 2017.

[14] Hunt WH. 6.05 - Metal Matrix Composites. In: Kelly A, Zweben C, editors. Comprehensive Composite Materials. Oxford: Pergamon; 2000. p. 57-66.

[15] Fishman SG, Rozner AG, Wiley RC, Wishard WN. Composite tungsten-steel armor penetrators. Google Patents; 1990.
[16] Park S-J, Seo M-K. Chapter 7 - Types of Composites. In: Park S-J, Seo M-K, editors. Interface Science and Technology: Elsevier; 2011. p. 501-629.
[17] Chawla KK. Ceramic matrix composites: Springer Science & Business Media; 2013.
[18] Kainer KU. Basics of metal matrix composites: Wiley Online Library; 2006.
[19] Haghshenas M. Metal–matrix composites. Reference Module in Materials Science and Materials Engineering. 2016:03950-3.
[20] Kainer KU. Metal matrix composites: custom-made materials for automotive and aerospace engineering: John Wiley & Sons; 2006.
[21] Batraev I, Chaitanya S, Cheng X, Dudina DV, Krishnaraj V, Kumar R, et al. Metal matrix composites: materials, manufacturing and engineering: Walter de Gruyter GmbH & Co KG; 2014.
[22] Narasimha BG, Krishna VM, Xavior AM. A review on processing of particulate metal matrix composites and its properties. International Journal of Applied Engineering Research. 2013;8:647-66.
[23] Rosso M. Ceramic and metal matrix composites: Routes and properties. Journal of Materials Processing Technology. 2006;175:364-75.
[24] Prasad SV, Asthana R. Aluminum Metal-Matrix Composites for Automotive Applications: Tribological Considerations. Tribology Letters. 2004;17:445-53.
[25] Hu W, Huang Z, Zheng G, Wang Y, Lei C, Cai L, et al. Optimizing the microstructure and mechanical behaviors of in-situ TiC-γ′/Ni composites by subsequent thermal treatment. Journal of Alloys and Compounds. 2019;774:739-47.
[26] Davim JP. Metal Matrix Composites, Materials, Manufacturing and Engineering2014.
[27] Kouzeli M, Mortensen A. Size dependent strengthening in particle reinforced aluminium. Acta Materialia. 2002;50:39-51.
[28] Kim S-H, Hahn HT. Size effect in particulate metal matrix composites: an analytical approach. Advanced Composite Materials. 2006;15:175-91.
[29] Sova A, Papyrin A, Smurov I. Influence of Ceramic Powder Size on Process of Cermet Coating Formation by Cold Spray. Journal of Thermal Spray Technology. 2009;18:633.
[30] Tzamtzis S, Barekar N, Babu NH, Patel J, Dhindaw B, Fan Z. Processing of advanced Al/SiC particulate metal matrix composites under intensive shearing–A novel Rheo-process. Composites Part A: Applied science and manufacturing. 2009;40:144-51.

[31] Naher S, Brabazon D, Looney L. Development and assessment of a new quick quench stir caster design for the production of metal matrix composites. Journal of Materials Processing Technology. 2005;166:430-9.
[32] Dasgupta R. Aluminium alloy-based metal matrix composites: a potential material for wear resistant applications. ISRN metallurgy. 2012;2012.
[33] Murthy HA, Singh SK. Influence of TiC particulate reinforcement on the corrosion behaviour of Al 6061 metal matrix composites. Adv Mater Lett. 2015;6:633-40.
[34] Torres B, Garrido M, Rico A, Rodrigo P, Campo M, Rams J. Wear behaviour of thermal spray Al/SiCp coatings. Wear. 2010;268:828-36.
[35] Gopalakrishnan S, Murugan N. Production and wear characterisation of AA 6061 matrix titanium carbide particulate reinforced composite by enhanced stir casting method. Composites Part B: Engineering. 2012;43:302-8.
[36] Mavhungu ST, Akinlabi ET, Onitiri MA, Varachia FM. Aluminum Matrix Composites for Industrial Use: Advances and Trends. Procedia Manufacturing. 2017;7:178-82.
[37] Selcuk C, Kennedy A. Al–TiC composite made by the addition of master alloys pellets synthesised from reacted elemental powders. Materials Letters. 2006;60:3364-6.
[38] Huttunen-Saarivirta E. Microstructure, fabrication and properties of quasicrystalline Al–Cu–Fe alloys: a review. Journal of Alloys and Compounds. 2004;363:154-78.
[39] Deuis R, Yellup J, Subramanian C. Metal-matrix composite coatings by PTA surfacing. Composites science and technology. 1998;58:299-309.
[40] Mao J, Shasha l, Zhang Y, Chu X, Yang Z. The stability of TiC surfaces in the environment with various carbon chemical potential and surface defects2016.
[41] Du B, Paital SR, Dahotre NB. Phase constituents and microstructure of laser synthesized TiB 2–TiC reinforced composite coating on steel. Scripta Materialia. 2008;59:1147-50.
[42] Vallauri D, Adrian IA, Chrysanthou A. TiC–TiB 2 composites: a review of phase relationships, processing and properties. Journal of the European Ceramic Society. 2008;28:1697-713.
[43] Lee K, Sim H, Kwon H. Reaction products of Al/TiC composites fabricated by the pressureless infiltration technique. Metallurgical and Materials Transactions A. 2005;36:2517-27.
[44] Senthilkumar V, Omprakash BU. Effect of Titanium Carbide particle addition in the aluminium composite on EDM process parameters. Journal of Manufacturing Processes. 2011;13:60-6.
[45] Durlu N. Titanium carbide based composites for high temperature applications. Journal of the European Ceramic Society. 1999;19:2415-9.

[46] Sahoo CK, Masanta M. Microstructure and mechanical properties of TiC-Ni coating on AISI304 steel produced by TIG cladding process. Journal of Materials Processing Technology. 2017;240:126-37.
[47] Shin Y, Li XS, Wang C, Coleman JR, Exarhos GJ. Synthesis of Hierarchical Titanium Carbide from Titania-Coated Cellulose Paper. Advanced Materials. 2004;16:1212-5.
[48] Karantzalis A, Wyatt S, Kennedy A. The mechanical properties of Al-TiC metal matrix composites fabricated by a flux-casting technique. Materials Science and Engineering: A. 1997;237:200-6.
[49] Kishore DSC, Rao KP, Ramesh A. Optimization of machining parameters for improving cutting force and surface roughness in turning of Al6061-TiC in-situ metal matrix composites by using Taguchi method. Materials Today: Proceedings. 2015;2:3075-83.
[50] Du B, Wang X, Zou Z. Microstructure and Tribological Behavior of Laser in Situ Synthesized TiC-Reinforced Fe-Based Composite Coatings. Tribology Letters. 2011;43:295-301.
[51] Chawla KK. Composite materials: science and engineering: Springer Science & Business Media; 2012.
[52] Yang H, Jiang L, Balog M, Krizik P, Schoenung JM. Reinforcement size dependence of load bearing capacity in ultrafine-grained metal matrix composites. Metallurgical and Materials Transactions A. 2017;48:4385-92.
[53] Lee SM, Jung JH, Fleury E, Kim WT, Kim DH. Metal matrix composites reinforced by gas-atomised Al-Cu-Fe powders. Materials Science and Engineering: A. 2000;294-296:99-103.
[54] Clyne T, Withers P. An introduction to metal matrix composites: Cambridge university press; 1995.
[55] Gibson I, Rosen D, Stucker B. Directed Energy Deposition Processes. 2015. p. 245-68.
[56] Prusov E, Deev V, Rakhuba E. Aluminum Matrix In-Situ Composites Reinforced with Mg2Si and Al3Ti2019.
[57] Chawla KK. Metal matrix composites. Materials Science and Technology. 2006.
[58] Cui C, Shen Y, Meng F, Kang S. Review on fabrication methods of in situ metal matrix composites. Cailiao Kexue Yu Jishu(Journal of Materials Science & Technology)(China)(USA). 2000;16:619-26.
[59] Sivaprasad K, Babu SK, Natarajan S, Narayanasamy R, Kumar BA, Dinesh G. Study on abrasive and erosive wear behaviour of Al 6063/TiB2in situ composites. Materials Science and Engineering: A. 2008;498:495-500.

[60] Contreras A, Angeles-Chávez C, Flores O, Perez R. Structural, morphological and interfacial characterization of Al–Mg/TiC composites. Materials Characterization. 2007;58:685-93.
[61] Lloyd D. Particle reinforced aluminium and magnesium matrix composites. International materials reviews. 1994;39:1-23.
[62] Tjong SC, Ma Z. Microstructural and mechanical characteristics of in situ metal matrix composites. Materials Science and Engineering: R: Reports. 2000;29:49-113.
[63] Bannan J, Temple RI, Jones R. In situfabrication of titanium carbide reinforced copper MMC. Materials Science and Technology. 2013;19:1148-50.
[64] Hardwicke CU, Lau Y-C. Advances in Thermal Spray Coatings for Gas Turbines and Energy Generation: A Review. Journal of Thermal Spray Technology. 2013;22:564-76.
[65] Maev RG, Leshchynsky V. Introduction to low pressure gas dynamic spray: physics and technology: John Wiley & Sons; 2009.
[66] Guo X, Chen J, Yu H, Liao H, Coddet C. A study on the microstructure and tribological behavior of cold-sprayed metal matrix composites reinforced by particulate quasicrystal. Surface and Coatings Technology. 2015;268:94-8.
[67] Papyrin A, Kosarev V, Klinkov S, Alkhimov A, Fomin VM. Cold spray technology: Elsevier; 2006.
[68] J. V, L. G, H. H, E. L. A systematic approach to material eligibility for the cold-spray process. 2005;14:125–33.
[69] Morgan R, Fox P, Pattison J, Sutcliffe C, O'Neill W. Analysis of cold gas dynamically sprayed aluminium deposits. Materials Letters. 2004;58:1317-20.
[70] Ghelichi R, Guagliano M. Coating by the cold spray process: a state of the art. Frattura ed Integrità Strutturale. 2009:30.
[71] Guillem-Marti J, Cinca N, Punset M, Cano IG, Gil FJ, Guilemany JM, et al. Porous titanium-hydroxyapatite composite coating obtained on titanium by cold gas spray with high bond strength for biomedical applications. Colloids and Surfaces B: Biointerfaces. 2019;180:245-53.
[72] Yin S, Cavaliere P, Aldwell B, Jenkins R, Liao H, Li W, et al. Cold spray additive manufacturing and repair: Fundamentals and applications. Additive Manufacturing. 2018;21:628-50.
[73] Ma W, Xie Y, Chen C, Fukanuma H, Wang J, Ren Z, et al. Microstructural and mechanical properties of high-performance Inconel 718 alloy by cold spraying. Journal of Alloys and Compounds. 2019;792:456-67.

[74] Pattison J, Celotto S, Morgan R, Bray M, O'Neill W. Cold gas dynamic manufacturing: A non-thermal approach to freeform fabrication. International Journal of Machine Tools and Manufacture. 2007;47:627-34.
[75] Rokni MR, Widener CA, Champagne VK, Crawford GA. Microstructure and mechanical properties of cold sprayed 7075 deposition during non-isothermal annealing. Surface and Coatings Technology. 2015;276:305-15.
[76] Bray M, Cockburn A, O'Neill W. The Laser-assisted Cold Spray process and deposit characterisation. Surface and Coatings Technology. 2009;203:2851-7.
[77] Assadi H, Gärtner F, Stoltenhoff T, Kreye H. Bonding mechanism in cold gas spraying. Acta Materialia. 2003;51:4379-94.
[78] Swaroopini AS, Kumar MG, Kumar TN. Numerical Simulation and Optimization of High Performance Supersonic Nozzle at Different Conical Angles. International Journal of Research in Engineering and Technology (IJRET). 2015;4.
[79] Podrabinnik P, Grigoriev S, Shishkovsky I. Laser post annealing of cold-sprayed Al/alumina–Ni composite coatings. Surface and Coatings Technology. 2015;271:265-8.
[80] Wisconsin Uo. Cold spray Program. 2014.
[81] Rolland G, Sallamand P, Guipont V, Jeandin M, Boller E, Bourda C. Damage study of cold-sprayed composite materials for application to electrical contacts. Journal of thermal spray technology. 2012;21:758-72.
[82] Prabhu B, Suryanarayana C, An L, Vaidyanathan R. Synthesis and characterization of high volume fraction Al–Al 2 O 3 nanocomposite powders by high-energy milling. Materials Science and Engineering: A. 2006;425:192-200.
[83] Hussain TY, S. and Li, C.-J. Modern Cold Spray; Materials, Process, and Applications. London: Springer; 2015.
[84] Moridi A, Hassani-Gangaraj S, Guagliano M, Dao M. Cold spray coating: review of material systems and future perspectives. Surface Engineering. 2014;30:369-95.
[85] Champagne VK. The Cold Spray Material Deposition Process-fundmentals and applications. Woodhead: CRC press,1-7.; 2007.
[86] A. S, KashirinO., KlyuevT., Buzdygar. Metal particle deposition stimulation by surface abrasive treatment in gas dynamic spraying. Journal of Thermal Spray Technology. 2006;15.
[87] Wang H-T, Li C-J, Yang G-J, Li C-X, Zhang Q, Li W-Y. Microstructural characterization of cold-sprayed nanostructured FeAl intermetallic compound coating and its ball-milled feedstock powders. Journal of thermal spray technology. 2007;16:669-76.

[88] Maestracci R, Sova A, Jeandin M, Malhaire J-M, Movchan I, Bertrand P, et al. Deposition of composite coatings by cold spray using stainless steel 316L, copper and Tribaloy T-700 powder mixtures. Surface and Coatings Technology. 2016;287:1-8.
[89] Suryanarayana C. Nanocrystalline materials. International Materials Reviews. 1995;40:41-64.
[90] li W, Assadi H, Gärtner F, Yin S. A Review of Advanced Composite and Nanostructured Coatings by Solid-State Cold Spraying Process2018.
[91] Aldwell B, Yin S, McDonnell KA, Trimble D, Hussain T, Lupoi R. A novel method for metal–diamond composite coating deposition with cold spray and formation mechanism. Scripta Materialia. 2016;115:10-3.
[92] Zhu L, Jen T-C, Pan Y-T, Chen H-S. Particle bonding mechanism in cold gas dynamic spray: A three-dimensional approach. Journal of Thermal Spray Technology. 2017;26:1859-73.
[93] Sova A, Grigoriev S, Kochetkova A, Smurov I. Influence of powder injection point position on efficiency of powder preheating in cold spray: Numerical study. Surface and Coatings Technology. 2014;242:226-31.
[94] Schmidt T, Gärtner F, Assadi H, Kreye H. Development of a generalized parameter window for cold spray deposition. Acta materialia. 2006;54:729-42.
[95] Kotteda VMK, Mittal S. Flow in a planar convergent–divergent nozzle2016.
[96] Seitzman JM. Isentropic Flow with Area Change. 2002.
[97] Maev RG, Leshchynsky V. Cold gas dynamic spray: CRC Press; 2016.
[98] Dykhuizen R, Smith M, Gilmore D, Neiser R, Jiang X, Sampath S. Impact of high velocity cold spray particles. Journal of Thermal Spray Technology. 1999;8:559-64.
[99] Eskin D, Voropaev S, Dorokhov I. Effect of particle-size distribution on wall friction in high-velocity gas-dynamic apparatuses. Theoretical Foundations of Chemical Engineering. 2003;37:122-30.
[100] Alkhimov A, Kosarev V, Klinkov S. The features of cold spray nozzle design. Journal of thermal spray technology. 2001;10:375-81.
[101] Assadi H, Schmidt T, Richter H, Kliemann J-O, Binder K, Gärtner F, et al. On Parameter Selection in Cold Spraying. Journal of Thermal Spray Technology. 2011;20:1161-76.
[102] Grujicic M, Zhao CL, Tong C, DeRosset WS, Helfritch D. Analysis of the impact velocity of powder particles in the cold-gas dynamic-spray process. Materials Science and Engineering: A. 2004;368:222-30.
[103] Kang K, Won J, Bae G, Ha S, Lee C. Interfacial bonding and microstructural evolution of Al in kinetic spraying. Journal of Materials Science. 2012;47:4649-59.

[104] King PC, Busch C, Kittel-Sherri T, Jahedi M, Gulizia S. Interface melding in cold spray titanium particle impact. Surface and Coatings Technology. 2014;239:191-9.
[105] Vidaller MV, List A, Gaertner F, Klassen T, Dosta S, Guilemany JM. Single impact bonding of cold sprayed Ti-6Al-4V powders on different substrates. Journal of Thermal Spray Technology. 2015;24:644-58.
[106] Chun D-M, Ahn S-H. Deposition mechanism of dry sprayed ceramic particles at room temperature using a nano-particle deposition system. Acta Materialia. 2011;59:2693-703.
[107] Grujicic M, Zhao CL, DeRosset WS, Helfritch D. Adiabatic shear instability based mechanism for particles/substrate bonding in the cold-gas dynamic-spray process. Materials & Design. 2004;25:681-8.
[108] Hassani-Gangaraj M, Veysset D, Champagne VK, Nelson KA, Schuh CA. Adiabatic shear instability is not necessary for adhesion in cold spray. Acta Materialia. 2018;158:430-9.
[109] Hussain T, McCartney DG, Shipway PH, Zhang D. Bonding Mechanisms in Cold Spraying: The Contributions of Metallurgical and Mechanical Components. Journal of Thermal Spray Technology. 2009;18:364-79.
[110] Xie Y, Yin S, Chen C, Planche M-P, Liao H, Lupoi R. New insights into the coating/substrate interfacial bonding mechanism in cold spray. Scripta Materialia. 2016;125:1-4.
[111] Li W, Assadi H, Gaertner F, Yin S. A review of advanced composite and nanostructured coatings by solid-state cold spraying process. Critical Reviews in Solid State and Materials Sciences. 2018:1-48.
[112] Villafuerte J. Modern cold spray: materials, process, and applications: Springer; 2015.
[113] Sova A, Kosarev V, Papyrin A, Smurov I. Effect of ceramic particle velocity on cold spray deposition of metal-ceramic coatings. Journal of thermal spray technology. 2011;20:285-91.
[114] Kliemann J-O, Gutzmann H, Gärtner F, Hübner H, Borchers C, Klassen T. Formation of cold-sprayed ceramic titanium dioxide layers on metal surfaces. Journal of Thermal Spray Technology. 2011;20:292-8.
[115] Fan SQ, Yang GJ, Li CJ, Liu GJ, Li CX, Zhang LZ. Characterization of microstructure of Nano-TiO2 coating deposited by vacuum cold spraying. Journal of Thermal Spray Technology. 2006;15:513-7.
[116] Fernandez R, Jodoin B. Cold Spray Aluminum–Alumina Cermet Coatings: Effect of Alumina Content. Journal of Thermal Spray Technology. 2018;27:603-23.

[117] Triantou KI, Pantelis DI, Guipont V, Jeandin M. Microstructure and tribological behavior of copper and composite copper+ alumina cold sprayed coatings for various alumina contents. Wear. 2015;336:96-107.
[118] Chivavibul P, Watanabe M, Kuroda S, Shinoda K. Effects of carbide size and Co content on the microstructure and mechanical properties of HVOF-sprayed WC–Co coatings. Surface and Coatings Technology. 2007;202:509-21.
[119] Tao Y, Xiong T, Sun C, Kong L, Cui X, Li T, et al. Microstructure and corrosion performance of a cold sprayed aluminium coating on AZ91D magnesium alloy. Corrosion Science. 2010;52:3191-7.
[120] Zhang D, Shipway P, McCartney D. Cold gas dynamic spraying of aluminum: the role of substrate characteristics in deposit formation. Journal of Thermal Spray Technology. 2005;14:109-16.
[121] Irissou E, Legoux J-G, Arsenault B, Moreau C. Investigation of Al-Al2O3 Cold Spray Coating Formation and Properties. Journal of Thermal Spray Technology. 2007;16:661-8.
[122] Diab M, Pang X, Jahed H. The effect of pure aluminum cold spray coating on corrosion and corrosion fatigue of magnesium (3% Al-1% Zn) extrusion. Surface and Coatings Technology. 2017;309:423-35.
[123] Spencer K, Zhang MX. Heat treatment of cold spray coatings to form protective intermetallic layers. Scripta Materialia. 2009;61:44-7.
[124] Sova A, Klinkov S, Kosarev V, Ryashin N, Smurov I. Preliminary study on deposition of aluminium and copper powders by cold spray micronozzle using helium. Surface and Coatings Technology. 2013;220:98-101.
[125] López AJ, Torres B, Taltavull C, Rams J. Influence of high velocity oxygen-fuel spraying parameters on the wear resistance of Al–SiC composite coatings deposited on ZE41A magnesium alloy. Materials & Design. 2013;43:144-52.
[126] Moridi A, Hassani-Gangaraj SM, Guagliano M, Dao M. Cold spray coating: review of material systems and future perspectives. Surface Engineering. 2014;30:369-95.
[127] Naveen Kumar G, Narayanasamy R, Natarajan S, Kumaresh Babu SP, Sivaprasad K, Sivasankaran S. Dry sliding wear behaviour of AA 6351-ZrB2 in situ composite at room temperature. Materials & Design. 2010;31:1526-32.
[128] Leshchynsky V, Papyrin A, Bielousova O, Yadroitsava I, Smurov I. Impact particle behavior in cold gas dynamic spray of composite coatings. Proceedings of the international thermal spray conference, Hamburg, Germany2011. p. 27-9.
[129] Ramesh C, Khan AA, Ravikumar N, Savanprabhu P. Prediction of wear coefficient of Al6061–TiO 2 composites. Wear. 2005;259:602-8.

[130] Umanath K, Palanikumar K, Selvamani S. Analysis of dry sliding wear behaviour of Al6061/SiC/Al 2 O 3 hybrid metal matrix composites. Composites Part B: Engineering. 2013;53:159-68.
[131] Rokni MR, Widener CA, Champagne VR. Microstructural Evolution of 6061 Aluminum Gas-Atomized Powder and High-Pressure Cold-Sprayed Deposition. Journal of Thermal Spray Technology. 2014;23:514-24.
[132] Rokni MR, Widener CA, Ozdemir OC, Crawford GA. Microstructure and mechanical properties of cold sprayed 6061 Al in As-sprayed and heat treated condition. Surface and Coatings Technology. 2017;309:641-50.
[133] Gavras AG, Lados DA, Champagne VK, Warren RJ. Effects of processing on microstructure evolution and fatigue crack growth mechanisms in cold-spray 6061 aluminum alloy. International Journal of Fatigue. 2018;110:49-62.
[134] Champagne V, Helfritch D. Critical assessment 11: structural repairs by cold spray. Materials Science and Technology. 2015;31:627-34.
[135] Kök M, Özdin K. Wear resistance of aluminium alloy and its composites reinforced by Al2O3 particles. Journal of Materials Processing Technology. 2007;183:301-9.
[136] Muvvala G, Patra Karmakar D, Nath AK. In-process detection of microstructural changes in laser cladding of in-situ Inconel 718/TiC metal matrix composite coating. Journal of Alloys and Compounds. 2018;740:545-58.
[137] Yang L, Li Z, Zhang Y, Wei S, Liu F. Al-TiC in situ composite coating fabricated by low power pulsed laser cladding on AZ91D magnesium alloy. Applied Surface Science. 2018;435:1187-98.
[138] He X, Kong D, Song R. Microstructures and properties of laser cladding Al-TiC-CeO2 composite coatings. Materials. 2018;11:198.
[139] Ao S, Wang T, Huang Y, Dai Y, Cai Y, Luo Z. The Wear Properties of TiC/Al-Based Composite Coating Applied by Laser Cladding. Metals. 2018;8:975.
[140] Zhang X, Zhang K, Ma J, Wang Y. Effect of Laser Cladding Al Ni TiC Powder on Microstructure and Properties of Aluminum Alloy. Journal of Minerals and Materials Characterization and Engineering. 2017;5:29-38.
[141] Mondal K, Koc R, Fan C. HVOF Thermal Spray TiC/TiB2 Coatings for AUSC Boiler/Turbine Components for Enhanced Corrosion Protection. Southern Illinois Univ., Carbondale, IL (United States); 2016.
[142] Bobzin K, Öte M, Knoch M, Liao X, Sommer J. Application of TiC reinforced Fe-based coatings by means of High Velocity Air Fuel Spraying. IOP Conference Series: Materials Science and Engineering: IOP Publishing; 2017. p. 012014.
[143] Bolelli G, Colella A, Lusvarghi L, Puddu P, Rigon R, Sassatelli P, et al. Properties of HVOF-sprayed TiC-FeCrAl coatings. Wear. 2019;418-419:36-51.

[144] Amiriyan M, Alamdari HD, Blais C, Savoie S, Schulz R, Gariépy M. Dry sliding wear behavior of Fe3Al and Fe3Al/TiC coatings prepared by HVOF. Wear. 2015;342-343:154-62.
[145] Myalska H, Michalska JK, Moskal G, Szymański K. Effect of nano-sized TiC powder on microstructure and the corrosion resistance of WC-Co thermal spray coatings. Surface and Coatings Technology. 2017;318:270-8.
[146] Chen H, Du Y, Wang D, Zhang C, Yang G, Liu B, et al. TiC/Ti3AlC2–Co plasma-sprayed coatings with excellent high-temperature tribological properties. Ceramics International. 2018;44:22520-8.
[147] Hou QY, Luo LM, Huang ZY, Wang P, Ding TT, Wu YC. Comparison of W–TiC composite coatings fabricated by atmospheric plasma spraying and supersonic atmospheric plasma spraying. Fusion Engineering and Design. 2016;105:77-85.
[148] Pan X, Niu Y, Liu T, Zhong X, Li C, Shi M, et al. Ablation behaviors of ZrC-TiC coatings prepared by vacuum plasma spray: Above 2000 °C. Journal of the European Ceramic Society. 2019.
[149] Sivkov A, Shanenkov I, Pak A, Gerasimov D, Shanenkova Y. Deposition of a TiC/Ti coating with a strong substrate adhesion using a high-speed plasma jet. Surface and Coatings Technology. 2016;291:1-6.
[150] Xu J, Zou B, Tao S, Zhang M, Cao X. Fabrication and properties of Al2O3–TiB2–TiC/Al metal matrix composite coatings by atmospheric plasma spraying of SHS powders. Journal of Alloys and Compounds. 2016;672:251-9.
[151] Emamian A, Corbin SF, Khajepour A. Effect of laser cladding process parameters on clad quality and in-situ formed microstructure of Fe–TiC composite coatings. Surface and Coatings Technology. 2010;205:2007-15.
[152] Ao S, Wang T, Huang Y, Dai Y, Cai Y, Luo Z. The Wear Properties of TiC/Al-Based Composite Coating Applied by Laser Cladding2018.
[153] Munagala VNV, Torgerson TB, Scharf TW, Chromik RR. High temperature friction and wear behavior of cold-sprayed Ti6Al4V and Ti6Al4V-TiC composite coatings. Wear. 2019;426-427:357-69.
[154] Kusiński J, Kac S, Kowalski K, Dosta S, Georgiou E, Garcia-Forgas J, et al. Microstructure and Properties of TiC/Ti Coatings Deposited by the Supersonic Cold Gas Spray Technique. Archives of Metallurgy and Materials. 2018.
[155] Sisson RD. Heat Treatment. In: Buschow KHJ, Cahn RW, Flemings MC, Ilschner B, Kramer EJ, Mahajan S, et al., editors. Encyclopedia of Materials: Science and Technology. Oxford: Elsevier; 2001. p. 3736-41.
[156] Rajan T, Sharma C, Sharma A. Heat treatment: Principles and techniques: PHI Learning Pvt. Ltd.; 2011.

[157] Kaufman JG, Rooy EL. Aluminum alloy castings: properties, processes, and applications: Asm International; 2004.
[158] Swamy NP, Ramesh C, Chandrashekar T. Effect of heat treatment on strength and abrasive wear behaviour of Al6061-SiCp composites. Bulletin of Materials Science. 2010;33:49-54.
[159] Reddy AC, Kotiveerachari B. Influence of microstructural changes caused by ageing on wear behaviour of Al6061/SiC composites. Journal of Metallurgy & Materials Science. 2011;53:31-9.
[160] Pitchuka SB, Lahiri D, Sundararajan G, Agarwal A. Scratch-Induced Deformation Behavior of Cold-Sprayed Aluminum Amorphous/Nanocrystalline Coatings at Multiple Load Scales. Journal of thermal spray technology. 2014;23:502-13.
[161] Chavan NM, Ramakrishna M, Phani PS, Rao DS, Sundararajan G. The influence of process parameters and heat treatment on the properties of cold sprayed silver coatings. Surface and Coatings Technology. 2011;205:4798-807.
[162] Phani PS, Rao DS, Joshi S, Sundararajan G. Effect of process parameters and heat treatments on properties of cold sprayed copper coatings. Journal of Thermal Spray Technology. 2007;16:425-34.
[163] Li W-Y, Li C-J, Liao H. Effect of annealing treatment on the microstructure and properties of cold-sprayed Cu coating. Journal of Thermal Spray Technology. 2006;15:206-11.
[164] Li WY, Zhang C, Guo X, Xu J, Li CJ, Liao H, et al. Ti and Ti-6Al-4V Coatings by Cold Spraying and Microstructure Modification by Heat Treatment. Advanced Engineering Materials. 2007;9:418-23.
[165] Yilbas BS, Shuja SZ. Laser Surface Processing and Model Studies. : Springer; 2013.
[166] Abioye TE. Laser deposition of Inconel 625/tungsten carbide composite coatings by powder and wire feedstock [Doctoral dissertation]: University of Nottingham; 2014.
[167] Tian YS, Chen CZ, Li ST, Huo QH. Research progress on laser surface modification of titanium alloys. Applied Surface Science. 2005;242:177-84.
[168] Zhou S, Huang Y, Zeng X, Hu Q. Microstructure characteristics of Ni-based WC composite coatings by laser induction hybrid rapid cladding. Materials Science and Engineering: A. 2008;480:564-72.
[169] Farahmand P, Kovacevic R. An experimental–numerical investigation of heat distribution and stress field in single- and multi-track laser cladding by a high-power direct diode laser. Optics & Laser Technology. 2014;63:154-68.

[170] Farahmand P, Liu S, Zhang Z, Kovacevic R. Laser cladding assisted by induction heating of Ni–WC composite enhanced by nano-WC and La2O3. Ceramics International. 2014;40:15421-38.
[171] Mann BS, Arya V, Pant BK. High-Power Diode Laser Surface Treated HVOF Coating to Combat High Energy Particle Impact Wear. Journal of Materials Engineering and Performance. 2013;22:1995-2004.
[172] Cerri W, Martinella R, Mor GP, Bianchi P, Angelo DD. Laser deposition of carbide-reinforced coatings. Surface and Coatings Technology. 1991;49:40-5.
[173] Vilar R. Laser cladding. Journal of laser applications. 1999;11:64-79.
[174] Doubenskaia M, Gilmutdinov AK, Nagulin KY. Laser cladding of metal matrix composites reinforced by cermet inclusions for dry friction applications at ambient and elevated temperatures. Surface and Coatings Technology. 2015;276:696-703.
[175] Yang S, Evans JRG. A multi-component powder dispensing system for three dimensional functional gradients. Materials Science and Engineering: A. 2004;379:351-9.
[176] De Hosson JTM. Proceedings of ASTRA-2003. 2003:368.
[177] Dahotre NB. Laser surface engineering. Advanced materials & processes. 2002;160:35-9.
[178] De Oliveira U, Ocelik V, De Hosson JTM. Analysis of coaxial laser cladding processing conditions. Surface and Coatings Technology. 2005;197:127-36.
[179] Toyserkani E, Khajepour A, Corbin SF. Laser cladding: CRC press; 2004.
[180] Dubourg L, Ursescu D, Hlawka F, Cornet A. Laser cladding of MMC coatings on aluminium substrate: influence of composition and microstructure on mechanical properties. Wear. 2005;258:1745-54.
[181] Riveiro A, Mejías A, Lusquiños F, del Val J, Comesaña R, Pardo J, et al. Laser cladding of aluminium on AISI 304 stainless steel with high-power diode lasers. Surface and Coatings Technology. 2014;253:214-20.
[182] Ocelík V, Eekma M, Hemmati I, De Hosson JTM. Elimination of Start/Stop defects in laser cladding. Surface and Coatings Technology. 2012;206:2403-9.
[183] Erfanmanesh M, Abdollah-Pour H, Mohammadian-Semnani H, Shoja-Razavi R. An empirical-statistical model for laser cladding of WC-12Co powder on AISI 321 stainless steel. Optics & Laser Technology. 2017;97:180-6.
[184] Zhang H, Yu H, Chen C. In-situ forming composite coating by laser cladding C/B4C. Materials and Manufacturing Processes. 2015;30:743-7.
[185] Wang L, Pratt P, Felicelli SD, El Kadiri H, Berry JT, Wang PT, et al. Pore Formation in Laser-Assisted Powder Deposition Process. Journal of Manufacturing Science and Engineering. 2009;131:051008--9.

[186] Wang L, Pratt P, Felicelli S, El Kadiri H, Berry J, Wang P, et al. Pore formation in laser-assisted powder deposition process. Journal of Manufacturing Science and Engineering. 2009;131:051008.
[187] Ignat S, Sallamand P, Grevey D, Lambertin M. Magnesium alloys laser (Nd: YAG) cladding and alloying with side injection of aluminium powder. Applied Surface Science. 2004;225:124-34.
[188] Lee H-K. Effects of the cladding parameters on the deposition efficiency in pulsed Nd: YAG laser cladding. Journal of materials processing technology. 2008;202:321-7.
[189] Lee H-K. Effects of the cladding parameters on the deposition efficiency in pulsed Nd:YAG laser cladding. Journal of Materials Processing Technology. 2008;202:321-7.
[190] Devesse W, De Baere D, Guillaume P. Modeling of laser beam and powder flow interaction in laser cladding using ray-tracing. Journal of Laser Applications. 2015;27:S29208.
[191] Uenishi K, Kobayashi KF. Formation of surface layer based on Al3Ti on aluminum by laser cladding and its compatibility with ceramics. Intermetallics. 1999;7:553-9.
[192] Lin J. A simple model of powder catchment in coaxial laser cladding. Optics & Laser Technology. 1999;31:233-8.
[193] Ready JF. Industrial applications of lasers. 2 ed. London: Academic Press; 1997.
[194] Naeem M. Laser Processing of Reflective Materials. Laser Technik Journal. 2013;10:18-20.
[195] Miyamoto I, Knorovsky G. Laser microwelding. Microjoining and Nanojoining: Elsevier; 2008. p. 345-417.
[196] Pierron N, Sallamand P, Matteï S. Study of magnesium and aluminum alloys absorption coefficient during Nd: YAG laser interaction. Applied Surface Science. 2007;253:3208-14.
[197] Liu W, DuPont J. Fabrication of functionally graded TiC/Ti composites by laser engineered net shaping. Scripta Materialia. 2003;48:1337-42.
[198] Quazi M, Fazal M, Haseeb A, Yusof F, Masjuki H, Arslan A. Laser-based Surface Modifications of Aluminum and its Alloys. Critical Reviews in Solid State and Materials Sciences. 2015:1-26.
[199] Karamış M, Cerit AA, Selçuk B, Nair F. The effects of different ceramics size and volume fraction on wear behavior of Al matrix composites (for automobile cam material). Wear. 2012;289:73-81.
[200] Li J, Luo X, Li GJ. Effect of Y2O3 on the sliding wear resistance of TiB/TiC-reinforced composite coatings fabricated by laser cladding. Wear. 2014;310:72-82.
[201] Farahmand P, Frosell T, McGregor M, Kovacevic R. Comparative study of the slurry erosion behavior of laser cladded Ni-WC coating modified by nanocrystalline WC

and La2O3. The International Journal of Advanced Manufacturing Technology. 2015;79:1607-21.
[202] Du B, Paital SR, Dahotre NB. Synthesis of TiB2–TiC/Fe nano-composite coating by laser surface engineering. Optics & Laser Technology. 2013;45:647-53.
[203] Surappa M. Aluminium matrix composites: Challenges and opportunities. Sadhana. 2003;28:319-34.
[204] Li J, Chen C, Squartini T, He Q. A study on wear resistance and microcrack of the Ti3Al/TiAl+TiC ceramic layer deposited by laser cladding on Ti–6Al–4V alloy. Applied Surface Science. 2010;257:1550-5.
[205] Emamian A, Corbin SF, Khajepour A. The influence of combined laser parameters on in-situ formed TiC morphology during laser cladding. Surface and Coatings Technology. 2011;206:124-31.
[206] Sampedro J, Pérez I, Carcel B, Ramos JA, Amigó V. Laser Cladding of TiC for Better Titanium Components. Physics Procedia. 2011;12:313-22.
[207] Yan H, Zhang J, Zhang P, Yu Z, Li C, Xu P, et al. Laser cladding of Co-based alloy/TiC/CaF2 self-lubricating composite coatings on copper for continuous casting mold. Surface and Coatings Technology. 2013;232:362-9.
[208] Yu M, Li WY, Suo XK, Liao HL. Effects of gas temperature and ceramic particle content on microstructure and microhardness of cold sprayed SiCp/Al 5056 composite coatings. Surface and Coatings Technology. 2013;220:102-6.
[209] Yu M, Suo XK, Li WY, Wang YY, Liao HL. Microstructure, mechanical property and wear performance of cold sprayed Al5056/SiCp composite coatings: Effect of reinforcement content. Applied Surface Science. 2014;289:188-96.
[210] El-Eskandarany MS. 2 - The history and necessity of mechanical alloying. In: El-Eskandarany MS, editor. Mechanical Alloying (Second Edition). Oxford: William Andrew Publishing; 2015. p. 13-47.
[211] Zhang FL, Zhu M, Wang CY. Parameters optimization in the planetary ball milling of nanostructured tungsten carbide/cobalt powder. International Journal of Refractory Metals and Hard Materials. 2008;26:329-33.
[212] Zhang D. Processing of advanced materials using high-energy mechanical milling. Progress in Materials Science. 2004;49:537-60.
[213] Zhang F, Wang C, Zhu M. Nanostructured WC/Co composite powder prepared by high energy ball milling. Scripta materialia. 2003;49:1123-8.
[214] Zhang D, Cai R, Zhou Y, Shao Z, Liao X-Z, Ma Z-F. Effect of milling method and time on the properties and electrochemical performance of LiFePO4/C composites prepared by ball milling and thermal treatment. Electrochimica Acta. 2010;55:2653-61.

[215] Wang Y, Li Y, Rong C, Liu JP. Sm–Co hard magnetic nanoparticles prepared by surfactant-assisted ball milling. Nanotechnology. 2007;18:465701.
[216] Chakka V, Altuncevahir B, Jin Z, Li Y, Liu J. Magnetic nanoparticles produced by surfactant-assisted ball milling. Journal of applied physics. 2006;99:08E912.
[217] Chandran M, Kumaran C, Gowthama S, Shanmugam P, Natarajan R, Bhattacharya S, et al. Chemical vapor deposition of diamond coatings on tungsten carbide (WC–Co) riveting inserts. International Journal of Refractory Metals and Hard Materials. 2013;37:117-20.
[218] Savvides N, Bell T. Microhardness and Young's modulus of diamond and diamondlike carbon films. Journal of applied physics. 1992;72:2791-6.
[219] He X-M, Li W-Z. Ion beam assisted deposition of diamond-like carbon onto steel materials: preparation and advantages. Surface and Coatings Technology. 1996;84:414-9.
[220] Leon CA, Drew RAL. Preparation of nickel-coated powders as precursors to reinforce MMCs. Journal of Materials Science. 2000;35:4763-8.
[221] Liu Z, Jian L, Tao W. Preparation of WC–Co composite powder by electroless plating and its application in laser cladding. Materials Letters. 2006;60:1956-9.
[222] Davydova A, Domashenkov A, Sova A, Movtchan I, Bertrand P, Desplanques B, et al. Selective laser melting of boron carbide particles coated by a cobalt-based metal layer. Journal of Materials Processing Technology. 2016;229:361-6.
[223] Feng C, Guipont V, Jeandin M, Amsellem O, Pauchet F, Saenger R, et al. B4C/Ni Composite Coatings Prepared by Cold Spray of Blended or CVD-Coated Powders. Journal of Thermal Spray Technology. 2012;21:561-70.
[224] Jafari M, Enayati M, Salehi M, Nahvi S, Han J, Park C. High temperature oxidation behavior of micro/nanostructured WC-Co coatings deposited from Ni-coated powders using high velocity oxygen fuel spraying. Surface and Coatings Technology. 2016;302:426-37.
[225] Mallory GO, Hajdu JB. Electroless plating: fundamentals and applications: William Andrew; 1990.
[226] Hai H, Ahn J, Kim D, Lee J, Chung H, Kim C. Developing process for coating copper particles with silver by electroless plating method. Surface and Coatings Technology. 2006;201:3788-92.
[227] Mirzamohammadi S, Khorsand H, Aliofkhazraei M. Effect of different organic solvents on electrodeposition and wear behavior of Ni-alumina nanocomposite coatings. Surface and Coatings Technology. 2017;313:202-13.
[228] Grigoriev S, Okunkova A, Sova A, Bertrand P, Smurov I. Cold spraying: From process fundamentals towards advanced applications. Surface and Coatings Technology. 2015;268:77-84.

[229] Richer P, Jodoin B, Ajdelsztajn L. Substrate roughness and thickness effects on cold spray nanocrystalline Al− Mg coatings. Journal of thermal spray technology. 2006;15:246-54.
[230] Handbook A. Aluminum and aluminum alloys. ASM international. 1993:117.
[231] Goodship V, Jacobs D. Polyvinyl alcohol: materials, processing and applications: Smithers Rapra Technology; 2009.
[232] Clare A, Kennedy A. Additive Manufacturing. Google Patents; 2014.
[233] Li Q, Rudolph V, Weigl B, Earl A. Interparticle van der Waals force in powder flowability and compactibility. International journal of pharmaceutics. 2004;280:77-93.
[234] Hare C, Zafar U, Ghadiri M, Freeman T, Clayton J, Murtagh M. Analysis of the dynamics of the FT4 powder rheometer. Powder Technology. 2015;285:123-7.
[235] Freeman R. Measuring the flow properties of consolidated, conditioned and aerated powders—a comparative study using a powder rheometer and a rotational shear cell. Powder Technology. 2007;174:25-33.
[236] Tajally M, Huda Z, Masjuki H. A comparative analysis of tensile and impact-toughness behavior of cold-worked and annealed 7075 aluminum alloy. International journal of impact engineering. 2010;37:425-32.
[237] Yang S, Evans J. Metering and dispensing of powder; the quest for new solid freeforming techniques. Powder Technology. 2007;178:56-72.
[238] Lu Y, Zheng Y, Song W. Laser induced removal of spherical particles from silicon wafers. Journal of Applied Physics. 2000;87:1534-9.
[239] Hart A. Effect of particle size on detergent powders flowability and tabletability. J Chem Eng Process Technol. 2015;6:215-8.
[240] Heckel R. Density-pressure relationships in powder compaction. Trans Metall Soc AIME. 1961;221:671-5.
[241] Stanford MK, Eylon D, DellaCorte C. Effect of particle morphology on flow characteristics of a composite plasma spray powder. Journal of Thermal Spray Technology. 2004;13:586-92.
[242] Park JM, Yu J-H, Kang TG, Kim SJ, Park SJ. Particle size effect on the magneto-rheological behavior of powder injection molding feedstock. Materials Characterization. 2014;94:19-25.
[243] Champagne VK. The cold spray materials deposition process: fundamentals and applications: Elsevier; 2007.
[244] Stoltenhoff T, Kreye H, Richter H. An analysis of the cold spray process and its coatings. Journal of Thermal Spray Technology. 2002;11:542-50.

[245] Wei Y-K, Luo X-T, Li C-X, Li C-J. Optimization of in-situ shot-peening-assisted cold spraying parameters for full corrosion protection of Mg alloy by fully dense Al-based alloy coating. Journal of Thermal Spray Technology. 2017;26:173-83.
[246] Van Steenkiste T, Smith J, Teets R. Aluminum coatings via kinetic spray with relatively large powder particles. Surface and Coatings Technology. 2002;154:237-52.
[247] Ozdemir OC, Widener CA, Carter MJ, Johnson KW. Predicting the Effects of Powder Feeding Rates on Particle Impact Conditions and Cold Spray Deposited Coatings. Journal of Thermal Spray Technology. 2017;26:1598-615.
[248] Li C-J, Li W-Y. Deposition characteristics of titanium coating in cold spraying. Surface and Coatings Technology. 2003;167:278-83.
[249] Tao Y, Xiong T, Sun C, Jin H, Du H, Li T. Effect of α-Al 2 O 3 on the properties of cold sprayed Al/α-Al 2 O 3 composite coatings on AZ91D magnesium alloy. Applied Surface Science. 2009;256:261-6.
[250] Spencer K, Fabijanic D, Zhang M-X. The use of Al–Al2O3 cold spray coatings to improve the surface properties of magnesium alloys. Surface and Coatings Technology. 2009;204:336-44.
[251] Lee YTR, Hussain T, Fisher GA, McDonald AG. Cold-Sprayed Metal Matrix Composite Coatings. Cold-Spray Coatings: Springer; 2018. p. 275-95.
[252] Irissou E, Legoux J-G, Arsenault B, Moreau C. Investigation of Al-Al 2 O 3 cold spray coating formation and properties. Journal of Thermal Spray Technology. 2007;16:661-8.
[253] Hussain T, McCartney D, Shipway P. Impact phenomena in cold-spraying of titanium onto various ferrous alloys. Surface and Coatings Technology. 2011;205:5021-7.
[254] Klinkov S, Kosarev V. Measurements of cold spray deposition efficiency. Journal of Thermal Spray Technology. 2006;15:364.
[255] Bae G, Xiong Y, Kumar S, Kang K, Lee C. General aspects of interface bonding in kinetic sprayed coatings. Acta Materialia. 2008;56:4858-68.
[256] Sova A, Kosarev VF, Papyrin A, Smurov I. Effect of Ceramic Particle Velocity on Cold Spray Deposition of Metal-Ceramic Coatings. Journal of Thermal Spray Technology. 2011;20:285-91.
[257] Koivuluoto H, Lagerbom J, Kylmälahti M, Vuoristo P. Microstructure and mechanical properties of low-pressure cold-sprayed (LPCS) coatings. Journal of Thermal Spray Technology. 2008;17:721-7.
[258] Rokni M, Nutt S, Widener C, Champagne V, Hrabe R. Review of relationship between particle deformation, coating microstructure, and properties in high-pressure cold spray. Journal of thermal spray technology. 2017;26:1308-55.

[259] Koivuluoto H, Vuoristo P. Effect of Ceramic Particles on Properties of Cold-Sprayed Ni-20Cr+Al2O3 Coatings. Journal of Thermal Spray Technology. 2009;18:555.
[260] Lee YTR, Ashrafizadeh H, Fisher G, McDonald A. Effect of type of reinforcing particles on the deposition efficiency and wear resistance of low-pressure cold-sprayed metal matrix composite coatings. Surface and Coatings Technology. 2017;324:190-200.
[261] Grard CAM. Aluminium and its alloys1922.
[262] Wei Y-K, Luo X-T, Li C-X, Li C-J. Optimization of In-Situ Shot-Peening-Assisted Cold Spraying Parameters for Full Corrosion Protection of Mg Alloy by Fully Dense Al-Based Alloy Coating. Journal of Thermal Spray Technology. 2017;26:173-83.
[263] Messer B, Dais S, Wolf D. Detection of vacancy-induced self-diffusion by rotating-frame spin-lattice relaxation in aluminum. Paper from" Magnetic Resonance and Related Phenomena". 1975;2.
[264] Huang R, Sone M, Ma W, Fukanuma H. The effects of heat treatment on the mechanical properties of cold-sprayed coatings. Surface and Coatings Technology. 2015;261:278-88.
[265] Van Loo F, Rieck G. Diffusion in the titanium-aluminium system—I. Interdiffusion between solid Al and Ti or Ti-Al alloys. Acta Metallurgica. 1973;21:61-71.
[266] Okura A, Motoki K. Rate of formation of intermetallic compounds in aluminium matrix-carbon fibre composites. Composites Science and Technology. 1985;24:243-52.
[267] Arabgol Z, Assadi H, Schmidt T, Gärtner F, Klassen T. Analysis of thermal history and residual stress in cold-sprayed coatings. Journal of Thermal Spray Technology. 2014;23:84-90.
[268] Moridi A. Powder Consolidation Using Cold Spray: Process Modeling and Emerging Applications: Springer; 2016.
[269] Chen R-Y, Chu H-Y, Lai C-C, Wu C-T. Effects of annealing temperature on the mechanical properties and sensitization of 5083-H116 aluminum alloy. Proceedings of the Institution of Mechanical Engineers, Part L: Journal of Materials: Design and Applications. 2015;229:339-46.
[270] Cantera EL, Mellor B. Fracture toughness and crack morphologies in eroded WC–Co–Cr thermally sprayed coatings. Materials Letters. 1998;37:201-10.
[271] Lee C, Han J, Yoon J, Shin M, Kwun S. A study on powder mixing for high fracture toughness and wear resistance of WC–Co–Cr coatings sprayed by HVOF. Surface and coatings technology. 2010;204:2223-9.
[272] Hashempour M, Razavizadeh H, Rezaie H. Investigation on wear mechanism of thermochemically fabricated W–Cu composites. Wear. 2010;269:405-15.

[273] Guilemany J, Dosta S, Miguel J. The enhancement of the properties of WC-Co HVOF coatings through the use of nanostructured and microstructured feedstock powders. Surface and Coatings Technology. 2006;201:1180-90.
[274] Melendez N, Narulkar V, Fisher G, McDonald A. Effect of reinforcing particles on the wear rate of low-pressure cold-sprayed WC-based MMC coatings. Wear. 2013;306:185-95.
[275] Qiao Y, Fischer TE, Dent A. The effects of fuel chemistry and feedstock powder structure on the mechanical and tribological properties of HVOF thermal-sprayed WC–Co coatings with very fine structures. Surface and Coatings Technology. 2003;172:24-41.
[276] Guilemany JM, Dosta S, Miguel JR. The enhancement of the properties of WC-Co HVOF coatings through the use of nanostructured and microstructured feedstock powders. Surface and Coatings Technology. 2006;201:1180-90.
[277] Oberle T. Properties influencing wear of metals. Journal of Metals. 1951;3:438-&.
[278] Pitchuka SB, Boesl B, Zhang C, Lahiri D, Nieto A, Sundararajan G, et al. Dry sliding wear behavior of cold sprayed aluminum amorphous/nanocrystalline alloy coatings. Surface and Coatings Technology. 2014;238:118-25.
[279] Lou Q, Zhou J, He B, Zhou H. Fiber lasers and their coherent beam combination. Optics and Photonics News. 2008;19:46-51.
[280] Kumar S, Chakraborty M, Subramanya Sarma V, Murty BS. Tensile and wear behaviour of in situ Al–7Si/TiB2 particulate composites. Wear. 2008;265:134-42.
[281] Xiong Y, Smugeresky JE, Ajdelsztajn L, Schoenung JM. Fabrication of WC–Co cermets by laser engineered net shaping. Materials Science and Engineering: A. 2008;493:261-6.
[282] Al-Hamdani KS, Murray JW, Hussain T, Clare AT. Heat-treatment and mechanical properties of cold-sprayed high strength Al alloys from satellited feedstocks. Surface and Coatings Technology. 2019;374:21-31.
[283] Sing SL, Yeong WY, Wiria FE, Tay BY, Zhao Z, Zhao L, et al. Direct selective laser sintering and melting of ceramics: a review. Rapid Prototyping Journal. 2017;23:611-23.
[284] Lee J-Y, Jo W-K. Control of methyl tertiary-butyl ether via carbon-doped photocatalysts under visible-light irradiation. Environmental Engineering Research. 2012;17:179-84.
[285] Partes K. Analytical model of the catchment efficiency in high speed laser cladding. Surface and Coatings Technology. 2009;204:366-71.
[286] Huang Y-L, Liu J, Ma N-H, Li J-G. Three-dimensional analytical model on laser-powder interaction during laser cladding. Journal of Laser Applications. 2006;18:42-6.

[287] Sheikholeslami M, Chamkha AJ. Influence of Lorentz forces on nanofluid forced convection considering Marangoni convection. Journal of Molecular Liquids. 2017;225:750-7.
[288] Magyari E, Chamkha AJ. Exact analytical results for the thermosolutal MHD Marangoni boundary layers. International Journal of Thermal Sciences. 2008;47:848-57.
[289] Goodarzi DM, Pekkarinen J, Salminen A. Effect of process parameters in laser cladding on substrate melted areas and the substrate melted shape. Journal of Laser Applications. 2015;27:S29201.
[290] Candel J, Amigó V, Ramos J, Busquets D. Sliding wear resistance of TiCp reinforced titanium composite coating produced by laser cladding. Surface and Coatings Technology. 2010;204:3161-6.
[291] Okamoto H. C-Ti (carbon-titanium). Journal of Phase Equilibria and Diffusion. 1998;19:89-.
[292] Bandyopadhyay D, Sharma R, Chakraborti N. The Ti-Al-C system (titanium-aluminum-carbon). Journal of phase equilibria. 2000;21:195-8.
[293] Nakano T, Negishi A, Hayashi K, Umakoshi Y. Ordering process of Al5Ti3, h-Al2Ti and r-Al2Ti with f.c.c.-based long-period superstructures in rapidly solidified Al-rich TiAl alloys. Acta Materialia. 1999;47:1091-104.
[294] Liu X, Liu L, Sun B, Li B, Ke X. The preparation of titanium carbide thin film of Ti6Al4V at low temperature and study of friction and wear properties2016.
[295] Benci JE, Ma JC, Feist TP. Structure and Microstructure of Al 2 Ti Intermetallic Alloy. MRS Online Proceedings Library Archive. 1992;288.
[296] Farahmand P, Frosell T, McGregor M, Kovacevic R. Comparative study of the slurry erosion behavior of laser cladded Ni-WC coating modified by nanocrystalline WC and La 2 O 3. The International Journal of Advanced Manufacturing Technology. 2015;79:1607-21.
[297] Nakano T, Hagihara K, Seno T, Sumida N, Yamamoto M, Umakoshi Y. Stress anomaly in Al-rich Ti-Al single crystals deformed by the motion of 1/2 «110] ordinary dislocations. Philosophical magazine letters. 1998;78:385-91.
[298] Hata S, Shiraishi K, Itakura M, Kuwano N, Nakano T, Umakoshi Y. Application of FIB microsampling technique to long-period ordered TiAl single crystal with composition gradient. Microscopy. 2004;53:537-40.
[299] Kravchenko Y, Borysiuk V, Pogrebnjak A, Kylyshkanov M, Iatsunskyi I, Smyrnova K. Characteristics of Arc-PVD TiAlSiY and (TiAlSiY) N coatings. 2017 IEEE 7th International Conference Nanomaterials: Application & Properties (NAP): IEEE; 2017. p. 01FNC2-1-FNC2-4.

[300] Li M, Huang J, Zhu Y, Li Z. Effect of heat input on the microstructure of in-situ synthesized TiN–TiB/Ti based composite coating by laser cladding. Surface and Coatings Technology. 2012;206:4021-6.
[301] Xue P, Meng Q, Chen S, Liang L, Liu Z, Chen R. Tribological property of (TiC-TiB 2) p Ni ceramics prepared by field-activated and pressure-assisted synthesis. Rare Metals. 2011;30:599-603.
[302] Cai Y, Luo Z, Feng M, Liu Z, Huang Z, Zeng Y. The effect of TiC/Al 2 O 3 composite ceramic reinforcement on tribological behavior of laser cladding Ni60 alloys coatings. Surface and Coatings Technology. 2016;291:222-9.
[303] Cai Y, Luo Z, Feng M, Liu Z, Huang Z, Zeng Y. The effect of TiC/Al2O3 composite ceramic reinforcement on tribological behavior of laser cladding Ni60 alloys coatings. Surface and Coatings Technology. 2016;291:222-9.
[304] Prasad B, Prasad S, Das A. Mechanisms of material removal and subsurface work hardening during low-stress abrasion of a squeeze-cast aluminium alloy-Al2O3 fibre composite. Materials Science and Engineering: A. 1992;156:205-9.
[305] Xu J, Liu W, Zhong M. Microstructure and dry sliding wear behavior of MoS2/TiC/Ni composite coatings prepared by laser cladding. Surface and Coatings Technology. 2006;200:4227-32.

Appendixes

Appendix 1: Parameters set and the average of three measurements for each clad.

	Sample No.	E_{eff} (J/mm^2)	PDD (g/mm^2)	Dilution (%)	Clad area (mm^2)	Clad form
Blended	1	104	0.0028	28	0.8	Clad/bonded
	2	104	0.0037	25	1.17	Clad/bonded
	3	104	0.0056	19	1.43	Clad/bonded
	4	104	0.0075	X	X	No clad
	5	122	0.0028	57	1.25	Clad/bonded
	6	122	0.0037	49	1.34	Clad/bonded
	7	122	0.0056	41	1.63	Clad/bonded
	8	122	0.0075	X	X	Clad/bonded
	9	140	0.0028	X	X	No clad
	10	140	0.0037	X	X	No clad
	11	140	0.0056	28	1.92	Clad/bonded
	12	140	0.0075	X	X	Clad/no bond
Satellited	13	104	0.0028	39	1.38	Clad/bonded
	14	104	0.0037	31	1.61	Clad/bonded
	15	104	0.0056	22.2	1.79	Clad/bonded
	16	104	0.0075	X	X	No clad
	17	122	0.0028	63	1.45	Clad/bonded
	18	122	0.0037	52	1.81	Clad/bonded
	19	122	0.0056	44	2.204	Clad/bonded
	20	122	0.0075	X	X	Clad/detached
	21	140	0.0028	X	X	No clad

	22	140	0.0037	X	X	No clad
	23	140	0.0056	52	2.44	Clad/bonded
	24	140	0.0075	50	4.1	Clad/bonded

Appendix 2: Ti - C binary phase diagram [Okamoto, 1998].

